University of Wroclaw

Faculty of Physics and Astronomy
Institute of Theoretical Physics

Consistent Many-Body Models of Lepton-Nucleus Scattering in the Energy Range Between 500 and 1200 MeV

Jakub Żmuda

PhD thesis

advisor

prof. dr hab. Jan Sobczyk

Wrocław, February 26, 2014

Konsystentne wielociałowe modele rozpraszania leptonów na jądrach atomowych w zakresie energii od 500 do 1200 MeV.

Jakub Żmuda

Rozprawa doktorska napisona pod kierunkiem

prof. dr hab. Jana Sobczyka

Streszczenie

Niniejsza rozprawa doktorska poświęcona jest szeroko rozumianemu problemowi oddziaływań leptonów z jądrami atomowymi, który to posiada szczególną wagę dla neutrinowych eksperymentów oscylacyjnych. Wstępne rozdziały tej pracy zawierają omówienie problemu oscylacji neutrin oraz sposobów ich pomiaru w eksperymentach akceleratorowych oraz głównych rodzajów reakcji leptonów z tarczą hadronową i jądrową. Ze względu na rozległość tematu skupiono się na typach oddziaływań ważnych dla doświadczeń z energią wiązki w zakresie od ~ 500 do ~ 1200 MeV takich, jak T2K, w którym to autor niniejszej rozprawy uczestniczy. Zakres badań obejmuje proces kwazielastyczny, produkcję pojedynczych pionów oraz tzw. "prądy wymiany mezonów" prowadzące do oddziaływań wielonukleonowych. W większości przypadków korzysta się tu ze zunifikowanego opisu opartego na efektywnej teorii pola, w której to główne stopnie swobody stanowią bariony i mezony, oraz na formalizmie tensora polaryzacyjnego.

W części poświęconej procesowi kwazielastycznemu wprowadza się ogólny formalizm oddziaływań leptonów z tarczą hadronową i jądrową, który używany jest potem w całej rozprawie, włączając w to również tensor polaryzacyjny. Wyprowadza się tam wzory na przekrój czynny dla lokalnego i globalnego relatywistycznego gazu Fermiego. Wyniki dla obu modeli są porównywane dla danych doświadczalnych z inkluzywnego rozpraszania elektronów na węglu. Pokazuje się również metodę otrzymania jądrowej funkcji spektralnej z użyciem nierelatywistycznej teorii wielu ciał i tensora polaryzacyjnego. Następnie prezentuje się wyniki pracy, w której zastosowano implementację gazu Fermiego i funkcji spektralnej w generatorze odziaływań neutrin NuWro do dopasowania masy aksjalnej nukleonu do danych eksperymentu MiniBooNE. Analizowany parametr jest niezwykle ważny w zrozumieniu aksjalnego prądu nukleonowego. Głównym rezultatem tych rozważań jest obserwacja, że jeżel potraktuje się dane MiniBooNE jako pochodzące tylko z oddziaływania kwazielastycznego na jądrze węgla, dostaje się masę aksjalną różniącą się istotnie od wyników starszych

eksperymentów przeprowadzanych na deuterze (gdzie efekty jądrowe można łatwo kontrolować) oraz wyliczeń teoretycznych opartych na hipotezie częściowo zachowanego prądu aksjalnego. Rozbieżność ta wynosi ponad 30% i różni się od dawnych wyników o 5 odchyleń standardowych. Sugeruje to istnienie dodatkowych kanałów rozpraszania, których eksperyment MiniBooNE nie bierze pod uwagę.

Szczególną uwagę poświęca się w niniejszej rozprawie procesowi produkcji pojedynczych pionów. Rozpatruje się trzy rodzaje tarcz (swobodny nukleon, deuter oraz jądro atomowe w ujęciu lokalnego gazu Fermiego) oraz dwa modele tła nierezonansowego. Dodatkowo sprawdza się różne opisy rezonansu $\Delta(1232)$, który daje znaczną część wkładu do produkcji pionów w rozpatrywanym przedziale energii. Modele testowane są najpierw na danych z inkluzywnego rozpraszania elektronów na protonie oraz neutrinoprodukcji pionów na deuterze w eksperymencie ANL. Dzięki temu sprawdza się mocne i słabe strony każdego z podejść. W kolejnym kroku sprawda się wpływ poszczególnych efektów jądrowych na produkcję pionów. Rozwija się tam jedno z podejść poprzez podanie przepisu na policzenie w sposób dokładny całek metodą Monte Carlo, które w dostępnej literaturze zawsze rozwiązuje się w sposób przybliżony. Dokładne omówienie efektów jądrowych zaczyna się od wpływu ruchu Fermiego i zakazu Pauliego, a kończy na nieperturbacyjnej energii własnej rezonansu Δ. Ta ostatnia prowadzi do rozpadów bezpionowych, w których z jądra wybijanych jest kilka nukleonów. Głównym wynikiem tutaj jest znalezienie wyraźnej zależności procentowego udziału rozpadów bezpionowych od nenergii neutrina, co jest niezgodne z dotychczasowymi założeniami stałego udziału 20% używanego w większości generatorów Monte Carlo. Dodatkowo sprawdza się wpływ efektów jądrowych i tła nierezonansowego na stosunki przekrojów czynnych na oddziaływanie neutrin mionowych i elektronowych. Dodatkowym rezultatem jest porównanie do przekrojów czynnych na produkcje pionów opublikowanych przez eksperyment MiniBooNE. Okazuje się, że teoretyczne obliczenia niedoszacowują mierzone przekroje czynne. Prawdopodobną przyczyną są dodatkowe kanały produkcji pionów w oddziaływaniu z tarczą jądrową, którch brak we wszystkich popularnych modelach.

Końcowy rozdział poświęcono przeglądowi wybranych modeli prądów wymiany mezonów. Omawia się implementację modelu z IFIC w generatorze NuWro a także porównanie właściwości tego modelu z uprzednio zaimplementowanymi modelami TEM oraz modelem grupy z Lyon. Pokazuje się problemy z rekonstrukcją energii neutrina dla zdarzeń wygenerowanych w ramach prądów wymiany mezonów oraz wkład autora rozprawy do analizy oscylacyjnej T2K. W końcowej sekcji rozdziału oblicza się teoretyczny wzór na jeden z wkładów do prądów wymiany mezonów w modelu IFIC i omawia problemy z rozbieżnościami części diagramów.

Acknowledgments

A lot has changed in the field of neutrino physics since Wolfgang Pauli proposed existence of a new particle in his letter to "Radioactive Ladies and Gentlemen" in 1930 and first detection in 1956 by Frederic Reines and Clyde Cowan. We already know neutrinos are massive and nowadays these particles may be the only accessible window for physics beyond standard model, as ATLAS and CMS experiments LHC have discovered a particle being presumably the Higgs boson and there are no signs of supersymmetry yet. Leptonc CP violation may be also soon discovered, but in order to make such experiments one has to understand properly the lepton-nucleus interactions.

I have entered the field of neutrino physics during time of great experimental and theoretical activity. Several major neutrino experiments are currently running or finishing their data taking (T2K, ICARUS, MiniBooNE, OPERA, DayaBay, RENO, Double Chooz and others) and more are planned for the future. They have provided us with exciting results, like nonzero value of $\sin^2(2\Theta_{13})$, and a lot of cross section data to analyze. This includes the first double-differential cross section measurements, which were not available up until 2010 due to very large experimental errors. Experimental activity has motivated an extensive research in the field of neutrino-nucleus interactions clearly seen in the NuInt conference series and number of published papers. This has opened a path for my thesis topic and allowed to meet a lot of interesting physicists working in the subjest

My PhD studies in Wroclaw were a great adventure. I have learned a lot about the importance of lepton-nucleus interaction studies together with a multitude of both theoretical and numerical techniques required to carry on necessary calculations. Scientific project I have undertaken would not be possible without the support of many people both in the scientific work and everyday life. I would like to thank everybody who helped me in coming this far.

First of all I would like to show my gratitude to my advisor, Prof. Jan Sobczyk, for encouraging me to take the path of neutrino physics and his constant support and guidance since the time of my masters degree studies. Thanks to him I could also meet a lot of interesting scientists, take part in multiple schools and conferences as well as participate in the T2K experiment, which is a very interesting and unusual experience for a theorist like me.

I am grateful to Dr. Krzysztof Graczyk and Dr. Luis Alvarez-Ruso for a long cooperation and many fruitful discussions which helped me solve a lot of problems I have encountered. Here I would like to thank also Prof. Juan Nieves, Prof. Manuel Jose Vicente-Vacas and Dr. Cezary Juszczak for their help.

Great atmosphere at work is also important. For lots of great time I would like to thank my past and present room mates Tomasz Golan, Jakub Jankowski and Łukasz and Sebastian Juchnowski. Their presence always helped to cheer me up. I would also like to thank all the friends from IFIC, whom I did not mention before and all experimentalists (especially the members of Polish Neutrino Groups: Dr. Justyna Łagoda, Dr. Jacek Świerblewski, Dr. Jacek Holeczek), with whom I've spent some wonderful time constructing and taking care of SMRD detector in Japan.

I feel specially grateful to my family, which has shown me support during my physics studies in so many ways I am unable to list them in this short paragraph. Last, but not least, I would like to thank Anna who has brought a lot of joy into my life.

This thesis has been supported by grants 4525/PB/IFT/11 (Polish National Science Cen-

ter UMO-2011/01/N/ST2/03224), 4433/PB/IFT/10 (N N202 368439), 4574/PB/IFT/12 (UMO-2011/01/M/ST2/02578) and 2293/M/IFT/12.

Abstract

This dissertation is devoted to the widely understood topic of lepton-nucleus interactions, which is specially important to neutrino oscillation experiments. We devote the introductory chapters to overview main aspects of neutrino oscillations, lepton-nucleon and lepton-nucleus interaction channels and why it is so important to understand all the dynamical processes behind them. Because of complexity of this problem main focus is given to three of them: quasielastic scattering, single pion production and meson exchange currents, which give rise to most of the neutrino cross sections for energies from $E_\nu \sim 500$ MeV up to $E_\nu \sim 1.2$ GeV. This range is important from the point of view of T2K experiment, in which the author of hereby dissertation participates. All calculations in this dissertation for atomic nuclei are carried out in an unified approach based on effective field theory with hadronic degree of freedom and polarization tensor formalism.

In chapter devoted to the quasielastic process we derive basic formulas for lepton-nucleus scatering and the polarization tensor. We calculate the cross sections for electron scattering in the local and global fermi gas models. We show also how one can derive a spectral function within the polarization tensor formalism. We compare the results for local and global Fermi gas to inclusive electron scattering data. Then we present our results concerning the nucleon axial mass fits to MiniBooNE data using both spectral function and Fermi gas models implemented within NuWro Monte Carlo generator of neutrino interactions. The fitted parameter is very important for understanding of axial part of nucleon weak current. Our main result is that if one treats the MiniBoonE data as coming from a pure quasielastic process, one obtains huge discrepancy with previous axial mass measurements carried out on deuteron target, where one could easily control all nuclear effects. This discrepancy is at the level of over 30% and has statistical significance of over 5 σ (standard deviation). This suggests existence of scattering channels neglected in the MiniBooNE data analysis.

Special attention is paid to pion production on three types of targets: free nucleon, deuteron and atomic nucleus. We investigate different descriptions of Δ resonance, which is a leading contribution to the $\nu_\mu p \to \mu^- p \pi^+$ reaction as well as two nonresonant background models. Comparisons are made both to inclusive electron-proton scattering as well as pion neutrinoproduction off deuteron data. As a result we are able to point out the main differences between considered models with their strong and weak points.
In the next step we investigate in details the impact of nuclear effects on single pion neutrinoproduction cross section. We develop one of the nonresonant background models by giving a prescription how to perform an exact cross section integration on atomic nucleus by using Monte Carlo routines, omitting various approximations used in the literature. An impact of nuclear effects starting with Fermi motion and Pauli exclusion principle and finishing with in-medium modifications of the $\Delta(1232)$ resonance properties are discussed. Dependence of the fraction of $\Delta(1232)$ decays into $np-nh$ states on incident neutrino energy is estimated. It appears to be strongly neutrino energy-dependent, in contradiction to presently assumed constant fraction of 20%, which is used in present neutrino Monte Carlo generators. An impact of various ingredients of the model on a ratio of muon to electron neutrino cross sections is investigated in detail. Our main result is that one can not reproduce the total single pion production cross section published by MiniBooNE within considered models. Second result is that the ratios of muon to electron neutrino cross sections depend only on the introduction of nonresonant background.

Finally, we review the main features of chosen meson exchange current models. We

discuss our implementation of the IFIC model in NuWro Monte Carlo generator of neutrino interactions, general properties of meson exchange current cross sections generated within three models available now within our Monte Carlo as well as our contribution to T2K oscillation analysis. Output of the neutrino energy reconstruction procedure for MEC events is shown. In the last section we show an example calculation of theoretical MEC cross section in the framework of IFIC model and discuss the divergency problem in one of the contributions.

List of publications

- Theoretical papers:
  - C. Juszczak, J.T. Sobczyk, and J. Żmuda, *"Extraction of the axial mass parameter from MiniBooNE neutrino quasielastic double differential cross-section data"*, Phys. Rev. C**82**, 045502 (2010).
  - J. T. Sobczyk. and J. Żmuda, *"On Impact of Nuclear Effects on Weak Pion Production in Sub 1 GeV Energy Region"*, arXiv:1210.6149 [nucl-th], 2012. (accepted for publication in Phys. Rev. C)
- Experimental papers:
  - K. Abe,... J.Żmuda *et al.* [T2K collaboration] *"Indication of Electron Neutrino Appearance from an Accelerator-produced Off-axis Muon Neutrino Beam"*, Phys. Rev. Lett. **107** (2011) 041801 (2011).
  - K. Abe,... J.Żmuda *et al.* [T2K collaboration], *"The T2K Experiment"*, Nucl. Instrum. Meth. A**659** (2011) 106-135 (2011).
  - C. Rubbia,... J.Żmuda *et al.* [ICARUS collaboration], *"Underground operation of the ICARUS T600 LAr-TPC: first results"*, JINST **6** (2011) P07011 (2011).
  - K. Abe,... J.Żmuda *et al.* [T2K collaboration], *"First Muon-Neutrino Disappearance Study with an Off-Axis Beam"*, Phys. Rev. D**85** 031103 (2012).
  - K. Abe,... J.Żmuda *et al.* [T2K collaboration], *"Measurements of the T2K neutrino beam properties using the INGRID on-axis near detector"*, Nucl. Instrum. Meth. A**694**, 211-223 (2012).
  - K. Abe,... J.Żmuda *et al.* [T2K collaboration], *"The T2K Neutrino Flux Prediction"*, Phys. Rev. D**87**, 012001 (2013).
- Proceedings:
  - J. Sobczyk, J. Żmuda, *"On extraction of oscillation parameters"*, CERN Yellow Reports (2010).
  - M. Ziembicki,... J.Żmuda et al., *"The SMRD subdetector at the T2K near detector station"*, Acta Phys. Polon. B**41** (2010) 1579-1584 (2010).
  - J. Żmuda, *"Electron-nucleus scattering process at intermediate energy transfers"*, AIP Conf. Proc. **1405** 33-38 (2011).
  - T. Golan, J. T. Sobczyk and J. Żmuda, *"NuWro: the Wrocław Monte Carlo Generator of Neutrino Interactions"*, Nucl. Phys. B Proc. Suppl. **229-232**, 499 (2012).

List of abbreviations

This is a list of common abbreviations used in this thesis together with the page number, where they first appear.

- ANL: Argonne National Laboratory, pg. 30.
- BNL: Brookhaven National Laboratory, pg. 30.
- CC: charged-current, pg. 1.
- CΔP: crossed Delta pole (current), pg. 81.
- CCQE: charged-current quasielastic, pg. 3.
- CMS: center-of-mass system, pg. 87.
- CNP: crossed nucleon pole (curent), pg. 81.
- CRPA: continuum random phase approximation, pg. 23.
- CT: contact term (current), pg. 81.
- CVC: conserved vector current, pg. 20.
- DIS: deep inelastic scattering, pg. 22.
- ΔP: Delta pole (current), pg. 81.
- EFT: effective field theory, pg. 22.
- F-N: Fogli-Nardulli, pg. 82.
- FG: Fermi gas, pg. 27.
- FSI: final state interactions, pg. 3.
- GR: giant resonances, pg. 22.
- GSL: GNU Scientific Library, pg. 101.
- HNV: Hernandez, Nieves, Valverde, pg. 30.
- IA: impulse approximation, pg. 25.
- IFIC: Instituto di Fisica Corpuscular, pg. 4.
- LDA: local density approximation, pg. 49.
- LFG: local Fermi gas, pg. 34.
- MEC: meson exchange currents, pg. 23.
- MC: Monte Carlo, pg. 3.

- NC: neutral current, pg. 2.
- NP: nucleon pole (current), pg. 81.
- (N)NMBT: (nonrelativistic) nuclear many-body theory, pg. 22.
- PCAC: partially conserved axial current, pg. 21.
- PDD: pionless Delta decay, pg. 29.
- PIF: pion-in-flight (current), pg. 81.
- PP: pion pole (current), pg. 81.
- PWIA: plane wave impulse approximation, pg. 33.
- QCD: quantum chromodynamics, pg. 20.
- QE: quasielastic, pg. 22.
- RDWIA: relativistic distorted wave impulse approximation, pg. 73.
- RFG: relativistic Fermi gas, pg. 23.
- RNMBT: relativistic nuclear many-body theory, pg. 22.
- RPA: random phase approximation, pg. 23.
- RPWIA: relativistic plane wave impulse approximation, pg. 119.
- RS: Rein Sehgal, pg. 30.
- SF: spectral function pg. 23.
- SM: standard model pg. 1.
- SPP: single pion production pg. 23.

Contents

1 Introduction **1**
1.1 Overview and organization of the dissertation chapters 3

2 Neutrino oscillations **7**

3 Interactions of weak and electromagnetic probes **17**
3.1 Weak and electromagnetic interactions of leptons and quarks 17
3.2 Weak and electromagnetic interactions with hadrons 20
3.3 Interactions with atomic nuclei 21
3.4 Main model uncertainties and systematic errors for neutrino energies from 500 to 1200 MeV. 24
3.4.1 Quasielastic scattering 24
3.4.2 Single pion production 28
3.4.3 Meson exchange currents 31
3.5 NuWro Monte Carlo generator of neutrino interactions 36

4 General formalism of lepton-nucleon and lepton-nucleus scattering **37**
4.1 Polarization tensor 41
4.2 Impulse approximation and De Forest prescription 44
4.3 Global and local Fermi gas 46
4.4 Spectral function 57
4.4.1 Nucleon propagator in the NMBT 57
4.4.2 Scalar response of nuclear matter 60
4.4.3 Derivation of the spectral function 63

5 Spectral function and MiniBooNE M_A fits **71**
5.1 M_A fits 71
5.1.1 Definition of χ^2 72
5.1.2 Momentum transfer cut 75
5.1.3 Main result 75
5.2 Conclusions from the MiniBooNE M_A fits 77

6 Single pion production **79**
6.1 General formalism 79
6.1.1 SPP dynamics 81
6.1.2 Resonant process 84
6.1.3 Form factors of the $\Delta(1232)$ resonance 84
6.1.4 $\Delta(1232)$ Width 87
6.1.5 Second resonance region 89
6.2 Integration of the SPP cross section on free nucleons 92
6.2.1 Results for free nucleon: pion electroproduction 94
6.2.2 Results for free nucleon: neutrino bubble chamber experiments 98
6.3 SPP on deuteron: neutrino bubble chamber experiments 99
6.3.1 Summary of SPP on free nucleon and deuteron targets 105
6.4 SPP on atomic nuclei 106
6.4.1 Δ self-energy in nuclear matter 108

6.4.2 Numerical procedures . . . 112
6.4.3 Results . . . 117
6.5 Summary and conclusions from SPP on atomic nuclei . . . 126

7 Meson exchange currents 129
7.1 General idea beyond the chosen MEC models . . . 129
7.1.1 IFIC model . . . 129
7.1.2 Transverse Enhancement Model . . . 130
7.2 NuWro implementation . . . 131
7.3 From SPP to MEC in IFIC model . . . 137

8 Conclusions 143

A Units, physical constants and conventions 147
A.1 Metric and four-vectors . . . 147
A.2 Isospin operators and transitions . . . 148
A.2.1 Nucleons . . . 148
A.2.2 Pions . . . 149
A.2.3 Δ resonance . . . 150
A.2.4 Electromagnetic and weak CC isospin transitions . . . 152
A.3 Free fields . . . 154
A.3.1 Free-pion field . . . 154
A.3.2 Free Dirac fields and Dirac matrices . . . 155
A.4 Free Rarita-Schwinger fields . . . 157

B Neutrino-nucleus cross section derivation 159

C Nucleon propagator in the Fermi gas model 161

D Electron QE cross section from the direct contraction of leptonic and hadronic tensors 165

E Alternative vector and axial form factor sets 169
E.1 Nucleon form factors . . . 169
E.2 Alternative sets of $\Delta(1232)$ form factors . . . 169
E.2.1 Vector form factors . . . 169
E.2.2 Axial form factors . . . 172

F Resonance decay widths 173
F.1 Spin 1/2 resosnace decay . . . 173
F.2 Spin 3/2 resosnace decay . . . 174

G SPP hadronic and leptonic tensors contraction simplification. 177

H Vector current conservation in HNV model 181

I Numerical procedures **183**
I.1 Basic code functionalities for scattering off free nucleon and deuteron 185
I.1.1 Basic functions for scattering off free nucleon 186
I.1.2 Basic functions for scattering off deuteron 187
I.2 Basic code functionalities for scattering off atomic nuclei 187
I.2.1 Basic functions for approximate calculation 187
I.2.2 Basic functions for MC integration 190

J Total SPP cross section tables for ^{12}C **191**

1 Introduction

Main motivation of hereby thesis concerning lepton-nucleus interaction problem lies within neutrino oscillation accelerator experiments. The neutrino physics is one of the most rapidly developing branches of elementary particle physics in the course of past 50 years. Being the lightest and most weakly interacting particles in the present standard model (SM), neutrinos display many surprising properties. One of most known of them is the ability of changing their leptonic flavor during propagation -"oscillation". In the presently used experimental sources neutrinos are always produced in pair with one of the charged leptons: electron, muon or taon. After propagating some distance from their source they may produce a totally different kind of lepton in the charged-current (CC) interaction with the target (assuming their energy to be sufficient to produce an on-shell particle). We believe the source of neutrino oscillation to lie within composite structure of neutrino flavor eigenstates, which in basic theory are unitary combinations of three mass eigenstates. The exact pattern of oscillations is governed by the set of SM parameters, which are being still measured with increasing accuracy by many experimental groups. These parameters are the three neutrino flavor mixing angles: Θ_{23}, Θ_{13} and Θ_{12}, which connect the flavor states to mass eigenstates of neutrinos and the two squared mass differences Δm^2_{12} and Δm^2_{23} together with their signs (mass hierarchy).

Other neutrino properties are still hypothetical, *i. e.* the leptonic CP symmetry violation and non-SM interactions, Majorana nature of neutrinos and sterile (decoupled from the charged lepton sector) neutrino flavors. All of the above mentioned phenomena, with the exception of Majorana neutrino interactions, may be discovered in oscillation experiments.

There are many modern experiments aiming to measure the neutrino oscillation parameters. They can be divided into groups depending on whether they are neutrino appearance/disappearance experiments or according to the neutrino source. The sources are either natural or artificial. We will name only the most popular experiments. Among the natural neutrino sources are the Sun (SNO, Borexino, Super-Kamiokande), collisions of energetic particles with Earth's atmosphere (Super-Kamiokande), cosmological sources (ANTARES, Ice Cube) and Supernovae explosions. The present artificial neutrino sources are the nuclear reactors (Daya Bay, Double Chooz, RENO) and accelerator beams (MiniBooNE, SciBooNE, MINOS, T2K, Opera, ICARUS, NOvA, LBNE).

The first experimental indication of the presence of neutrino oscillations was so-called "solar neutrino problem", resulting from the Homestake Experiment measurement of solar electron neutrino flux (final results in the Ref. [1]). It has shown, that the flux of neutrinos coming from the Sun is much lower, than predicted by any solar model of nuclear synthesis. The only reasonable hypothesis was that the neutrinos have changed their flavor during propagation from the source. This experiment has resulted in a Nobel Prize for R. Davis in 2002. A convincing proof (or, at least, a very strong indication) of the neutrino oscillation phenomenon has been given by the Super-Kamiokande experiment (first evidence in Ref. [2] and oscillation parameter measurement in Ref. [3]). It allowed to check the theoretical prediction of neutrino oscillations against the atmospheric neutrinos propagating along different path lengths deduced from angular correlations between charged lepton appearing in the detector and initial neutrino trajectory. At present there are many more neutrino oscillation experiments running. The T2K experiment, which is one of the core examples in this dissertation, measures the muon neutrino disappearance due to the oscillations. It operates at the baseline of the length of 295 [km], using the beamline in J-PARC as the ν_μ source and Super-

Kamiokande as the far detector. It measures the Θ_{23} and Δm^2_{23}, which are the leading order parameters responsible for the ν_μ oscillations. It was also supposed to answer the question, whether θ_{13} is nonzero by searching for the ν_e appearance. In 2011 T2K has found an electron neutrino appearance signal (Ref. [4]), giving $0.03(0.04) < \sin^2 2\theta_{13} < 0.28(0.34)$ for $\delta_{\rm CP} = 0$ and a normal (inverted) hierarchy. Unfortunately, the statistical significance was only at the level of 2.5σ. These results have been followed in a short period of time by precise reactor experiment measurements made by Daya Bay ($\sin^2 2\theta_{13} = 0.092 \pm 0.016(\text{stat}) \pm 0.005(\text{syst})$ at 5.2σ confidence level, Ref. [5]), RENO ($\sin^2 2\theta_{13} = 0.113 \pm 0.013(\text{stat.}) \pm 0.019(\text{syst.})$ at 4.9σ confidence level, (Ref. [6]) and Double Chooz ($\sin^2 2\theta_{13} = 0.109 \pm 0.030(\text{stat}) \pm 0.025(\text{syst})$ at 2.9σ confidence level, (Ref. [7]). Finally, in Ref. [8] T2K has reported another partial result $\sin^2 2\theta_{13} = 0.088^{+0.049}_{-0.039}(\text{stat} + \text{syst})$ for eleven electron neutrino appearance candidates compared to the previous six. All of these results agree on nonzero θ_{13} and the values agree up to the experimental uncertainties. This was a big success of experimental neutrino physics. Values of θ_{13} as large as those reported by 4 independent experiments open a possibility for δ_{CP} measurements in the future.

The pursue of precision oscillation measurements is motivated by two main questions. The first one concerns possibility of leptonic CP violation, believed to be connected to leptogenesis, which introduced matter-antimatter asymmetry of the Universe. Analogous mechanisms are driven by the CP violation in the quark sector, but it is well known that baryogenesis itself is not able to provide a satisfactory explanation. The second motivation to have as precise oscillation experiments as possible is connected to the question about possible extensions of SM, which include "sterile" neutrino flavors. These hypothetic particles interact differently from the rest of neutrinos. Experimental results from LSND and also MiniBooNE experiments suggest their existence, though their statistical significance is too low to draw any certain conclusions. One of the goals of present T2K experiment is the search of these sterile neutrinos in neutral current (NC) ν_μ interactions.

The new generation of upcoming and presently run neutrino experiments is sensitive to systematic errors. One of the most important sources is the lack of knowledge of precise neutrino cross sections for neutrino energies around 1 GeV. In spite of recent efforts in establishing these cross sections, *e. g.* Refs. [9, 10] the overall uncertainties are still at the level of 20-30%. There are two main sources of our lack of knowledge of these cross sections:

- The poor knowledge of both neutrino flux spectrum and normalization. We still do not have electrically neutral particle monoenergetic sources.
- The interaction with target itself is a complicated problem. Complex structures: nucleons are bound inside another complex structure: the nucleus.

In this thesis we will focus mainly on the interaction problem in the above mentioned 1 GeV neutrino energy region. There are also many experiments dedicated mainly to the problem of neutrino-nucleus interactions (SciBooNE, MINERvA, T2K near ND280 detector). The measured cross section is still carrying large errors. Until very recently there were no available measurements of double-differential neutrino cross sections, but currently we have at least two papers in this topic: [11, 12]. Unfortunately, the data quality will never be as good as for the electron scattering experiments, where one can control both the flux and energy up to very high precision. All nuclear models are thus firstly tested on electron scattering data samples, under the assumption of independence of main nuclear dynamic features under the interchange between weak and electromagnetic interactions. Throughout

this thesis we will also test many effects firstly on electron scattering data samples, where a direct comparison to data is possible.

Typical neutrino beams are wide-band in energy, even the modern off-axis beam used in T2K has a long high-energy tail. One of the basic tools in neutrino oscillation parameter reconstruction experiments is the neutrino energy spectrum analysis (see *e. g.* Ref. [13]). Since neutrinos are never seen directly, one has to rely upon the observed charged lepton kinematics. This can be done with satisfying accuracy only for charged-current quasielastic (CCQE) events, in which neutrinos interact with a single nucleon, leading to its removal from nucleus. For these events the nucleon-at-rest target approximation can be done and a value close to true neutrino energy can be extracted. Other dynamics give largely biased and/or widely spread reconstructed spectrum. These more complicated, than CCQE, processes require knowledge about the hadronic target system excitations. The information about outgoing hadrons is either absent or obscured by the strong final state interactions (FSI). These non-CCQE dynamics can be taken into account only by the means of Monte Carlo (MC) simulations, which take both theoretical calculations as well as independent experimental data (*e. g.* pion-nucleus scattering measurements) as an input. In experimental neutrino physics one expects to get as realistic simulation of event distribution in the detector and its dependence on oscillation parameters as possible, because all uncertainties of numbers of events (thus of the cross sections) coming from each dynamical process contribute to the systematic error of neutrino energy spectrum reconstruction. Other uncertainties coming from non-CCQE channels are connected to the particle identification problem. One of the most important topics is the production and decay of neutral pion π^0, which may mimic the electron neutrino appearance signal in the detector. Another pion-related issue is the misidentification of high-momentum charged pions with muons in water Cherenkov detectors. Both problems are very important to the T2K experiment and put the pion production and propagation in nuclear matter in the center of attention for many research groups. One of the ideas to bypass these problems is to put a near detector by the neutrino source which will both monitor the beam intensity and constrain systematic errors coming from different interaction modes by studying neutrino interactions. This is the case for example in T2K experiment, which has constructed the near ND280 detector almost at the beam source. Nevertheless, simultaneous theoretical studies are required.

From the above mentioned reasons lot of effort is being put into the development of neutrino MC generators, largely by encoding more and more complicated dynamical models, which are expected to give the results as close to reality as possible. The presented studies will be useful for oscillation analysis in T2K experiment, in which the Wroclaw Neutrino Division participates including the author of hereby dissertation.

1.1 Overview and organization of the dissertation chapters

This dissertation aims at being a review of chosen aspects of neutrino physics and interactions of leptons with hadronic and nuclear targets. It's organization concept is to start from an overview most basic ideas of neutrino interactions and physics and then follow through more and more advanced topics of nuclear dynamics, trying to answer questions about basic lepton-nucleus interaction properties. This includes considerations of axial nucleon weak coupling strength and proper treatment of the lightest $\Delta(1232)$ isobar and nonresonant background in single pion production process both on free nucleons as well as various nuclear targets. The latter topic will be given most attention, since pion production dynamics

contribute a major part of the systematic error-producing background in neutrino accelerator experiments with neutrino beam energy centered around 1 GeV (see *e. g.* Ref. [11]). We shall also discuss basic features of the multi-nucleon meson exchange currents and their implementation in Monte Carlo.

This thesis is organized as follows:

Chapter 2 is an overview of the basic physical concepts in neutrino oscillations together with basic ideas in oscillation experiments.

Chapter 3 is devoted to an overview of weak and electromagnetic interactions starting from the lepton and quark currents in the standard model (section 3.1), through the concept of weak charged-current and electromagnetic interactions of hadrons in section 3.2 to the basic overview of possible interaction dynamics with nuclear targets in section 3.3. Section 3.4 introduces the main theoretical and experimental uncertainties in neutrino interaction modes under consideration: quasielastic scattering, single pion production and meson exchange currents. In section 3.5 we make an overview of NuWro neutrino interaction generator, which is used in some of the following analyses.

Chapter 4 gives basic derivations and notions of the formalism used for lepton-nucleus interactions modeling in this thesis. We start from the general overview of one-boson-exchange interaction cross sections, then in section 4.1 we introduce the polarization tensor, which is the main tool in deriving all scattering observables in following chapters. The next section 4.2 will explain the notion of "impulse approximation" and De Forest prescription, which will be commonly referred to. Finally, in sections 4.3 and 4.4 we will discuss the chosen models of the single-nucleon excitation: the global and local Fermi gas and nuclear spectral function. We will show our results of electron quasielastic scattering in local and global Fermi gas models.

Chapter 5 presents our results published in Ref. [14]. It is devoted to the problem of basic axial nucleon coupling and its parameterization confronted to MiniBooNE experiment data. Influence of different dynamical models on this procedure is discussed in details. We show the results of our fits to MiniBooNE data using both Fermi gas and spectral function formalisms.

Chapter 6 concerns the single pion production process. It begins with an introduction to this problem, then starting from section 6.1.1 it gives an overview of chosen pion production models, including two nonresonant backgrounds. In the sections 6.2 and 6.3 we will show our results using these models for lepton scattering off nucleon and deuteron targets together with comparison to pion electro- and neutrinoproduction data from inclusive electron and bubble chamber neutrino scattering experiments. We show the basic differences between these models, nuclear effects of deuteron as well as the impact of different Δresonance axial coupling parameters. Finally, in section 6.4 we shall show our results published in Ref. [15], where we discuss the single pion production process on atomic nuclei with medium modifications of the Δ resonance properties. Our results show the impact of different nuclear model components and details of dynamical model on pion production cross sections.

Chapter 7 gives an overview of the concepts of different meson exchange current models. We show our implementation of IFIC (from Instituto di Fisica Corpuscular in Valencia) model in NuWro and basic results, including the impact on neutrino energy reconstruction procedure and meson exchange current cross sections resulting from different models. This implementation is presently used to produce event samples for T2K oscillation analysis. We finish this chapter with a general scheme showing how to calculate the meson exchange current cross section and outline the biggest computational problems in section 7.3.

Finally, in chapter 8 we will summarize the main outcomes of hereby research.

2 Neutrino oscillations

The neutrinos are very uncanny particles. Besides unimaginably small cross sections and masses they can change their identity- the flavor. Let us perform a gedanken experiment with a source of neutrinos of only one flavor. At the initial point with coordinate $x_0 \equiv (t = 0, \boldsymbol{x} = 0)$ we have an accelerator producing muon neutrinos (ν_μ) in a state $|\nu_\mu(x_0)\rangle$. We let them travel a distance L (all flavor states will be denoted by Greek letters). At the distance L we put a particle detector. Normally one would expect to find only muon

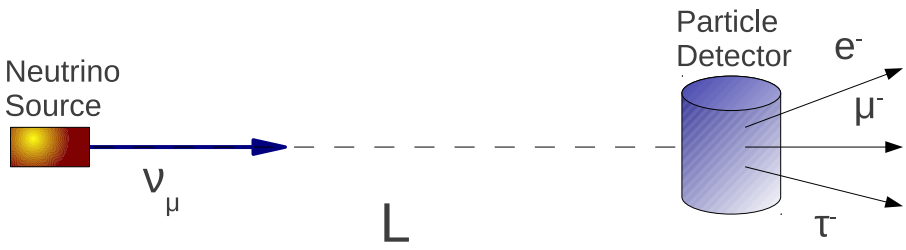

Figure 1: Muon neutrino oscillation experiment.

neutrinos coming from the beam by looking for muons appearing inside of it. But instead we find also other types of leptons (Fig. 1). Electrons and sometimes even taons (if the beam energy is sufficient). This phenomenon is called the "oscillation". It can be explained using the basic principles of quantum mechanics.
For more detailed explanation it is necessary to know the Standard Model of weak and electromagnetic interactions. This model has been developed thanks to Weinberg, Glashow and Salam (Refs. [16, 17, 18, 19, 20]). In SM the lepton masses are generated by the coupling of lepton fields to Higgs field. After the spontaneous gauge symmetry breaking it can appear that the flavor states of quarks and leptons are different from the states with defined masses. This phenomenon is modeled for quarks by the so-called Cabibbo-Kobayashi-Maskawa mixing matrix. Because the quarks are confined, it is impossible to measure their oscillations (at least directly). The neutrinos interact weakly and can propagate freely, thus it is possible to make a direct search for their oscillations. In the following subsection we will discuss the oscillation mechanism very briefly. More detailed discussion on the Standard Model as well as quark and lepton mixings can be found for example in Ref. [21] or Ref. [22].

We would like to prepare the initial neutrino flavor state $|\nu_\alpha(x_0)\rangle$ in such a manner, that the probability of detecting a different state ν_β at coordinates x_1 is nonzero, e.g. $|\langle\nu_\beta(x_1)|\nu_\alpha(x_0)\rangle|^2 \neq 0$. The usual way too meet this goal is to assume all the neutrino *flavor* states are a mixture of different *mass* eigenstates (denoted by Roman letters), rather than pure states:

$$|\nu_\alpha\rangle = \sum_i U^*_{\alpha i} |\nu_i\rangle \tag{2.1}$$

Here it is convenient to explain the meaning of the "mass eigenstate". It is a state, which in the particle rest frame fulfills the following Schrödinger equation:

$$i\frac{\partial}{\partial \tau_i} |\nu_i(\tau_i)\rangle = m_i |\nu_i(\tau_i)\rangle \tag{2.2}$$

with τ_i being the particle's proper time and we are working in a $\hbar = c = 1$ unit system. Thus it is an eigenstate of the Hamiltonian a free particle with mass m_i. the solution to the above equation is:

$$|\nu_i(\tau_i)\rangle = e^{-im_i\tau_i} |\nu_i(0)\rangle \tag{2.3}$$

The reason, why we use the "proper time" will explain itself in a while. Now we need to discuss the mixing matrix properties. If one wants the state orthonormality condition to be fulfilled the mixing matrix $U_{i\alpha}$ can not be completely arbitrary. At the same point of space and time we would like to have:

$$\delta_{\alpha\beta} = \langle \nu_\beta(x)|\nu'_\alpha(x)\rangle = \sum_{i,j} U_{\beta j} U^*_{\alpha i} \langle \nu_j|\nu_i\rangle = \sum_i U^*_{\alpha i} U_{\beta i} = \left(U^\dagger U\right)_{\alpha\beta} \tag{2.4}$$

thus the neutrino mixing matrix has to be unitary[1]. Under the assumption of three lepton flavors and three mass eigenstates, the most general form of the mixing matrix is as follows:

$$U = \begin{pmatrix} U_{e1} & U_{e2} & U_{e3} \\ U_{\mu 1} & U_{\mu 2} & U_{\mu 3} \\ U_{\tau 1} & U_{\tau 2} & U_{\tau 3} \end{pmatrix}. \tag{2.5}$$

Each row contains the information about mass eigenstate contents of given neutrino flavor state. The matrix elements $U_{\alpha i}$ can be complex numbers. The mixing matrix U is unitary $N \times N$ matrix, so it depends upon $N^2 = 9$ independent parameters. This includes $\frac{N(N-1)}{2} = 3$ mixing angles connected to real rotations of neutrino state vector and $\frac{N(N+1)}{2} = 6$ complex phases. Not all phases are physical, all measurable effects occur only in the weak charged current. The exact number of independent parameters depends on whether the neutrinos are Dirac or Majorana particles. This corresponds to the type of lepton mass terms, which enter into the electroweak Lagrangian. We shall discuss this issue only briefly, for more details see *e. g.* Ref. [22]. One can assume, that Higgs multiplets couple to the lepton fields as well. Then the symmetry breaking can give rise to Dirac mass term. It has the following form connecting both left- and right- handed components of fields:

$$\mathcal{L}^D_m = -\overline{l}'_L M'^l l'_R - \overline{\nu}'_L M'^\nu \nu'_R + h.c. \tag{2.6}$$

The mass matrix is, in general, nondiagonal. The fields l' and ν' are defined as:

$$l'_{L/R} \equiv \begin{pmatrix} l'_{e\ L/R} \\ l'_{\mu\ L/R} \\ l'_{\tau\ L/R} \end{pmatrix};\ \nu'_{L/R} \equiv \begin{pmatrix} \nu'_{e\ L/R} \\ \nu'_{\mu\ L/R} \\ \nu'_{\tau\ L/R} \end{pmatrix} \tag{2.7}$$

and they are equivalent to true flavor eigenstates. Furthermore, we have introduced here also the right-handed components of neutrino fields, which are assumed to be sterile (*i. e.* they do not enter into the weak charged current interaction with charged leptons). The mass matrix can be diagonalized using four unitary matrices $V^{l/\nu}_{L/R}$, which act upon the lepton state vectors in following way:

$$V^{l\dagger}_{L/R} l'_{L/R} = l_{L/R} = \begin{pmatrix} l_{e\ L/R} \\ l_{\mu\ L/R} \\ l_{\tau\ L/R} \end{pmatrix};\ V^{\nu\dagger}_{L/R} \nu'_{L/R} = \nu_{L/R} = \begin{pmatrix} \nu_{1\ L/R} \\ \nu_{2\ L/R} \\ \nu_{3\ L/R} \end{pmatrix} \tag{2.8}$$

[1]This is, however, the truth only if there are no more lepton families, than predicted by the Standard Model.

where now $l_{\alpha\ L/R}$,$\alpha = e, \mu, \tau$ are lepton mass eigenstates and $\nu_{k\ L/R}$, $k = 1, 2, 3$ are neutrino mass eigenstates. Under this transformation the Dirac mass Lagrangian becomes:

$$\mathcal{L}_m^D = -\bar{l}_L M^l l_R - \overline{\nu}_L M^\nu \nu_R + h.c. = -\sum_{\alpha=e,\mu,\tau} \bar{l}_{\alpha\ L} m_\alpha l_{\alpha\ R} + \sum_{k=1,2,3} \overline{\nu}_{k\ L} m_k \nu_{k\ R} + h.c. \quad (2.9)$$

We have diagonalized the $M^{l/\nu}$. Kinetic terms of the Lagrangian are invariant under such transformations. We are interested in the weak charged current of leptons:

$$j_{CC}^\mu = 2 \sum_{\alpha=e,\mu\tau} \bar{l}'_{\alpha L} \gamma^\mu \nu'_{\alpha L} = 2\bar{l}_L \gamma^\mu U^* \nu_L;\ U^* = V_L^{l\dagger} V_L^\nu. \quad (2.10)$$

This is the origin of U, the neutrino mixing matrix. It allows us to write the charged current just like in the standard model considerations:

$$j_{CC}^\mu = 2 \sum_{\alpha=e,\mu,\tau} \bar{l}_{\alpha L} \gamma^\mu \nu_{\alpha L}. \quad (2.11)$$

Each lepton field l_α and ν_α carries the lepton number $L_\alpha = +1$, and antilepton fields carry $L_\alpha = -1$. Since neutrinos oscillate only the total lepton number is conserved in SM: $L = L_e + L_\mu + L_\tau$. For the Dirac neutrinos the whole Lagrangian is invariant under global rephasing of lepton fields:

$$\nu_k \to e^{i\phi_k} \nu_k\ (k = 1, 2, 3);\ l_\alpha \to e^{i\phi_\alpha} l_\alpha \quad (2.12)$$

with the exception of charged current piece:

$$j_{CC}^\mu = 2e^{i(\phi_1 - \phi_e)} \sum_{\alpha=e,\mu,\tau} \sum_{k=1,2,3} l_{\alpha L} \gamma^\mu e^{i(\phi_e - \phi_\alpha)} U_{\alpha k}^* e^{i(\phi_k - \phi_1)} \nu_k. \quad (2.13)$$

There are five phases all together, which can be used to eliminate 5 out of 6 phases in the mixing matrix U. Thus the Dirac neutrinos can have only one independent mixing phase.

Now we assume the neutrinos to be Majorana particles:

$$\begin{aligned} \nu &= \nu_L + \nu_L^C \\ \nu &= \nu^C \end{aligned} \quad (2.14)$$

so the neutrino is its own antiparticle. We have introduced C- the charge-conjugation operator. Since $\nu_R = V\overline{\nu}_L^T$ one can construct corresponding mass term:

$$\mathcal{L}_m^M = -\frac{m}{2}(\overline{\nu}_L^C \nu_L + \overline{\nu}_L \nu_L^c) = -\frac{m}{2}\overline{\nu}\nu. \quad (2.15)$$

It clearly leads to the lepton number violation $\Delta L = \pm 2$, so one can expect exotic processes, like the neutrinoless double β-decay, to take place. The advantage is that we have only the left-handed chirality neutrinos. After the diagonalization procedure the neutrino Majorana mass term can be expressed as:

$$\mathcal{L}_m^M = \frac{1}{2} \sum_{k=1}^{3} m_k \nu_{kL}^T C^\dagger \nu_{kL} + h.c. \quad (2.16)$$

It is no longer invariant under the neutrino field rephasing (2.12). Thus Majorana neutrinos mixing has two additional complex phases.

In the three-neutrino flavor and mass state case one can parametrize the mixing matrix in terms of real rotations combined with complex CP-violating phases:

$$
\begin{aligned}
U &= \begin{pmatrix} c_{12}c_{13} & s_{12}c_{13} & s_{13}e^{-i\delta} \\ -s_{12}c_{23} - c_{12}s_{23}s_{13}e^{i\delta} & c_{12}c_{23} - s_{12}s_{23}s_{13}e^{i\delta} & s_{23}c_{13} \\ s_{12}s_{23} - c_{12}c_{23}s_{13}e^{i\delta} & -c_{12}s_{23} - s_{12}c_{23}s_{13}e^{i\delta} & c_{23}c_{13} \end{pmatrix} \times \\
&\times \begin{pmatrix} 1 & 0 & 0 \\ 0 & e^{i\frac{\alpha_{21}}{2}} & 0 \\ 0 & 0 & e^{i\frac{\alpha_{31}}{2}} \end{pmatrix}
\end{aligned} \tag{2.17}
$$

with $c_{ij} = \cos(\theta_{ij})$, $s_{ij} = \sin(\theta_{ij})$ for $\theta_{ij} \in [0, 1]$ and $\delta/\ \alpha_{ij}$ being the Dirac/Majorana CP-violation phases. Together with two squared mass differences, Δm^2_{12} and Δm^2_{23} and mass hierarchy (normal hierarchy if $m_1 < m_2 < m_3$ or inverted hierarchy if $m_3 < m_1 < m_2$) they form a complete information about neutrino oscillation pattern. Good review about the current knowledge of these parameters can be found in Ref. [23], together with description of present oscillation experimental methods.

Let us calculate now the neutrino oscillation probability:

$$
\begin{aligned}
|\langle \nu_\beta(y)|\nu_\alpha(x)\rangle|^2 &= \left|\sum_{i,j} U^*_{\alpha i}U_{j\beta}\,\langle \nu_j(y)|\nu_i(x)\rangle\right|^2 = \left|\sum_{i} U^*_{\alpha i}U_{i\beta}\,\langle \nu_i(y)|\nu_i(x)\rangle\right|^2 = \\
&= \sum_{i,j} U^*_{\alpha i}U_{i\beta}U_{\alpha j}U^*_{j\beta}\,\langle \nu_i(y)|\nu_i(x)\rangle\,\langle \nu_j(y)|\nu_j(x)\rangle^* = \\
&= \sum_i |U_{\alpha i}|^2\,|U_{\beta i}|^2 + \sum_{i\neq j} U^*_{\alpha i}U_{i\beta}U_{\alpha j}U^*_{j\beta}\langle \nu_i(y)|\nu_i(x)\rangle\langle \nu_j(y)|\nu_j(x)\rangle^*.
\end{aligned} \tag{2.18}
$$

What we need now is the neutrino mass eigenstate propagation amplitude. The solution given in Eq. (2.3) will be used to write down the amplitude the particle rest frame:

$$
\langle \nu_i(0)|\nu_i(\tau_i)\rangle \tag{2.19}
$$

A convenient choice of the coordinate system is the one, in which the distance L is taken along the neutrino beam direction, *e. g.* :

$$
m_i\tau_i = E_i t - p_i L \tag{2.20}
$$

for each mass eigenstate i. The desired propagation amplitude will be:

$$
\langle \nu_i(0)|\nu_i(\tau_i)\rangle = e^{-i(E_i t - p_i L)}. \tag{2.21}
$$

The neutrinos produced by a source are coming in wave packets constructed from mass eigenstates, whose propagation is described by the above-mentioned formula. The oscillation phenomenon is described by the interference of propagation amplitudes of different mass eigenstates, as one can see in Eq. (2.18). If we assume, that the neutrino source is constant in time, then we measure something proportional to the time average of the probability formula. Now let us take a look at the time-dependence part:

$$
\left\langle e^{-i(E_i - E_j)t}\right\rangle_t = 0 \tag{2.22}
$$

unless $E_i = E_j$. Following this argument the oscillation should come from mass eigenstates having the same energy (approach by Stodolsky). If all $E_i = E_j$, then the interference terms will become:

$$\langle \nu_i(y)|\nu_i(x)\rangle \langle \nu_j(y)|\nu_j(x)\rangle^* = e^{i(p_i - p_j)L} \tag{2.23}$$

Here we have to make another assumption: the energy of neutrinos is of the order of 10^6 eV (MeV) or grater, thus the particles are ultra-relativistic with their rest mass being of the order of 1 eV. One can then expand the formula connecting relativistic momentum and energy in powers of $\frac{E}{M}$[2]:

$$p_i = \sqrt{E^2 - m_i^2} = E - \frac{m_i^2}{2E} + \mathcal{O}\left(\frac{m_i}{E}\right)^4. \tag{2.24}$$

we have arrived at a point, where it is possible to define the interference terms leading to oscillation probability:

$$|\langle \nu_\beta(y)|\nu_\alpha(x)\rangle|^2 = \sum_i |U_{\alpha i}|^2 |U_{\beta i}|^2 + \sum_{i\neq j} U^*_{\alpha i} U_{i\beta} U_{\alpha j} U^*_{j\beta} \exp(i\frac{(m_j^2 - m_i^2)L}{2E}) \tag{2.25}$$

We arrive at the conclusion, that neutrinos must be massive in order to oscillate. Moreover, at least one of the masses must be different from the others. To make the further discussion more clear some elementary algebra is needed. Let us denote:

$$\Delta m_{ij}^2 \equiv m_i^2 - m_j^2 \tag{2.26}$$

We shall go back into the oscillation probability formula and after some algebraic manipulations and using the mixing matrix unitarity we obtain the final formula:

$$\begin{aligned} |\langle \nu_\beta(y)|\nu_\alpha(x)\rangle|^2 &= \delta_{\alpha\beta} - 4\sum_{i>j} \Re\left[U^*_{\alpha i} U_{\beta i} U_{\alpha j} U^*_{\beta j}\right] \sin^2\left(\frac{\Delta m_{ij}^2 L}{4E}\right) + \\ &+ 2\sum_{i>j} \Im\left[U^*_{\alpha i} U_{\beta i} U_{\alpha j} U^*_{\beta i}\right] \sin\left(\frac{\Delta m_{ij}^2 L}{2E}\right) \end{aligned} \tag{2.27}$$

The above formula has a big advantage over the previous one (2.25). First of all it became apparent, that if $x = y$ there are no oscillations.
Secondly, quantum theories are assumed to be CPT- invariant. Thus one should get the same physics after switching from the particles to antiparticles (C), making a mirror image of the space (P) and reversing the time flow (T). Let us take a look at the anti-neutrino oscillation probability:

$$P\left(\overline{\nu}_\alpha \to \overline{\nu}_\beta\right) \overset{CPT}{=} P\left(\nu_\beta \to \nu_\alpha\right) = P\left(\nu_\alpha \to \nu_\beta, U \to U^*\right) \tag{2.28}$$

Thus:

$$\begin{aligned} P\left(\overline{\nu}_\alpha \to \overline{\nu}_\beta\right) &= \delta_{\alpha\beta} - 4\sum_{i>j} \Re\left[U^*_{\alpha i} U_{\beta i} U_{\alpha j} U^*_{\beta j}\right]^2 \sin\left(\frac{\Delta m_{ij}^2 L}{4E}\right) + \\ &\overset{!!!}{-} 2\sum_{i>j} \Im\left[U^*_{\alpha i} U_{\beta i} U_{\alpha j} U^*_{\beta j}\right] \sin\left(\frac{\Delta m_{ij}^2 L}{2E}\right) \end{aligned} \tag{2.29}$$

[2]The more popular approach, as seen for example in Particle Data Group listings, assumes the mass eigenstates to have the same momenta. The result are the same, but it is harder to show, how to keep the mass states coherent over time.

This means, that if the mixing matrix U is complex, the oscillation probabilities for neutrinos and antineutrinos can[3] be different. This has further, deeper, consequences. It means that in the neutrino physics CP symmetry can be broken. This is a subject of several proposed and ongoing experimental studies. Now we can divide the oscillation probability into two parts:

$$\begin{aligned} P\left(\nu_\alpha/\overline{\nu}_\alpha \to \nu_\beta/\overline{\nu}_\beta\right) &= \underbrace{\delta_{\alpha\beta} - 4\sum_{i>j} \Re\left[U^*_{\alpha i}U_{\beta i}U_{\alpha j}U^*_{\beta j}\right]\sin^2\left(\frac{\Delta m^2_{ij}L}{4E}\right)}_{CP-conserving} + \\ &+/- \underbrace{2\sum_{i>j} \Im\left[U^*_{\alpha i}U_{\beta i}U_{\alpha j}U^*_{\beta j}\right]\sin\left(\frac{\Delta m^2_{ij}L}{2E}\right)}_{CP-violating} \end{aligned} \tag{2.30}$$

From the experimentalists point of view one can detect the neutrino oscillations in two ways:

1. Search for the appearance of $\nu_\alpha \neq \nu_\beta$ from a ν_α source. Done by searching for the charged leptons from CC neutrino interactions. (*appearance* experiment)

2. Search for lacks of known ν_α flux.(*disappearance* experiment)

Both methods require intense neutrino sources, big detectors and lots of time (*weak* interactions). An experimentalist has to know where to put the detector in order to get the best result. After restoring all $\hbar$ and c in the oscillation formula:

$$\frac{\Delta m^2_{ij}L}{4E} = 1.27\Delta m^2_{ij}(eV^2)L(km)/E(GeV) \tag{2.31}$$

The experiments sensitivity to measured $\Delta m^2_{ij}(eV^2)$ is governed by the $\frac{E(GeV)}{L(km)}$ fraction. Because the $\sin\left(\frac{\Delta m^2_{ij}L}{4E}\right)$ has to reach reasonably large values, the approximate experiment sensitivity is given by:

$$\Delta m^2_{ij}(eV^2) \propto \frac{E(GeV)}{L(km)}. \tag{2.32}$$

It is also worthy to mention, that the neutrino oscillation experiments are able only to give the difference between squared masses, not the neutrino masses themselves. An important remark on the CP violation experiments in neutrino sector comes from the fact, that neutrinos usually propagate through matter. Neutrinos and antineutrinos interact differently with the surrounding matter (Fig. 2). The absence of positrons produces a difference between the charged current interactions of neutrinos and antineutrinos, leading to the so-called "matter effect". It produces a fake CP violation pattern. In the figure 3 we have plotted difference between neutrino and antineutrino oscillation caused by the presence of matter at the density of Sun's core. Here a two-neutrino (e and μ) flavor approximation has been used with the squared mass difference $\Delta m^2 = 7.59 \times 10^{-5}$ eV^2 and mixing angle $\sin(2\Theta) = 0.93$. Thus the neutrino experimentalists have to be very careful while planning their experimental setups:

[3]But do not have to, think for example about an overall phase of the type $e^{i\phi}$!

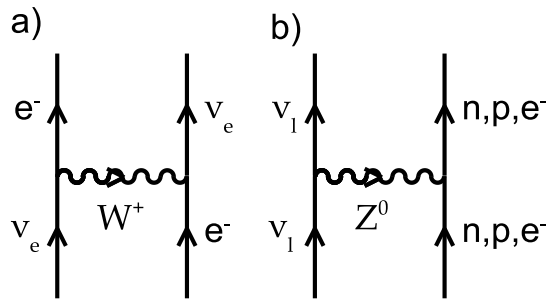

Figure 2: Neutrino interactions, which give rise to the matter potential.

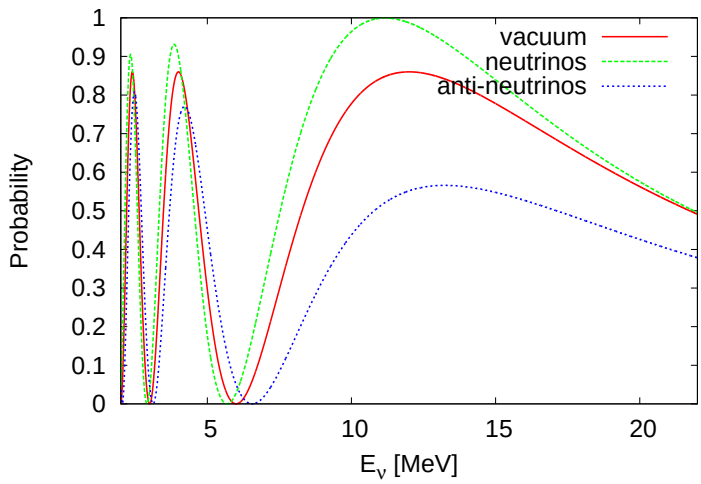

Figure 3: Matter effect example for $(\nu_e \to \nu_\mu)$ and $(\overline{\nu}_e \to \overline{\nu}_\mu)$ as a function of neutrino energy for the two neutrino oscillation case and fixed distance $L \approx 31[km]$ with the matter density of 31 g/cm^3.

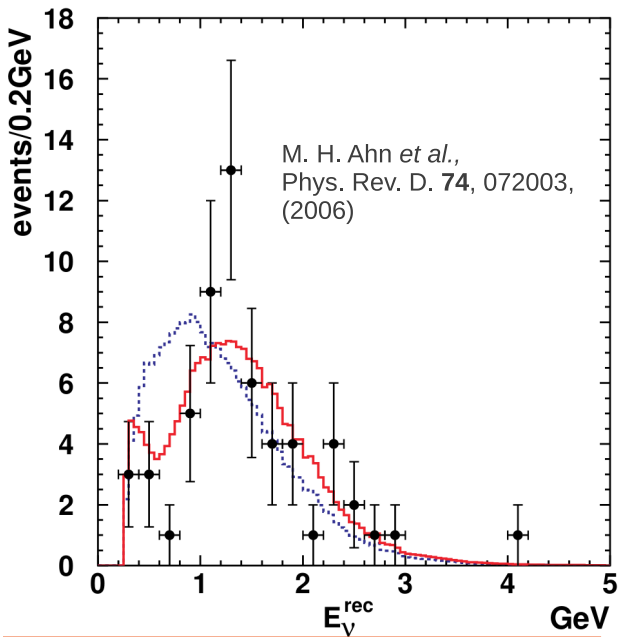

Figure 4: Plot showing the main result from Ref. [13]. The $E_{rec.}$ distribution for event sample containing single muon events. Points with error bars are data. The solid red curve is the best fit spectrum with neutrino oscillation and the dashed blue curve is the expectation without oscillation. These histograms are normalized by the number of single-muon events observed in K2K (58).

not only they must find optimal distance/energy ration but also take multiple effects, like the matter influence, into account.

The true challenge of neutrino oscillation experiments is the measurement itself. Not only we do not know the exact neutrino beam spectrum, but also our knowledge about neutrino interactions within the target is, in the best case, not exactly complete. We want to extract the knowledge about the energy spectrum of neutrinos interacting at the far detector. As mentioned in the introduction, this can not be done directly. Very often one refers to the "reconstructed energy" observable -$E_{rec.}$. It bases only on the outgoing charged lepton kinematics. All complicated nuclear dynamics are neglected and the scattering process is assumed to take place on a single nucleon at rest. Sometimes one adds a small binding energy ϵ_b to the energy balance. Let us assume we want to reconstruct the energy of muon neutrino. There are two observables taken into account: the muon production angle Θ_μ with respect to the neutrino beam direction and the muon energy ε_μ (or, alternatively, its momentum p_μ). The resulting formula is:

$$E_{rec} = \frac{\varepsilon_\mu(M - \epsilon_b) + \frac{1}{2}(2M\epsilon_b - \epsilon_b^2 - m_\mu^2)}{(M - \epsilon_b) - \varepsilon_\mu + p_\mu \cos(\Theta_\mu)}. \tag{2.33}$$

Most valuable results are obtained from this procedure only for CCQE events, which give the reconstructed energy values narrowly peaked around the actual neutrino energy. In disappearance experiments experimentalists are searching for a "dent" in predicted neutrino spectrum without oscillations. By measuring its position and depth one can deduce the values of Δm^2 (dent's position) and mixing angle Θ (dent's depth). Results of such searches are depicted in Fig. 4, which is taken from Ref. [13]. One can see the event distribution in

reconstructed neutrino energy measured by K2K together the predicted distribution without oscillation and with fitted oscillation parameters. Limitations to events with only one muon visible in the final state is done due to higher probability, that they are CCQE in origin. As one can see, the oscillation pattern is clearly visible ("dent" and shift of the spectrum), and the best fit values are $\Delta m^2 = 2.8 \times 10^{-3}$ [eV^2] and $\sin^2(2\Theta) = 1$ in the two-neutrino flavor approximation (μ and τ).

The main question now is: how does one produce predictions of reconstructed energy spectra given by Eq. (2.33)? There are many experimental inputs, such as the beam energy spectrum, which can be measured in the near detector placed by the beam source, high-energy neutrino backgrounds and hardware issues like detector efficiency and resolution. In this dissertation we shall focus on the main theoretical aspect: neutrino-nucleus interactions within the target. All predictions of what we observe in the detector and how it depends on neutrino oscillation parameters, regardless on the chosen observable to be $E_{rec.}$ or single event likelihood or Q^2-distribution, are made using the available MC tools. These tools require our best theoretical knowledge of neutrino interactions available at predicted beam energy range. Otherwise we can not be sure, whether our oscillation effect predictions match what is measured. All uncertainties on CCQE and non-CCQE interaction channels contribute to the systematic errors. Due to low statistics and large statistical uncertainties the discrepancy between MC predictions and data in K2K seems to lie in the range of one standard deviation from most of the measured data points (Fig. 4). Present and future accelerator experiments, like T2K, will have much higher event statistics. Preliminary expectations for the T2K experiment were, that in the far Super-Kamiokande detector one would collect about 1600 ν_μCC events/year if there were no oscillations [24, 25]. In practice, the event rate is calculated with respect to the number of protons delivered on target in the neutrino beam facility (p.o.t.). For the first three runs (with a long break due to March 2011 earthquake) T2K delivered 3.01×10^{20} p.o.t. with expected 200 $\nu_\mu CC$ events with no oscillation. The T2K experiment is expected to run for the next few years with possible beam intensity upgrades. One can compare these numbers and expectations to to total 1×10^{20} p.o.t. delivered in K2K ([13]). Thus the problem of data-MC discrepancies driven by systematic errors becomes even more important. We will discuss some of the main issues of neutrino interaction physics in 1 [GeV] energy range, but first we need to introduce the main neutrino interaction properties on nuclear and subnuclear targets.

3 Interactions of weak and electromagnetic probes

In this section we will focus on the main aspects of weak and electromagnetic probe interactions with nuclear and subnuclear targets. The following paragraph will be devoted to a very brief weak and electromagnetic current description in the Standard Model. More detailed discussion of the electroweak theory containing step-by step derivations, quark mass state mixings, Higgs boson properties etc. can be found *e. g.* in Refs. [21] and [22].

3.1 Weak and electromagnetic interactions of leptons and quarks

From the historical point of view weak interactions have been discovered in the neutron beta-decay process, depicted in Fig. 5. One had to propose an adequate form of Hamiltonian for this process. Weak gauge bosons as well as quarks were unknown at that time. Experiments

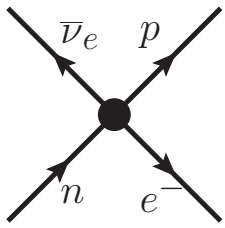

Figure 5: Neutron β-decay before the introduction of quarks and $W^{\pm}$ bosons to theory.

have shown, that observed neutrinos always have left-handed *chirality* [4]. The neutron decay rate has been used to establish weak coupling constant and the fixed neutrino chirality required the neutron decay Hamiltonian to contain parity-breaking terms. Feynman and Gell-Mann in Ref. [26] have proposed its form connecting the left-handed components of fermionic currents (neutron-proton and electron-neutrino):

$$\begin{aligned} \mathcal{H} &= \frac{G_F}{\sqrt{2}} 4\overline{p}_L \gamma_\mu n_L \overline{e}_L \gamma^\mu \nu_{eL} + h.c. \\ &= \frac{G_F}{\sqrt{2}} \overline{p} \gamma_\mu (1-\gamma_5) n \overline{e} \gamma^\mu (1-\gamma_5) \nu_e + h.c. \end{aligned} \tag{3.1}$$

with G_F being the Fermi coupling constant, $n_{(L)}$, $p_{(L)}$, $e_{(l)}$ and $\nu_{e(L)}$ represent the (left-handed) components of Dirac neutron, proton, electron and neutrino fields. The $\frac{1-\gamma_5}{2}$ is the left-handed helicity projection operator. The above Hamiltonian, although successful at low interaction energies, has a few drawbacks. This type of interaction is nonrenormalizable, so one can consider only tree-level processes, like the one in Fig. 5. And since the electromagnetic interaction is carried by a photon, one expected there exists also one responsible for the weak interaction as well.

[4] The chirality should not be confused with helicity. The fixed left-hander/right-handed chirality component of any fermion is constructed by acting with $\frac{1\pm\gamma^5}{2}$ projection operator on the spinor representing the fermionic field. The second one is just a projection of the spin on the direction of movement $\hat{\Sigma}\hat{p}$, $\hat{\Sigma}$ being the spin and $\hat{p}$- momentum operators. Since the neutrinos are massive, the fixed helicity makes no sense: one can always find a rest frame, or a frame, where neutrino moves in the opposite direction, changing the sign of its momentum, but not the third component of spin.

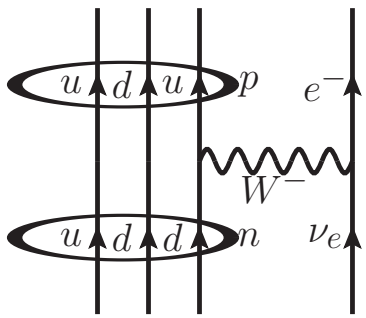

Figure 6: Neutron β-decay after the introduction of quarks and $W^{\pm}$ bosons to theory.

Approximately 10 years later S. Weinberg in Ref. [19] has proposed an unified model of weak and electromagnetic interactions based on spontaneously broken $SU(2) \times U(1)$ symmetry. The charge changing weak interaction connects left-handed components of the local $SU(2)$ symmetry doublets. These contain "up" and "down" types of quarks or charged lepton and corresponding neutrino.

$$\psi_L = \begin{pmatrix} u_L \\ d_L \end{pmatrix} \text{ or } \begin{pmatrix} l_L^- \\ \nu_{lL} \end{pmatrix} \tag{3.2}$$

The right-handed fields enter the Lagrangian as $SU(2)$ singlets. The electromagnetic interaction connects both left- and right-handed fields. Thus one needed to introduce an extra symmetry group $U(1)$ of the hypercharge Y in order to incorporate the electrodynamics as well. The presence of local $SU(2)$ gauge generates current:

$$\boldsymbol{j}^{\mu}(x) = \overline{\psi}_L(x)\gamma^{\mu}\frac{\boldsymbol{\tau}}{2}\psi_L(x). \tag{3.3}$$

In the above equation $\frac{\boldsymbol{\tau}}{2}$ are the isospin-1/2 $SU(2)$ algebra elements. Here we use Pauli matrices, as explained in Appendix A.2.1. The derivative acting on the right-handed components will not be affected. It can be broken to two pieces incorporating the charged current interactions known from β-decays, pion physics or muon decays:

$$j_{\mu}(x) = 2(j_{\mu}^1 + ij_{\mu}^2) = \overline{\psi}_L(x)\gamma_{\mu}(\tau^1 + i\tau^2)\psi_L(x) = \overline{\psi}_L^+(x)\gamma_{\mu}\psi_L^-(x). \tag{3.4}$$

Here ψ_L^+ and ψ_L^- are the upper/lower components of the left-handed isotopic doublets. By "upper components" we mean $\overline{\psi}_L^+ = u_L$ or $\overline{\psi}_L^+ = l_L^-$ and by "lower components" $\overline{\psi}_L^- = d_L$ or $\overline{\psi}_L^- = \nu_L$.
The second part of our current conserves the charge:

$$j_{\mu}^3(x) = \overline{\psi}_L(x)\gamma_{\mu}\frac{1}{2}\tau_3\psi_L(x) = \frac{1}{2}\left(\overline{\psi}_L^+(x)\gamma_{\mu}\psi_L^+(x) - \overline{\psi}_L^-(x)\gamma_{\mu}\psi_L^-(x)\right). \tag{3.5}$$

The $U(1)_Y$ symmetry is connected to the hypercharges of left- and right-handed field components. In order to identify the hypercharges one uses the Gell-Mann-Nishijima relation connecting the isotopic spin I_3 and hypercharge Y to the electric charge Q:

$$Q = I_3 + \frac{1}{2}Y. \tag{3.6}$$

Table 1: Hypercharges

Field	q_L	u_R	d_R	l_L	l_R^-	ν_{lR}
Y	1/3	4/3	-2/3	-1	-2	0

and the phenomenological electric charges: $Q^{up} = \frac{2}{3}$ for the u, c, t quarks, $Q^{down} = -\frac{1}{3}$ for the d, s, b quarks, $Q^{e^-,\mu^-,\tau^-} = -1$ for the charged leptons and $Q^{\nu} = 0$ for all neutrinos. The hypercharges of isodoublets and singlets of fields have been summarized in table 1. The hypercharge symmetry generates another current:

$$j_\mu^Y = Y_L^{doub}\overline{\psi}_L\gamma_\mu\psi_L + Y_R^+\overline{\psi}_R^+\gamma\mu\psi_R^+ + Y_R^-\overline{\psi}_R^-\gamma\mu\psi_R^- \tag{3.7}$$

which is connected to the total electromagnetic current by a relation:

$$j_\mu^{EM} = \frac{1}{2}j_\mu^Y + j_\mu^3. \tag{3.8}$$

After spontaneous symmetry breaking the interaction Lagrangian of SM can be expressed in the terms of physical fields:

$$\mathcal{L}_{I\ SM} = \left(-\frac{g}{2\sqrt{2}}j_\mu^{CC}W^{-\mu} + h.c.\right) - \frac{g}{2\cos\Theta_W}j_\mu^{NC}Z^\mu - ej_\mu^{EM}A^\mu. \tag{3.9}$$

By $W^\pm$ we denote the massive charged W-boson fields, by Z^0 the neutral weak boson field and by A^μ- the photon field. The coupling constant g is the initial $SU(2)$ gauge coupling and e- the electric charge. The Weinberg angle is denoted by Θ_W. The corresponding charged currents are:

$$\begin{aligned} j_\mu^{CC} &= 2\overline{u}_L\gamma_\mu d_L\ (\text{"}up\text{"}\ and\ \text{"}down\text{"}\ quarks) \\ j_\mu^{CC} &= 2\overline{\nu}_{lL}\gamma_\mu l_L\ (neutrinos\ and\ leptons) \end{aligned} \tag{3.10}$$

the electromagnetic currents:

$$\begin{aligned} j_\mu^{EM} &= \sum_{q=u,d,c,s,t,b} e_q\overline{q}\gamma_\mu q\ (\text{"}up\text{"}\ and\ \text{"}down\text{"}\ quarks) \\ j_\mu^{EM} &= -\overline{l}\gamma_\mu l\ (charged\ leptons) \end{aligned} \tag{3.11}$$

with e_q being the quark charge: 2/3 for u, c, t and $-1/3$ for d, s, b. Notice, that the neutrinos, as neutral particles, do not have any electromagnetic interactions. Finally, the neutral current is defined as:

$$j_\mu^{NC} = 2j_\mu^3 - 2\sin^2\Theta_W j_\mu^{EM} \tag{3.12}$$

both for quarks and leptons. Furthermore, the weak charged current can be decomposed into the "vector" and "axial vector" (or axial parts). Starting from Eq. (3.10):

$$j_\mu^{CC} = 2\overline{\psi}_L^+\gamma_\mu\psi_L^- = \overline{\psi}^+(\gamma_\mu - \gamma_\mu\gamma^5)\psi^- = V_\mu - A_\mu. \tag{3.13}$$

With these prescriptions one is capable of calculating all processes concerning the weak and electromagnetic interactions of particles. This includes more detailed picture of neutron decay (Fig. 6) showing transitions between down and up quarks together with a virtual W-boson emission.

3.2 Weak and electromagnetic interactions with hadrons

Throughout this thesis we will always work in the low-energy regime, where the full charged current interaction Lagrangian given by Eq. (3.9) can be successfully replaced by the Fermi contact interaction given by equation similar to Eq. (3.1). However, the general considerations within SM will be useful in justifying the form of electromagnetic and weak interactions with hadrons and nuclei. For example, the proton and neutron masses are almost identical and their electric charges differ by 1. Thus we may consider them to be an isospin doublet, transforming according to the $SU(2)$ symmetry. Historically speaking, the notion of isospin has been first introduced in the nuclear physics, concerning protons and neutrons. Although hadrons are complex structures dressed in the nonperturbative quantum chromodynamics (QCD) effects, they are believed to form the same kind of weak and electromagnetic currents, as leptons and quarks. In this limit one may write down their electromagnetic current as:

$$J^{\mu}_{EM} = \tilde{j}^{\mu}_{3} + \frac{1}{2}\tilde{j}^{\mu}_{Y} \tag{3.14}$$

with first component being the isospin current and the second- the hypercharge current. The tilde sign has been introduced in order to distinguish between the interactions on point-like Dirac particles and complex-structured hadrons. Unfortunately, the theory does not support us with exact calculations of these currents, thus the information about inner hadronic structure is parametrized in the terms of form factors. The most general form of on-shell nucleon electromagnetic current is:

$$\tilde{j}^{N\mu}(q) \;=\; F^{N}_{1}(Q^2)\gamma^{\mu} + \frac{i}{2M}\sigma^{\mu\alpha}q_{\alpha}F^{N}_{2}(Q^2) \tag{3.15}$$

with q^{μ} being the four-momentum transfer, $Q^2 = -q^2$ and F^{N}_{i} being the electromagnetic form factors of nucleon of isospin $N = p, n$. The number of independent electromagnetic form factors for on-shell nucleons is limited to two. This results from application of the Dirac equation and electromagnetic current conservation. The weak charged current of nucleons can be decomposed into the vector and axial parts, as in Eq. (3.13):

$$j^{\mu}_{CCN}(q) \;=\; V^{\mu}(q) - A^{\mu}(q). \tag{3.16}$$

The vector part of the weak charged current can be written analogous to Eq. (3.4):

$$V^{\mu}_{CC} = \tilde{j}^{\mu}_{(v)1} + i\tilde{j}^{\mu}_{(v)2}. \tag{3.17}$$

The general neutral vector current form is more complex from Eq. (3.12) and reads:

$$V^{\mu}_{NC} = (1 - 2\sin^2(\Theta_W))\tilde{j}^{\mu}_{(v)3} - \sin^2(\Theta_W)\tilde{j}^{\mu}_{(v)Y} - \frac{1}{2}\tilde{j}^{\mu}_{(v)s}. \tag{3.18}$$

The last term comes from the strange sea quarks and can be obtained within the limit of the exact $SU(3)$ flavor symmetry limit between u, d and s quarks in QCD and their weak interactions. Moreover, the currents $\tilde{j}^{\mu}_{(v)i}$ are assumed to be identical to the SM isospin current. This is the so-called conserved vector current hypothesis (CVC), which results in the conservation of J^{μ}_{EM} and $V^{\mu}_{CC/NC}$.

The vector part of charged current is expressed through an analogous set of form factors as in the case of electromagnetic current:

$$V^{\mu}(q) \;=\; F_1^V(Q^2)\gamma^{\mu} + \frac{i}{2M}\sigma^{\mu\alpha}q_{\alpha}F_2^V(Q^2) \tag{3.19}$$

with $F_i^V = F_i^p - F_i^n$. Derivation of the relation between weak vector and electromagnetic nucleon form factors can be found in Appendix A.2.4.

For the axial part we use the following prescription:

$$A^{\mu}(q) \;=\; G^A(Q^2)\gamma^{\mu}\gamma^5 + \gamma^5\frac{q^{\mu}}{M}G_P(Q^2). \tag{3.20}$$

In the most simple form of this current one assumes that there are only two axial form factors: pseudovector $G_A(Q^2)$ and pseudoscalar $G_P(Q^2)$. The so-called "second-class currents" connected to tensor axial form factor are neglected. Furthermore, the axial components of weak hadronic currents are conserved only in the limit of zero pion mass. This is the so-called partially conserved axial current (PCAC) hypothesis. Under this assumption, one can relate the pseudoscalar and pseudovector form factors (detailed derivation in *e. g.* Ref. [27], Ch. 42.12):

$$G_P(Q^2) \;=\; \frac{2M^2}{m_{\pi}^2 - q^2}G_A(Q^2). \tag{3.21}$$

After applying the Dirac equation one can simplify the axial current to:

$$A^{\mu}(q) \;=\; G^A(Q^2)\left(\gamma^{\mu}\gamma^5 + \frac{\not{q}}{m_{\pi}^2 - q^2}q^{\mu}\gamma^5\right). \tag{3.22}$$

with only one axial form factor, $G_A(Q^2)$. Whereas it's value for $Q^2 = 0$ is well known from the β-decay experiments, the exact Q^2-dependence is an issue of still ongoing debate. It has a crucial role in all neutrino experiments since it produces the leading contribution to the quasielastic scattering of neutrinos off nucleons. We shall analyze it in more details in the Chapter 5.

PCAC can be also used to connect the value of axial form form factors in the lepton scattering in the limit $q^2 \to 0$ (four-momentum transfer squared) through the so-called Goldberger-Treiman relations, which hold up to a rather small error (see Ref. [28] for the original derivation)

Analogous construction of currents, with the help of CVC and PCAC can be done also in the case of nucleon-resonance transitions. It depends on the exact isospin representation, to which the baryonic resonance corresponds. For example, all charge states of the $\Delta(1232)$ resonance form a multiplet of the isospin-3/2 representation. This procedure allows one to construct the general excitation vertex together with appropriate isospin Clebsch-Gordan coefficients. These coefficients are calculated in the Appendix A.2.4, which gives also the relations between electromagnetic and weak CC resonance form factors.

3.3 Interactions with atomic nuclei

In the case of lepton-nucleus interactions one has to take into account not only the inner hadron structure but also complicated many-body physics of the target system. Dominating phenomena, which occur during such process, are strongly dependent on the interaction

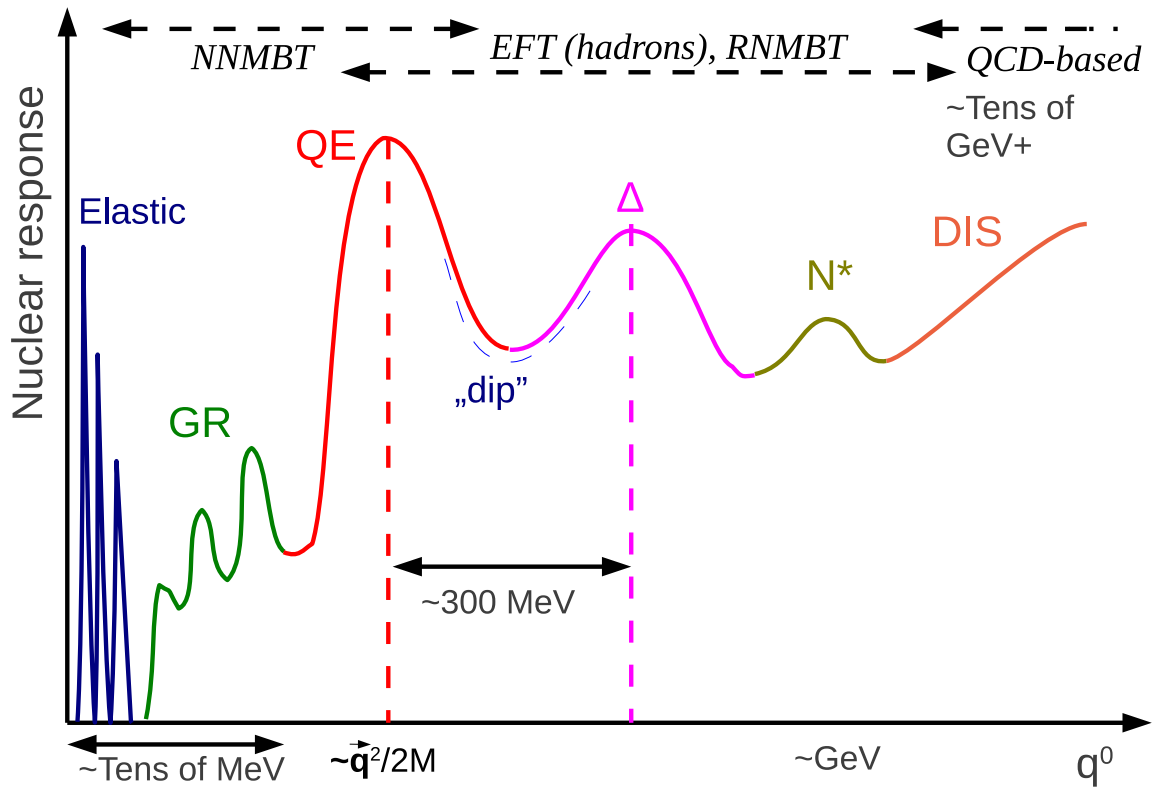

Figure 7: Schematic plot of nuclear response to scattering of an electron probe at different energy transfers q^0. Target response regions from the left: elastic, giant resonances (GR), quasielastic (QE), dip region, Δ-peak, second/heavier resonance region (N^*), deep inelastic scattering (DIS) together with corresponding energy scales and theoretical approaches used in the nuclear phenomena modeling. The latter include nonrelativistic and relativistic nuclear many-body theories (NNMBT/RNMBT), effective field theories (EFT) with hadrons being the degree of freedom and for the highest energies QCD-based theories.

energy scale. These phenomena have been well observed and documented in the case of electron scattering. It is believed, that due to the nature of electromagnetic and weak interactions, connected through the standard model, an analogous picture should appear also for the neutrino scattering. Unfortunately, it is impossible to produce so far a monoenergetic neutrino beam, which would help in high-precision probing of the weak nuclear structure. Even if one would overcome this difficulty, the weak nature of neutrino interactions would require several years of data taking. In the Fig. 7 we have made a schematic plot of nuclear response to leptonic probe as a function of energy transferred to the nuclear system, q^0. Starting from the left and lowest energy transfers of ∼few MeV we see a series of sharp peaks corresponding to elastic scattering, where the probe scatters off the whole nucleus, leaving it an either ground state or exciting single nucleons to discrete excitation levels. When the energy transfer grows to ∼tens of MeV one can produce collective excitation modes of the nucleus called the giant resonances. At slightly bigger energies one reaches the region, where the main part of scattering process can be (in a better or worse approximation) described as an interaction with a single quasifree nucleon, this we call it quasielastic process. It is seen as the so-called quasielastic peak on the plot. The dominating dynamics is described by an excitation of nucleon from the nucleus ground state, which leaves an unoccupied state, the

hole. Thus we usually denote it also as $1p1h$ excitation.
Around 300 MeV to the right one can see another peak. It is formed from the $\Delta(1232)$ resonance excitation (sometimes denoted by Δh). Much broader from QE peak, as Δ is not a stable particle, it is connected strongly to single pion production process (SPP). The pion production may be connected to the nucleus excitation, leading to $npnh1\pi$ (mostly $1p1h1\pi$) final states or it may not lead to any nucleus excitation (coherent process). Between QE and Δ peaks there is a "dip", in which large part of the cross section is believed to come from multinucleon currents driven by meson exchange processes. Hence they are named meson exchange currents (MEC). They excite at least two nucleons from the ground state, leading to $2p2h$, $3p3h$... $npnh$ excitations. The energy transfer region, in which they play important role, is much larger, than just the "dip" region. It is believed to start from the QE peak and go beyond Δ excitation (since Δ decay in nuclear matter may excite $npnh$ states through virtual pion exchange). In general, this phenomenon is very hard to measure, since all hadrons outgoing primary interaction vertices undergo strong FSI, which obscure the initial dynamics. Thus it is easy to misidentify the origin of each recorded event. Moreover, many detectors track only the outgoing charged leptons, giving no or very little information about hadrons. An attempt of measuring MEC events would require at least a very sensitive detector with 4π acceptance for lepton-hadron coincidence.
For higher energy transfers one excites a series of heavier resonances, which form broad peaks due to large overlap in the allowed kinematic excitation and decay regions. Finally, one reaches the DIS region, where the processes take place on quarks, rather than whole hadrons. The exact definition of DIS can be confusing, because in neutrino experiments and MC generators one labels "DIS" all events more inelastic, than SPP.

The lepton-nucleus scattering process is modeled within different formalisms, depending on the energy scale. For elastic and GR regions one has to take into account the discrete excitation levels of a many-hadron system starting from single nucleon excitations, which can be accounted for in a shell model, ending on more complicated many-body excitations with possible nucleon removal in GR region. There one has to use more sophisticated techniques, like different types of (continuum) random phase approximation ((C)RPA). All of them are calculated within nonrelativistic nuclear many body theory, which gives a prescription how to deal with complex interacting systems within quantum mechanics formalism.

Starting from QE peak the relativistic corrections become more and more important, thus one has to switch to effective field theories of hadronic systems, where the main degree of freedom are the nucleons, nucleon resonances and mesons described within relativistic quantum field theory. Many groups uses a simplified picture of the nucleus: relativistic Fermi gas (RFG). Some try to incorporate also various many-body effects in relativistic nuclear many-body theory. An example approach is the relativistic shell model, in which one solves the Dirac equation in a potential well in order to get the single-nucleon wave function set instead of RFG plane waves. Independently, there exist several nonrelativistic model of the $1p1h$ excitations in the QE region, such as the nuclear spectral functions (SF), which account for nucleon short- and long- range correlations basing both on mean-field corrections to their self-energy and on the knowledge of discrete nuclear structure and excitation spectrum.

While moving to higher energy transfers, EFT can describe the SPP and heavier resonance N^* excitation, but at some point it becomes ineffective. It works as long as one can describe all physics using tree-level amplitudes.

Finally, one increases the energy transfer to the point, where only the QCD-based techniques can describe the lepton-nucleus scattering. The interaction takes place basically on

quarks and hadrons production is effectively described by various quark jet hadronization models.

Separate problem arises from the possible modification of hadron properties in the presence of nuclear matter: modification of their masses and basic electromagnetic and weak form factors. Most of the research groups specializing in lepton-nucleus scattering assume, that nucleon and resonance form factors are the same, as in the free case, since there is no way of measuring their modifications inside of the nucleus.

Throughout this thesis the main focus will be given to nuclear dynamics from QE to Δ peaks. This region gives rise to a large fraction of neutrino interactions for the T2K experiment beam energies. Consequently, all systematic errors and nuclear model uncertainties connected to neutrino-nucleus interaction channels in this energy region are of the utter importance for accelerator neutrino oscillation experiments with beam energies peaked around 1 GeV. We shall briefly discuss main problems in the next paragraph.

3.4 Main model uncertainties and systematic errors for neutrino energies from 500 to 1200 MeV.

In the previous sections we have introduced some of the general aspects of lepton-nucleon and lepton-nucleus interactions. There are many unknowns and uncertainties in theoretical models of lepton-nucleus interactions, which are affecting neutrino oscillation parameter measurements in accelerator experiments. Our main example here will be the T2K experiment, whose main concerns and systematic error sources have been pointed out *e. g.* in Ref. [8]. We shall review the dynamical interaction channels, which are subject of this dissertation, together with their main uncertainties and systematic errors, which they introduce in the main example experiment (basing on Ref. [8]). We will also give a more detailed introduction and motivation to the main research topics presented here.

3.4.1 Quasielastic scattering

This is the main dynamical process giving rise to neutrino-nucleus cross section at T2K energies. One assumes the interaction to take place on one of the nucleons inside the nucleus, leading to its excitation. The QE process is ilustated in Fig. 8 assuming the initial nucleon state N can be separated from the rest of nucleus. This assumption is the so-called "impulse approximation". More details on IA are given in section 4.2. The main concerns here are the details of nuclear effect modeling and lacks of knowledge about the nucleon axial current. We shall start our discussion with the latter problem. We assume the weak nucleon vertex to have the on-shell form described by Eqs. (3.19, 3.22). As we have mentioned before, the vector part of nucleon weak charged current is well-established from electron scattering data and CVC. The axial part is rather poorly understood. This is a big hinderance for all neutrino experiments, as the axial nucleon current gives rise to most of the CCQE cross section. Usually one adopts a dipole form of the axial nucleon form factor:

$$G_A(Q^2) \quad = \quad \frac{g_A}{(1+\frac{Q^2}{M_A^2})^2} \tag{3.23}$$

where Q^2 is the squared four-momentum transfer. It's value at $Q^2 = 0$ ($g_A = 1.26\ldots$) has been established by the neutron β-decay experiments, but the exact Q^2-dependence governed by the nucleon axial mass, M_A, is still problematic. The axial mass can change the

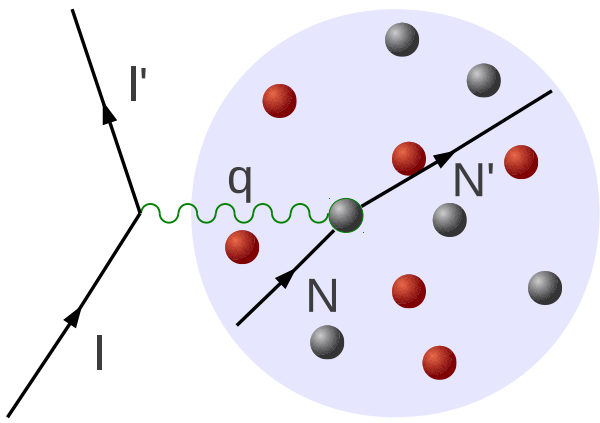

Figure 8: QE scattering process within impulse approximation (IA). Lepton probe with four-momentum l interacts with nucleon state with quantum numbers N by exchanging four-momentum q.

Experiment	Target	Cut in Q^2 [GeV^2]	$M_A GeV$
K2K[30]	oxygen	$Q^2 > 0.2$	1.2 ± 0.12
K2K[31]	carbon	$Q^2 > 0.2$	1.14 ± 0.11
MINOS[32]	iron	no cut	1.19 ± 0.17
MINOS[32]	iron	$Q^2 > 0.2$	1.26 ± 0.17
MiniBooNE[11]	carbon	no cut	1.35 ± 0.17
MiniBooNE[11]	carbon	$Q^2 > 0.25$	1.27 ± 0.14
NOMAD[33]	carbon	no cut	1.07 ± 0.07

Table 2: Recent M_A measurements

limiting value of CCQE cross section as $E_\nu \to \infty$ in a very significant way (shown analytically by A. Ankowski for dipole vector and axial form factors in Ref. [29]). The increase of the value of M_A from 1.03 to 1.35 GeV, the cross section and thus the expected number of CCQE events is raised by around 30%. This is a huge effect. Before the era of accelerator neutrino experiments most of the data about nucleon axial current came from measurements performed mostly on the deuterium target, and seemed to converge to the value of $M_A = 1.03$ GeV. This value is consistent with the weak pion-production measurements at low Q^2 where the PCAC based computations give the value of $M_A = 1.077 \pm 0.039$ GeV. In the first decade of 21st century multiple measurements of axial mass on nuclear targets have

been published by experimental groups (see Tab 2). Their central values are located above the one predicted using PCAC, but large errors seemed to make this deviation insignificant in most of the cases. The biggest controversy came with most recent results. In 2010 the MiniBooNE experiment has released the first measurement of muon neutrino charged current quasielastic double differential cross section in Ref. [11]. It was a very valuable result providing an unprecedented possibility to validate theoretical models. The MiniBooNE collaboration expected the published data to be a pure quasielastic process. They have made a huge effort to subtract from the event sample everything that was expected not to be quasielastic in origin. In the analysis they used NUANCE MC generator based on the Fermi gas model. Assumption was made, that main background source to CCQE process comes from single pion production events, where the pion gets absorbed or escapes detection by other means. They introduced an ad hoc correction function obtained by comparing the SPP events produced by NUANCE to a measured SPP event sample. The physics beyond the shape of this function is rather poorly understood. We shall address this issue in the chapter 6 devoted only to the SPP process on nucleons and atomic nuclei. In the neutrino- nucleus scattering at MiniBooNE energies there are many more possible sources of CCQE measurement errors coming either from the modifications of the CCQE cross section itself, like the spectral function or random phase approximation, or from backgrounds coming from multinucleon processes (*npnh* excitations). They have been disregarded by MiniBooNE, with the exception of simplified pionless Δ decay model implemented in NUANCE, which gives rise to some of the *npnh* excitations. The negligence of *npnh* dynamics in many experiments originates also from experimental limitations, as the scintillator and Cherenkov detectors can "see" hadrons only above Cherenkov kinetic energy threshold, which is higher for nucleons. Thus multinucleon ejection escapes detection in most of the cases. No direct indication of *npnh* neutrino scattering has been reported so far.

Being provided with the data, the authors of Ref. [11] tried to extract the axial mass M_A. They have used the Q^2 differential cross section shape and dipole axial form factor. Shape comparison method has the advantage of being independent on the total neutrino flux. MiniBooNE has obtained results varying from 1.27 ± 0.14 GeV (discarding events with $Q^2 < 0.25$ GeV) up to 1.35 ± 0.17 GeV (no cut). The cut in Q^2 is motivated by the breakdown of impulse approximation in low-Q^2 region (see Ref. [34] for more details) and is used by many experimental groups (see Tab. 2). The values of M_A obtained by MiniBooNE are higher, than the previous measurements on nuclear targets made by different collaborations. The MiniBooNE tried to do the same fit using normalized cross section, with similar result. There has been an attempt of solving the low-Q^2 problem by increasing the Pauli blocking effect by an effective parameter κ, which has been fitted simultaneously with M_A. The effect was negligible, giving κ consistent wit 1 (no modification). Also the MINOS collaboration proposed an ad hoc modification of the Pauli blocking in Ref. [32].

With such big discrepancies coming from different measurements the T2K experiment has decided to assume $M_A = 1.21$ GeV with possible variations in the range ± 0.43 GeV. This gives already a huge uncertainty on CCQE cross section predictions. Furthermore for higher M_A fitted by MiniBooNE the nominal theoretical predictions of Fermi gas model CCQE cross section do not match the high-energy measurements of NOMAD [33]. Assuming, that both experiments have had some problems with overall neutrino flux normalizations and in order to make the MiniBooNE and NOMAD consistent T2K has introduced three (sic!) independent cross section normalization factors for neutrino energies up to 1.5, from 1.5 to 3.5 and above 3.5 GeV. All of them have nominal value of 1, but the predicted error ranges

from 11 to 30%.

Thus the main question is, whether the source of the problems with MiniBooNE M_A and CCQE cross section measurement was lying in the dynamical model. In most of the MC

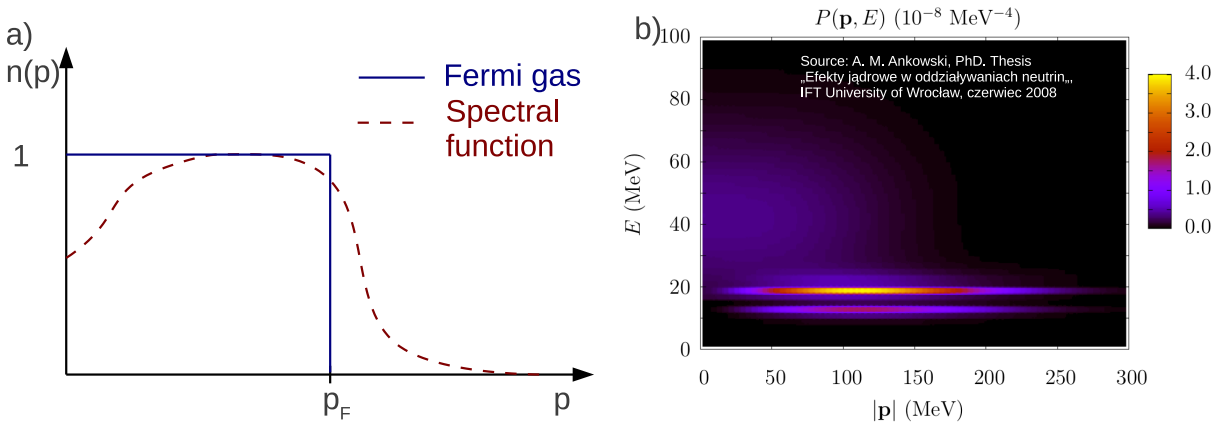

Figure 9: (Left) Schematic plot of initial occupation numbers of nucleon states with given spin and isospin in Fermi gas and spectral function. (Right) Actual spectral function of oxygen as a two-dimensional probability distribution of finding a neutron with removal energy E and momentum p from A. M. Ankowski PhD. thesis [35].

generators one uses the Fermi gas (FG) nucleus model by default. In this model nucleons are treated as a Fermi sea of independent fermions with momentum states filled up to the Fermi level characterized by maximal Fermi momentum p_F. This distribution is shown in Fig. 9 a). All nuclear binding effects are accounted for with an overall binding energy B subtracted from energy transfer. This model is used for example in T2K analysis with allowed uncertainty on Fermi momenta of ^{12}C $p_F = 217 \pm 30$ MeV and ^{16}O $p_F = 225 \pm 30$ (Ref. [8]). Theoretical picture in which the nucleus is treated as an infinite Fermi sea of nucleons is rather oversimplified. Nucleons are strongly correlated and inside the nucleus they form a set of well-distinct energy levels. A step toward more realistic treatment of CCQE process is introduction of the so-called "spectral function". This formalism uses both information from a set of experimental electron scattering data, which gives insight into the nucleon energy level and occupation number distributions as well as theoretical nucleon-nucleon correlation computations to form a probability distribution of finding a nucleon with momentum p and removal energy[5] E inside the nucleus. Detailed calculations can be found in Refs. [36, 37, 38, 39, 40]. Schematic plot of momentum occupation number is shown in Fig. 9 a) and an example two-dimensional neutron SF in Fig. 9 b). A basic derivation of SF can be found in chapter 4.4.

Being provided with implementation of SF in NuWro Monte Carlo generator of neutrino interactions [41, 42, 43] we have performed a fit to MiniBooNE CCQE data in order to check the resulting M_A. The procedure has been described in detail in chapter 5. Our central result, which been published in Ref. [14], shows that both FG and SF give the same answer of $M_A \approx 1350$ MeV. This is a strong indication, that the cross sections published by MiniBooNE are not only from CCQE process and one is missing an important dynamical

[5]Removal energy is defined using final nucleus energy E_{A-1}, nucleon mass M and initial nucleus mass M_A as $E = E_{A-1} + M - M_A$ with A being the target nucleus mass number. In this definition it is a sum of final nucleus mass and kinetic energy.

contribution in present MC generators.

Nevertheless, both SF and FG predict quite different number of CCQE events. MiniBooNE cross section normalizations obtained in our fits [6] from both models exclude each other at more, than 3σ. They also predict slightly different lepton kinematics (an example muon energy distribution change between FG ans SF can be found in Ref. [44]). Thus the T2K collaboration allowed for a smooth shift of lepton kinematics from FG to SF predictions with an extra control parameter x_{SF}, which may vary from 0 to 1. They use the event sets created with NuWro and they are working currently on their own implementation of SF as well.

3.4.2 Single pion production

There has been a lot of effort to understand better single pion production reactions in neutrino-nucleon and neutrino-nucleus scattering. An example process can be seen in Fig. 10. Motivations for SPP studies come from the neutrino oscillation experiments and their demand to reduce systematic errors. In a few GeV energy region characteristic for experiments like T2K, MINOS, NOvA, MiniBooNE and MicroBooNE the SPP channels account for a large fraction of the cross section (at 1 GeV on an isoscalar target about 1/3 of the cross section). For the neutrino energies under consideration SPP events with pions absorbed in nuclei form the biggest fraction of non-CCQE background. Pion absorption due to final state interactions has been discussed in this context in Ref. [45].

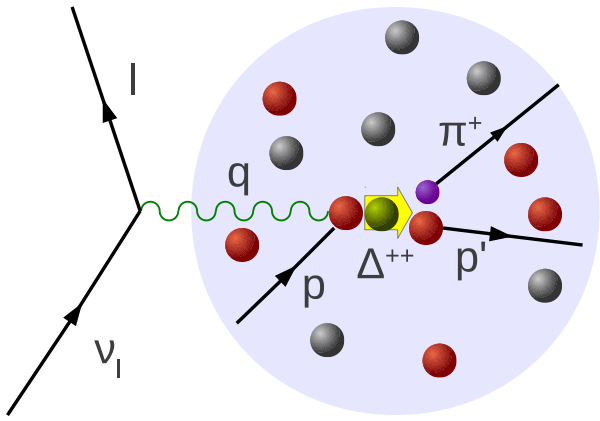

Figure 10: Resonant SPP process on proton in the dominant $\nu_l p \to l^- p \pi^+$ channel.

Another well known instance of the relevance of pion production channels in neutrino oscillation analysis is the neutral current π^0 production. The neutral pions give rise to events which can mimic $\nu_\mu \to \nu_e$ signal. It happens if one of the two photons from the π^0 decay remains undetected and the second one is misidentified as coming from an electron.

In this thesis we focus on neutrino energies below 1 [GeV], where SPP is dominated by the intermediate Δ resonance excitation. There are several challenges in the theoretical description of SPP reactions. The first one comes from uncertainties in the NΔ transition matrix element. The vector part is well-established thanks to photo- and electroproduction experiments, but as precise information on its axial counterpart is still missing. The axial

[6] Fitting procedure has assumed an overall data normalization error coming from MiniBooNE neutrino flux uncertainty, which has been treated as an independent fit parameter.

nucleon-Δ current is dominating in weak SPP cross sections on free nucleons. Because Δ is a spin- isospin-3/2 resonance, description of the axial nucleon-Δ transition requires four form factors (more details in section 6.1.3): C_3^A, C_4^A, C_5^A and C_6^A. All of them can be parameterized in a good approximation as functions of Q^2. Furthermore, usually one assumes $C_3^A \approx 0$ and relates C_6^A and C_4^A to C_5^A using PCAC and other theoretical assumptions. This leaves only one independent form factor $C_5^A(Q^2)$, which determines the axial contribution behavior. Its Q^2-dependence is governed again by "axial mass" parameter, $M_{A\Delta}$, which is a counterpart of nucleon axial mass. It is widely used to fit theoretical predictions to experimental data, like in Ref. [46] or Ref. [47]. Uncertainty on resonant axial mass is also taken into account in the T2K oscillation analysis [8]. We will show the SPP cross section dependence on C_5^A in section 6.3.

Moreover, it turned out, that resonant process alone can describe only the dominant $\nu_l p \to l^- p \pi^+$ channel in a satisfactory way. In order to describe all SPP channels simultaneously one needs to add a nonresonant background amplitudes. Several models of the background in electro- and neutrinoproduction exist (*e. g.* [48, 49, 46, 50, 51]). The first two references ([48, 49]) contain somewhat ad-hoc sets of Born SPP terms, the latter are based on more consistent field-theoretical approaches. Special attention will be given to the chiral model of [46]. Another problem is that the way of describing the Δ resonance propagator and decay vertex differs from model to model. The extracted Δ production form factors also differ with respect to how one defines "Delta" and "background" contributions.

In SPP on atomic nuclei several many-body effects become relevant. The most important nuclear effects going beyond Fermi motion and Pauli blocking are related to Δ in-medium self-energy. Its real part shifts the Δ pole, whereas its imaginary part corresponds to the medium-modified SPP and pionless Delta decay (PDD) processes. The latter process occurs when the resonance is absorbed by a pair of trio of nucleons by virtual meson exchange and gives rise to *npnh* dynamics. The problem of CC SPP on nuclei has been addressed in Refs. [52, 53, 56, 57] assuming Δ dominance model with many-body effects taken from Ref. [58]. The computations have shown a significant reduction of the pion production cross section. The above mentioned calculations did not include a nonresonant background. They lead to the conclusion that a fraction of Δ pionless decays has a rather mild dependence on the incident neutrino energy. Because of these results in some of the widely-used neutrino Monte Carlo generators PDD has been implemented as a constant fraction of about 20% of the total Δ production. This is the case in T2K, which uses NEUT for their analysis [8]. However, in the official analysis there is no *npnh* dynamics yet, thus PDD events are treated only as a modification of SPP in nuclear matter.

Weak single pion production processes are also important for the hadronic physics. They provide a valuable information both on the dynamical structure of the nucleon resonances and nonresonant contributions. This information is complementary to what is known from the electro- and photoproduction studies. This topic was studied in the MAINZ, BONN and TJNAF laboratories. The results give a good insight on the electromagnetic structure of nucleon resonances production, see for example a recent paper on the subject [59] and the underlying unitary isobar model for pion electroproduction [50]. The above mentioned analysis includes also a variety of resonances beyond $\Delta(1232)$. Three of them: $P_{11}(1440)$, $D_{13}(1525)$ and $S_{11}(1535)$ are relevant for the understanding of pion production process in the neutrino experiments like NOvA. We shall discuss their relevance for electron energies above 1 GeV in section 6.2, but for our main study for SPP on atomic nuclei below 1 GeV their contribution will be neglected. Electro- and photoproduction experiments can

also serve as a valuable source of information on final state interactions effects which are universal for all pion production experiments though a number of such studies is limited.

Experimental research of the weak SPP processes is also a remarkable challenge. The models of Δ excitations matrix elements and non-resonant background are still validated mainly on old low statistics bubble chamber experiments held in Argonne National Laboratory (ANL, [60, 61]) and Brookhaven National Laboratory (BNL, [62]). The non-resonant background is more important in two neutrino-neutron SPP channels where the cross sections are smaller than for neutrino-proton SPP reaction and the statistical uncertainties are larger. Recent experimental results on the charge current SPP reactions on atomic nuclei come mainly from the K2K ([63, 64]) and MiniBooNE experiments ([65, 66]). Unfortunately, the analysis of the underlying fundamental physical processes of pion production on nucleons is obscured by nuclear effects. There is an important impact of the nuclear medium on a primary interaction as well as on a redistribution of exclusive channels by FSI. The latter effect is usually divided into pion re-scattering, absorption, charge exchange and production of additional pions (for sufficiently high energies). These nuclear physics uncertainties are so large that MiniBooNE did not attempt to measure the characteristics of neutrino-*nucleon* SPP process and published the cross sections results with all the nuclear effects included (the signal events are those with a single pion leaving a nucleus).

In spite of these drawbacks T2K uses the MiniBooNE data to fine-tune NEUT SPP simulation on atomic nuclei by fitting several parameters ([8]), hoping it will give reasonable results on oxygen target. NEUT models the pion production channels using Rein-Sehgal (RS) model [67] for lepton-nucleon interaction based on the quark FKR model [68]. The RS model is rather outdated and its predictions are known to disagree with the precise experimental data for electron scattering [69]. Unsurprisingly, the required number of fit parameters is large. For the CC SPP process alone there are few independent parameters. First one is the resonance axial mass $M_{A\Delta} = 1.16 \pm 0.11$ GeV. It has been determined with lower accuracy, than in Ref. [47] on deuterium target. Second is the the total cross section normalization factor for neutrino energies below 2.5 GeV, which after the fit has been set to $x_1^{CC1\pi} = 1.63 \pm 0.43$. Such a discrepancy between RS model predictions and data is concerning. On top of that one had to introduce also an energy-dependent tuning in order to bring the calculated SPP cross section energy dependence in agreement with MiniBooNE data. These discrepancies show, that sometimes one lacks almost any predictive power for neutrino-nucleus SPP process and that it is very hard to get physically meaningful results. Thus we shall put a lot of stress on SPP in this dissertation, devoting the whole chapter 6 to it.

Our main goal is to discuss thoroughly theoretical models of pion production used in the current attempts to understand available experimental data. As said before, they should also be used in the estimation of non-CCQE contamination in CCQE-like samples of events allowing for a better insight into the neutrino oscillation phenomenon. In this thesis we focus mostly the model of weak SPP on nucleons based on Ref. [46]. It is often called the HNV model from the names of its creators (Hernandez, Nieves, Valverde). This model contains a nonresonant background based on a consistent effective field theory and thus it seems to be more reliable than the models presented in [49] or [48]. Impact of various ingredients of the model on the final results is discussed in detail. We will discuss a role of the nonresonant background contribution starting from free nucleon targets, through deuterium up to a more "complete" nucleus model based on Ref. [70]. We will also introduce an alternative nonresonant background description based on Fogli-Nardulli paper [48] and

compare it to the HNV results. During the discussion we will show also the impact of alternative Δ resonance excitation vertex and propagator description. For the SPP on atomic nuclei we re-calculate $np - nh$ contribution coming from the pionless Δ decays as well as discuss the simplest nuclear effects: Fermi motion and Pauli blocking. We also give a prescription how to perform cross section integration "exactly", avoiding many not-easy-to-control approximations present in Ref. [70]. Because of availability of large number of electron scattering data, we shall also perform many calculations of electromagnetic SPP processes to check our model predictions with higher accuracy data.

Special attention is given to the ν_μ/ν_e and $\overline{\nu}_\mu/\overline{\nu}_e$ cross section ratios, which can be very important for the $\nu_\mu \to \nu_e$ oscillation signal analysis, *e. g.* Ref. [8].

Final results for charged-current SPP on ^{12}C target are presented in the form of tables of total cross sections for both muon and electron (anti) neutrinos and neutrino energies up to 1 [GeV] in Appendix J. We calculate these cross sections separately with different approximations of nuclear effects and for separate pion charge channels. This format allows for a use in the evaluation of the systematic errors by experimental groups.

3.4.3 Meson exchange currents

Meson exchange currents are a type of nuclear dynamics, where the lepton interacts with more, than one nucleon at once. This is driven by the exchange of virtual mesons, which mediate nuclear forces. A schematic example of MEC process leading to $2p2h$ excitation can be seen in Fig. 11.

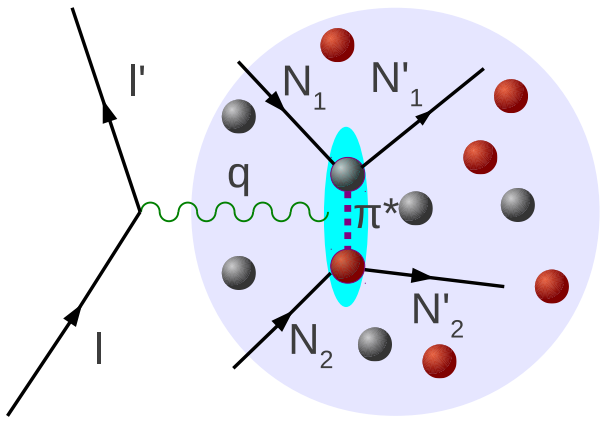

Figure 11: MEC process: interaction on a pair of nucleons correlated by virtual meson exchange (here- π^*).

MEC is under intensive study within the T2K collaboration. A lot of work is done in order to implement this interaction channel in NEUT and to estimate the impact of MEC on neutrino oscillation measurements. We have been asked to produce MEC event samples for T2K using our MC generator, NuWro. More details about this work can be found in chapter 7.

At present none of the detectors is capable to separate MEC events from CCQE-like samples, with the exception of MINERvA experiment. This experiment has recently published first result regarding MEC measurement for neutrino and antineutrino interactions in Refs. [71, 72]. They use extensively the NuWro MC generator of neutrino interactions in their analysis.

Experimentalists have to rely on MC simulations and until very recently, the MEC models were absent in MC generators, save for some simplified pionless Δ decay channels. NuWro was the first neutrino interaction MC generator, which incorporated MEC models in the code. The current works on MEC are motivated by possible neutrino energy reconstruction bias coming from MEC events.

From theoretical point of view the situation of MEC is also complicated. There are many approaches to computation of this contributio to lepton-nucleus cross section, which have been developed during past ~ 50 years. We will give here a historical introduction to the topic.

Problem of many-body nuclear currents has been studied by many research groups for a long period of time. One of the oldest papers in the topic was Ref. [73], where the role of meson-exchange currents in the excitation of nuclear states by electron scattering off carbon was investigated. The one-pion exchange correction to electron scattering form factors has been estimated. It has been found to be small for low values of the momentum transfer, but growing substantially as the transfer increases, even overcoming the contribution of the one-body operators.

Approximately one year later, the same authors have published a paper concerning Meson Exchange Currents effects in nuclear electromagnetic and weak processes [74]. Although it concerned low-energy phenomena of the exchange effect in the isovector and isoscalar magnetic moments of helium and tritium and in the Gamow-Teller matrix element for tritium beta-decay, it introduced quite sophisticated treatment of MEC effects. The one-pion-exchange process has been separated into Born and non-Born parts corresponding to the respective contributions in the process of weak or photoproduction of a pion by the nucleon. Additional corrections coming from dynamical models have been introduced: a phenomenological Lagrangian for the weak current and the Chew-Low model for the electromagnetic current together with the exchange operators due to the exchange of ρ and ω mesons in the vector dominance model.

The next decade has brought a significant development of the electron MEC models. One of the most important results in MEC study has been published by Van Orden and Donnelly in Refs. [75, 76]. The authors have investigated the inelastic electron scattering for energy and momentum transfer regions between QE and $\Delta(1232)$ peaks, basing on the Fermi Gas model of the nucleus. They have found the MEC contribution to be essential in order to understand the nuclear response in the mentioned region. The MEC have been found responsible for the measured cross section between both peaks in the so-called "dip" region, which could not be reproduced by the means of one-body excitation theoretical formalism. Also the missing part of transverse response has been (at least partially) restored by MEC. This was a very important result, indicating importance of the MEC effects in energy region, which is crucial for present neutrino experiments. The model missed the ρ and ω meson contributions present in [74].
This paper has been followed by many more, *e. g.* [77, 78, 79, 80], where the MEC effects have always been found important. In these papers one has also come to better understanding of the impact of nuclear medium effects on MEC, but all of them use Fermi gas model of the nucleus and differ on the total strength of MEC effects.

In the early 1990's researchers have found, that relativistic treatment of electron MEC is crucial and that a very important part comes from the two-body currents mediated through Δ resonance (papers of Dekker *et al.* [81, 82]), which motivated further studies of the Δ in-medium properties. This has been done in Ref. [83], where the Δ-h pair decay into a

$2p2h$ state has been calculated in a fully relativistic manner in infinite nuclear matter (in opposition to the nonrelativistic model of ref. [58]), leading to good agreement with the experimental data. In the same reference authors have gone beyond the usual Fermi gas ground state by evaluating the finite nuclear size effects by calculating realistic baryon density distributions in the nucleus, starting from relativistic mean field nucleon wave functions. In this approximations effects of finite nuclear system size were very moderate.

However, this result is different to what follows more realistic approaches to nuclear ground states. In Ref [84] in which the nuclear response was expressed in terms of the response of deuteron-like pairs of nuclear density, the authors found out that it is important to account in the initial state for the tensor correlations between np pairs. Only when these tensor correlations were included would the two-body terms give appreciable contributions to the quasielastic response. The impact of realistic nucleus model with the presence of nucleon-nucleon correlations on MEC at that time has also been investigated by the authors of Ref. [85]. After studying the two-body contribution to inclusive electron scattering off light nuclei they have obtained results better, than all plane wave impulse approximation (PWIA) computations, which tend to disagree with experimental data, especially for low momentum and energy transfers. Thus the proper treatment of nuclear forces and wave functions seems to play a major role in the understanding of lepton-nucleus scattering. It is worthy to mention here, that the idea of realistic treatment of nucleus in evaluation of MEC effects has already been present in [73].

Another important contribution to the field of MEC in electromagnetic interactions can be found in Ref. [86]. The authors have evaluated the MEC effects starting from model containing a set of pion electroproduction diagrams, which have been tested against experimental data. The paper contains a rich analysis of nuclear medium effects on inclusive electron scattering from QE peak up to Δ peak, including the spectral function and random phase approximation effects both in single nucleon and MEC channels. Another novelty was the introduction of two-pion production process as well as adding $2p2h1\pi$ contribution on top of the existing SPP and MEC diagrams using a consistent framework. They have obtained good agreement with existing inclusive electron data in the impulse approximation applicability regime. In spite of nonrelativistic treatment and Fermi gas vacuum state his is a step toward theory, where SPP and MEC are constructed in an unified way. This may be also an indication, that MEC should be consequently constructed basing on theory, which works in the SPP process.

Within the past $\sim$10 years still a lot of effort has been put in the electron scattering MEC development. Significant effort has been put to models basing on RFG ground state with superscaling [87, 88], although in Ref. [89] it is clearly stated, that realistic treatment of both nucleon wave functions and correlations is necessary to obtain correct two-body current description (at least in the case of light nuclei). Still, both the approaches from Ref. [87, 88] and Ref. [89] are missing tests of underlying meson amplitudes in pion production process, which would make their predictions reliable also in the SPP channel. This would indicate complete consistency of underlying theory.

Throughout past 4 decades many groups have addressed the problem of MEC in electron scattering. Following different approaches and approximations they agreed only in the point, that MEC effects cannot be neglected. The total strength of MEC differs from model to model. From this history it follows, that in order to understand the MEC phenomenon one needs:

- Consistent description of meson production diagrams, which is the starting point of MEC construction.
- Proper treatment of in-medium modifications of nucleon and $\Delta(1232)$ resonance properties.
- Realistic description of many-body nuclear system together with nucleon-nucleon correlations.

Even in the field of electron scattering proper treatment of MEC remains until today an opened question and topic of sophisticated research.

In the case of neutrino scattering there are not as many models and papers on the MEC effects, as in the electron case. Historically, the investigation of the effect was done by Marteau in his PhD thesis and published in Ref. [90]. The model describes neutrino-nucleus interactions from QE to Δ excitation regions. It incorporates many-body RPA correlations. Nuclear response is described by the means of polarization propagator and the whole cross section is parametrized by means of response functions. Nuclear ground state is assumed to be local Fermi gas (LFG). MEC effects are introduced both through pion correlation diagrams and pionless Δ decays parametrized in the form of Δ self-energy (Ref. [58] and nucleon correlation diagrams. The model allows the intermediate pions in RPA series to go on-shell, leading to prediction for coherent pion production. In a later paper [91] Martini, Marteau and others demonstrated, that the MEC is important in understanding of the MiniBooNE muon neutrino CC cross section measurement. Because of the place of origin, we shall call this approach the "Lyon model".

The IFIC group in Ref. [70] has proposed MEC based on HNV SPP model [46]. This work it is a continuation of the idea from [86], but with more relativistic approach to MEC contribution. The HNV model treats pion production amplitudes within a consistent effective field theory. The Valencia group has more MEC amplitudes, than the authors of Ref. [91]. They also base the Δ medium effects on Ref. [58]. Lyon group misses some of the many-body corrections present in [86], as well as the two-pion and $2p2h1\pi$ channels. A deficiency of this approach is the fact, that HNV model does not describe all pion isospin channels equally well and that nuclear effects are treated on the level of LFG. In spite of that, in Ref. [92] this group has performed an axial mass fit to MiniBooNE double-differential CC cross sections, obtaining result in full agreement with the world average of 1.03 GeV. This result is a strong indication, that one needs to incorporate MEC effects in order to understand the neutrino-nucleus scattering process.

Another microscopic model of MEC in neutrino scattering has been proposed in [93]. It includes the same type of MEC amplitudes as [90] and takes RFG as a ground state. They do not include the axial and vector-axial contributions to MEC, which is a drawback with respect to the previously mentioned models. This approach is a continuation of the thirty years old electron MEC papers (Refs. [75, 76]).

There exist also effective MEC models: transverse enhancement model (TEM) from Ref. [94], which parameterizes the MEC effects as a modification of magnetic nucleon form factors and Dytman model, which is developed by experimentalists on purely phenomenological arguments [95]. Both give rather unrealistic predictions for double-differential cross sections for fixed lepton energy, but after integrating over the broad MiniBooNE flux they give reasonable answers.

All of the mentioned models seem to agree more or less with the neutrino scattering cross sections published by MiniBooNE, but they tend to disagree on the size of MEC effects. This is possible, because the MiniBooNE collaboration CCQE measurement has huge errors published without any covariance matrix, which gives the correlations between different data points and their systematic and statistical uncertainties. Thus one can always get a statistically plausible fit even with neutrino interaction models neglecting MEC (this was the case in Ref. [14]). In order to show the discrepancies between different MEC models we compared the cross section per neutron for 1 GeV muon neutrinos scattering off carbon. Biggest value is obtained in Lyon group model [96], 3.73×10^{-39} cm^2, which is 44% compared to quasielastic cross section in that paper. Smaller value has been obtained in IFIC model [97], 2.15×10^{-39} cm^2, which gives roughly 22% ratio to quasielastic channel cross section from that reference. Smaller contribution from MEC is obtained in [98], 1.75×10^{-39} cm^2 20% compared to the QE cross section and in TEM [94], where it is roughly 2×10^{-39} cm^2 on free nucleon target (21% MEC/EL). The latter two models do not have the axial contribution to MEC and [98] does not include MEC in the axial-vector response. Thus it is not surprising, that for antineutrinos the disagreement on the size of MEC effects is even bigger. Authors of [98] obtain in [93] exactly the same value as for neutrinos (lack of the axial-vector MEC responses), but now MEC/QE is roughly 57%, as expected with reduced QE antineutrino cross section. Other models show reduction of the MEC cross section: Lyon model [96] 1.65×10^{-39} cm^2 (60% MEC/QE), IFIC model [99] 0.77×10^{-39} cm^2 (27% MEC/QE) and TEM [94] 0.5×10^{-39} cm^2 (15% MEC/EL). The biggest reduction is seen in the TEM model (factor of 4). It includes vector MEC contribution calculated as an effective parametrization of nucleon magnetic form factors, thus it enters as a part of the vector nucleon current. It does not alter the axial part, but it gives rise to the vector-axial interference with axial nucleon current, which is destructive in the antineutrino case. Difference between Lyon and IFIC results comes from different foundations of MEC diagrams and slightly different treatment of nuclear effects.

We have stated previously, that MEC contribution should be constructed starting from a consistent meson production model. Here we need to stress, that there exist SPP models alternative to HNV model, which is the base for IFIC MEC calculations. Good example can be found in [51], which predicts rather different SPP, than HNV. One can expect, that if one constructs MEC model using as a basis different SPP model, results should differ in a significant manner. This leaves an open path to study correlation between MEC and underlying SPP theory.

In a summary: only one of the above mentioned MEC models tries to construct MEC diagrams basing on a consistent SPP theory and neither of them treats the nucleus in a realistic manner. Their results disagree at large. This leaves the neutrino scattering MEC topic a problem even more opened and interesting for future research, than in the electron scattering case.

Neither of the existing microscopic MEC models can be used for neutrino energies above 1.0-1.5 GeV. Only the effective TEM can give meaningful results above that limit. With increasing energy other physical channels open starting from heavier nucleon resonance and multi-pion production, through contributions from heavier mesons, like vector rho meson, strange particles up to the point, where the hadronic effective field theories fail to describe any physical process. The effective field theory works as long as one can use only tree level amplitudes and can not be extended to large energies, which causes the $\sim$1.5 GeV limitation.

There still exist the problem of nuclear correlation effects in MEC together with realistic

treatment of nucleus wave functions. All of the present neutrino scattering MEC models are based on FG vacuum state. This may lead to unrealistic predictions of MEC effects, as shown in Ref. [85]. The nuclear effects have to be treated beyond the mean-field approximation, otherwise one will most likely not obtain any suitable modifications of the model predictions, as in Ref. [83].

3.5 NuWro Monte Carlo generator of neutrino interactions

For any practical neutrino scattering analysis one needs to have a Monte Carlo simulation. In this thesis we shall use the NuWro MC generator of neutrino interactions, which is an open-source software. It has been developed on Wroclaw University [41, 42, 43] since 2005. We base this chapter on informations from Ref. [100] and our own experience with this code. Currently NuWro is capable of simulating all of the nuclear dynamics required by accelerator oscillation experiments: QE scattering (QEL), single pion production (RES), coherent pion production (COH), meson exchange currents (MEC) and deep inelastic scattering (DIS) both for neutral and charged-current interactions. All of these dynamics can be turned on and off as required by the user. It is capable to cover the neutrino energy range from 100 MeV up to TeV.

Quasielastic scattering is implemented basing on the Llewelyn-Smith formalism [101]. It provides several options for nucleon form factors and dynamical models: local and global relativistic Fermi gas as well as nuclear SF for a series of nuclei (^{12}C, ^{16}O, ^{40}Ar -effective "grid SF", ^{40}Ca, ^{48}Ca, ^{56}Fe). Recently ring random phase approximation [102, 103] has been added on top of the LFG model.

The RES channel describes SPP process dominated by intermediate Δ resonance excitation for hadronic invariant mass $W < 1.6$ GeV, following the model from Ref. [104], different from usual Rein-Sehgal approach [67]. There is also an effective contribution of nonresonant background. It is simulated as a fraction of DIS process for $W \in (1.3, 1.6)$ GeV in a way, which guarantees smooth passage to the DIS channel with growing W.

The coherent pion production (COH) is a process, in which the atomic nucleus is left in its ground state. The NuWro generator uses an implementation of Rein-Sehgal coherent SPP model from Ref. [105].

MEC is the newest channel implemented in NuWro. It is based on the algorithm of nucleon ejection from Ref. [106]. Three MEC models have been implemented. This includes: the Lyon group model [107], the IFIC model [70] and the TEM [94]. In hereby dissertation special attention will be given to the implementation of IFIC model in NuWro.

Deep inelastic scattering in NuWro means more inelastic channels, than SPP. All DIS channel total cross sections are evaluated using Bodek-Yang model [108]. In general, it is used to model cross sections for $W > 1.6$ GeV, but for specific quark configurations hadronization for smaller values of W (down to 1.2 GeV) is modeled with the Pythia6 hadronization routine [109, 42, 110] in order to make a meaningful crossing to the RES region.

All hadrons produced by NuWro are then re-processed by final state interaction algorithm. The FSI model has been also recently developed by implementing the Oset model of effective pion-nucleon interactions [111] and various options of "formation time" (minimal time, after which the newly formed particle can interact). The detailed description of current FSI model can be found in Ref. [100].

On top of the initial and final state interactions NuWro has a large data set of experimental neutrion beams as well as a newly added detector geometry module for realistic experimental events simulations. With all these fits NuWro is becoming a fully-fledged MC event generator ready for use in neutrino experiments. It is available from repository:

`http://borg.ift.uni.wroc.pl/gitweb/?p=nuwro`

The short user's manual can be found in Ref. [43].

4 General formalism of lepton-nucleon and lepton-nucleus scattering

Throughout this thesis we are interested in unpolarized lepton scattering cross sections. The one boson exchange (OBE) approximation is used, *i. e.* the incoming lepton interchanges only one boson with hadronic system. Derivation of scattering cross section for neutrinos can be found in Appendix B. The basic cross-section formula for the electromagnetic or weak charged-current lepton inclusive differential cross section with respect to the final lepton energy E' and solid angle Ω' is:

$$\frac{d^3\sigma}{d\Omega' dE'} = F_l(Q^2)\frac{|\boldsymbol{l'}|}{\sqrt{(l\cdot P_i)^2}}L_{\mu\nu}W^{\mu\nu} \tag{4.1}$$

$$F_l(Q^2) = \begin{cases} \frac{2\alpha^2}{Q^4}, \text{ electrons} \\ \frac{G_F^2\cos^2\theta_C}{4\pi^2}, \text{ neutrinos} \end{cases}$$

$$L_{\mu\nu} = \begin{cases} \frac{1}{4}\mathrm{Tr}\left[(\not{l}' + m_e)\gamma_\mu(\not{l} + m_e)\gamma_\nu\right] \approx l_\mu l'_\nu + l'_\mu l_\nu - g_{\mu\nu}ll', \text{ electrons} \\ \frac{1}{8}\mathrm{Tr}[(\not{l}' + m_x)\gamma_\mu(1\mp\gamma^5)(\not{l} + m_{\nu_x})\gamma_\nu(1\mp\gamma^5)] \approx \\ \approx l_\mu l'_\nu + l'_\mu l_\nu - g_{\mu\nu}ll' \pm i\epsilon_{\mu\nu\alpha\beta}l'^\alpha l^\beta, \text{ neutrinos} \end{cases} \tag{4.2}$$

In the energy regime under consideration one can put $m_e \approx 0$ and $m_{\nu_x} \approx 0$, hence the approximation in the leptonic tensor, $L_{\mu\nu}$. The "+" sign is used for neutrinos and the "−" for antineutrinos. We are assuming the flux of leptons with four-momentum l interacting with hadronic target with four-momentum P_i, hence the $\frac{1}{\sqrt{(l\cdot P_i)^2}}$ factor. Usually the target nucleus is assumed to be at rest and $P_i = (M_i, \mathbf{0})$ with M_i denoting the nucleus mass. As for the couplings, in the case of electromagnetic interactions the fine structure constant is approximately $\alpha = \frac{e^2}{4\pi} \approx \frac{1}{137}$. For the weak interactions the Fermi constant is $G_F = 1.1664 * 10^{-11}/MeV^2$ and the cosine of Cabibbo angle is $\cos(\Theta_C) = 0.974$. Furthermore l^μ and l'^μ denote initial/final lepton four-momenta, $q^2 \equiv -Q^2 = (l - l')^2$ is the squared four-momentum transfer. In the laboratory frame we assume the momentum transfer to be directed along the Z-axis and the scattering to take place in the X-Z plane. The whole dynamical information about nuclear system response is included in nuclear tensor $W^{\mu\nu}$. It

is defined in the following way:

$$
\begin{aligned}
W^{\mu\nu} &\equiv \overline{\sum_i}\sum_f \delta(E_i+q^0-E_f)\Big\langle f\Big|\int d^3x e^{i\boldsymbol{qx}}\hat{J}^\mu(\boldsymbol{x})\Big|i\Big\rangle\Big(\Big\langle f\Big|\int d^3y e^{i\boldsymbol{qy}}\hat{J}^\nu(\boldsymbol{y})\Big|i\Big\rangle\Big)^* E_i = \\
&= (2\pi)^3\Omega\overline{\sum_i}\sum_f \Big\langle f\Big|\hat{J}^\mu(0)\Big|i\Big\rangle\Big(\Big\langle f\Big|\hat{J}^\nu(0)\Big|i\Big\rangle\Big)^* E_i\delta^4(q+P_i-P_f) = \\
&= \Omega\overline{\sum_i}\sum_f \int d^3x e^{\pm i(\boldsymbol{q}+\boldsymbol{P_i}-\boldsymbol{P_f})\boldsymbol{x}}\Big\langle f\Big|\hat{J}^\mu(0)\Big|i\Big\rangle\Big(\Big\langle f\Big|\hat{J}^\nu(0)\Big|i\Big\rangle\Big)^* E_i\delta(E_i+q^0-E_f) \qquad (4.3)
\end{aligned}
$$

with Ω being the nuclear system quantization volume and E_i- the energy of target nucleus. The third line in above equation follows from the Heisenberg equations of motion:

$$\hat{O}(\boldsymbol{x}) = e^{-i\hat{\boldsymbol{p}}\boldsymbol{x}}\hat{O}(0)e^{i\hat{\boldsymbol{p}}\boldsymbol{x}}.$$

and includes manipulations with Dirac/Kronecker delta functions in infinite/finite space: [7]:

$$(2\pi)^3\delta^3(\boldsymbol{q}+\boldsymbol{P_i}-\boldsymbol{P_f}) = \int d^3x e^{\pm i(\boldsymbol{q}+\boldsymbol{P_i}-\boldsymbol{P_f})\boldsymbol{x}} = \lim_{\Omega\to\infty}\Omega\delta_{\boldsymbol{q}+\boldsymbol{P_i},\boldsymbol{P_f}}. \qquad (4.4)$$

The form of nuclear tensor starting in second line of Eq. (4.3) is less general because it assumes $|i\rangle$, $|f\rangle$ to be momentum eigenstates.

Rosenbluth separation in electron scattering

Many physical observables in electron scattering can be obtained by extracting the separate "longitudinal" and "transverse" responses of nuclear system. One of the cases is the extraction of magnetic nucleon form factor. The procedure of separation of nuclear system responses has been introduced by Rosenbluth in Ref. [112]. Here we will do a quick calculation to demonstrate how it works. The hadronic tensor must be built from the Lorentz vectors which are at our disposal. It can be shown, that the general form of the current conserving

$$q_\mu W^{\mu\nu} = q_\nu W^{\mu\nu} = 0 \qquad (4.5)$$

nuclear tensor is:

$$W^{\mu\nu} = W_1(q^2, q\cdot P_i)\left(\frac{q^\mu q^\nu}{q_\mu^2} - g^{\mu\nu}\right) + \frac{W_2(q^2, q\cdot P_i)}{M_i^2}\left(P_i^\mu - \frac{P_i\cdot q}{q_\mu^2}q^\mu\right)\left(P_i^\nu - \frac{P_i\cdot q}{q_\mu^2}q^\nu\right). \qquad (4.6)$$

The scalar functions W_1 and W_2 are called *structure functions* and there are only two of them in the electromagnetic scattering processes. They are functions of two arguments.

We will contract the leptonic and nuclear tensors in order to find a most general formula for the cross section. In the computations we use the fact that also the leptonic tensor satisfies:

[7] The Fourier transformation for nuclear current may be confusing, normally $f(q) = \int d^4x f(x)e^{iqx}$ with (+,-,-,-) metric. The sign switch happens due to the definition of physical momentum transfer $q = l - l' = P_f - P_i$ and the 4-momentum conservation, hence the nuclear and leptonic currents will have different signs of q in the exponential.

$$q_\mu L^{\mu\nu} = q_\nu L^{\mu\nu} = 0. \tag{4.7}$$

Thus the contraction of electromagnetic leptonic and nuclear tensors will be:

$$\begin{aligned} L_{\mu\nu}W^{\mu\nu} &= \left(l_\mu l'_\nu + l'_\mu l_\nu - g_{\mu\nu} l\cdot l'\right)\left[W_1\left(\frac{q^\mu q^\nu}{q_\mu^2} - g^{\mu\nu}\right) + \frac{W_2}{M_i^2}\left(P_i^\mu - \frac{P_i\cdot q}{q_\mu^2}q^\mu\right)\left(P_i^\nu - \frac{P_i\cdot q}{q_\mu^2}q^\nu\right)\right] = \\ &= 2W_1 l\cdot l' + \frac{W_2}{M_i^2}\left(2(l\cdot P_i)(l'\cdot P_i) - P_i^2(l\cdot l')\right). \end{aligned} \tag{4.8}$$

For this scattering process we can express $l\cdot l'$ in the ultrarelativistic approximation:

$$\begin{aligned} l\cdot l' &= E(\boldsymbol{l})E(\boldsymbol{l'}) - \boldsymbol{l}\boldsymbol{l'} \approx E(\boldsymbol{l})E(\boldsymbol{l'}) - E(\boldsymbol{l})E(\boldsymbol{l'})\cos(\Theta) = \\ &= 2E(\boldsymbol{l})E(\boldsymbol{l'})\sin^2\left(\frac{\Theta}{2}\right) \end{aligned} \tag{4.9}$$

with Θ being the laboratory frame scattering angle.

$$L_{\mu\nu}W^{\mu\nu} = 4W_1 E(\boldsymbol{l})E(\boldsymbol{l'})\sin^2\left(\frac{\Theta}{2}\right) + 2W_2 E(\boldsymbol{l})E(\boldsymbol{l'})\cos^2\left(\frac{\Theta}{2}\right). \tag{4.10}$$

We insert this result into the cross section formula. Further simplification comes from expressing the formulas in the laboratory frame of resting nucleus ($P_i^\mu = (M_i, \mathbf{0})$).:

$$\begin{aligned} d\sigma &= \frac{4\alpha^2}{q_\mu^4}\frac{d^3 l'}{2E(\boldsymbol{l'})}\frac{1}{\sqrt{(l\cdot p_i)^2}}\left[4W_1 E(\boldsymbol{l})E(\boldsymbol{l'})\sin^2\left(\frac{\Theta}{2}\right) + 2W_2 E(\boldsymbol{l})E(\boldsymbol{l'})\cos^2\left(\frac{\Theta}{2}\right)\right] = \\ &= \frac{4\alpha^2}{q_\mu^4}\frac{\boldsymbol{l'}^2 dl' d\Omega}{2E(\boldsymbol{l'})}\frac{1}{E(\boldsymbol{l})M_i}\left[4W_1 E(\boldsymbol{l})E(\boldsymbol{l'})\sin^2\left(\frac{\Theta}{2}\right) + 2W_2 E(\boldsymbol{l})E(\boldsymbol{l'})\cos^2\left(\frac{\Theta}{2}\right)\right]. \end{aligned} \tag{4.11}$$

Because

$$dl' = \frac{dl'}{dE(\boldsymbol{l'})}dE(\boldsymbol{l'}) = \frac{E(\boldsymbol{l'})}{l'}dE(\boldsymbol{l'}) \approx dE(\boldsymbol{l'}) \tag{4.12}$$

we can rewrite the cross section formula, as:

$$d\sigma = \frac{4\alpha^2}{q_\mu^4 M_i}E(\boldsymbol{l'})^2 dE(\boldsymbol{l'})d\Omega'\left[2W_1\sin^2\left(\frac{\Theta}{2}\right) + W_2\cos^2\left(\frac{\Theta}{2}\right)\right]. \tag{4.13}$$

The laboratory frame 4-momentum transfer can also be expressed in the energy and angle variables:

$$\begin{aligned} q_\mu^2 &= (l-l')_\mu(l-l')^\mu = E(\boldsymbol{l})^2 + E(\boldsymbol{l'})^2 - 2E(\boldsymbol{l})E(\boldsymbol{l'}) - \boldsymbol{l}^2 - \boldsymbol{l'}^2 + 2|\boldsymbol{l}||\boldsymbol{l'}|\cos(\Theta) = \\ &= -4E(\boldsymbol{l})E(\boldsymbol{l'})\sin^2\left(\frac{\Theta}{2}\right). \end{aligned} \tag{4.14}$$

It will further simplify the cross section formula:

$$\begin{aligned} \frac{d\sigma}{dE(\boldsymbol{l'})d\Omega'} &= \frac{\alpha^2\cos^2\left(\frac{\Theta}{2}\right)}{4E(\boldsymbol{l})^2 M_i\sin^4\left(\frac{\Theta}{2}\right)}\left[2W_1\,\mathrm{tg}^2\left(\frac{\Theta}{2}\right) + W_2\right] = \\ &= \frac{\sigma_M}{M_i}\left[2W_1\,\mathrm{tg}^2\left(\frac{\Theta}{2}\right) + W_2\right]. \end{aligned} \tag{4.15}$$

In the above formula we have extracted the classical Mott scattering cross section:

$$\sigma_M = \frac{\alpha^2 \cos^2\left(\frac{\Theta}{2}\right)}{4E(\boldsymbol{l})^2 \sin^4\left(\frac{\Theta}{2}\right)}. \tag{4.16}$$

Eq. (4.15) represents the most general form for the inclusive electron-nucleus cross section. We need a nuclear model in order to evaluate W_j.

An important observation is that we need not to know all the components of $W^{\mu\nu}$. In fact, we see from the above expression that only two combinations of them enter the inclusive cross section formula. We have assumed that the 4-momentum transfer in LAB frame is:

$$q^\mu = (q^0, 0, 0, q). \tag{4.17}$$

We introduce an orthonormal set of three 4-vectors which are perpendicular to the 4-momentum transfer:

$$\begin{aligned} x_s^\mu &= \frac{1}{\sqrt{Q^2}}(q, 0, 0, q^0) \\ x_1^\mu &= (0, 1, 0, 0) \\ x_2^\mu &= (0, 0, 1, 0). \end{aligned} \tag{4.18}$$

This choice is rather unusual, because in most of the cases one chooses the polarization vectors of gauge boson:

$$\begin{aligned} x_l^\mu &= \frac{1}{\sqrt{Q^2}}(q, 0, 0, q^0) \\ x_+^\mu &= -\frac{1}{\sqrt{2}}(0, 1, i, 0) \\ x_-^\mu &= \frac{1}{\sqrt{2}}(0, 1, -i, 0). \end{aligned} \tag{4.19}$$

which gives an immediate answer to the definitions of "longitudinal" and "transverse" as response functions to the longitudinal and transverse modes of gauge boson. However, as long the set is orthonormal and one of the vectors corresponds to longitudinal polarization (as does x_s^μ), the choice of transverse basis representation for transverse response separation is completely arbitrary. It would make a difference *e. g.* with polarized cross section and helicity amplitude measurements, where it is necessary to separate the left- and right- handed transverse boson polarization modes. We contract the 4-vectors from Eq. (4.18) with the formula which expresses $W^{\mu\nu}$ in terms of W_j:

$$\begin{aligned} x_{s\mu}x_{s\nu}W^{\mu\nu} &= [q^2W^{00} + q_0^2W^{33} - q^0q(W^{30} + W^{03})]/Q^2 = \\ &= [(q_0^2 - q^2)W_1 + q^2W_2]/Q^2 \\ x_{1\mu}x_{1\nu}W^{\mu\nu} &= W_1(-x_{1\mu}x_1^\mu) = W_1 = W_{11} \\ x_{2\mu}x_{2\nu}W^{\mu\nu} &= W_1(-x_{2\mu}x_2^\mu) = W_1 = W_{22} \\ 0 &= q_\mu W^{\mu 0} = q^0W^{00} - qW^{03} = q^0W^{00} - qW^{30} \\ 0 &= q_\mu W^{\mu 3} = q^0W^{03} - qW^{33} \\ 0 &= q_\mu W^{\mu 1} = q^0W^{01} - qW^{31} \\ 0 &= q_\mu W^{\mu 2} = q^0W^{02} - qW^{32}. \end{aligned} \tag{4.20}$$

They are only diagonal elements of $W^{\mu\nu}$ which matter. Moreover:

$$W^{33} = \frac{q_0^2}{q^2} W^{00}. \tag{4.21}$$

We find

$$(q^2 - q_0^2)W^{00} + (q_0^2 - q^2)\frac{q_0^2}{q^2}W^{00} = \frac{q_\mu^4}{q^2}W^{00} = (q_0^2 - q^2)W_1 + q^2 W_2 \tag{4.22}$$

and the result is:

$$\begin{aligned} W_1 &= W^{11} = W^{22} = \frac{1}{2}(W^{11} + W^{22}) \equiv \frac{1}{2}R_T \\ W_2 &= \frac{Q^4}{q^4}W^{00} + \frac{Q^2}{q^2}W_1 = \frac{Q^4}{q^4}W^{00} + \frac{Q^2}{q^2}\frac{1}{2}(W^{11} + W^{22}) \equiv .\frac{Q^4}{q^4}R_L + \frac{1}{2}\frac{Q^2}{q^2}R_T. \end{aligned} \tag{4.23}$$

The chosen combinations of the hadronic tensor can be used in the final expression for the inclusive cross section:

$$\begin{aligned} \frac{d\sigma}{dE(\boldsymbol{k'})d\Omega'} &= \frac{\sigma_M}{M_i}\left[2W^{11}\,\mathrm{tg}^2\left(\frac{\Theta}{2}\right) + \frac{Q^4}{q^4}W^{00} - \frac{Q^2}{q^2}W^{11}\right] = \\ &= \frac{\sigma_M}{M_i}\left[R_T\left(\mathrm{tg}^2\left(\frac{\Theta}{2}\right) + \frac{1}{2}\frac{Q^2}{q^2}\right) + \frac{Q^4}{q^4}R_L\right]. \end{aligned} \tag{4.24}$$

The above expression corresponds to the so-called "Rosenbluth separation" to longitudinal and transverse nuclear system responses. It has been named after the author of Ref. [112].

4.1 Polarization tensor

In order to introduce the polarization tensor formalism the following distribution property is needed:

$$\frac{1}{x \pm i\varepsilon} = \mathcal{P}_{\frac{1}{x}} \mp i\pi\delta(x); \qquad \delta(x) = \mp\frac{1}{\pi}\Im\frac{1}{x \pm i\varepsilon}. \tag{4.25}$$

By applying it to Eq. (4.3) we obtain

$$\begin{aligned} L_{\mu\nu}W^{\mu\nu} &= -\frac{1}{\pi}L_{\mu\nu}\overline{\sum_i}\sum_f\int d^3x e^{-i(\boldsymbol{q}+\boldsymbol{P_i}-\boldsymbol{P_f})\boldsymbol{x}}\left\langle f\left|\hat{J}^\mu(0)\right|i\right\rangle\left(\left\langle f\left|\hat{J}^\nu(0)\right|i\right\rangle\right)^* \\ &\quad \Im\left(\frac{1}{q^0+E_i-E_f+i\varepsilon}\right)\Omega E_i = \\ &= -\frac{1}{\pi}\Im\left(L_{\mu\nu}\overline{\sum_i}\sum_f\int d^3x e^{-i(\boldsymbol{q}+\boldsymbol{P_i}-\boldsymbol{P_f})\boldsymbol{x}}\frac{\left\langle f\left|\hat{J}^\mu(0)\right|i\right\rangle\left(\left\langle f\left|\hat{J}^\nu(0)\right|i\right\rangle\right)^*}{q^0+E_i-E_f+i\varepsilon}\Omega E_i\right). \end{aligned} \tag{4.26}$$

Notice, that we need to work with the full contraction of $L_{\mu\nu}W^{\mu\nu}$. This happens due to the fact, that for the weak processes both $L^{\mu\nu}$ and $W^{\mu\nu}$ are complex. Using the argument, that

the cross section should be a real number and that the imaginary part of leptonic tensor is antisymmetric, one can write down the general decomposition of these tensors:

$$\begin{aligned} L_{\mu\nu} &= L^S_{\mu\nu} + iL^A_{\mu\nu} \\ W_{\mu\nu} &= W^S_{\mu\nu} + iW^A_{\mu\nu} \end{aligned} \tag{4.27}$$

where the "S" and "A" indices refer to real symmetric/antisymmetric components of he tensors. The contraction of both is always real. Since we will have to extract the imaginary parts coming from the poles inside nuclear tensor, we need to do all following manipulations either with $L_{\mu\nu}W^{\mu\nu}$ or separately with symmetric and antisymmetric parts of $W^{\mu\nu}$. We choose the first option. We introduce $\tilde{L}_{\mu\nu}\tilde{W}^{\mu\nu}$ such that $\tilde{L}_{\mu\nu}\tilde{W}^{\mu\nu} = L_{\mu\nu}W^{\mu\nu}$ as long as $q^0 > 0$. This condition is met when we add/subtract to $L_{\mu\nu}W^{\mu\nu}$ an expression, which has pole at a point different from $q^0 + E_i = E_f$. Because the final goal is to have time-ordered operators in the cross section expression the additional term should describe processes with different direction of the time flow, thus with $q^\mu \to -q^\mu$. For the leptonic tensor it is readily done by substituting $L_{\mu\nu} \to L_{\mu\nu}(l \leftrightarrow l') = L_{\nu\mu}$. For the whole contraction one has to add a term:

$$\begin{aligned} &L_{\nu\mu}W^{\mu\nu}(P_i, -q) = \\ &= L_{\nu\mu}\overline{\sum_i}\sum_f \delta(E_f+q^0-E_i)\left\langle f \left| \int d^3x e^{-i\boldsymbol{qx}}\hat{J}^\mu(\boldsymbol{x}) \right| i \right\rangle \left(\left\langle f \left| \int d^3y e^{-i\boldsymbol{qy}}\hat{J}^\nu(\boldsymbol{y}) \right| i \right\rangle\right)^* E_i = \\ &= \frac{1}{\pi}\Im\left(L_{\nu\mu}\Omega\overline{\sum_i}\sum_f \int d^3x e^{-i(\boldsymbol{q}+\boldsymbol{P_f}-\boldsymbol{P_i})\boldsymbol{x}} \frac{\left\langle i \left| \hat{J}^\nu(0) \right| f \right\rangle \left(\left\langle i \left| \hat{J}^\mu(0) \right| f \right\rangle\right)^*}{q^0 + E_f - E_i - i\varepsilon} E_i\right). \end{aligned} \tag{4.28}$$

The last equality can be obtained by performing the same steps and assumptions as previously. One has to use the fact, that the nuclear current operator has to be self- adjoint. Finally, one has to replace dummy summation indices $\mu \leftrightarrow \nu$ in the above expression and add it to Eq. (4.26). The extended contraction is thus defined as:

$$\overline{L_{\mu\nu}W^{\mu\nu}}(P_i, q) \equiv L_{\mu\nu}W^{\mu\nu}(P_i, q) + L_{\nu\mu}W^{\mu\nu}(P_i, -q). \tag{4.29}$$

The extended tensor structure is more general than $W^{\mu\nu}$ but it contains contributions, which are nonphysical from the lepton scattering process point of view. Because the part we added is zero in all physical scattering channels, we may write for our purpose $\overline{L_{\mu\nu}W^{\mu\nu}}(P_i, q) = L_{\mu\nu}W^{\mu\nu}$. Thus the drawback of this method is that one has to check the energy conservation and physical interpretation of the results while calculating the cross section.

One has to put the nuclear currents in a time-ordered product, which we will do in the following steps:

$$\begin{aligned} L_{\mu\nu}W^{\mu\nu} &= -\frac{1}{\pi}\Im\left(L_{\mu\nu}\Omega\overline{\sum_i}\sum_f \int d^3x e^{-i(\boldsymbol{q}+\boldsymbol{P_i}-\boldsymbol{P_f})\boldsymbol{x}} \frac{\left\langle f \left| \hat{J}^\mu(0) \right| i \right\rangle \left(\left\langle f \left| \hat{J}^\nu(0) \right| i \right\rangle\right)^*}{q^0+E_i-E_f+i\varepsilon} E_i\right) + \\ &+ \frac{1}{\pi}\Im\left(L_{\mu\nu}\Omega\overline{\sum_i}\sum_f \int d^3x e^{-i(\boldsymbol{q}+\boldsymbol{P_f}-\boldsymbol{P_i})\boldsymbol{x}} \frac{\left\langle i \left| \hat{J}^\mu(0) \right| f \right\rangle \left(\left\langle i \left| \hat{J}^\nu(0) \right| f \right\rangle\right)^*}{q^0 + E_f - E_i - i\varepsilon} E_i\right). \end{aligned} \tag{4.30}$$

One would like to extract the theta functions of the time argument. This can be done by using the following properties of distributions:

$$\begin{aligned}
\frac{1}{a+i\varepsilon} &= -i\int dx^0 e^{ix^0 a}\Theta(x^0) \\
\frac{1}{a-i\varepsilon} &= i\int dx^0 e^{-ix^0 a}\Theta(x^0) = i\int dx^0 e^{ix^0 a}\Theta(-x^0).
\end{aligned} \tag{4.31}$$

This standard manipulation (used for example in the calculation of QFT propagators) leads to:

$$\begin{aligned}
L_{\mu\nu}W^{\mu\nu} &= -\frac{1}{\pi}\Im\left(L_{\mu\nu}\Omega\overline{\sum_i}\sum_f(-i)\int d^4x e^{i(q^0+E_i-E_f)x^0}e^{-i(\boldsymbol{q}+\boldsymbol{P_i}-\boldsymbol{P_f})\boldsymbol{x}}\right. \\
&\quad \left.\Theta(x^0)\left\langle f\left|\hat{J}^\mu(0)\right|i\right\rangle\left(\left\langle f\left|\hat{J}^\nu(0)\right|i\right\rangle\right)^* E_i\right) + \\
&+ \frac{1}{\pi}\Im\left(L_{\mu\nu}\Omega\overline{\sum_i}\sum_f i\int d^4x e^{i(q^0+E_f-E_i)x^0}e^{-i(\boldsymbol{q}+\boldsymbol{P_f}-\boldsymbol{P_i})\boldsymbol{x}}\right. \\
&\quad \left.\Theta(-x^0)\left\langle i\left|\hat{J}^\mu(0)\right|f\right\rangle\left(\left\langle i\left|\hat{J}^\nu(0)\right|f\right\rangle\right)^* E_i\right) = \\
&= -\frac{1}{\pi}\Im\left(L_{\mu\nu}\Omega\overline{\sum_i}\sum_f(-i)\int d^4x e^{iqx}\Theta(x^0)\left\langle f\left|\hat{J}^\mu(0)\right|i\right\rangle\left(\left\langle f\left|\hat{J}^\nu(x)\right|i\right\rangle\right)^* E_i\right) + \\
&+ \frac{1}{\pi}\Im\left(L_{\mu\nu}\Omega\overline{\sum_i}\sum_f i\int d^4x e^{iqx}\Theta(-x^0)\left\langle i\left|\hat{J}^\mu(0)\right|f\right\rangle\left(\left\langle i\left|\hat{J}^\nu(x)\right|f\right\rangle\right)^* E_i\right) = \\
&= \Im\left(L_{\mu\nu}\Omega\frac{i}{\pi}\int d^4x e^{iqx}\overline{\sum_i}\left\langle i\left|T\left\{\hat{J}^{\nu\dagger}(x)\hat{J}^\mu(0)\right\}\right|i\right\rangle E_i\right) \equiv \\
&\equiv -\frac{1}{\pi}\Im\left(L_{\mu\nu}\Pi^{\mu\nu}(q)\right).
\end{aligned} \tag{4.32}$$

Thus we have introduced the **polarization tensor**:

$$\Pi^{\mu\nu}(q) \equiv i\Omega\int d^4x e^{iqx}\overline{\sum_i}\left\langle i\left|T\left\{\hat{J}^{\nu\dagger}(x)\hat{J}^\mu(0)\right\}\right|i\right\rangle E_i \tag{4.33}$$

After going from the Heisenberg to the interaction representation of currents one can rewrite the above expression as:

$$\Pi^{\mu\nu}(q) \equiv i\Omega\int d^4x e^{iqx}\overline{\sum_i}\left\langle i\left|T\left\{\hat{J}_I^{\nu\dagger}(x)\hat{J}_I^\mu(0)\exp\left(-i\int d^4y\hat{H}_{int.}(y)\right)\right\}\right|i\right\rangle E_i \tag{4.34}$$

The above formula is very convenient in all types of nuclear system response computations. Unfortunately, the nature of strong interactions does not allow us to formulate an exact description of both the nuclear current operators $\hat{J}^\mu(x)$, nuclear ground state $|i\rangle$ and the interactions hidden in the quantum field theoretical expansion of nuclear current time-ordered product. Hence one must rely on approximations.

4.2 Impulse approximation and De Forest prescription

In the Eqs. (4.1) and (4.34) one requires information about initial nucleus four-momentum. In the laboratory frame, where most of the calculations are made, initial nucleus energy E_i is equal to its mass M_i. It is very convenient to cancel out all the nuclear mass factors, which leads to:

$$\frac{d^3\sigma}{dq^0 d\Omega'} = F_l(Q^2)\frac{|\boldsymbol{l'}|}{|\boldsymbol{l}|}\frac{-1}{\pi}\Im\left(L_{\mu\nu}\tilde{\Pi}^{\mu\nu}\right) \tag{4.35}$$

with polarization tensor defined as:

$$-i\tilde{\Pi}^{\mu\nu}(q) \equiv \Omega\int d^4x e^{iqx}\overline{\sum_i}\left\langle i\left|T\left\{\hat{J}_I^{\nu\dagger}(x)\hat{J}_I^{\mu}(0)\exp\left(-i\int d^4y\hat{H}_{int.}(y)\right)\right\}\right|i\right\rangle. \tag{4.36}$$

From now on whenever we refer to $\Pi^{\mu\nu}$ we mean the Eq. (4.36) without the nucleus mass inside. There is still a problem of energy conservation in Eq. (4.3), $M_i{+}q^0{=}E_f$, because it describes an excitation of the whole nuclear system. Here some approximations have to be made. Firstly, the target nucleus consists of A nucleons being bound by nuclear forces and we assume the probe to scatter off one chosen nucleon bound in a nuclear system. In the so-called "impulse approximation" we can break the wave function of initial state into parts describing the target nucleon and the rest of the system of $A-1$ nucleons:

$$|\psi_i\rangle = |p_i, s_i, \tau_i\rangle \otimes |(A-1)_i\rangle \tag{4.37}$$

with p, s, τ being the nucleon momentum, spin and isospin. Here we must state, that the choice of set of quantum numbers describing our nucleon is arbitrary. The one used here corresponds to the "plane wave impulse approximation" because the nucleon is described by a set of plane waves. The same procedure can be applied for two-body currents, where we separate out two nucleons and neglect the nucleon-nucleon correlations:

$$|\psi_i\rangle = \left|p_i^{(1)}, s_i^{(1)}, \tau_i^{(1)}\right\rangle \otimes \left|p_i^{(2)}, s_i^{(2)}, \tau_i^{(2)}\right\rangle \otimes |(A-2)_i\rangle\,. \tag{4.38}$$

This is beyond the range of IA, where only single-nucleon currents are taken into account. In the following considerations we will focus mostly on the more simple one-nucleon excitation case.

The nucleon inside nucleus is bound by strong forces and does not propagate on its mass shell. This means its wave function is not a solution to the free Dirac equation and the nucleon's form factors may differ from the free case. A simple solution has been introduced by De Forest in Ref. [113]. One simply takes into account the nucleon removal energy E defined as:

$$E = E_{A-1} + M - M_i. \tag{4.39}$$

It is assumed here, that the initial nucleus consists of the target nucleon and the final nucleus with energy E_{A-1}, so the struck nucleon energy can be defined as $M_A - E_{A-1} = M - E$. In general, E_{A-1} consists both of nuclear system excitation energy in its mass frame and kinetic energy T_{A-1}. Thus the remnant nucleus may carry away part of the momentum transfer. We denote it as $\boldsymbol{p_{A-1}}$. In most of the cases it is assumed here, that the remnant nucleus mass is much greater, than the nucleon mass, *i. e.* $M_{A-1} \gg M$. Thus we can neglect

the nucleus recoil effect, setting $\boldsymbol{p_{A-1}} \approx 0$. Another common simplification is to assume the removal energy to be constant with respect to the target nucleon variables and 4-momentum transfer. We assume the initial nucleon energy

$$E_N = \sqrt{\boldsymbol{p}_i^2 + M^2} - B \tag{4.40}$$

with B being the constant binding energy. This leads to conclusion, that one can approximate $M_i = M_{A-1} + E_N$ and $E_f = M_{A-1} + E_{N'}$. This means all the energy and momentum transfer goes to the chosen nucleon and that we disregard all changes in the $A-1$ nucleon system wave function (we neglect FSI), *i. e.* :

$$|(A-1)_i\rangle = |(A-1)_f\rangle \tag{4.41}$$

and as such we break also the final nuclear state into the outgoing nucleon and remnant nucleus:

$$|\psi_f\rangle = |p_f, s_f, \tau_f\rangle \otimes |(A-1)_f\rangle \,. \tag{4.42}$$

Within IA and with the above mentioned simplifications we can re-write the energy conservation relation:

$$\begin{aligned} \delta(M_i + q^0 - E_f) &\approx \delta(M_{A-1} + E_N + q^0 - (M_{A-1} + E_{N'})) = \\ &= \delta(E_N + q^0 - E_{N'}). \end{aligned} \tag{4.43}$$

This prescription can be generalized to any number of involved nucleons and hadrons produced in the final state. For example in two-body interaction case we break the system into two chosen nucleons and $A-2$ nucleon remnant and use appropriate two-body currents, approximating the energy conservation relation by:

$$\begin{aligned} \delta(M_i + q^0 - E_f) &\approx \delta(M_{A-2} + E_{N1} + E_{N2} + q^0 - (M_{A-2} + E_{N1'} + E_{N2'})) = \\ &= \delta(E_{N1} + E_{N2} + q^0 - E_{N1'} - E_{N2'}) \end{aligned} \tag{4.44}$$

The mentioned simplifications are used throughout this thesis unless specified otherwise. All effects of nucleus mass change etc. can be incorporated into the binding energy B. Furthermore, the usual assumption in the De Forest prescription is that the nucleons stay on their mass shell, and that one takes into account the binding effects by modifying the energy transfer:

$$q^0 \to \tilde{q}^0 = q^0 - B. \tag{4.45}$$

This substitution is widely used, but has many shortcomings. One of them is breakdown of the vector current conservation. Normally for the purely vector components of the leptonic and nuclear tensor one has:

$$q^\mu L^V_{\mu\nu} = q^\mu W^V_{\mu\nu} = 0. \tag{4.46}$$

After applying Eq. (4.45) this behavior changes to:

$$\begin{aligned} q^\mu L^V_{\mu\nu} &= 0 \\ q^\mu W^V_{\mu\nu} &\neq 0 \\ \tilde{q}^\mu W^V_{\mu\nu} &= 0. \end{aligned} \tag{4.47}$$

The last equation follows from the fact, that the vector part of nuclear tensor given in a general form by Eq. (4.6) is now constructed using $\tilde{q}^\mu = (\tilde{q}^0, \boldsymbol{q})$.

4.3 Global and local Fermi gas

The Fermi gas model of nucleus is the most simple picture of nucleus. One assumes the ground state to be a Fermi sea of protons and neutrons filled up completely to a certain Fermi level described by Fermi momentum, k_F. The construction is following. For the $\psi(x)$ we take the free quantum Dirac field:

$$\psi(x) = \frac{1}{\sqrt{\Omega}} \sum_{\substack{\boldsymbol{k}\boldsymbol{k'} \\ ss'}} \frac{1}{\sqrt{2k^0}} \left[a_{\boldsymbol{k}s} u_{s\alpha}(\boldsymbol{k}) e^{-ikx'} + b^\dagger_{\boldsymbol{k},s} v_{s\alpha}(\boldsymbol{k}) e^{ikx'} \right].$$

The model is determined by the way in which creation and annihilation operators act on the ground state.

$$\begin{aligned} b_{\boldsymbol{k},s} \left|0\right\rangle &= 0 \qquad \text{always} \\ a^\dagger_{\boldsymbol{k},s} \left|0\right\rangle &= 0 \qquad \text{for } \ |\boldsymbol{k}| < k_f \\ a_{\boldsymbol{k},s} \left|0\right\rangle &= 0 \qquad \text{for } \ |\boldsymbol{k}| > k_f \end{aligned} \tag{4.48}$$

This definition assumes, that all particle states are filled up to the Fermi level. Here we can calculate an example polarization tensor in the easiest case: the quasielastic scattering off Fermi gas. All nucleon-nucleon interactions are absent and we excite a single particle-hole pair out of the ground state. In this lowest order the polarization tensor is

$$i\Pi^{(0)\mu\nu}(q) = \Omega \int d^4x e^{iqx} \left\langle 0 \left| T \left\{ \hat{J}^{\nu\dagger}(x) \hat{J}^\mu(0) \right\} \right| 0 \right\rangle. \tag{4.49}$$

One can express the single nucleon current operators in a space coordinate representation as:

$$\begin{aligned} \hat{J}^\mu_V(x) &= \overline{\psi}(x) \left[\gamma^\mu \hat{F}_1 + \sigma^{\mu\alpha} \overleftrightarrow{\partial}_\alpha \frac{\hat{F}_2}{M} \right] \psi(x) \\ \hat{J}^\mu_A(x) &= \overline{\psi}(x) \left[\hat{G}_A \gamma^\mu \gamma^5 + \frac{2}{i} \frac{\overleftrightarrow{\partial^\mu}}{M} \gamma^5 \hat{G}_P \right] \psi(x) \end{aligned} \tag{4.50}$$

The operator $\overleftrightarrow{\partial^\mu} = \frac{1}{2}\left(\overleftarrow{\partial^\mu} + \overrightarrow{\partial^\mu}\right)$ picks up the momentum difference from Fourier modes of field operators, *e. g.*:

$$\begin{aligned} \overline{\psi}(x) \overleftrightarrow{\partial^\mu} \psi(x) &= \frac{1}{2\Omega} \sum_{\substack{\boldsymbol{k}\boldsymbol{k'} \\ ss'}} \frac{1}{2\sqrt{E(\boldsymbol{k})E(\boldsymbol{k'})}} \left\{ \partial^\mu \left[a^\dagger_{\boldsymbol{k'}s'} \overline{u}_{s'}(\boldsymbol{k'}) e^{ik'x} + b_{\boldsymbol{k'},s'} \overline{v}_{s'}(\boldsymbol{k'}) e^{-ik'x} \right] \cdot \right. \\ &\cdot \left[a_{\boldsymbol{k}s} u_s(\boldsymbol{k}) e^{-ikx} + b^\dagger_{\boldsymbol{k},s} v_s(\boldsymbol{k}) e^{ikx} \right] + \\ &+ \left[a^\dagger_{\boldsymbol{k'}s'} \overline{u}_{s'}(\boldsymbol{k'}) e^{ik'x} + b_{\boldsymbol{k'},s'} \overline{v}_{s'}(\boldsymbol{k'}) e^{-ik'x} \right] \cdot \\ &\cdot \left. \partial^\mu \left[a_{\boldsymbol{k}s} u_s(\boldsymbol{k}) e^{-ikx} + b^\dagger_{\boldsymbol{k},s} v_s(\boldsymbol{k}) e^{ikx} \right] \right\} = \end{aligned}$$

$$
\begin{aligned}
&= \frac{i}{2\Omega}\sum_{\substack{\boldsymbol{k}\boldsymbol{k'}\\ ss'}}\frac{1}{2\sqrt{E(\boldsymbol{k})E(\boldsymbol{k'})}}\Big[(k'-k)^{\mu}a^{\dagger}_{\boldsymbol{k'}s'}a_{\boldsymbol{k}s}\overline{u}_{s'}(\boldsymbol{k'})u_s(\boldsymbol{k})e^{i(k'-k)x}+\\
&+ (k'+k)^{\mu}a^{\dagger}_{\boldsymbol{k'}s'}b^{\dagger}_{\boldsymbol{k},s}\overline{u}_{s'}(\boldsymbol{k'})v_s(\boldsymbol{k})e^{i(k'+k)x}+\\
&- (k'+k)^{\mu}b_{\boldsymbol{k'},s'}a_{\boldsymbol{k}s}\overline{v}_{s'}(\boldsymbol{k'})u_s(\boldsymbol{k})e^{-i(k'+k)x}+\\
&- (k'-k)^{\mu}b_{\boldsymbol{k'},s'}b^{\dagger}_{\boldsymbol{k},s}\overline{v}_{s'}(\boldsymbol{k'})v_s(\boldsymbol{k})e^{-i(k'-k)x}\Big] \qquad (4.51)
\end{aligned}
$$

thus for the nucleon momentum eigenstates it literally produces the $\frac{i}{2}q^{\mu}$ needed in momentum representation of the nucleon electromagnetic and weak currents. The drawback of such representation is that one can not always express it as a finite series of $\overleftrightarrow{\partial^{\mu}}$ operators, as in the case of nucleon form factors. For example a dipole axial form factor $G_A(Q^2)\propto\frac{1}{(1+\frac{Q^2}{M_A^2})^2}$ would require an expansion of denominator into an infinite series of differential operators. It is easy to check that the current operator is self-adjoint.

$$
\begin{aligned}
\hat{J}^{\mu\dagger}_V(x) &= \psi^{\dagger}(x)\gamma^0\left[\gamma^0\gamma^{\mu\dagger}\hat{F}_1\gamma^0+\left(\gamma^0\frac{-i}{2}[\gamma^{\alpha\dagger},\gamma^{\mu\dagger}]\overleftrightarrow{\partial_{\alpha}}\frac{\hat{F}_2}{M}\gamma^0\right)\right]\gamma^0\psi(x)=\overline{\psi}(x)\hat{\Gamma}^{\mu}_V\psi(x)\\
\hat{J}^{\mu\dagger}_A(x) &= \psi^{\dagger}(x)\gamma^0\left[\hat{G}_A\gamma^0\gamma^5\gamma^{\mu\dagger}\gamma^0-\frac{2}{i}\frac{\overleftrightarrow{\partial^{\mu}}}{M}\gamma^0\gamma^5\gamma^0\hat{G}_P\right]\gamma^0\psi(x)=\bar{\psi}(x)\hat{\Gamma}^{\mu}_A\psi(x). \qquad (4.52)
\end{aligned}
$$

Last equality was obtained from:

$$
\gamma^0\gamma^{\dagger\mu}\gamma^0=\gamma^{\mu}. \qquad (4.53)
$$

In order to get explicit partial derivatives we must introduce space-time separation of the current arguments. Also spinor indices are explicitly shown.

$$
\begin{aligned}
i\Pi^{(0)\mu\nu}(q) &= \Omega\int d^4x e^{iqx}\left\langle 0\left|T\left\{\bar{\psi}_{\alpha}(x)\hat{\Gamma}^{\nu}_{\alpha\beta}\psi_{\beta}(x)\bar{\psi}_{\lambda}(0)\hat{\Gamma}^{\mu}_{\lambda\delta}\psi_{\delta}(0)\right\}\right|0\right\rangle=\\
&= \lim_{\substack{y\to x^-,z_1\to 0^+\\ z_2\to 0^-}}\Omega\int d^4x e^{iqx}\langle 0|T\Big\{\bar{\psi}_{\alpha}(x)\hat{\Gamma}^{\nu}_{\alpha\beta}(x,y)\psi_{\beta}(y)\\
&\quad \bar{\psi}_{\lambda}(z_1)\hat{\Gamma}^{\mu}_{\lambda\delta}(z_1,z_2)\psi_{\delta}(z_2)\Big\}|0\rangle\,. \qquad (4.54)
\end{aligned}
$$

The limits of the type $y\to x^-$ have been introduced in order to make some of the appearing Green functions well-defined, as well as the $\hat{\Gamma}^{\mu}_{\lambda\delta}(0)$. Without assigned coordinate it would be impossible to use the differential vertex function from Eq. (4.50).
It is convenient to introduce space-time coordinates in the current operator too, according to the arguments of appropriate spinor fields:

$$
\hat{\Gamma}^{\mu}(x,y)\equiv\gamma^{\mu}\hat{F}_1(x,y)+\sigma^{\mu\alpha}\left(\frac{\overleftarrow{\partial}}{\partial x^{\alpha}}+\frac{\overrightarrow{\partial}}{\partial y^{\alpha}}\right)\frac{\hat{F}_2(x,y)}{2M}. \qquad (4.55)
$$

With $\hat{F}_{1,2}(x,y)$ being power series in $(\frac{\overleftarrow{\partial}}{\partial x^{\alpha}}+\frac{\overrightarrow{\partial}}{\partial y^{\alpha}})$ according to this convention. We introduce Dirac field propagator into our equations:

$$iG^{(0)}_{\alpha\beta}(y-x) =< 0|T\{\psi_\alpha(y)\bar{\psi}_\beta(x)\}|0 > .$$

and get two terms:

$$\begin{aligned} i\Pi^{(0)\mu\nu}(q) &= \lim_{\substack{y\to x^-, z_1\to 0^- \\ z_2\to z_1^-}} \Omega \int d^4x e^{iqx} \Big[iG^{(0)}_{\beta\alpha}(y-x) iG^{(0)}_{\delta\lambda}(z_2-z_1) + \\ & iG^{(0)}_{\delta\alpha}(z_2-x) iG^{(0)}_{\beta\lambda}(y-z_1)\Big] \hat{\Gamma}^\nu_{\alpha\beta}(x,y)\hat{\Gamma}^\mu_{\lambda\delta}(z_1,z_2). \end{aligned} \tag{4.56}$$

The first term corresponds to a disconnected diagram. It contributes to the normalization of the ground state only and we drop it out.
After dropping the disconnected terms two of the introduced limits become superfluous and it is enough to keep just one in order to define the vertex operator in an appropriate manner. Vertex operators will be thus again functions of one variable.
It is useful to introduce Fourier transform of the polarization propagator:

$$\begin{aligned} i\Pi^{(0)\mu\nu}(q) &= \lim_{z_1\to 0^-} \Omega \int d^4x e^{iqx} \int \frac{d^4p_1}{(2\pi)^4} \int \frac{d^4p_2}{(2\pi)^4} G^{(0)}_{\delta\alpha}(p_1) e^{-ip_1(z_1-x)} \\ & G^{(0)}_{\beta\lambda}(p_2) e^{-ip_2(x-z_1)} \hat{\Gamma}^\nu_{\alpha\beta}(x)\hat{\Gamma}^\mu_{\lambda\delta}(z_1) = \\ &= \lim_{z_1\to 0^-} \Omega \int d^4x e^{iqx} \int \frac{d^4p_1}{(2\pi)^4} \int \frac{d^4p_2}{(2\pi)^4} \\ & Tr\left\{ G^{(0)}(p_1) e^{ip_1x} \hat{\Gamma}^\nu(x) e^{-ip_2x} G^{(0)}(p_2) e^{ip_2z_1} \hat{\Gamma}^\mu(z_1) e^{-ip_1z_1} \right\} = \\ &= \Omega \int d^4x \int \frac{d^4p_1}{(2\pi)^4} \int \frac{d^4p_2}{(2\pi)^4} e^{i(q+p_1-p_2)x} \\ & \mathrm{Tr}\big\{ G^{(0)}(p_1)\Gamma^\nu(p_1,p_2) G^{(0)}(p_2)\Gamma^\mu(p_2,p_1)\big\}, \end{aligned} \tag{4.57}$$

where:

$$\begin{aligned} \Gamma^\nu_V(p_1,p_2) &\equiv \gamma^\nu F_1\left((p_1-p_2)^2\right) + i\sigma^{\nu\alpha}(p_1-p_2)_\alpha \frac{F_2\left((p_1-p_2)^2\right)}{2M} \\ \Gamma^\nu_A(p_1,p_2) &\equiv G_A\left((p_1-p_2)^2\right)\left(\gamma^\mu + \frac{\gamma^\alpha(p_1-p_2)_\alpha(p_1-p_2)^\mu}{m_\pi^2-(p_1-p_2)^2}\right)\gamma^5. \end{aligned} \tag{4.58}$$

We perform the Fourier transformation and obtain:

$$i\Pi^{(0)\mu\nu}(q) = \int \frac{d^4p}{(2\pi)^4} Tr\left\{ G^{(0)}(p)\Gamma^\nu(-q) G^{(0)}(p+q)\Gamma^\mu(q)\right\} \Omega M_i \tag{4.59}$$

The above equation can be used to calculate the double-differential cross section in the Fermi gas model. There are two popular approaches. One of them assumes the nucleus to have one mean Fermi momentum k_F and binding energy B both for protons and neutrons. We incorporate this binding into the definition of q^0, as in Eq. (4.45). Furthermore we always use a mean binding energy B of the nucleus both for global and local nuclear matter density QE scattering calculations. It is called "global Fermi gas" or just Fermi gas. It has also a constant quantization volume:

$$\Omega = \frac{3\pi^2}{k_F^3}. \tag{4.60}$$

The other approach assumes, that the Fermi momentum depends on local nuclear matter density for nucleons of isospin N. It is the framework of local density approximation (LDA). The local Fermi momenta calculated from relation $k_F^N(\boldsymbol{r}) = (3\pi^2\rho(\boldsymbol{r})^N)^{\frac{1}{3}}$. The proton density profiles are established through electron scattering experiments and fitted to the two and three parameter Fermi distributions or harmonic oscillator density profiles. Neutron densities are either assumed to be close in shape to the charged proton distributions or calculated from the nuclear many body theory. In this thesis the harmonic oscillator density profiles from Ref. [114] are used:

$$\rho(\boldsymbol{r}) = \rho_0 \left(1 + a\,(r/R)^2\right) \exp\left[-\,(r/R)^2\right] \tag{4.61}$$

with corrections to parameters a and R calculated in Ref. [115]. These corrections take into account, that neutrons and protons have finite radii. We call tis approach local Fermi gas.

Example calculation for electron scattering.

A good exercise and example is to perform the analytic calculation for local and global Fermi gas $1p1h$ cross section in the case of electron scattering, using both Rosenbluth separation formulation and the direct contraction of leptonic and nuclear tensors. The relativistic Fermi Gas of noninteracting nucleons can be described with following polarization tensor:

$$i\Pi^{\mu\nu}_{RFG} = \Omega \int \frac{d^4p}{(2\pi)^4} \mathrm{Tr}[G_N(p+q)V^\mu G_N(p)V^\nu] \tag{4.62}$$

Here the notation reads:

$$\begin{aligned}
\Omega &= \begin{cases} \frac{3\pi^2}{k_F^3} & FG \\ 4\pi \int r^2 dr & LFG \end{cases} \\
G_N(p) &= (\not{p} + M) D_N(p) \\
D_N(p) &= \frac{1}{E(p) + p^0 - i\epsilon} \left(\frac{n_N(p)\Theta(p^0)}{p^0 - E(p) - i\epsilon} + \frac{1 - n_N(p)\Theta(p^0)}{p^0 - E(p) + i\epsilon} \right) \\
V^\mu &= \gamma^\mu (F_1 + F_2) - \frac{(p+p')^\mu F_2}{2M}
\end{aligned} \tag{4.63}$$

The above version of nucleon electromagnetic vertices, V^μ, can be obtained from Eq. (3.15) by applying Dirac equation on nucleon spinors, assuming both initial and final nucleons to be on their mass shell. The relativistic nucleon propagator in FG model is calculated in the Appendix C. We have dropped the antinucleon part of the RFG nucleon propagator, because we work in the energy transfer regime below the nucleon-antinucleon pair creation threshold. We would like to calculate the integral over p_0. Let us take a look at the Fig. 12. Due to Jordan theorem we are free to add the integral over semi-circle in either upper or lower half-plane. We see that only terms with poles on both sides of the $\Re p_0$ axis contribute. Terms with poles on the same side of the $\Re p_0$ axis will be integrated out by closing the contour always on the opposite demiplane. The integral itself can be performed, because all the terms are $\propto \frac{1}{p_0^2}$ and Dirac spinors and $\Gamma(q)$ do not depend on p_0. We choose to integrate

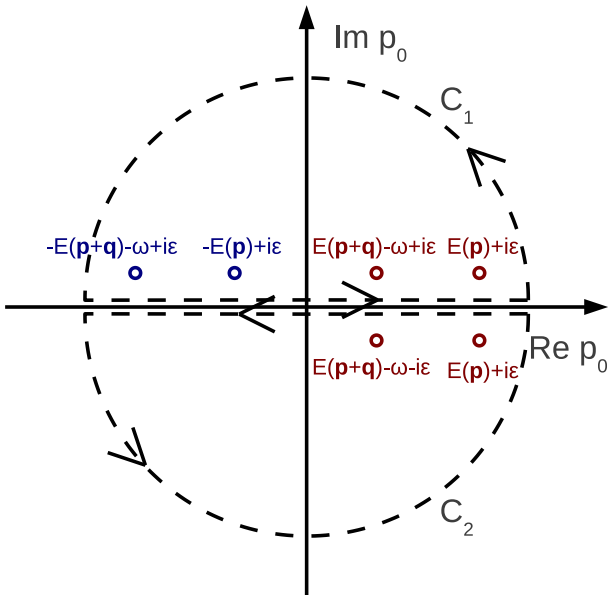

Figure 12: Placement of the poles in one-loop polarisation tensor. Red color for the particle propagator poles, blue for the antiparticle propagator poles. We neglect the antiparticle part in our calculation assuming the energy transfer to be too small to produce nucleon-antinucleon pairs.

along the contour C_1 and the polarization tensor becomes:

$$\begin{aligned} i\Pi^{\mu\nu}_{RFG} &= i\Omega \int \frac{d^4p}{(2\pi)^4} \left\{ \frac{1}{2E(p)(E(p+q)+E(p)+q^0)} \frac{(1-n_N(p'))n_N(p)}{q^0+E(p)-E(p+q)+i\epsilon} + \right. \\ &+ \left. \frac{1}{2E(p+q)(E(p)+E(p+q)-q^0)} \frac{(1-n_N(p))n_N(p+q)}{E(p+q)-q^0-E(p)+i\epsilon} \right\} \cdot \\ &\cdot \ \mathrm{Tr}[(\not{p}+M)V^\mu(\not{p}'+M)V^\nu]. \end{aligned} \tag{4.64}$$

Now it is easy to see, that the imaginary part of $\Pi^{\mu\nu}$ is obtained by placing all nucleon propagators on their mass shell. There exists a more general set of rules referred to as "Cutkosky rules" by the authors of Ref. [70]. They refer to the paper of Cutkosky (Ref. [116]) about the discontinuities of Feynman amplitudes and to optical theorem. We shall only give a very general outline and idea of the proof. The optical theorem says, that for a well-defined unitary S-matrix one can easily proof that the T-matrix ($S = \mathbb{1} + iT$) satisfies:

$$2\Im T = TT^\dagger \tag{4.65}$$

and thus:

$$2\Im \langle i|T|i\rangle = \langle i|TT^\dagger|i\rangle = \sum_f |\langle f|T|i\rangle|^2 \propto \sigma^{total}_{i\to f} \propto \int d(phase-space) \left[-\frac{1}{\pi}\Im(L_{\mu\nu}\Pi^{\mu\nu})\right] \tag{4.66}$$

In the last step we have inserted a complete set of final states as in the derivation of polarization tensor in section 4.1. Since all final states are on-shell one can prove now,

that for all physical scattering processes one obtains the imaginary part of contraction of polarization propagator with leptonic tensor by putting the final state particle propagators on their mass shell. This is illustrated in the Fig. 13 for the case of RFG, where $\sum_f |f\rangle\langle f|$

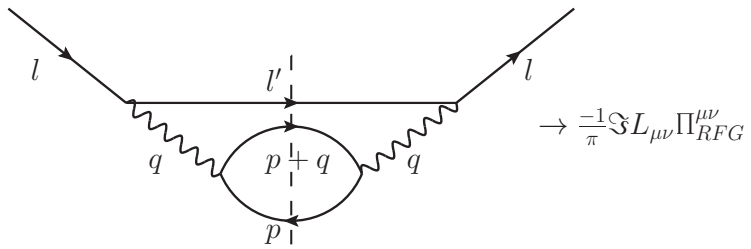

Figure 13: Illustration of Cutkosky cut in the RFG vacuum-vacuum Feynman diagram giving rise to the cross section in lepton scattering.

represents now the complete sum over on-shell particle-hole pairs and outgoing leptons. This can be done for every interaction channel, where we have more complicated final states. Thus one can also calculate the imaginary part of Eq. (4.62) by replacing:

$$\begin{aligned}
D_N(p) &\rightarrow i\Im D_N(p)\theta(p^0) = \frac{i\pi}{2E(p)}(2n_N(p)-1)\delta(p^0-E(p)) \\
D_N(p)D_N(p+q) &\rightarrow \frac{(i\pi)^2}{4E(p)E(p')}(2n_N(p)-1)(2n_N(p')-1) \\
&\quad \delta(p^0+q^0-E(p'))\delta(p^0-E(p)) = \\
&= \frac{-(\pi)^2}{4E(p)E(p')}(2n_N(p)(n_N(p')-1)+2n_N(p')(n_N(p)-1)+1) \\
&\quad \delta(p^0+q^0-E(p'))\delta(p^0-E(p)) = \\
&= \frac{2\pi^2}{4E(p)E(p')}\left(n_N(p)(1-n_N(p'))+n_N(p')(1-n_N(p))-1\right) \\
&\quad \delta(p^0+q^0-E(p'))\delta(p^0-E(p)). \qquad (4.67)
\end{aligned}$$

This technique can save some time while performing calculations of more complicated contributions to polarization tensor containing multiple propagators of nucleons, mesons etc. The part of $\Im\Pi^{\mu\nu}$ (Eq. 4.64) which does not contain the state density $n_N(p)$, is a vacuum contribution. By substituting $\boldsymbol{p} \rightarrow -\boldsymbol{p}-\boldsymbol{q}$ in the part with $1-n(p)$ one can show, that it contributes only for $q^0 < 0$. Hence the desired polarization propagator is:

$$\frac{-1}{\pi}\Im\Pi^{\mu\nu}_{RFG}(q) = \Omega\int\frac{d^3p}{(2\pi)^3}\frac{n_N(p)(1-n_N(p+q))}{E(p)E(p+q)}A^{\mu\nu}_N\delta(E(p+q)-E(p)-q^0) \qquad (4.68)$$

with the hadronic tensor defined as:

$$A^{\mu\nu} = \frac{1}{4}\mathrm{Tr}[(\not{p}+M)V^\mu(\not{p}'+M)V^\nu]. \qquad (4.69)$$

Let us evaluate the Dirac matrices traces first:

$$
\begin{aligned}
&\mathrm{Tr}\ \left[(\not{p}+M)\left(\gamma^\nu(F_1+F_2)-\frac{(p+p')^\nu}{2M}\right)(\not{p}'+M)\left(\gamma^\mu(F_1+F_2)-\frac{(p+p')^\mu}{2M}\right)\right]= \\
&= \left(\mathrm{Tr}\left[\not{p}\gamma^\nu\not{p}'\gamma^\mu\right]+M^2\mathrm{Tr}\left[\gamma^\mu\gamma^\nu\right]\right)(F_1+F_2)^2+ \\
&+ \frac{(p+p')^\nu(p+p')^\mu}{4M^2}\left(\mathrm{Tr}\left[\gamma^\mu\gamma^\nu\right]+4M^2\right)F_2^2+ \\
&- \frac{(p+p')^\nu}{2M}\mathrm{Tr}\left[(\not{p}+M)(\not{p}'+M)\gamma^\mu\right]F_2(F_1+F_2)+ \\
&- \frac{(p+p')^\mu}{2M}\mathrm{Tr}\left[(\not{p}+M)(\not{p}'+M)\gamma^\nu\right]F_2(F_1+F_2)= \\
&= 4\left[\left(2p^\mu p^\nu+p^\mu q^\nu+p^\nu q^\mu-g^{\mu\nu}(p\cdot(p+q)-M^2)\right)(F_1+F_2)^2+\right. \\
&+ (2p+q)^\mu(2p+q)^\nu\frac{p\cdot(p+q)+M^2}{4M^2}F_2^2+ \\
&- \left.(2p+q)^\mu(2p+q)^\nu F_2(F_1+F_2)\right]. \qquad (4.70)
\end{aligned}
$$

In the above explicit 4-momentum conservation $p'=p+q$ and on-shell condition $p_\mu^2=M^2$ have been used. Using again the on-shell relations one can show:

$$
M^2={p'}_\mu^2=p_\mu^2+2p\cdot q+q_\mu^2\rightarrow p\cdot q=-\frac{1}{2}q_\mu^2. \qquad (4.71)
$$

Thus with a little algebraic manipulation:

$$
\begin{aligned}
A^{\mu\nu} &= (2p^\mu p^\nu+p^\mu q^\nu+p^\nu q^\mu+\frac{1}{2}q_\mu^2 g^{\mu\nu})(F_1+F_2)^2+ \qquad (4.72)\\
&+ 2(2p^\mu p^\nu+p^\mu q^\nu+p^\nu q^\mu+\frac{1}{2}q^\mu q^\nu)\frac{1}{2}(1-\frac{q_\mu^2}{4M^2})F_2^2+ \\
&- 2(2p^\mu p^\nu+p^\mu q^\nu+p^\nu q^\mu+\frac{1}{2}q^\mu q^\nu)(F_2^2+F_1F_2)= \\
&= (2p^\mu p^\nu+p^\mu q^\nu+p^\nu q^\mu)\left(F_1^2-\frac{q_\mu^2}{4M^2}F_2^2\right)+\frac{1}{2}q_\mu^2 g^{\mu\nu}(F_1+F_2)^2+ \\
&- q^\mu q^\nu\left(F_1F_2+\frac{1}{2}(1+\frac{q_\mu^2}{4M^2})F_2^2)\right).
\end{aligned}
$$

Quick check of the formula by testing the gauge invariance:

$$
\begin{aligned}
q_\mu A^{\mu\nu} &= (2p\cdot qp^\nu+p\cdot qq^\nu+p^\nu q_\mu^2)\left(F_1^2-\frac{q_\mu^2}{4M^2}F_2^2\right)+\frac{1}{2}q_\mu^2 q^\nu(F_1+F_2)^2+ \qquad (4.73)\\
&- q_\mu^2 q^\nu\left(F_1F_2+\frac{1}{2}(1+\frac{q_\mu^2}{4M^2})F_2^2)\right)= \\
&= (-q_\mu^2 p^\nu-\frac{1}{2}q_\mu^2 q^\nu+p^\nu q_\mu^2)\left(F_1^2-\frac{q_\mu^2}{4M^2}F_2^2\right)+\frac{1}{2}q_\mu^2 q^\nu(F_1+F_2)^2+ \\
&- q_\mu^2 q^\nu\left(F_1F_2+\frac{1}{2}(1+\frac{q_\mu^2}{4M^2})F_2^2)\right)\equiv 0.
\end{aligned}
$$

Thus for the on-shell nucleons one preserves the gauge invariance. We would like to account for the nucleon binding inside the target nucleus. We shall use the De Forest prescription

from Eq. (4.45):

$$q^\mu \to \tilde{q}^\mu = (q^0 - B, \boldsymbol{q}) = (\tilde{q^0}, \boldsymbol{q}). \tag{4.74}$$

We will obtain a re-defined hadronic tensor:

$$\begin{aligned} \tilde{A}^{\mu\nu} &= (2p^\mu p^\nu + p^\mu \tilde{q}^\nu + p^\nu \tilde{q}^\mu)\left(F_1^2 - \frac{\tilde{q}_\mu^2}{4M^2}F_2^2\right) + \frac{1}{2}\tilde{q}_\mu^2 g^{\mu\nu}(F_1+F_2)^2 + \\ &- \tilde{q}^\mu\tilde{q}^\nu\left(F_1F_2 + \frac{1}{2}(1+\frac{\tilde{q}_\mu^2}{4M^2})F_2^2)\right). \end{aligned} \tag{4.75}$$

This form of the tensor obeys:

$$\tilde{q}_\mu \tilde{A}^{\mu\nu} = 0 \tag{4.76}$$

breaking the normal gauge invariance condition. This follows strictly the prediction of Eq. (4.46). One can also try to account for binding and medium effects by correcting nucleon energy dispersion relation $E(p) = \sqrt{\boldsymbol{p}^2 + M^2}$ by an in-medium self-energy. For each $1p1h$ calculation one has to find the proper integration limits. Let us begin with a general integral:

$$\begin{aligned} &\int \frac{d^3p}{(2\pi)^3}\frac{n_N(p)(1-n_N(p+q))}{E(p)E(p+q)}\delta(E(p+q)-E(p)-\tilde{q}^0)(\ldots) = \\ &= \frac{1}{4\pi^2}\int_0^{2\pi}\frac{d\phi}{2\pi}\int_{-1}^{1}d\mu\int_0^{k_F}p^2dp\frac{\Theta(|\boldsymbol{p}+\boldsymbol{q}|-k_F)}{E(p)E(p+q)}\delta(E(p+q)-E(p)-\tilde{q}^0)(\ldots) \end{aligned} \tag{4.77}$$

where we have introduced a short notation $\mu \equiv \cos(\Theta)$.

It is convenient to use the energy conservation to perform the azimuthal angle integral.

$$\begin{aligned} \sqrt{p^2+q^2+2pq\mu_0+M^2} &= \sqrt{p^2+M^2}+\tilde{q}^0 \\ \mu_0 = \frac{q_\mu^2 + 2E(p)\tilde{q}^0}{2pq}. \end{aligned} \tag{4.78}$$

And the Jacobian is:

$$\frac{df}{d\mu} = \frac{pq}{E(p+q)}. \tag{4.79}$$

Thus the integral becomes:

$$\begin{aligned} &\frac{1}{4\pi^2}\int_0^{2\pi}\frac{d\phi}{2\pi}\int_{-1}^{1}d\mu\int_0^{k_F}p^2dp\frac{\Theta(|\boldsymbol{p}+\boldsymbol{q}|-k_F)}{E(p)E(p+q)}\delta(E(p+q)-E(p)-\tilde{q}^0)(\ldots) = \\ &= \frac{1}{4\pi^2 q}\int_0^{2\pi}\frac{d\phi}{2\pi}\int_{p_{min}}^{k_F}\frac{pdp}{E(p)}(\ldots) = \frac{1}{4\pi^2 q}\int_0^{2\pi}\frac{d\phi}{2\pi}\int_{E_{min}}^{E_F}dE(p)(\ldots). \end{aligned} \tag{4.80}$$

In the last step the integration variable has been switched to nucleon energy, which is more convenient in the relativistic case.

First we shall calculate the energy conservation condition from $\mu \in [-1,1]$. Limiting cases are $\mu = \pm 1$. Thus we need to solve following equation:

$$\begin{aligned}
\left|\frac{q_\mu^2 + 2E(p)\tilde{q}^0}{2pq}\right| &= 1 \\
(q_\mu^2 + 2E(p)\tilde{q}^0)^2 = 4p^2q^2 &= 4(E(p)^2 - M^2)q^2 \\
E(p)^2 + E(p)\tilde{q}^0 + \frac{q_\mu^2}{4} + \frac{M^2q^2}{q_\mu^2} &= 0 \\
\Delta &= q^2\left(1 - \frac{4M^2}{q_\mu^2}\right) \\
E(p) &= \frac{1}{2}\left(-\tilde{q}^0 + q\sqrt{1 - \frac{4M^2}{q_\mu^2}}\right).
\end{aligned} \tag{4.81}$$

Another limits come from the condition $E(p) > M$ and $E(p) + \tilde{q}^0 > E_F$ ("Pauli blocking", (PB)). The final integration limit can be expressed as:

$$E_{min.} = max\left\{M, E_F - \tilde{q}^0, \frac{1}{2}\left(-\tilde{q}^0 + q\sqrt{1 - \frac{4M^2}{\tilde{q}_\mu^2}}\right)\right\}. \tag{4.82}$$

Knowing this one can re- express the polarization tensor:

$$\frac{-1}{\pi}\Im\Pi^{\mu\nu}_{RFG}(q) = \frac{\Omega}{4\pi^2 q}\int_0^{2\pi}\frac{d\phi}{2\pi}\int_{E_{min}}^{E_F} dE(p)A_N^{\mu\nu}. \tag{4.83}$$

Using this expression one can calculate the cross section. There are two possibilities to proceed: either the Rosenbluth separation into R_L and R_T or direct contraction of tensors. We shall use the quicker Rosenbluth separation technique, obtaining the separation to longitudinal and transverse cross sections in laboratory frame. The latter method is used in Appendix D. We shall start from the Eq. (4.24) with the longitudinal and transverse responses defined as:

$$\begin{aligned}
R_L &= \frac{-1}{\pi}\Im\Pi^{00} \\
R_T &= \frac{-1}{\pi}\Im(\Pi^{11} + \Pi^{22}) \equiv \frac{-2}{\pi}\Im\Pi^{11} (\text{because here } \Im\Pi^{11} = \Im\Pi^{22}).
\end{aligned} \tag{4.84}$$

The longitudinal response in the $1p1h$ RFG:

$$\begin{aligned}
R_L &= \frac{-1}{\pi}\Im\Pi^{00}_{RFG}(q) = \frac{\Omega}{4\pi^2 q}\int_0^{2\pi}\frac{d\phi}{2\pi}\int_{E_{min}}^{E_F} dE(p)A_N^{00} = \\
&= \frac{\Omega}{4\pi^2 q}\int_0^{2\pi}\frac{d\phi}{2\pi}\int_{E_{min}}^{E_F} dE(p)(2E(p)^2 + 2\tilde{q^0}E(p))\left(F_1^2 - \frac{\tilde{q}_\mu^2}{4M^2}F_2^2\right) + \frac{1}{2}\tilde{q}_\mu^2(F_1+F_2)^2 + \\
&- \tilde{q^0}^2\left(F_1F_2 + \frac{1}{2}(1 + \frac{\tilde{q}_\mu^2}{4M^2})F_2^2)\right) = \\
&= \frac{\Omega}{4\pi^2 q}\left[(\frac{2}{3}E(p)^3 + \tilde{q^0}E(p)^2)\left(F_1^2 - \frac{\tilde{q}_\mu^2}{4M^2}F_2^2\right) + \frac{1}{2}\tilde{q}_\mu^2 E(p)(F_1+F_2)^2 + \right. \\
&- \left.\tilde{q^0}^2 E(p)\left(F_1F_2 + \frac{1}{2}(1 + \frac{\tilde{q}_\mu^2}{4M^2})F_2^2)\right)\right]_{E_{min}}^{E_F}.
\end{aligned} \tag{4.85}$$

The transverse response:

$$
\begin{aligned}
R_T &= \frac{-2}{\pi}\Im\Pi^{11}_{RFG}(q) = \frac{\Omega}{2\pi^2 q}\int_0^{2\pi}\frac{d\phi}{2\pi}\int_{E_{min}}^{E_F} dE(p)A^{11}_N = \\
&= \frac{\Omega}{2\pi^2 q}\int_0^{2\pi}\frac{d\phi}{2\pi}\int_{E_{min}}^{E_F} dE(p)(2p_1^2)\left(F_1^2 - \frac{\tilde{q}_\mu^2}{4M^2}F_2^2\right) - \frac{1}{2}\tilde{q}_\mu^2(F_1+F_2)^2.
\end{aligned}
\tag{4.86}
$$

The p_1^2:

$$
\begin{aligned}
p_1^2 &= p^2\sin^2\Theta_p\sin^2\phi_p = \left(E(p)^2 - M^2 - \frac{(2E(p)\tilde{q^0} + \tilde{q}_\mu^2)^2}{4q^2}\right) = \\
&= p^2\sin^2\Theta_p\sin^2\phi_p = \left(-E(p)^2\frac{\tilde{q}_\mu^2}{q^2} - E(p)\tilde{q^0}\frac{\tilde{q}_\mu^2}{q^2} - M^2 - \frac{\tilde{q}_\mu^4}{4q^2}\right)\sin^2\phi_p.
\end{aligned}
\tag{4.87}
$$

And $\int_0^{2\pi}\frac{d\phi}{2\pi}\sin^2\phi = \frac{1}{2}$, thus

$$
\begin{aligned}
R_T &= -\frac{\Omega}{2\pi^2 q}\Bigg[\left(\frac{E(p)^3}{3}\frac{\tilde{q}_\mu^2}{q^2} + \frac{E(p)^2\tilde{q^0}\tilde{q}_\mu^2}{2q^2} + E(p)(M^2 + \frac{\tilde{q}_\mu^4}{4q^2})\right)\left(F_1^2 - \frac{\tilde{q}_\mu^2}{4M^2}F_2^2\right) + \\
&+ \frac{E(p)}{2}\tilde{q}_\mu^2(F_1+F_2)^2\Bigg]_{E_{min}}^{E_F}.
\end{aligned}
\tag{4.88}
$$

The cross section (per nucleon) in the FG case:

$$
\begin{aligned}
\frac{d\sigma}{d\Omega dE'} &= \frac{3\sigma_{Mott}}{4k_F^3 q}\Bigg\{\frac{q_\mu^4}{\boldsymbol{q}^4}\Bigg[(\frac{2}{3}E(p)^3 + \tilde{q^0}E(p)^2)\left(F_1^2 - \frac{\tilde{q}_\mu^2}{4M^2}F_2^2\right) + \\
&+ \frac{1}{2}\tilde{q}_\mu^2 E(p)(F_1+F_2)^2 - \tilde{q^0}^2 E(p)\left(F_1F_2 + \frac{1}{2}(1 + \frac{\tilde{q}_\mu^2}{4M^2})F_2^2)\right)\Bigg]_{E_{min}}^{E_F} + \\
&- \left(-\frac{q_\mu^2}{\boldsymbol{q}^2} + 2\,\mathrm{tg}^2\left(\frac{\theta}{2}\right)\right)\Bigg[\left(\frac{E(p)^3}{3}\frac{\tilde{q}_\mu^2}{q^2} + \frac{E(p)^2\tilde{q^0}\tilde{q}_\mu^2}{2q^2} + E(p)(M^2 + \frac{\tilde{q}_\mu^4}{4q^2})\right) \\
&\left(F_1^2 - \frac{\tilde{q}_\mu^2}{4M^2}F_2^2\right) + \frac{E(p)}{2}\tilde{q}_\mu^2(F_1+F_2)^2\Bigg]_{E_{min}}^{E_F}\Bigg\}.
\end{aligned}
\tag{4.89}
$$

The cross section (total for protons/neutrons) in the LFG case:

$$
\begin{aligned}
\frac{d\sigma}{d\Omega dE'} &= \frac{\sigma_{Mott}}{\pi q}\int r^2 dr\Bigg\{\frac{q_\mu^4}{\boldsymbol{q}^4}\Bigg[(\frac{2}{3}E(p)^3 + \tilde{q^0}E(p)^2)\left(F_1^2 - \frac{\tilde{q}_\mu^2}{4M^2}F_2^2\right) + \\
&+ \frac{1}{2}\tilde{q}_\mu^2 E(p)(F_1+F_2)^2 - \tilde{q^0}^2 E(p)\left(F_1F_2 + \frac{1}{2}(1 + \frac{\tilde{q}_\mu^2}{4M^2})F_2^2)\right)\Bigg]_{E_{min}}^{E_F} + \\
&- \left(-\frac{q_\mu^2}{\boldsymbol{q}^2} + 2\,\mathrm{tg}^2\left(\frac{\theta}{2}\right)\right)\Bigg[\left(\frac{E(p)^3}{3}\frac{\tilde{q}_\mu^2}{q^2} + \frac{E(p)^2\tilde{q^0}\tilde{q}_\mu^2}{2q^2} + E(p)(M^2 + \frac{\tilde{q}_\mu^4}{4q^2})\right) \\
&\left(F_1^2 - \frac{\tilde{q}_\mu^2}{4M^2}F_2^2\right) + \frac{E(p)}{2}\tilde{q}_\mu^2(F_1+F_2)^2\Bigg]_{E_{min}(r)}^{E_F(r)}\Bigg\}.
\end{aligned}
\tag{4.90}
$$

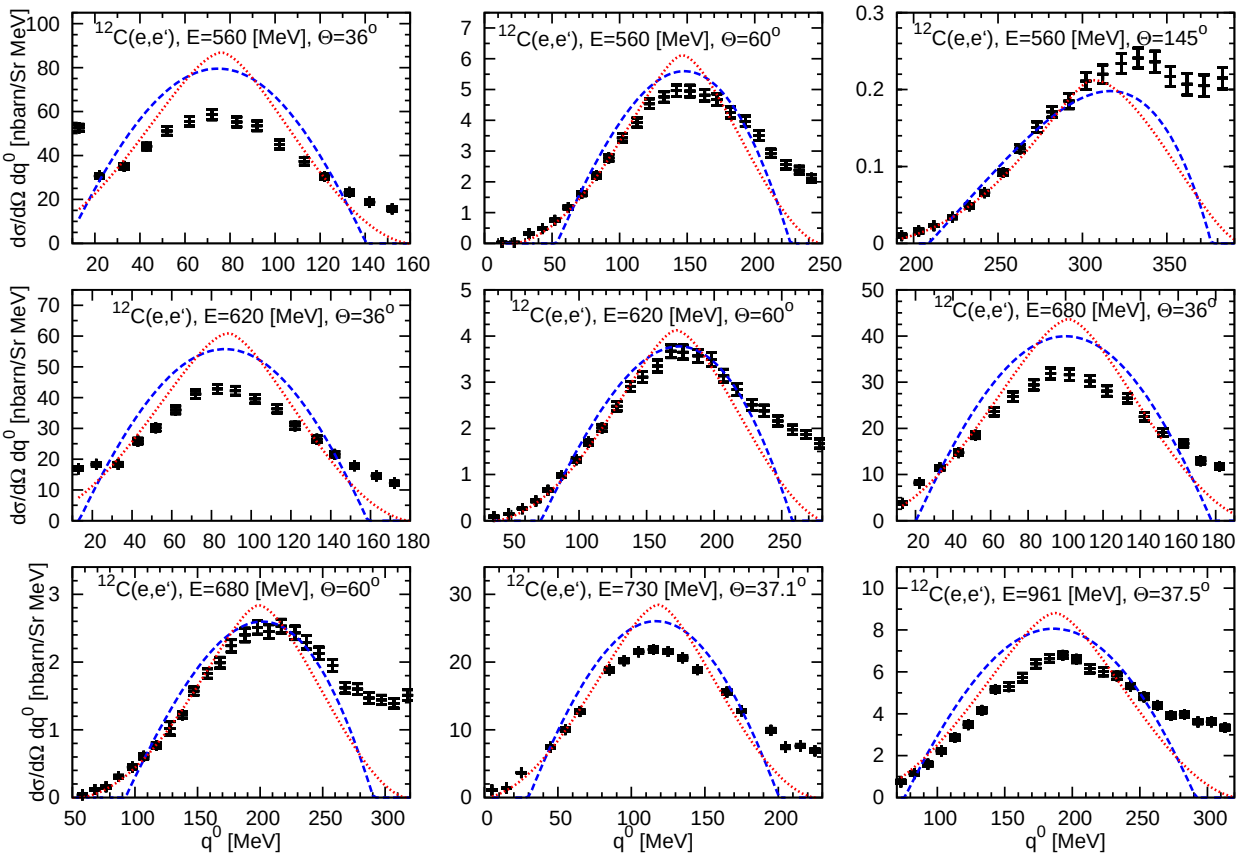

Figure 14: Relativistic local (dotted red lines) and global (dashed blue lines) Fermi gas quasielastic double-differential cross sections for inclusive electron scattering off carbon. Mean $k_F \approx 206$ MeV for global FG and $B = 17$ MeV in both cases. Data (black points with error bars) taken from Ref. [117] (electron energy up to 680 MeV), Ref. [118] (electron energy 730 MeV) and Ref. [119] (electron energy 961 MeV). Approximate momentum transfer $|\boldsymbol{q}|$ at the quasielastic peak is from the left to right and top to bottom: 330, 503, 780, 370, 555, 400, 605, 440 and 585 MeV.

The above analytic formula can be used to perform a quick check of FG/LFG QE scattering predictions against available experimental data. An alternative method of obtaining it, the direct contraction of tensors, is shown in Appendix D.

We have plotted some example double differential cross section calculated within global and local Fermi gas models for inclusive scattering off carbon. They are shown in the Fig. 14. We use here the Galster electromagnetic form factor set given in Appendix E.1. For the global FG we have calculated mean momentum from LFG distribution. In both cases we use the same constant binding energy. The local Fermi gas seems to give a better overall agreement with the data, but in both cases discrepancies are large. We see, that the bigger the momentum transfer at the quasielastic peak is, the better agreement with data we have. The worst agreement is seen for ($E = 560$ MeV, $\Theta = 36^o$) and for ($E = 630$ MeV, $\Theta = 36^o$), where the momentum transfer seems to be below the impulse approximations applicability limit. This is confirmed by the presence of sudden cross section increase with dropping energy transfer at low energy transfer slopes, which means the scattering is described there by collective phenomena. Nevertheless, one has to go beyond the simple FG model in order

to get a realistic description of QE scattering. Unfortunately, most of the present neutrino experiments are preferring to use FG in oscillation analysis due to its simplicity giving a high speed of event production in MC simulations. This is not exactly the case in T2K, which takes into account also the spectral function effects using the data sets created by Wroclaw group with NuWro [8]. They also work on their own implementation of SF. One has to keep in mind, that it is impossible to reproduce any collective excitations with SF, as it is formulated within the impulse approximation formalism.

4.4 Spectral function

In the previous section we have discussed the simple Fermi gas model, which treats the nucleus as an infinite Fermi sea of noninteracting nucleons. In reality it is well known, that nucleon-nucleon correlations are strong. There are several models trying to take into account a realistic description of nuclear ground and excited states. In the first approach one can construct the shell model nucleon orbitals, which correspond to the solutions to Schrödinger/Dirac equations in a central mean field potential. This approach gives a rather realistic spectrum of nucleon energy levels, but it fails to reproduce the electron scattering data, unless one assumes the valence nucleon orbital occupational number to be at the level of 80% [120, 121]. The deviation from fully occupied states arises from nucleon-nucleon correlations, which are missing in the mean-field solutions to the shell model.

These correlations can be divided into two basic classes. The long range correlations are responsible for collective nuclear excitation, like giant resonances, which occur at low energy and momentum transfers (tens of MeV). In this kinematic region leptonic probes interact with multiple nucleons simultaneously and these interactions can not be described by the means of impulse approximation. For higher lepton energies we encounter so-called "short range correlations" (SRC), which are connected to the nucleon-nucleon repulsive force at close range interactions. They lead to creation of nucleon pairs with high relative momentum.

We would like to give an idea, how one can describe the spectral function in the framework of NMBT. This requires a short introduction to the topic, which is not very familiar to particle physicists. We will start wit the basic definitions and formulas of propagators (Green functions) and the scalar response of nuclei. For simplicity we will omit the isospin indices.

4.4.1 Nucleon propagator in the NMBT

We shall now go beyond the approximations given by Eqs. (4.41) and (4.45). The relativistic field-theoretical formulation is not a good starting point for microscopic calculations of nuclear many-body problem. Most of the effects discussed here occurs at energy scales, where the exactly relativistic treatment of bound nucleon wave functions is not a necessity. Moreover, the plane wave basis of Dirac fermions is rather useless in solving a many-body bound state problem and one would have to use the relativistic fermionic wave functions in spherical basis. In order to simplify the considerations we shall work here within the nonrelativistic nuclear many-body theory formalism. The definition of the Green function is almost the same, as in the relativistic QFT:

$$iG_{\alpha\beta}(x',x) \equiv \left\langle \psi_0^A \left| T\left\{ \hat{\psi}_\alpha(x') \hat{\psi}^\dagger_\beta(x) \right\} \right| \psi_0^A \right\rangle . \tag{4.91}$$

Here $\left|\psi_0^A\right\rangle$ denotes the ground state of A-body system. The difference is, that here we have two-component spinor field operators with no antiparticle part. For translationally invariant systems we have a plane-wave solution to a free Schrödinger equation:

$$
\begin{aligned}
i\partial_t\psi(\boldsymbol{x},t) &= \frac{\nabla^2}{2m}\psi(\boldsymbol{x},t) && (4.92)\\
\psi_\alpha(\boldsymbol{x},t) &= \frac{1}{\sqrt{\Omega}}\sum_{\boldsymbol{k}} c_{\boldsymbol{k}\alpha}e^{-i(E_k t-\boldsymbol{k}\boldsymbol{x})} = \psi_\alpha(x). && (4.93)
\end{aligned}
$$

with Ω being the quantization space volume. The operators $c_{\boldsymbol{k}\alpha}$ annihilate a fermion with momentum $\boldsymbol{k}$ and spin α. These operators satisfy standard anticommutation relations:

$$
\left\{c_{\boldsymbol{k},s}, c^\dagger_{\boldsymbol{k}',s'}\right\} = \delta_{\boldsymbol{k}\boldsymbol{k}'}\delta_{ss'} \tag{4.94}
$$

We use the letter "c" in order to avoid confusion with relativistic Dirac field operators. All techniques, like the time-ordered products, perturbative expansion of the S-matrix and Wick's theorem exist in the NMBT as well. The main difference is that one uses nonrelativistic representation of matter fields and potentials instead of gauge bosons. A good description can be found in the textbook of Fetter and Walecka [122], in this paragraph we shall follow the considerations from chapter 7.
We introduce here the spectral representation of a NMBT Green function. We can evaluate the following type type of two-point Green function for a generic A-body system ground state:

$$
\begin{aligned}
iG_{\alpha\beta}(x',x) &= \left\langle\psi_0^A\left|\hat\psi_\alpha(x')\hat\psi^\dagger_\beta(x)\right|\psi_0^A\right\rangle\Theta(t'-t) + \\
&- \left\langle\psi_0^A\left|\hat\psi^\dagger_\beta(x)\hat\psi_\alpha(x')\right|\psi_0^A\right\rangle\Theta(t-t') = \\
&= \sum_n\Big[\left\langle\psi_0^A\left|\hat\psi_\alpha(x')\right|\psi_n^{A+1}\right\rangle\left\langle\psi_n^{A+1}\left|\hat\psi^\dagger_\beta(x)\right|\psi_0^A\right\rangle\Theta(t'-t) + \\
&- \left\langle\psi_0^A\left|\hat\psi^\dagger_\beta(x)\right|\psi_n^{A-1}\right\rangle\left\langle\psi_n^{A-1}\left|\hat\psi_\alpha(x')\right|\psi_0^A\right\rangle\Theta(t-t')\Big]. && (4.95)
\end{aligned}
$$

Where we have inserted the complete set of states for systems containing $A\pm 1$ particles $\sum_n|\psi_n^{A\pm1}\rangle\langle\psi_n^{A\pm1}|$ between the field operators. In general, they may have different excitation spectra. We are considering translationally invariant systems with field operators given by Eq. (4.92). We can use the Heisenberg equations of motion:

$$
\hat O(x) = e^{i\hat P x}O(0)e^{-i\hat P x} \tag{4.96}
$$

in order to extract the spatial dependence out of matrix elements.

$$
\begin{aligned}
&iG_{\alpha\beta}(x'-x) = \\
&= \sum_n\Big[\left\langle\psi_0^A\left|\hat\psi_\alpha(0)\right|\psi_n^{A+1}\right\rangle\left\langle\psi_n^{A+1}\left|\hat\psi^\dagger_\beta(0)\right|\psi_0^A\right\rangle e^{-i(E_n^{A+1}-E_0^A)(t'-t)}e^{i\boldsymbol{p}_{\boldsymbol{n}}^{\boldsymbol{A+1}}(\boldsymbol{x}'-\boldsymbol{x})}\Theta(t'-t) + \\
&- \left\langle\psi_0^A\left|\hat\psi^\dagger_\beta(0)\right|\psi_n^{A-1}\right\rangle\left\langle\psi_n^{A-1}\left|\hat\psi_\alpha(0)\right|\psi_0^A\right\rangle e^{-i(E_n^{A-1}-E_0^A)(t-t')}e^{i\boldsymbol{p}_{\boldsymbol{n}}^{\boldsymbol{A-1}}(\boldsymbol{x}-\boldsymbol{x}')}\Theta(t-t')\Big]. && (4.97)
\end{aligned}
$$

We assume here, that the initial state has zero momentum, *i. e.* $\boldsymbol{p}_{\boldsymbol{0}}^{\boldsymbol{A}} = 0$. In translationally invariant system Green functions depend only on the coordinate difference, hence the

replacement $G(x',x) \to G(x'-x)$. We can easily get the Fourier representation of this function:

$$
\begin{aligned}
iG_{\alpha\beta}(\boldsymbol{p},p^0) = & \int d^4(x'-x)e^{i\left(p^0(t'-t)-\boldsymbol{p}(\boldsymbol{x'}-\boldsymbol{x})\right)} \cdot \\
& \cdot \sum_n \Big[\Big\langle \psi_0^A \Big| \hat{\psi}_\alpha(0) \Big| \psi_n^{A+1} \Big\rangle \Big\langle \psi_n^{A+1} \Big| \hat{\psi}_\beta^\dagger(0) \Big| \psi_0^A \Big\rangle \cdot \\
& \cdot e^{-i(E_n^{A+1}-E)(t'-t)} e^{i\boldsymbol{p_n^{A+1}}(\boldsymbol{x'}-\boldsymbol{x})} \Theta(t'-t) + \\
& - \Big\langle \psi_0^A \Big| \hat{\psi}_\beta^\dagger(0) \Big| \psi_n^{A-1} \Big\rangle \Big\langle \psi_n^{A-1} \Big| \hat{\psi}_\alpha(0) \Big| \psi_0^A \Big\rangle \cdot \\
& \cdot e^{-i(E_n^{A-1}-E)(t-t')} e^{i\boldsymbol{p_n^{A-1}}(\boldsymbol{x}-\boldsymbol{x'})} \Theta(t-t') \Big] .
\end{aligned} \tag{4.98}
$$

We shall use the identity:

$$
\int dx \Theta(\pm x) e^{ip^0 x} = \frac{\pm i}{p^0 \pm i\varepsilon} \tag{4.99}
$$

and perform the spatial integral. The final form of the Green function is as follows:

$$
\begin{aligned}
G_{\alpha\beta}(\boldsymbol{p},p^0) &= \Omega \sum_n \delta_{\boldsymbol{p},\boldsymbol{p_n^{A+1}}} \frac{\Big\langle \psi_0^A \Big| \hat{\psi}_\alpha(0) \Big| \psi_n^{A+1} \Big\rangle \Big\langle \psi_n^{A+1} \Big| \hat{\psi}_\beta^\dagger(0) \Big| \psi_0^A \Big\rangle}{p^0 - (E_n^{A+1} - E_0^A) + i\varepsilon} + \\
&+ \Omega \sum_n \delta_{-\boldsymbol{p},\boldsymbol{p_n^{A-1}}} \frac{\Big\langle \psi_0^A \Big| \hat{\psi}_\beta^\dagger(0) \Big| \psi_n^{A-1} \Big\rangle \Big\langle \psi_n^{A-1} \Big| \hat{\psi}_\alpha(0) \Big| \psi_0^A \Big\rangle}{p^0 + (E_n^{A-1} - E_0^A) - i\varepsilon}.
\end{aligned} \tag{4.100}
$$

This is the so-called Lehmann spectral representation of the Green function. The form of Green function from Eq. (4.100) holds for all systems with time-independent Hamiltonian.[8] The spatially uniform system is needed for us to introduce spectral functions in the future. Using the momentum Dirac delta functions and form of field operators given by Eq. (4.92) one can see, that this Green function has nonzero contribution only from field modes carrying momentum $\boldsymbol{p}$:

$$
\begin{aligned}
G_{\alpha\beta}(\boldsymbol{p},p^0) &= \sum_n \frac{\Big\langle \psi_0^A \left| c_{\boldsymbol{p}\alpha} \right| \psi_n^{A+1}, \boldsymbol{p} \Big\rangle \Big\langle \psi_n^{A+1}, \boldsymbol{p} \Big| c_{\boldsymbol{p}\beta}^\dagger \Big| \psi_0^A \Big\rangle}{p^0 - (E_n^{A+1} - E_0^A) + i\varepsilon} + \\
&+ \sum_n \frac{\Big\langle \psi_0^A \Big| c_{\boldsymbol{p}\beta}^\dagger \Big| \psi_n^{A-1}, -\boldsymbol{p} \Big\rangle \Big\langle \psi_n^{A-1}, -\boldsymbol{p} \left| c_{\boldsymbol{p}\alpha} \right| \psi_0^A \Big\rangle}{p^0 + (E_n^{A-1} - E_0^A) - i\varepsilon}.
\end{aligned} \tag{4.102}
$$

[8] In general, the system does not have to be translationally invariant. This allows us to perform the time Fourier transformation:

$$
\begin{aligned}
G_{\alpha\beta}(\boldsymbol{x'},\boldsymbol{x},p^0) &= \sum_n \frac{\Big\langle \psi_0^A \Big| \hat{\psi}_\alpha(\boldsymbol{x'}) \Big| \psi_n^{A+1} \Big\rangle \Big\langle \psi_n^{A-1} \Big| \hat{\psi}_\beta^\dagger(\boldsymbol{x}) \Big| \psi_0^A \Big\rangle}{p^0 - (E_n^{A+1} - E_0^A) + i\varepsilon} + \\
&+ \sum_n \frac{\Big\langle \psi_0^A \Big| \hat{\psi}_\beta^\dagger(\boldsymbol{x}) \Big| \psi_n^{A-1} \Big\rangle \Big\langle \psi_n^{A-1} \Big| \hat{\psi}_\alpha(\boldsymbol{x'}) \Big| \psi_0^A \Big\rangle}{p^0 + (E_n^{A-1} - E_0^A) - i\varepsilon}
\end{aligned} \tag{4.101}
$$

but transformation of the spatial coordinates have to be performed separately for x and x'.

We can also assume, that for the systems with rotational invariance of ground state and Hamiltonian Green functions are diagonal in the spin indices and the spin dependence factors out:

$$\begin{aligned} G_{\alpha\beta}(\boldsymbol{p}, p^0) &= \sum_n \frac{\left\langle \psi_0^A \left| c_{\boldsymbol{p}} \right| \psi_n^{A+1}, \boldsymbol{p} \right\rangle \left\langle \psi_n^{A+1}, \boldsymbol{p} \left| c_{\boldsymbol{p}}^\dagger \right| \psi_0^A \right\rangle}{p^0 - (E_n^{A+1} - E_0^A) + i\varepsilon} \delta_{\alpha\beta} + \\ &+ \sum_n \frac{\left\langle \psi_0^A \left| c_{\boldsymbol{p}}^\dagger \right| \psi_n^{A-1}, -\boldsymbol{p} \right\rangle \left\langle \psi_n^{A-1}, -\boldsymbol{p} \left| c_{\boldsymbol{p}} \right| \psi_0^A \right\rangle}{p^0 + (E_n^{A-1} - E_0^A) - i\varepsilon} \delta_{\alpha\beta} = \\ &= G(\boldsymbol{p}, p^0) \delta_{\alpha\beta} \end{aligned} \tag{4.103}$$

We will be able to simplify some of the future considerations by dropping the spin indices as well.

4.4.2 Scalar response of nuclear matter

The NMBT nuclear scalar response function for given energy and momentum transfer $(q^0, \mathbf{q})$ is defined as:

$$S(\mathbf{q}, q^0) = \frac{1}{\pi} \Im \left\langle \psi_0^A \left| \rho_{\mathbf{q}}^\dagger \frac{1}{H - E_0^A - q^0 - i\epsilon} \rho_{\mathbf{q}} \right| \psi_0^A \right\rangle \tag{4.104}$$

where nucleon density fluctuation induced by the probe is $\rho_{\mathbf{q}} = \sum_{\mathbf{k}} c_{\mathbf{k}+\mathbf{q}} c_{\mathbf{k}}^\dagger$. For the sake of simplicity we assume spin- and isospin-independence in all of hereby calculations. In the above equation H denotes the Hamiltonian of our system and E_0^A its ground level energy of A-body system (nucleus). The scalar response function defies the way nuclear matter reacts to an external scalar probe, which deposites four-momentum q^μ. This is basically what we need in the computation of the lepton-nucleus cross section in the one-body current approximation. We assume that $q^0 \geq 0$. We observe that from the definition of $\rho_{\mathbf{q}}$ it follows that:

$$\rho_{\mathbf{q}}^\dagger = \rho_{-\mathbf{q}}. \tag{4.105}$$

Following the Fetter-Walecka textbook, chapter 17, we introduce a complete set of nucleus states:

$$\mathbf{1} = \sum_n |n\rangle\langle n| \tag{4.106}$$

satisfying $H|n\rangle = E_n |n\rangle$, obtaining:

$$\begin{aligned} S(\mathbf{q}, q^0) &= \frac{1}{\pi} \Im \sum_n \left\langle \psi_0^A \left| \rho_{\mathbf{q}}^\dagger |n >< n| \frac{1}{H - E_0^A - q^0 - i\epsilon} \rho_{\mathbf{q}} \right| \psi_0^A \right\rangle = \\ &= \frac{1}{\pi} \Im \sum_n \frac{\left\langle \psi_0^A \left| \rho_{\mathbf{q}}^\dagger \right| n \right\rangle \left\langle n \left| \rho_{\mathbf{q}} \right| \psi_0^A \right\rangle}{E_n - E_0^A - q^0 - i\epsilon} = \\ &= \frac{1}{\pi} \Im \sum_n \left(\frac{\left\langle \psi_0^A \left| \rho_{\mathbf{q}}^\dagger \right| n \right\rangle \left\langle n \left| \rho_{\mathbf{q}} \right| \psi_0^A \right\rangle}{E_n - E_0^A - q^0 - i\epsilon} - \frac{\left\langle \psi_0^A \left| \rho_{\mathbf{q}} \right| n \right\rangle \left\langle n \left| \rho_{\mathbf{q}}^\dagger \right| \psi_0^A \right\rangle}{E_0^A - E_n - q^0 + i\epsilon}. \right) \end{aligned} \tag{4.107}$$

We have added the term which is always equal zero due to the fact, that for the physical processes $q^0 > 0$, and $E_0^A - E_n < 0$ from the definition of an excited state. The reason is that we would like to express the scalar response function by the means of scalar (*i. e.* no vector or axial structure at external vertices) polarization tensor. We define now the scalar polarization tensor as:

$$i\Pi^s(x,y) \equiv \left\langle \psi_0^A \left| T\rho(\boldsymbol{x},x^0)\rho(\boldsymbol{y},y^0) \right| \psi_0^A \right\rangle = \left\langle \psi_0^A \left| T\psi^\dagger(x)\psi(x)\psi^\dagger(y)\psi(y) \right| \psi_0^A \right\rangle . \quad (4.108)$$

The above form of the tensor is very similar to Eq. (4.33), but it assumes a more general spatially non-uniform system at this point. Actually, these two tensors are almost identical objects if one notices that if one removes the Dirac vertex structure from one-body currents (*e. g.* from Eq. (4.50)) one is left with a one-body state density operator:

$$\rho(x) = \overline{\psi}(x)\psi(x) \quad (4.109)$$

which becomes:

$$\rho(x) = \sum_\alpha \psi_\alpha^\dagger(x)\psi_\alpha(x) \quad (4.110)$$

in the nonrelativistic case. Operators $\rho(\boldsymbol{x})$ is the Fourier transform of $\rho(\boldsymbol{q})$:

$$\rho(\boldsymbol{q}) = \int d^3x \rho(\boldsymbol{x}) e^{i\boldsymbol{xq}}. \quad (4.111)$$

It is important to notice that

$$\rho(\boldsymbol{x}) = \int \frac{d^3q}{(2\pi)^3} \rho(\boldsymbol{q}) e^{-i\boldsymbol{xq}} \quad (4.112)$$

and

$$\rho(\boldsymbol{x})^\dagger = \int \frac{d^3q}{(2\pi)^3} \rho(\boldsymbol{q})^\dagger e^{i\boldsymbol{xq}} = \int \frac{d^3q}{(2\pi)^3} \rho(-\boldsymbol{q}) e^{i\boldsymbol{xq}} = \int \frac{d^3q}{(2\pi)^3} \rho(\boldsymbol{q}) e^{-i\boldsymbol{xq}} = \rho(\boldsymbol{x}). \quad (4.113)$$

The ρ's dependence on time is defined in the Heisenberg picture. From the definition of the polarization tensor (Eq. (4.108) it follows that:

$$\begin{aligned}
i\Pi(x,y) &= \Theta(x^0-y^0) \left\langle \psi_0^A \left| \rho(\boldsymbol{x},x^0)\rho(\boldsymbol{y},y^0) \right| \psi_0^A \right\rangle \\
&+ \Theta(y^0-x^0) \left\langle \psi_0^A \left| \rho(\boldsymbol{y},y^0)\rho(\boldsymbol{x},x^0) \right| \psi_0^A \right\rangle = \\
&= \Theta(x^0-y^0) \left\langle \psi_0^A \left| e^{iHx^0}\rho(\boldsymbol{x})e^{-iHx^0}e^{iHy^0}\rho(\boldsymbol{y})e^{-iHy^0} \right| \psi_0^A \right\rangle + \\
&+ \Theta(y^0-x^0) \left\langle \psi_0^A \left| e^{iHy^0}\rho(\boldsymbol{y})e^{-iHy^0}e^{iHx^0}\rho(\boldsymbol{x})e^{-iHx^0} \right| \psi_0^A \right\rangle = \\
&= \Theta(x^0-y^0) e^{iE_0(x^0-y^0)} \left\langle \psi_0^A \left| \rho(\boldsymbol{x})e^{iH(y^0-x^0)}\rho(\boldsymbol{y}) \right| \psi_0^A \right\rangle + \\
&+ \Theta(y^0-x^0) e^{iE_0(y^0-x^0)} \left\langle \psi_0^A \left| \rho(\boldsymbol{y})e^{iH(x^0-y^0)}\rho(\boldsymbol{x}) \right| \psi_0^A \right\rangle . \quad (4.114)
\end{aligned}$$

We insert the complete set of states and obtain:

$$\begin{aligned}
i\Pi(x,y) &= \Theta(x^0-y^0) \sum_n e^{i(E_0-E_n)(x^0-y^0)} \left\langle \psi_0^A \left| \rho(\boldsymbol{x}) \right| n \right\rangle \left\langle n \left| \rho(\boldsymbol{y}) \right| \psi_0^A \right\rangle + \\
&+ \Theta(y^0-x^0) \sum_n e^{i(E_0-E_n)(y^0-x^0)} \left\langle \psi_0^A \left| \rho(\boldsymbol{y}) \right| n \right\rangle \left\langle n \left| \rho(\boldsymbol{x}) \right| \psi_0^A \right\rangle . \quad (4.115)
\end{aligned}$$

At this point we need the integral representation of the Θ function:

$$\Theta(t) = -\int \frac{dq^0}{2\pi i} \frac{e^{-iq^0 t}}{q^0 + i\epsilon}$$

and we express:

$$\begin{aligned}
\Theta(x^0 - y^0) &= -\int \frac{dq^0}{2\pi i} \frac{e^{-iq^0(x^0-y^0)}}{q^0 + i\epsilon} \\
\Theta(y^0 - x^0) &= \int \frac{dq^0}{2\pi i} \frac{e^{iq^0(y^0-x^0)}}{q^0 - i\epsilon}.
\end{aligned}$$

We get:

$$\begin{aligned}
i\Pi(x,y) &= -\int \frac{dq^0}{2\pi i} \sum_n e^{i(x^0-y^0)((E_0-E_n)-q^0)} \left\langle \psi_0^A \left| \rho(\boldsymbol{x}) \right| n \right\rangle \left\langle n \left| \rho(\boldsymbol{y}) \right| \psi_0^A \right\rangle \frac{1}{q^0 + i\epsilon} + \\
&+ \int \frac{dq^0}{2\pi i} \sum_n e^{i(y^0-x^0)((E_0-E_n)+q^0)} \left\langle \psi_0^A \left| \rho(\boldsymbol{y}) \right| n \right\rangle \left\langle n \left| \rho(\boldsymbol{x}) \right| \psi_0^A \right\rangle \frac{1}{q^0 - i\epsilon} = \\
&= -\int \frac{dq^0}{2\pi i} \sum_n e^{-i(x^0-y^0)q^0} \left\langle \psi_0^A \left| \rho(\boldsymbol{x}) \right| n \right\rangle \left\langle n \left| \rho(\boldsymbol{y}) \right| \psi_0^A \right\rangle \frac{1}{q^0 + (E_0 - E_n) + i\epsilon} + \\
&+ \int \frac{dq^0}{2\pi i} \sum_n e^{i(y^0-x^0)q^0} \left\langle \psi_0^A \left| \rho(\boldsymbol{y}) \right| n \right\rangle \left\langle n \left| \rho(\boldsymbol{x}) \right| \psi_0^A \right\rangle \frac{1}{q^0 + (E_n - E_0) - i\epsilon}. \quad (4.116)
\end{aligned}$$

We use Fourier transforms of the density operator:

$$\begin{aligned}
\rho(\boldsymbol{x}) &= \int \rho(\boldsymbol{q}_1)^\dagger e^{i\boldsymbol{x}\boldsymbol{q}_1} \frac{d^3 q_1}{(2\pi)^3} \\
\rho(\boldsymbol{y}) &= \int \rho(\boldsymbol{q}_2) e^{-i\boldsymbol{y}\boldsymbol{q}_2} \frac{d^3 q_2}{(2\pi)^3}
\end{aligned}$$

and the final expression for the scalar polarization tensor reads:

$$\begin{aligned}
i\Pi(x,y) &= \int \frac{dq^0}{2\pi i} \int \frac{d^3 q_1}{(2\pi)^3} \int \frac{d^3 q_2}{(2\pi)^3} \sum_n e^{-i(x^0-y^0)q^0} e^{i\boldsymbol{x}\boldsymbol{q}_1} e^{-i\boldsymbol{y}\boldsymbol{q}_2} \\
&\left(-\frac{\left\langle \psi_0^A \left| \rho(\boldsymbol{q}_1)^\dagger \right| n \right\rangle \left\langle n \left| \rho(\boldsymbol{q}_2) \right| \psi_0^A \right\rangle}{q^0 + (E_0 - E_n) + i\epsilon} + \frac{\left\langle \psi_0^A \left| \rho(\boldsymbol{q}_2) \right| n \right\rangle \left\langle n \left| \rho(\boldsymbol{q}_1)^\dagger \right| \psi_0^A \right\rangle}{q^0 + (E_n - E_0) - i\epsilon} \right). \quad (4.117)
\end{aligned}$$

The polarization tensor in the momentum space is defined as:

$$i\Pi(x,y) = \int \frac{dq^0}{2\pi} \int \frac{d^3 q_1}{(2\pi)^3} \int \frac{d^3 q_2}{(2\pi)^3} e^{-i(x^0-y^0)q^0} e^{i\boldsymbol{x}\boldsymbol{q}_1} e^{-i\boldsymbol{y}\boldsymbol{q}_2} i\Pi(\boldsymbol{q}_1, \boldsymbol{q}_2, q^0) \quad (4.118)$$

so that

$$i\Pi(\boldsymbol{q}_1, \boldsymbol{q}_2, q^0) = i\sum_n \left(\frac{\left\langle \psi_0^A \left| \rho(\boldsymbol{q}_1)^\dagger \right| n \right\rangle \left\langle n \left| \rho(\boldsymbol{q}_2) \right| \psi_0^A \right\rangle}{q^0 + (E_0 - E_n) + i\epsilon} - \frac{\left\langle \psi_0^A \left| \rho(\boldsymbol{q}_2) \right| n \right\rangle \left\langle n \left| \rho(\boldsymbol{q}_1)^\dagger \right| \psi_0^A \right\rangle}{q^0 + (E_n - E_0) - i\epsilon} \right) \quad (4.119)$$

We conclude that the imaginary part of scalar polarization propagator is proportional to nuclear matter response function:

$$S(\boldsymbol{q}, q^0) = -\frac{1}{\pi} \Im \Pi(\boldsymbol{q}, \boldsymbol{q}, q^0). \quad (4.120)$$

This identity is going to be useful in the derivation of nuclear SF.

4.4.3 Derivation of the spectral function

In Ref. [37] the NMBT nuclear scalar response function for given energy and momentum transfer $(q^0, \mathbf{q})$ has been expressed by a braid of particle and hole spectral functions:

$$S(\mathbf{q}, q^0) = \int \frac{d^3p}{(2\pi)^3} \int dE S_p(\boldsymbol{q}+\boldsymbol{p}, E-q^0) S_h(p, E). \tag{4.121}$$

which are defined as:

$$\begin{aligned} S_h(\boldsymbol{k}, E) &= \sum_n \left| \left\langle \psi_n^{A-1} \left| c_{\boldsymbol{k}} \right| \psi_0^A \right\rangle \right|^2 \delta(E+\varepsilon_n^-) \\ S_p(\boldsymbol{k}, E) &= \sum_n \left| \left\langle \psi_n^{A+1} \left| c_{\boldsymbol{k}}^\dagger \right| \psi_0^A \right\rangle \right|^2 \delta(E+\varepsilon_n^+). \end{aligned} \tag{4.122}$$

In the above formulas $\left|\psi_0^A\right\rangle$ denotes the ground state of nuclear N-particle system and $\left\langle\psi_n^{N\pm1}\right|$ denote the n-th excited state of $N \pm 1$ nucleon system. The energies of the excited states are defined as:

$$\begin{aligned} \varepsilon_n^+ &\equiv E_n^{A+1} - E_0^A \\ \varepsilon_n^- &\equiv E_0^N - E_n^{A-1}. \end{aligned} \tag{4.123}$$

The hole spectral function $S_h(p, E)$ describes probability that the probe (here-electron or neutrino) interacts with a nucleon described by momentum $\boldsymbol{p}$ and removal energy E from the initial nucleus. In this manner one leaves a hole state with quantum numbers corresponding to the removed nucleon. The particle spectral function is the corresponding probability of the outgoing nucleon to occupy final state with momentum $\boldsymbol{p}+\boldsymbol{q}$ and energy $q^0 - E$. This is basically what we need in the computation of the lepton-nucleus cross section in the one-body current approximation. We assume that $q^0 \geq 0$. The hole SF arises naturally in the calculations of the neutrino QE cross section in the PWIA [123] *i. e.* assuming that the nucleon in the final state leaves the nucleus after primary interaction with no FSI effects. We would like to derive also its particle part.

The right- hand side of Eq. (4.121) can be derived using the one loop contribution to polarization propagator with fully dressed particle propagators. For simplicity we shall use consider only the spin/isospin-independent interaction.

We are looking now for the *scalar* response of the nuclear matter, hence the vertex, in which the 4-momentum transfer enters the system is structureless. Under the conditions mentioned in previous paragraph we write down the polarization tensor for translationally invariant system with time-independent Hamiltonian:

$$\Pi^s(q) \equiv i \int d^4x e^{iqx} \left\langle \psi_0^A \left| T\psi^\dagger(x)\psi(x)\psi^\dagger(0)\psi(0) \right| \psi_0^A \right\rangle \tag{4.124}$$

which can be expressed in the interaction picture as:

$$\Pi^s(q) \equiv i\int d^4x e^{iqx} \overline{\sum_i} \left\langle \psi_0^A \left| T\left\{ \psi_I^\dagger(x)\psi_I(x)\psi_I^\dagger(0)\psi_I(0) \exp\left(-i\int d^4y \hat{H}_{int.}(y) \right) \right\} \right| \psi_0^A \right\rangle . \tag{4.125}$$

In order to derive the nuclear SF we shall take into account terms, which can be treated as a single nucleon loop. The difference to calculations presented for RFG model in section

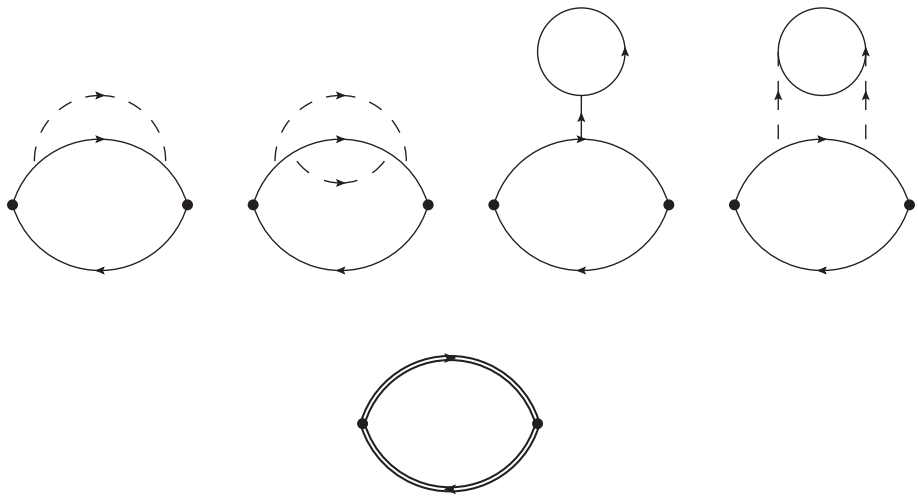

Figure 15: (Top) Example Feynman diagrams giving rise to the nuclear spectral function in the language of polarization propagator. The scalar line represents the effective nucleon-nucleon interaction of NMBT, solid lines represent nucleons. (Bottom) One-loop diagram representing the SF response, where the double lines represent nucleon propagators dressed in all the above self-interactions. This is the main difference with situation from Fig. 13.

4.3 is that now we do not limit ourselves to the lowest order free nucleon propagators, but we also take into account also the Feynman diagrams giving rise to nucleon self-energy. In general, these can be infinite sum of diagrams, which modify free propagator by means of the Dyson equation (which will be explained in more details). This situation is depicted in Fig. 15. Using the same steps as in section 4.3 one can write down the following polarization propagator:

$$\Pi^{s(1)}(\mathbf{q}, q^0) = i \int \frac{d^4p}{(2\pi)^4}\, iG(\mathbf{p}+\mathbf{q}, q^0+p_0)\; iG(\mathbf{p}, p_0) \tag{4.126}$$

where $G(\boldsymbol{p}, p^0)$ are scalar parts of nucleon propagator defined in Eq. (4.103). The index $s(1)$ stands for "one-loop scalar". We can insert now the Lehmann representation of propagator into the one-loop polarization propagator from Eq. (4.126). We obtain:

$$\begin{aligned} i\Pi^{s(1)}(\mathbf{q}, q^0) &= \int \frac{d^4p}{(2\pi)^4} \sum_{m,n} \Bigg\{ \Bigg[\frac{\langle \psi_0^A | c_{\boldsymbol{p}+\boldsymbol{q}} | \psi_m^{A+1} \rangle \langle \psi_m^{A+1} | c^\dagger_{\boldsymbol{p}+\boldsymbol{q}} | \psi_0^A \rangle}{q^0 + p_0 - \varepsilon_m^+ + i\eta} + \\ &+ \frac{\langle \psi_0^A | c^\dagger_{\boldsymbol{p}+\boldsymbol{q}} | \psi_m^{A-1} \rangle \langle \psi_m^{A-1} | c_{\boldsymbol{p}+\boldsymbol{q}} | \psi_0^A \rangle}{q^0 + p_0 - \varepsilon_m^- - i\eta} \Bigg] \times \\ &\times \Bigg[\frac{\langle \psi_0^A | c_{\boldsymbol{p}} | \psi_n^{A+1} \rangle \langle \psi_n^{A+1} | c^\dagger_{\boldsymbol{p}} | \psi_0^A \rangle}{p_0 - \varepsilon_n^+ + i\eta} + \\ &+ \frac{\langle \psi_0^A | c^\dagger_{\boldsymbol{p}} | \psi_n^{A-1} \rangle \langle \psi_n^{A-1} | c_{\boldsymbol{p}} | \psi_0^A \rangle}{p_0 - \varepsilon_n^- - i\eta} \Bigg] \Bigg\}. \end{aligned} \tag{4.127}$$

As one can see, this function after multiplying all terms in square brackets has four terms

with different pairs of poles.

$$
\begin{array}{llll}
a) \left\{ \begin{array}{lcl} p_0 & = & \varepsilon_m^+ - q^0 - i\eta \\ p_0 & = & \varepsilon_n^+ - i\eta \end{array} \right. & b) \left\{ \begin{array}{lcl} p_0 & = & \varepsilon_m^+ - q^0 - i\eta \\ p_0 & = & \varepsilon_n^- + i\eta \end{array} \right. \\
c) \left\{ \begin{array}{lcl} p_0 & = & \varepsilon_m^- - q^0 + i\eta \\ p_0 & = & \varepsilon_n^+ - i\eta \end{array} \right. & d) \left\{ \begin{array}{lcl} p_0 & = & \varepsilon_m^- - q^0 + i\eta \\ p_0 & = & \varepsilon_n^- + i\eta \end{array} \right.
\end{array}
\tag{4.128}
$$

Two of these terms have poles on the same side of the real axis and two on the opposite

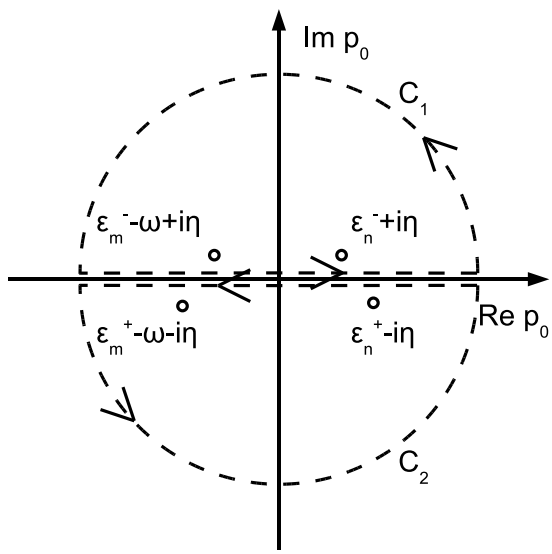

Figure 16: Localization of the poles of one loop insertion to the NMBT polarization propagator

sides. We shall use a theorem from Ref. [122]. For translationally invariant systems:

$$
G(\boldsymbol{k}, q^0) \propto \frac{1}{q^0}, \ |q^0| \to \infty. \tag{4.129}
$$

Now we can prove, that the choice between integration contours C_1 and C_2 (see Fig. 16) is arbitrary, because the convolution of two Green functions is proportional to $\frac{1}{p_0^2}$ when $p_0 \to \infty$. Therefore we shall close the contours in such a way, that terms a) and d) will drop out. This will make the computation significantly simpler. Integration of b) and c) around

C_2 yields:

$$
\begin{aligned}
i\Pi^{s(1)}(\mathbf{q},q^0) &= \oint_{C_2}\frac{dp_0}{2\pi}\int\frac{d^3p}{(2\pi)^3}\sum_{m,n}\left[\frac{\left|\left\langle\psi_m^{A+1}\right|c^\dagger_{\boldsymbol{p}+\boldsymbol{q}}\left|\psi_0^A\right\rangle\right|^2\left|\left\langle\psi_n^{A-1}\right|c_{\boldsymbol{p}}\left|\psi_0^A\right\rangle\right|^2}{(q^0+p_0-\varepsilon_m^+ + i\eta)(p_0-\varepsilon_n^- - i\eta)}+\right.\\
&+\left.\frac{\left|\left\langle\psi_m^{A-1}\right|c_{\boldsymbol{p}+\boldsymbol{q}}\left|\psi_0^A\right\rangle\right|^2\left|\left\langle\psi_n^{A+1}\right|c^\dagger_{\boldsymbol{p}}\left|\psi_0^A\right\rangle\right|^2}{(q^0+p_0-\varepsilon_m^- - i\eta)(p_0-\varepsilon_n^+ + i\eta)}\right]=\\
&=-2\pi i\int\frac{d^3p}{(2\pi)^4}\sum_{m,n}\left[\frac{\left|\left\langle\psi_m^{A+1}\right|c^\dagger_{\boldsymbol{p}+\boldsymbol{q}}\left|\psi_0^A\right\rangle\right|^2\left|\left\langle\psi_n^{A-1}\right|c_{\boldsymbol{p}}\left|\psi_0^A\right\rangle\right|^2}{-q^0+\varepsilon_m^+-\varepsilon_n^- - i\eta}+\right.\\
&+\left.\frac{\left|\left\langle\psi_m^{A-1}\right|c_{\boldsymbol{p}+\boldsymbol{q}}\left|\psi_0^A\right\rangle\right|^2\left|\left\langle\psi_n^{A+1}\right|c^\dagger_{\boldsymbol{p}}\left|\psi_0^A\right\rangle\right|^2}{q^0+\varepsilon_n^+-\varepsilon_m^- - i\eta}\right]=\\
&=-i\int\frac{d^3p}{(2\pi)^3}\sum_{m,n}\left[\frac{\left|\left\langle\psi_m^{A+1}\right|c^\dagger_{\boldsymbol{p}}\left|\psi_0^A\right\rangle\right|^2\left|\left\langle\psi_n^{A-1}\right|c_{\boldsymbol{p}+\boldsymbol{q}}\left|\psi_0^A\right\rangle\right|^2}{q^0+(\varepsilon_m^+-\varepsilon_n^-)-i\eta}\right.\\
&-\left.\frac{\left|\left\langle\psi_m^{A+1}\right|c^\dagger_{\boldsymbol{p}+\boldsymbol{q}}\left|\psi_0^A\right\rangle\right|^2\left|\left\langle\psi_n^{A-1}\right|c_{\boldsymbol{p}}\left|\psi_0^A\right\rangle\right|^2}{q^0-(\varepsilon_m^+-\varepsilon_n^-)+i\eta}\right]
\end{aligned}
\tag{4.130}
$$

where in the last step we have interchanged the dummy summation variables m and n. The minus sign comes from the fact, that if one wants to integrate over C_2 without changing the sign of q^0 one has to use negative orientation of the integration path. The form of Eq. (4.130) is very convenient for writing down the real and imaginary parts of polarization propagator. We can readily give the expression for the imaginary part:

$$
\begin{aligned}
-\frac{1}{\pi}\Im\Pi^{s(1)}(\mathbf{q},q^0) &= \int\frac{d^3p}{(2\pi)^3}\sum_{m,n}\\
&\left[\left|\left\langle\psi_m^{A+1}\right|c^\dagger_{\boldsymbol{p}}\left|\psi_0^A\right\rangle\right|^2\left|\left\langle\psi_n^{A-1}\right|c_{\boldsymbol{p}+\boldsymbol{q}}\left|\psi_0^A\right\rangle\right|^2\delta(q^0+(\varepsilon_m^+-\varepsilon_n^-))+\right.\\
&+\left.\left|\left\langle\psi_m^{A+1}\right|c^\dagger_{\boldsymbol{p}+\boldsymbol{q}}\left|\psi_0^A\right\rangle\right|^2\left|\left\langle\psi_n^{A-1}\right|c_{\boldsymbol{p}}\left|\psi_0^A\right\rangle\right|^2\delta(q^0-(\varepsilon_m^+-\varepsilon_n^-))\right]
\end{aligned}
\tag{4.131}
$$

as well as the real part:

$$
\begin{aligned}
-\frac{1}{\pi}\Re\Pi^{s(1)}(\mathbf{q},q^0) &= \frac{1}{\pi}\int\frac{d^3p}{(2\pi)^3}\mathcal{P}\sum_{m,n}\\
&\left[\frac{\left|\left\langle\psi_m^{A+1}\right|c^\dagger_{\boldsymbol{p}}\left|\psi_0^A\right\rangle\right|^2\left|\left\langle\psi_n^{A-1}\right|c_{\boldsymbol{p}+\boldsymbol{q}}\left|\psi_0^A\right\rangle\right|^2}{q^0+(\varepsilon_m^+-\varepsilon_n^-)}\right.\\
&-\left.\frac{\left|\left\langle\psi_m^{A+1}\right|c^\dagger_{\boldsymbol{p}+\boldsymbol{q}}\left|\psi_0^A\right\rangle\right|^2\left|\left\langle\psi_n^{A-1}\right|c_{\boldsymbol{p}}\left|\psi_0^A\right\rangle\right|^2}{q^0-(\varepsilon_m^+-\varepsilon_n^-)}\right]
\end{aligned}
\tag{4.132}
$$

where the $\mathcal{P}$ stands for the Cauchy's principal value, which has to be taken into account for the continuum part of the ε_m^+ and ε_n^- spectra. We shall now focus on the imaginary part.

The first term will always drop out, even for the non-uniform matter. The reason for that is the impossibility of fulfillment of energy conservation. In our case $q^0 > 0$, but the condition is:

$$\begin{aligned} q^0 &= -\varepsilon_m^+ + \varepsilon_n^- = E_0^A - E_m^{A+1} + E_0^A - E_n^{A-1} \pm E_0^{A-1} \pm E_0^{A+1} = \\ &= \mu^{A-1} - \mu^{A+1} + (E_0^{A+1} - E_m^{A+1}) + (E_0^{A-1} - E_n^{A-1}). \end{aligned} \tag{4.133}$$

The chemical potentials are defined with the ground state energies of systems having one more/one less particle:

$$\begin{aligned} \mu^{A+1} &\equiv E_0^{A+1} - E_0^A \\ \mu^{A-1} &\equiv E_0^A - E_0^{A-1}. \end{aligned} \tag{4.134}$$

The terms in parentheses in Eq. (4.133) are negative for $m, n \neq 0$ and zero otherwise. For the infinite uniform matter $\mu^{A-1} = \mu^{A+1}$. Thus for $q^0 > 0$ the first term always disappears. What we are left with is:

$$\begin{aligned} -\frac{1}{\pi}\Im\Pi^{s(1)}(\mathbf{q}, q^0) &= \int \frac{d^3p}{(2\pi)^3} \sum_{m,n} \left| \left\langle \psi_m^{A+1} \right| c_{\boldsymbol{p}+\boldsymbol{q}}^\dagger \left| \psi_0^A \right\rangle \right|^2 \left| \left\langle \psi_n^{A-1} \right| c_{\boldsymbol{p}} \left| \psi_0^A \right\rangle \right|^2 \\ &\quad \delta(q^0 - (\varepsilon_m^+ - \varepsilon_n^-)). \end{aligned} \tag{4.135}$$

The last identity comes from the Lehman representation of the Green function. Using these definitions one can write the imaginary part of polarization propagator in the language of nuclear spectral functions:

$$\begin{aligned} -\frac{1}{\pi}\Im\Pi^{s(1)}(\mathbf{q}, q^0) &= \int \frac{d^3p}{(2\pi)^3} \int dE \sum_{m,n} \left| \left\langle \psi_m^{A+1} \right| c_{\boldsymbol{p}+\boldsymbol{q}}^\dagger \left| \psi_0^A \right\rangle \right|^2 \delta(E - q^0 + \varepsilon_m^+) \times \\ &\times \left| \left\langle \psi_n^{A-1} \right| c_{\boldsymbol{p}} \left| \psi_0^A \right\rangle \right|^2 \delta(E + \varepsilon_n^-) = \\ &= \int \frac{d^3p}{(2\pi)^3} \int dE S_p(\boldsymbol{q} + \boldsymbol{p}, E - q^0) S_h(\boldsymbol{p}, E). \end{aligned} \tag{4.136}$$

This is (almost) the same formula, as the one used in Omar Benhar's group works (4.121), *e. g.* [37, 38, 36, 39, 40]). The difference is in particle spectral function energy argument (different sign, Benhar has $S_p(\boldsymbol{q} + \boldsymbol{p}, q^0 - E)$). We have also obtained the relation between SF and one-particle Green functions:

$$\begin{aligned} S_h(\boldsymbol{k}, E) &= \frac{1}{\pi}\Im G(\boldsymbol{k}, -E)\Theta(\mu^{A-1} + E) \\ S_p(\boldsymbol{k}, E) &= -\frac{1}{\pi}\Im G(\boldsymbol{k}, -E)\Theta(-(\mu^{A+1} + E)) \end{aligned} \tag{4.137}$$

which is useful in many practical calculations involving SRC contribution. Having these formulas we can try to evaluate the real and imaginary parts of both Green functions, as well as polarization propagators. In the NMBT language it is convenient to use the self-consistent Dyson equation for particle Green function in (nuclear) medium coming from irreducible self-energy insertion (see Fig. 17). The irreducible self-energy comes from irreducible Feynman diagrams, *i. e.* the diagrams, which can not be broken down along the nucleon propagator being dressed in self-energy into two or more subdiagrams. Example irreducible diagrams

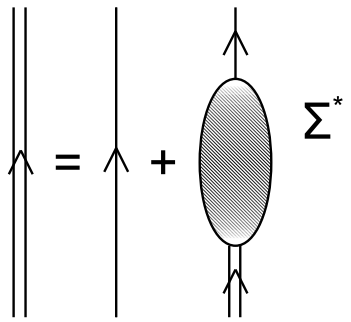

Figure 17: The graphical representation of Dyson equation. The full propagator is a sum of the free propagator and the convolution of full propagator with the irreducible self-energy Σ^*.

can be found in the Fig. 15. In the momentum representation (again the translational invariance is being assumed) this equation has the following form:

$$G_{\alpha\beta}(\boldsymbol{k}, k^0) = G^0_{\alpha\beta}(\boldsymbol{k}, k^0) + G_{\alpha\lambda}(\boldsymbol{k}, k^0)\Sigma^*_{\lambda\mu}(\boldsymbol{k}, k^0)G^0_{\mu\beta}(\boldsymbol{k}, k^0). \tag{4.138}$$

A very important property of this equation is that every insertion to the self energy coming from an irreducible Feynman diagram is automatically summed up to an infinite order. Therefore this method of calculating the Green function is nonperturbative.
To show a simple example we'll assume the spin independence of potential. It is possible to drop the indices and write down an explicit solution to this equation:

$$G(\boldsymbol{k}, k^0) = \frac{1}{[G^0(\boldsymbol{k}, k^0)]^{-1} - \Sigma^*(\boldsymbol{k}, k^0)} \tag{4.139}$$

where the inverted free particle propagator is simply $[G^0(\boldsymbol{k}, k^0)]^{-1} = k^0 - k^0_{\boldsymbol{k}}$. Knowing this one can evaluate the real and imaginary parts of Green function:

$$\begin{aligned}
\Re G(\boldsymbol{k}, k^0) &= \frac{1}{2}\left\{\frac{1}{k^0 - k^0_{\boldsymbol{k}} - \Sigma^*(\boldsymbol{k}, k^0)} + \frac{1}{k^0 - k^0_{\boldsymbol{k}} - (\Sigma^*(\boldsymbol{k}, k^0))^*}\right\} = \\
&= \frac{k^0 - k^0_{\boldsymbol{k}} - \Re\Sigma^*(\boldsymbol{k}, k^0)}{(k^0 - k^0_{\boldsymbol{k}} - \Re\Sigma^*(\boldsymbol{k}, k^0))^2 + (\Im\Sigma^*(\boldsymbol{k}, k^0))^2} \\
\Im G(\boldsymbol{k}, k^0) &= \frac{1}{2}\left\{\frac{1}{k^0 - k^0_{\boldsymbol{k}} - \Sigma^*(\boldsymbol{k}, k^0)} - \frac{1}{k^0 - k^0_{\boldsymbol{k}} - (\Sigma^*(\boldsymbol{k}, k^0))^*}\right\} = \\
&= \frac{\Im\Sigma^*(\boldsymbol{k}, k^0)}{(k^0 - k^0_{\boldsymbol{k}} - \Re\Sigma^*(\boldsymbol{k}, k^0))^2 + (\Im\Sigma^*(\boldsymbol{k}, k^0))^2}.
\end{aligned} \tag{4.140}$$

These identities and the relation of spectral functions to Green function (4.137) are the starting point of calculation of the nuclear medium SRC effect-driven spectral function part. The other part requires detailed analysis of discrete single-nucleon excitations of nuclear system and bases on localized many-body wave functions.

From the technical point of view one introduces the SF by following the replacement in FG integrations: One introduces the hole SF into usual FG integrals with following replacement:

$$\int \frac{d^3p}{(2\pi)^3} \frac{n_N(p)(1-n_N(p+q))}{E(p)E(p+q)} \delta(E(p+q)-E(p)-q^0+B)(\ldots) \rightarrow$$
$$\rightarrow \int \frac{d^3p}{(2\pi)^3} \int dE \frac{1}{E(p)E(p+q)} S_p(|\boldsymbol{p}+\boldsymbol{q}|, E-q^0) S_h(|\boldsymbol{p}|, E)(\ldots) \tag{4.141}$$

In many calculations the particle SF, which is connected to FSI) is neglected and one substitutes:

$$S_p(\boldsymbol{q}+\boldsymbol{p}, E-q^0) \quad \rightarrow \quad (1-n_N(p+q))\delta(E(p+q)-M-q^0+\tilde{E}). \tag{4.142}$$

with $n_N(p+q)$ being the occupation number of nucleon states with momentum $\boldsymbol{p}+\boldsymbol{q}$ and $\tilde{E} \equiv E + \varepsilon^+_{m_0} - E(p+q) + M$ assuming:

$$\left| \left\langle \psi^{A+1}_m \right| c^\dagger_{\boldsymbol{p}+\boldsymbol{q}} \left| \psi^A_0 \right\rangle \right|^2 \quad = \quad \begin{cases} 1-n_N(p+q) & m=m_0 \\ 0 & \text{otherwise} \end{cases} . \tag{4.143}$$

This assumption states, that we may reach only one final particle state, neglecting possible redistribution into different $\left\langle \psi^{A+1}_m \right|$ by FSI. This is the case *e. g.* in Ref. [35]. One introduces the hole SF into usual FG integrals with following replacement:

$$\int \frac{d^3p}{(2\pi)^3} \frac{n_N(p)(1-n_N(p+q))}{E(p)E(p+q)} \delta(E(p+q)-E(p)-q^0+B)(\ldots) \rightarrow$$
$$\rightarrow \int \frac{d^3p}{(2\pi)^3} \int d\tilde{E} \frac{(1-n_N(p+q))}{E(p)E(p+q)} S_h(|\boldsymbol{p}|, \tilde{E}) \delta(E(p+q)-M-q^0+\tilde{E})(\ldots). \tag{4.144}$$

An example plot of hole SF can be found in Fig. 9. Finally, assuming there is only one possible hole state with momentum $\boldsymbol{p}$ and our system is a Fermi gas:

$$\left| \left\langle \psi^{A-1}_n \right| c_{\boldsymbol{p}} \left| \psi^A_0 \right\rangle \right|^2 \quad = \quad \begin{cases} n_N(p) & n=n_0 \\ 0 & \text{otherwise} \end{cases} \tag{4.145}$$

one has to substitute

$$S_p(\boldsymbol{q}+\boldsymbol{p}, \tilde{E}-q^0) \quad \rightarrow \quad n_N(p)\delta(\tilde{E}+E(p)-B-M) \tag{4.146}$$

in order to get back to the usual RFG integration.

5 Spectral function and MiniBooNE M_A fits

So far we have worked within the framework disregarding nuclear many-body wave functions (4.41) and within the De Forest prescription given by Eq. (4.45). We would like to address the questions: how good are these approximations and do they have a large impact on extraction of physical observables from experimental data? We shall present here the work from Ref. [14].

Following the motivations outlined in section 3.4.1 and assuming the MiniBooNE data to be purely quasielastic, we decided to repeat the M_A fit using the nuclear models available in NuWro Monte Carlo generator [14]. The first fit has been performed using FG model. The second one has been performed with a nuclear hole spectral function (see Eq. (4.144), details of the model described in *e. g.* Ref. [40]). In the following paragraphs we shall describe our fitting procedure and main results.

5.1 M_A fits

In order to estimate how reliable is the value of M_A obtained from measurements on a nucleus target a good understanding of all the nuclear effects is required. In the first place, in order to extract the value of the parameter for the neutrino scattering on a *free nucleon*, one assumes that the neutrino nucleus scattering occurs on individual quasi-free nucleons (Impulse Approximation). This is well justified if typical values of the momentum transfer are sufficiently large $q \geq 350 - 400$ MeV/c, some authors assume even $q \geq 500$ MeV/c). To the contrary of what might be expected, in the case of neutrino QE interactions, a fraction of at least $15\% - 20\%$ of the total cross section comes from lower values of the momentum transfer, almost independently of the neutrino energy. For neutrino energies E_ν below 500 MeV the percentage is even higher, as shown in Ref. [34]. This manifests itself as the low Q^2 (typically $Q^2 <\sim 0.1$ GeV^2) problem. On the theoretical side, from the electron scattering data analysis it is known that the correct treatment of nucleus in the low momentum transfer region must account for collective effects (giant resonances) and computational techniques like RPA (or better- CRPA) should be applied [124]. The impact of the limitations of the IA on the extracted value of M_A will be discussed in detail in the next section. An important result of our investigation is that cuts on the momentum transfer make the fitted value of M_A smaller, but the effect is by not strong enough to explain the discrepancy with the old deuterium measurements.

The MiniBooNE experiment has calculated theoretical CCQE cross section within the global FG framework (described in section 4.3) in its M_A fits. This model is commonly chosen by experimental groups because it is determined by only two parameters: Fermi momentum k_F and binding energy B and the resulting cross sections can be expressed by simple analitic formulas. This makes it very easy to implement in MC generators. From the electron scattering experiments it is known that satisfactory agreement between FG and data is reached only for large enough values of the momentum transfer, in the region of the *quasi-elastic peak*. In neutrino experiments we can not avoid the low-q region. However, from a closer investigation of the electron scattering data, it is also known that the FG model is unable to correctly separate the longitudinal and transverse nuclear response functions from the Eq. (4.24).

More sophisticated approaches primarily used to describe nuclear effects in the electron scattering were later applied to neutrino interactions. Many of them are described

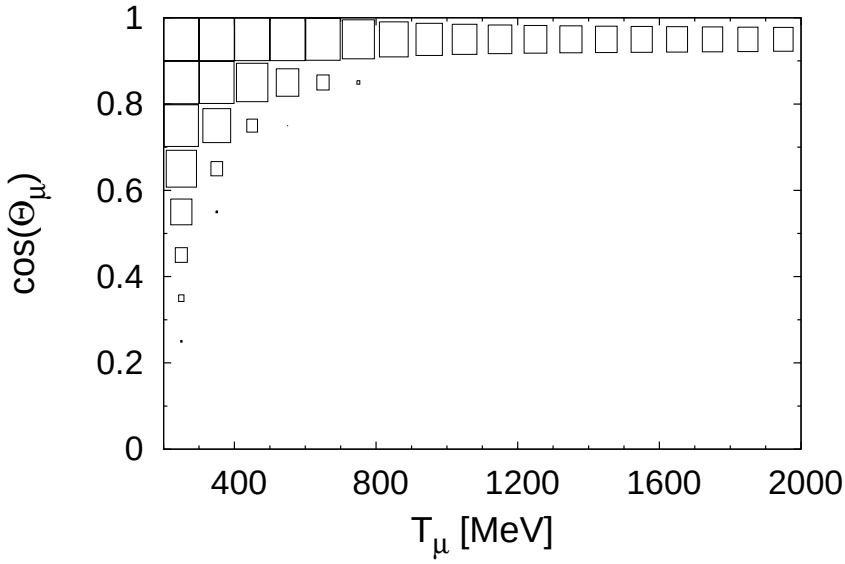

Figure 18: Contribution of events with momentum transfer lower than $q_{\rm cut} = 400$ MeV/c for the spectral function model. For each bin the contribution is proportional to the area.

in Refs. [125, 126, 127]. In our investigation we use the SF approach following Refs. [36] and [128, 129]. In the context of neutrino interactions its use has been advocated by Omar Benhar. The SF model (with FSI effects included) gives a very good agreement with the electron-nucleus cross section data in the quasi-elastic region for momentum transfers larger than ~ 350 MeV according to Refs. [38] and [39]. The available models of SF combine information from the mean field theory (shell model) and a contribution from the short range correlations (SRC). The shell model orbitals are clearly seen as wide slopes in the probability distribution. SRC part dominates for large values of the nucleon momentum. In our investigation we use the implementation of the SF formalism in the NuWro MC events generator [41, 42, 43]. For carbon, oxygen and iron NuWro uses tabularized spectral functions provided by Benhar. There also exist approximate models of SF for medium-sized nuclei like calcium and argon, which have been shown to provide a good agreement with the electron scattering data [130]. The full (hole and particle) SF arises naturally within the polarization tensor formalism. We have shown it on the general level in section 4.4.

5.1.1 Definition of χ^2

The MiniBooNE double differential CCQE cross section data is given in the form of the table in Ref. [11] with 20 bins in $\cos\theta$ and 18 bins in the muon kinetic energy T_μ spanning the region between 200 to 2000 MeV. There are 360 bins altogether and the double differential cross section is non-zero in 137 of them.

The single differential cross section in Q^2 is presented in the form of 17 bins covering the region from 0 to 2 GeV^2.

The fits to M_A are usually done only on the $d\sigma/dQ^2$ data. The MiniBooNE collaboration reported the value $M_A = 1.35 \pm 0.17$ GeV and in the recent paper Butkevich [131] obtained the values 1.37 ± 0.05 and 1.36 ± 0.05 for the two theoretical models used in the analysis

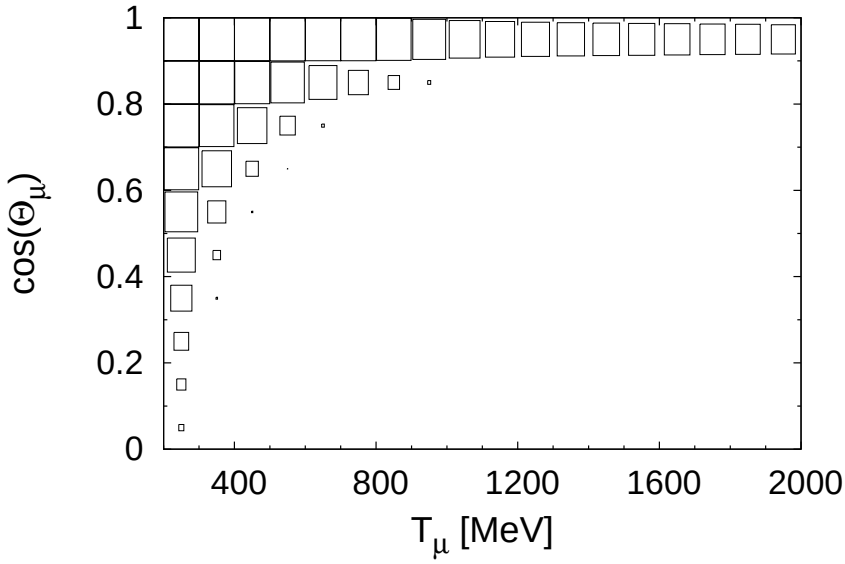

Figure 19: Contribution of events with momentum transfer lower than $q_{\rm cut} = 500$ MeV/c for the spectral function model. For each bin the contribution is proportional to the area.

(RDWIA - relativistic distorted wave impulse approximation and RFG). The agreement is very good, which is an interesting result because RDWIA is a sophisticated model which includes contribution from short range correlated nucleon pairs and corrections from the FSI effects. In the fitting procedure an impact of the overall (correlated) flux uncertainty was not taken into account.

We use the complete set of MiniBooNE data and this was the first M_A fit obtained from the distribution of events in the form of double differential cross section. On the theoretical side we compare two models: Fermi gas and spectral function both implemented in the NuWro MC events generator. In the case of the FG the parameters used in the simulations were: $k_F = 220$ MeV/c and $B = 34$ MeV. The SF approach is parameter free. Pauli blocking is imposed in both models. In the case of SF the Fermi momentum value needed for Pauli blocking was calculated within the local density approximation.

The samples of events were produced by NuWro for both the FG and SF models for the axial mass value changing in steps of 10 MeV in the $1-2$ GeV region.

It is well known that for the same value of M_A FG and SF predict quite different values of the total CCQE cross section and one could expect that the fitting procedure will give rise to very different values of M_A for the two models. In the Ref. [40] the conclusion is drawn that for the SF approach the best agreement with the data is obtained with $M_A = 1.6$ GeV. The total flux-averaged SF CCQE cross section at $M_A = 1.6$ GeV is approximately the same as the total flux-averaged RFG CCQE total cross section at $M_A = 1.4$ GeV.

Despite many efforts there is still a lot of uncertainty in the knowledge of the neutrino flux, see Ref. [132]. MiniBooNE collaboration estimates the overall fully correlated uncertainty as 10.7%. It is known that some other MiniBooNE measurements yield larger than expected cross sections [133] which are difficult to explain with standard theoretical models. On the other hand the reported ratio CCPi+/CCQE is in reasonable agreement with many models [134]. It seems necessary to include in the data analysis also the contribution coming from the fully correlated flux uncertainty. Being given the experimental errors in each bin

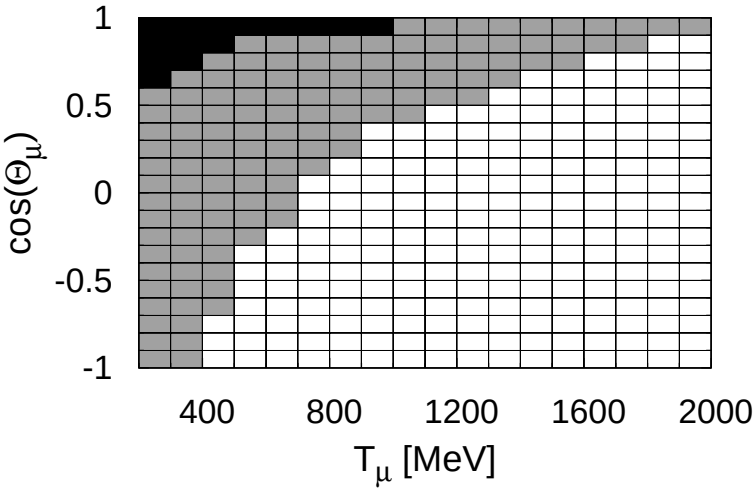

Figure 20: Bins excluded from the fitting procedure for $q_{\rm cut} = 400$ MeV/c are shown in black color. Bins with non-zero cross section measured by MiniBooNE are shown in grey color.

as well as the normalization uncertainty we can define a χ^2 measure. We shall apply the method of D'Agostini [135] and we construct the appropriate χ^2 function:

$$\chi^2(M_A,\lambda) = \sum_{i=1}^{n} \left(\frac{\left(\frac{d^2\sigma}{dT_\mu d\cos\theta}\right)_j^{exp} - \lambda \left(\frac{d^2\sigma}{dT_\mu d\cos\theta}(M_A)\right)_j^{th}}{\Delta\left(\frac{d^2\sigma}{dT_\mu d\cos\theta}\right)_j} \right)^2 + \left(\frac{\lambda^{-1}-1}{\Delta\lambda}\right)^2 . \quad (5.1)$$

$\left(\frac{d^2\sigma}{dT_\mu d\cos\theta}\right)_j^{exp}$ is the measured double differential cross section in the j-th bin with the uncertainty $\Delta\left(\frac{d^2\sigma}{dT_\mu d\cos\theta}\right)_j$ (all the uncertainties are also provided by MiniBooNE). $\left(\frac{d^2\sigma}{dT_\mu d\cos\theta}\right)_j^{th}$ is the theoretical prediction from either RFG or SF model for a fixed value of M_A. $\Delta\lambda = 0.107$ is the overall normalization uncertainty. The similar χ^2 was successfully applied in the reanalysis of the single pion production bubble chamber experiments data in Ref. [47]. It is noticeable, that exactly the same scheme has been adapted later in Ref. [92], where analogous fits have been performed in a model containing also the *npnh* excitations.

We also investigated the possible impact of the boundary bins in which MiniBooNE reported the vanishing cross section. For this aim we added those bins to the analysis and assumed that the uncertainty with which the null cross section is measured is equal to the average of uncertainties from all the neighboring bins. The proposed extension of the fitting procedure allows for a *punishment* of the models/parameter values which give rise to too large predictions in the kinematical region excluded by the MiniBooNE measurements. This extension had a very small impact on the final results, shifting the best fit value of the axial mass by a few MeV only. In what follows we present the results for the χ^2 calculated on the non-zero bins only.

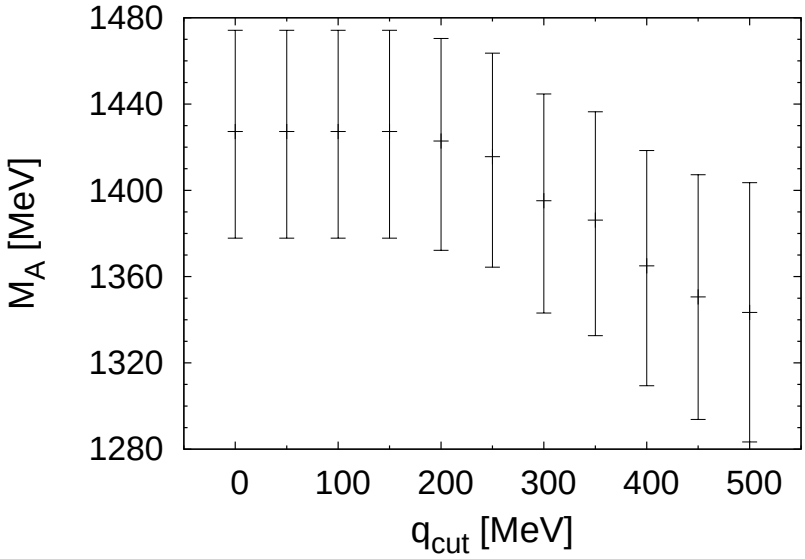

Figure 21: Best fit values of M_A and 1σ regions for SF model as functions of the low momentum transfer cut.

5.1.2 Momentum transfer cut

We propose a further refinement in the analysis. We exclude from the χ^2 expression Eq. (5.1) the bins with large contribution from events with small momentum transfer. The motivation was explained before: one cannot expect that the models based on the IA give reliable results in this kinematical region. In the Ref. [124] it was shown that inclusion of RPA correlations in theoretical model improves significantly the agreement in the distribution of events in the small Q^2 region. We introduce the momentum transfer cut parameter $q_{\rm cut}$ and change its value in steps of 50 MeV/c. The parameter is defined in such a way that the bins for which the contribution from $q < q_{\rm cut}$ is larger than 50% are not included in Eq. (5.1). In the Figs. 18 and 19 we show the contributions of events with the momentum transfer $q < q_{\rm cut} = 400$ MeV/c and $q < q_{\rm cut} = 500$ MeV/c for the SF, in every bin separately. The results for the RFG are very similar and there is no need to show them independently. The bins which are excluded from the fitting procedure are shown in the Fig. 20 as marked in the black color. For every value of $q_{\rm cut}$ the same bins survive for both RFG and SF models. For the value $q_{\rm cut} = 500$ MeV/c there are still 108 bins taken into account in the numerical analysis.

In a recent paper Butkevich [131] concludes that in some bins the predictions of the RDWIA and RFG models do not agree with the data. It is an interesting observation that most of these bins are excluded from our analysis. For example at $q_{\rm cut} = 400$ MeV/c only one bin pointed out by Butkevich is present in our analysis: $T_\mu \in (400, 500)$ MeV and $\cos\theta \in (0.7, 0.8)$.

5.1.3 Main result

Figs. 21 and 22 contain our main discovery: the best fit values of M_A for various choices of $q_{\rm cut}$ for both SF and RFG models. Contrary to what might be expected the values of the best fits for the SF model are only slightly smaller than for the RFG model. The reason is

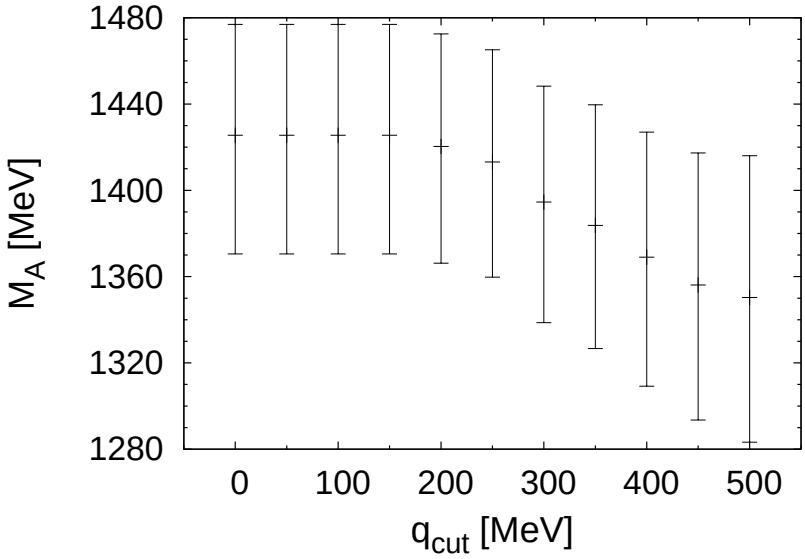

Figure 22: Best fit values of M_A and 1σ regions for RFG model as functions of the low momentum transfer cut.

in the interplay between M_A and λ parameters: the best fit for λ is in the case of SF much larger. For $q_{\rm cut} = 500$ MeV/c χ^2 becomes minimal at $\lambda = 1.06$ for RFG and $\lambda = 1.23$ for SF. The obtained best fit values for RFG and SF are very similar: $M_A = 1350 \pm 66$ MeV for RFG and $M_A = 1343 \pm 60$ MeV for SF. The minimal values of χ^2 are different, in the case of RFG they are always smaller. For example, for $q_{\rm cut} = 500$ MeV/c the minimal values are $\chi^2_{min} = 14.45$ (RFG) and $\chi^2_{min} = 23.2$ (SF). The χ^2/DOF is very small because experimental errors seem to be overestimated. Presumably there is a lot of correlation, but MiniBooNE did not provide the correlation matrix. It is interesting to see that as $q_{\rm cut}$ becomes larger the best fit value of M_A gets smaller, and there is less tension with the old bubble chamber measurements. The decline is noticeable but even if we take the maximal meaningful value of the cut, namely $q_{\rm cut} = 500$ MeV/c, we are still far away from the old world average $M_A = 1.03$ GeV.

In the Fig. 23 we show the two-dimensional $1-$ $3-$ and 5σ regions for $q_{\rm cut} = 500$ MeV/c. Because the best fit scale factors for both models are very different it is possible to show them in one figure. For the comparison we also show the old world average value of the axial mass $M_A = 1.03$ GeV. Our conclusion is that old and new measurements are incompatible, if one treats the data as a true CCQE sample. This is the most important result of our investigation.

We also checked the behavior of the best fits for M_A for even more restrictive cuts in the momentum transfer. We discovered that for $q_{\rm cut} > 550$ MeV/c the best fit values start to increase but simultaneously also the 1σ regions start to grow. The behavior of 1σ regions is what might be expected because as $q_{\rm cut}$ gets larger we loose more and more statistics and the predictions become less precise.

Finally we note that the best fit value for the axial mass from our analysis is very close to the values obtained by MiniBooNE and Butkevich from the 1-dimensional analysis of $d\sigma/dQ^2$. However, without the momentum transfer cut our results for M_A would be higher. The advantage of our analysis is that we use the full information provided by the MiniBooNE

collaboration and not only the Q^2 projection of the results.

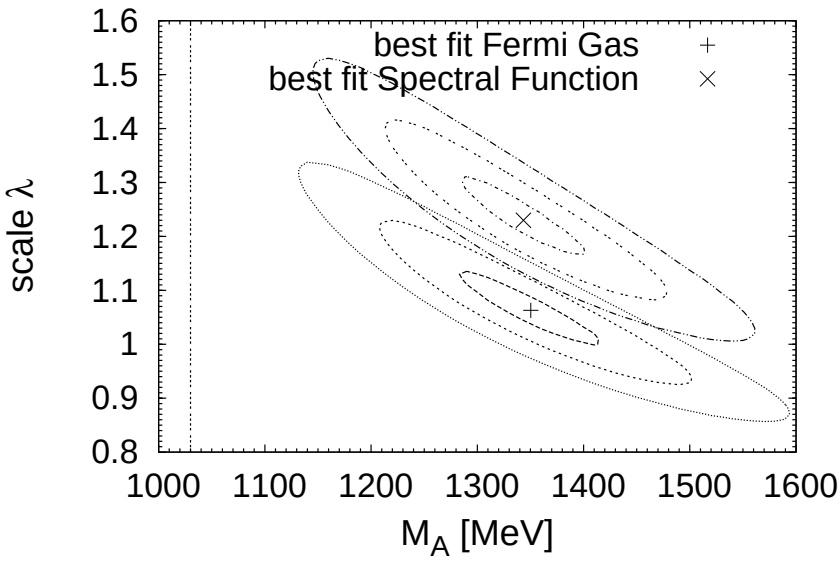

Figure 23: Best fit values of M_A and λ together with 1σ, 3σ, and 5σ regions for the $q_{\rm cut}$ = 500 MeV/c transfer momentum cut. The old M_A world average value is marked with a vertical line.

We compared the true data with the SF predictions for $M_A = 1.03$ GeV and $\lambda = 1$. The difference, shown in Fig. 24, can be treated as the contribution from a new dynamical mechanism going beyond the IA and/or $1p1h$ excitation.

5.2 Conclusions from the MiniBooNE M_A fits

In the comparison with the MiniBooNE CCQE double differential cross section data we used two nuclear models: the simplest nucleus Fermi gas model which is common in MC events generators and much more sophisticated spectral function model which is well tested on the electron scattering data in the quasi-elastic peak region. We eliminated from the discussion the bins dominated by the low momentum transfer events for which the IA based models are known to be unreliable. Our conclusion is that the new data are not compatible with the results from the old bubble chamber experiments on deuterium where the nuclear effects are easily put under control.

It is natural to consider the possibility that the disagreement is caused by the nuclear effects which were not taken into account in the models applied so far. We know from the electron scattering that there is a need for a new dynamical mechanism in the region between quasi-elastic and the Δ peaks, called the "dip" region. It is known that the MEC mechanism in which an electron interacts with a pair of nucleons exchanging a pion adds some cross section in the "dip" region, making the theoretical predictions more realistic in Refs. [107, 91, 92]. The MEC contributes to the transverse response function where the strength is missing. In the MEC reaction two nucleons can be ejected from the nucleus. If an analogous process happened in the case of 1 GeV neutrino scattering, the event would probably be categorized as QE-like. It is unlikely that both nucleons would be detected as they typically carry insufficient kinetic energy. Clearly such events would mislead the

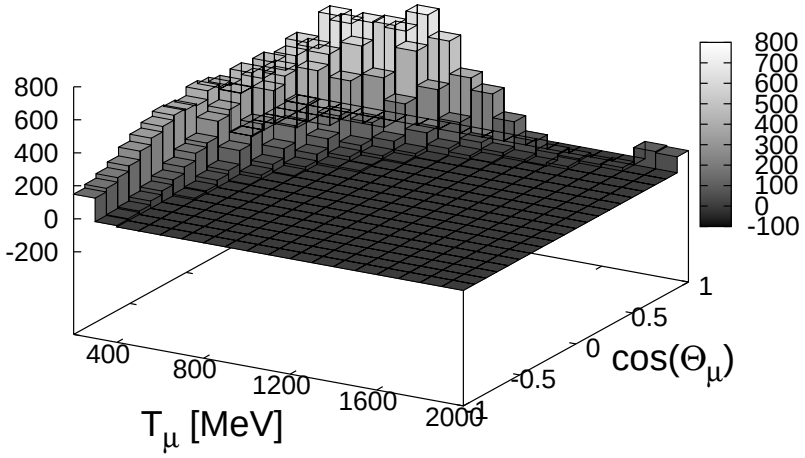

Figure 24: The difference between the double differential cross section measured by MiniBooNE and prediction from the SF model with $M_A = 1.03$ GeV without rescaling. The units are 10^{-41} cm^2/GeV/nucleon.

experimentalist and contribute to the measured CCQE double differential cross section. According to Marteau-Martini computations [91] (group from Lyon) the contribution to the CC cross section neglected in IA models is quite large. They developed the non-relativistic model that includes QE and Δ production primary interactions, RPA correlations, local density effects and also elementary 2p-2h excitations. In the Ref. [136] they have compared their model to MiniBooNE CCQE data, obtaining quite good agreement to the double-differential cross sections with $M_A = 1.03$ GeV. This comes from the fact, that in the case of the neutrino-carbon CCQE process, after averaging over the MiniBooNE beam, the nuclear effects are to increase the cross section per neutron from 7.46 to 9.13, in the units of 10^{-39}cm^2. This includes a reduction of the cross section due to the RPA effects and the increase due to the 2p-2h contribution. A fit to the MiniBooNE data has been done in Ref. [92] by the group of Nieves, Ruiz Simo and Vicente Vacas from IFIC. The have included the RPA effects in the QE channel together with MEC model based on the effective field theory diagrams used for SPP off nucleons in Ref. [46]. They have used the same χ^2 definition, as in Eq. (5.1) and obtained $M_A = 1.077 \pm 0.027$ GeV, which is in a full agreement with PCAC and old experiments on deuterium targets. As for the scale parameter they have obtained $\lambda = 0.917 \pm 0.029$, strongly correlated to M_A. The results from Lyon and IFIC are a strong indication, that one has to include *npnh* dynamics in order to understand the neutrino-nucleus interactions at MiniBooNE/T2K energies. One has to keep in mind, that there exist at least three MEC models, which seem to disagree on the above mentioned details, like the neutrino/antineutrino effects.

6 Single pion production

We would like to address now the SPP problem. The motivation for this research has been outlined in section 3.4.2. We will introduce the SPP formalism on free nucleons discussing both the dynamics of background and resonant contributions, then we will use the same formalism for deuterium target. Discussion about model uncertainties will be made. Finally, we will calculate SPP on atomic nuclei, giving attention to nuclear effects and confronting our results to MiniBooNE SPP data.

6.1 General formalism

We discuss charged current inelastic neutrino scattering off nucleons and nuclear targets. Six channels for single pion production induced by (anti)neutrino-nucleon interaction are considered,

$$\nu_\mu(l) + p(p) \rightarrow \mu^-(l') + \pi^+(k) + p(p') \tag{6.1}$$
$$\nu_\mu(l) + n(p) \rightarrow \mu^-(l') + \pi^0(k) + p(p') \tag{6.2}$$
$$\nu_\mu(l) + n(p) \rightarrow \mu^-(l') + \pi^+(k) + n(p') \tag{6.3}$$
$$\overline{\nu}(l) + n(p) \rightarrow \mu^+(l') + \pi^-(k) + n(p') \tag{6.4}$$
$$\overline{\nu}_\mu(l) + p(p) \rightarrow \mu^+(l') + \pi^0(k) + n(p') \tag{6.5}$$
$$\overline{\nu}(l) + p(p) \rightarrow \mu^+(l') + \pi^-(k) + n(p') \tag{6.6}$$

with l, l', p, p' and k being the neutrino, muon, initial nucleon, final nucleon and pion momenta respectively. For the pion electroproduction we define following channels:

$$e^-(l) + p(p) \rightarrow e^-(l') + \pi^+(k) + n(p') \tag{6.7}$$
$$e^-(l) + p(p) \rightarrow e^-(l') + \pi^0(k) + p(p') \tag{6.8}$$
$$e^-(l) + n(p) \rightarrow e^-(l') + \pi^-(k) + p(p') \tag{6.9}$$
$$e^-(l) + n(p) \rightarrow e^-(l') + \pi^0(k) + n(p'). \tag{6.10}$$

The SPP kinematics together with our notation of all necessary variables is illustrated in Fig. 25. The first process (6.1) on proton is dominated by resonant charged pion production through intermediate $\Delta^{++}(1232)$ state, although non negligible nonresonant background contribution may be still present. The supposed dominance of resonant pion production makes this channel attractive for the analysis of $\Delta(1232)$ properties. The other two channels (Eqs. (6.2) and (6.3)) are assumed to have large nonresonant pion production contribution and thus present more challenge for physicists (but also more interesting information about the single pion production dynamics). The four-momentum transfer is defined as:

$$q^\mu = l - l' = p' + k - p = (q^0, \boldsymbol{q}) \;\; Q^2 \equiv -q^2 \tag{6.11}$$

and the hadronic system invariant mass:

$$W^2 = s = (p+q)^2 = (p'+k)^2. \tag{6.12}$$

Furthermore, we assume the same laboratory frame, as for the quasielastic process, *i. e.* neutrino and muon scattering plane to be the x-z plane and the momentum transfer to be directed along z-axis:

$$\boldsymbol{q} = (0, 0, q). \tag{6.13}$$

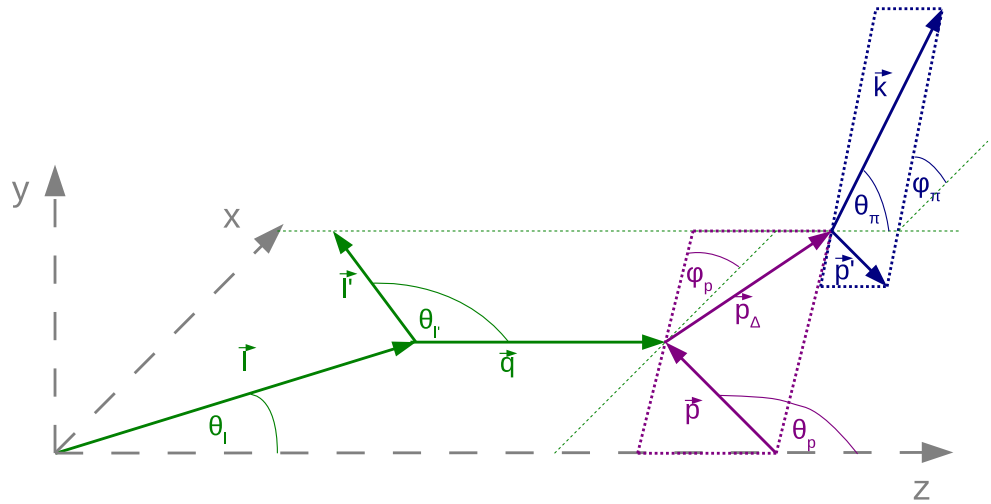

Figure 25: Kinematics and coordinate system for SPP on nucleon. By $\boldsymbol{l}$, $\boldsymbol{l'}$, $\boldsymbol{p}$, $\boldsymbol{p_\Delta}$, $\boldsymbol{p'}$ and $\boldsymbol{k}$ we denote the neutrino, muon, initial nucleon, intermediate virtual state (here-Δ) final nucleon and pion momenta. We distinguish the lepton scattering plane (green), $N\Delta$ plane (blue) and final $\pi N'$ plane (purple) with respective rotation angles w.r.t. to leptonic plane.

We shall start with the free nucleon SPP process. The inclusive double-differential cross section has the form:

$$\begin{aligned}
\frac{d^3\sigma}{d\Omega' dE'} &= \frac{|\boldsymbol{l'}|}{|\boldsymbol{l}|} 4\pi G_F^2 \cos^2(\Theta_C) \int \frac{d^3k}{(2\pi)^3 2E_\pi(k)} L_{\mu\nu} W^{\mu\nu} \\
W^{\mu\nu} &= \frac{1}{2} \int \frac{d^3p'}{(2\pi)^3} \frac{1}{4ME(p')} \overline{\sum_{spins}} \langle \pi N' \left| j^\mu_{cc}(0) \right| N \rangle \langle \pi N' \left| j^\nu_{cc}(0) \right| N \rangle^* \delta^{(4)}(p'+k-p-q) = \\
&= \frac{1}{128\pi^3 ME(p')} A^{\mu\nu} \delta(E(p') + E_\pi(k) - M - q^0). \qquad (6.14)
\end{aligned}$$

We take out the common Cabibbo angle factor out of weak charged current definition. After performing the summations over nucleon spins we can rewrite the hadronic tensor as:

$$A^{\mu\nu} = \mathrm{Tr}\left[(\not{p}' + M) s^\mu (\not{p} + M) \gamma^0 s^{\nu\dagger} \gamma^0\right] \qquad (6.15)$$

where the s^μ matrices contain all the dynamical information about the SPP process. These operators are called "reduced current matrix elements" and correspond to weak transition amplitudes:

$$\langle N'(p', s')\pi(k) \left| j^\mu_{cc} \right| N(p, s) \rangle = \overline{u}_{s'}(\boldsymbol{p'}) s^\mu u_s(\boldsymbol{p}). \qquad (6.16)$$

The double-differential cross section on free nucleons becomes then:

$$\frac{d^3\sigma}{d\Omega' dE'} = \frac{|\boldsymbol{l'}|}{|\boldsymbol{l}|} \frac{G_F^2 \cos^2(\Theta_C)}{512\pi^5 M} \int d\Omega_\pi \int_0^\infty \frac{\boldsymbol{k}^2 d|k|}{E_\pi(k) E_N(p')} L_{\mu\nu} A^{\mu\nu} \delta(E(p') + E_\pi(k) - M - q^0). \qquad (6.17)$$

As for the leptonic tensor under assumption of x-z scattering plane we find following angles in the laboratory frame:

$$\begin{aligned}
\cos(\Theta_\nu) &= \frac{E_\nu^2 + \boldsymbol{q}^2 - \boldsymbol{l'}^2}{2E_\nu q} \\
\cos(\Theta_\mu) &= -\frac{\boldsymbol{q}^2 + \boldsymbol{l'}^2 - E_\nu^2}{2|\boldsymbol{l'}|q}; \qquad (6.18)
\end{aligned}$$

which lead to the following lepton four-momenta:

$$
\begin{aligned}
l^{\mu}_{LAB} &= (E_\nu, \sin(\Theta_\nu)E_\nu, 0, \cos(\Theta_\nu)E_\nu) \\
l'^{\mu}_{LAB} &= (E_\mu, \sin(\Theta_\mu)|\boldsymbol{l'}|, 0, \cos(\Theta_\mu)|\boldsymbol{l'}|)
\end{aligned} \tag{6.19}
$$

In the next section we shall focus on the details of SPP dynamical models used in this dissertation.

6.1.1 SPP dynamics

The dynamics of SPP process is defined by a set of Feynman diagrams (Fig. 26) with vertices determined by the effective chiral field theory [46] (HNV model). The same set of diagrams describes also pion electroproduction, with the exception of pion pole diagram, which is purely axial. In the above mentioned model the reduced current matrix elements from Eq.

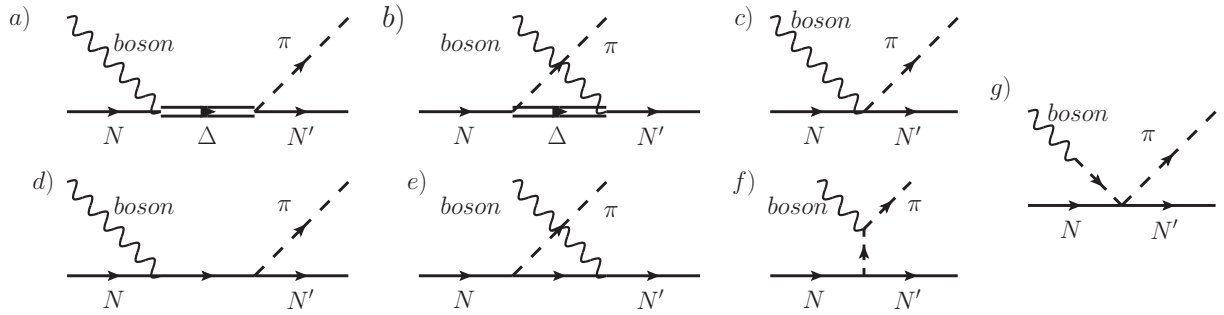

Figure 26: Basic pion production diagrams from [46]: a) Delta pole (ΔP), b) crossed Delta pole (CΔP), c) contact term (CT), d) nucleon pole (NP), e) crossed nucleon pole (CNP), f) pion-in-flight (PIF), g) pion pole (PP)

(6.16) are calculated to be (see: [46]):

$$
s^{\mu}_{\Delta P} = iC_{\Delta P}\frac{f^*}{m_\pi}k^\alpha G_{\alpha\beta}(p+q)\Gamma^{\beta\mu}(p,q) \tag{6.20}
$$

$$
s^{\mu}_{C\Delta P} = iC_{C\Delta P}\frac{f^*}{m_\pi}\gamma^0\left[\Gamma^{\alpha\mu}(p-k,-q)\right]^\dagger\gamma^0 G_{\alpha\beta}(p-k)k^\beta \tag{6.21}
$$

$$
s^{\mu}_{NP} = -iC_{NP}\frac{g_A}{\sqrt{2}f_\pi}\not{k}\gamma^5\frac{(\not{p}+\not{q}+M)}{(p+q)^2-M^2+i\epsilon}j^{\mu}_{CCN}(q)F_\pi(k-q) \tag{6.22}
$$

$$
s^{\mu}_{CNP} = -iC_{CNP}\frac{g_A}{\sqrt{2}f_\pi}j^{\mu}_{CCN}(q)\frac{(\not{p}-\not{k}+M)}{(p-k)^2-M^2+i\epsilon}\not{k}\gamma^5 F_\pi(k-q) \tag{6.23}
$$

$$
s^{\mu}_{CT} = -iC_{CT}\frac{1}{\sqrt{2}f_\pi}\gamma^\mu F_\pi(k-q)\left[g_A F^V_{CT}(q^2)\gamma^5 - F_\rho((q-k)^2)\right] \tag{6.24}
$$

$$
s^{\mu}_{PIF} = -iC_{PIF}\frac{g_A}{\sqrt{2}f_\pi}F^V_{PIF}(q^2)\frac{(2k-q)^\mu}{(k-q)^2-m_\pi^2}2M\gamma^5 F_\pi(k-q) \tag{6.25}
$$

$$
s^{\mu}_{PP} = -iC_{PP}\frac{1}{\sqrt{2}f_\pi}F_\rho(k-q)\frac{q^\mu\not{q}}{q^2-m_\pi^2} \tag{6.26}
$$

In our notation $f^* = 2.16$ is the $\pi N\Delta$ coupling constant. This value is slightly larger than 2.14 used in [46]. With our choice free $\Delta(1232)$ width is 0.118 GeV. The values of axial

couplings are standard: $g_A = 1.267$ and $f_\pi = 93$ MeV. We use averaged masses for nucleons and pions: $M = \frac{1}{2}(M_n + M_p)$, $m_\pi = \frac{1}{3}(m_{\pi^+} + m_{\pi^-} + m_{\pi^0})$ with the values given by Particle Data Group [23]. For the Δ-resonance contributions we assume $M_\Delta = 1.232$ GeV. In the Delta pole and crossed Delta pole amplitudes $G_{\alpha\beta}(p_\Delta)$ denotes the Rarita-Schwinger (spin-$\frac{3}{2}$ field) propagator. By $\Gamma^{\beta\mu}(p,q)$ we denote the Δ electroweak excitation vertex. We will give more details about the Δ propagator and decay width in the next subsection. The electroweak excitation vertex as well as the set of vector and axial form factors is described in Sec. 6.1.3. For the nucleon weak currents present in Eq. (6.22) and Eq. (6.23) we use the standard vector-axial prescription from Eq. (3.16).

From the conserved vector current hypothesis one can also get constraints on the form factors of contact term and pion-in-flight diagrams (see Appendix H):

$$F_{PIF}(Q^2) = F_{CT}(Q^2) = F_1^V(Q^2). \tag{6.27}$$

We choose the same nucleon form factors as in [46]. Details are described in the Appendix E.1. Our current matrix elements contain a virtual pion form factor $F_\pi(k-q)$ coming from the PIF term, where the W boson interacts with a virtual pion with momentum $a = k - q$. The CVC forces one to include it in several other background terms. F_π is assumed to have a monopole form:

$$F_\pi(a) = \frac{\Lambda_\pi^2 - m_\pi^2}{\Lambda_\pi^2 - a^2};\ \Lambda_\pi = 1.25\text{GeV}. \tag{6.28}$$

The ρ-meson form factor, having a monopole form $F_\rho(a) = \frac{1}{1-a^2/m_\rho^2}$; $m_\rho = 0.7758$ GeV., has been introduced in the PP term by the authors of [46] in order to account for the ρ-meson dominance of $\pi\pi NN$ coupling. Because of the partially conserved axial current hypothesis it has been also introduced in the axial part of CT. For each physical pion production channel there is a set of isospin Clebsch-Gordan coefficients C_i. For the electromagnetic process they are listed in the table 3 and for the νCC process in table 4. These coefficients can be

Table 3: Electromagnetic isospin coefficients of Eqs. (6.20-6.26)

Process	ΔP	CΔP	NP	CNP	Others
$e^- + p \to e^- + \pi^0 + p$	$\sqrt{\frac{2}{3}}$	$\sqrt{\frac{2}{3}}$	$\sqrt{\frac{1}{2}}$	$\sqrt{\frac{1}{2}}$	0
$e^- + p \to e^- + \pi^+ + n$	$-\sqrt{\frac{1}{3}}$	$\sqrt{\frac{1}{3}}$	1	1	-1
$e^- + n \to e^- + \pi^- + p$	$\sqrt{\frac{1}{3}}$	$-\sqrt{\frac{1}{3}}$	1	1	1
$e^- + n \to e^- + \pi^0 + n$	$\sqrt{\frac{2}{3}}$	$\sqrt{\frac{2}{3}}$	$-\sqrt{\frac{1}{2}}$	$-\sqrt{\frac{1}{2}}$	0

verified using the isospin relations from Appendix A.2). For the electromagnetic process we drop all purely axial contributions, *i. e.* the PP term, axial nucleon and Δ isobar currents as well as the part containing F_ρ in CT. In the computations of cross section on nuclear targets we sum up contributions from protons and neutrons in the incoherent way.

The Fogli-Nardulli (F-N) model [48], which in the past was considered as an alternative to the Rein-Sehgal model, contains contributions from three background terms: nucleon pole and crossed nucleon pole diagrams and direct neutrino-pion interaction diagram with pseudoscalar pion-nucleon coupling instead of the pseudovector one used in HNV model. They

Table 4: Charged current isospin coefficients of Eqs. (6.20-6.26)

Process	ΔP	CΔP	NP	CNP	Others
$\nu_l + p \to l^- + \pi^+ + p$	$\sqrt{3}$	$\sqrt{\frac{1}{3}}$	0	1	1
$\nu_l + n \to l^- + \pi^0 + p$	$-\sqrt{\frac{2}{3}}$	$\sqrt{\frac{2}{3}}$	$\sqrt{\frac{1}{2}}$	$-\sqrt{\frac{1}{2}}$	$-\sqrt{2}$
$\nu_l + n \to l^- + \pi^+ + n$	$\sqrt{\frac{1}{3}}$	$\sqrt{3}$	1	0	-1
$\overline{\nu}_l + n \to l^+ + \pi^- + n$	$\sqrt{3}$	$\sqrt{\frac{1}{3}}$	0	1	1
$\overline{\nu}_l + p \to l^+ + \pi^0 + n$	$\sqrt{\frac{2}{3}}$	$-\sqrt{\frac{2}{3}}$	$-\sqrt{\frac{1}{2}}$	$\sqrt{\frac{1}{2}}$	$\sqrt{2}$
$\overline{\nu}_l + p \to l^+ + \pi^- + p$	$\sqrt{\frac{1}{3}}$	$\sqrt{3}$	1	0	-1

use also a slightly different convention of the Δ propagator and form factors, but in order to make a meaningful comparisons to HNV model we willextract only their nonresonant terms. After a careful calculation and relative sign cross-checks we find the F-N background in our convention:

$$s_{NP}^{\mu\,(F-N)} = iC_{NP}\, g_{\pi NN}\gamma^5 \frac{(\not{p} + \not{q} + M)}{(p+q)^2 - M^2 + i\epsilon} j^{\mu}_{CCN}(q) \tag{6.29}$$

$$s_{CNP}^{\mu\,(F-N)} = iC_{CNP}\, g_{\pi NN} j^{\mu}_{CCN}(q) \frac{(\not{p} - \not{k} + M)}{(p-k)^2 - M^2 + i\epsilon}\gamma^5 \tag{6.30}$$

$$s_{PIF}^{\mu\,(F-N)} = -iC_{PIF}\, g_{\pi NN} \frac{(2k-q)^{\mu}}{(k-q)^2 - m_{\pi}^2}\gamma^5 \tilde{F}_{\pi}(k-q) \tag{6.31}$$

with $g_{\pi NN} = \sqrt{14.8 \cdot 4\pi}$ is the standard pion-nucleon coupling constant and $\tilde{F}_{\pi}(k-q) \equiv \frac{1}{1+Q^2/0.47\mathrm{GeV}^2}$ is the F-N virtual pion form factor. The nucleon Born terms have different signs with resonant term, than in HNV model The CΔP, CT and PP diagrams are absent, since they appear in a natural way only if one starts from the chiral field theory formalism. The fogli-Nardulli model does not include the pion form factor given by Eq. (6.28) either, only its older from $\tilde{F}_{\pi}$ in PIF term. We do not include nucleon resonances from the second resonance region, which are present in the Fogli-Nardulli paper, as long as we consider neutrino energies $E_{\nu} \leq 1$ GeV. We also use different nucleon and Δ form factors and Δ width, thus starting from this point we will refer to this approach as "Fogli-Nardulli type" (or "F-N type") model, as it is dfferent from the original Fogli-Nardulli paper.

In general, it should be possible also to add heavier resonances to the HNV model. However, these resonances have pole masses above the two pion production threshold and there is a significant branching ratio for decay channels with two pion in the final state. Thus the consistency would require to expand the effective field theory Lagrangian to higher order and add the two pion production terms as well, see [137, 138]. One should remember that the effective field theory works as long as one can use only tree level amplitudes and can not be extended to large energies. The authors of [137, 138] constrain predictions from the model to $E_{\nu} \leq 3$ GeV. This is rather unfortunate for experiments with a large fraction of higher energy neutrinos like MINERvA and LBNE which will probably have to rely on extrapolations from the DIS region justified by the quark-hadron duality hypothesis [139].

6.1.2 Resonant process

The $\Delta(1232)$ resonance excitation is very important for single pion production, because of it has only one strong decay channel into a πN pair. It is a spin-$\frac{3}{2}$ isospin- $\frac{3}{2}$ baryon. Here we treat it within the isobar framework. We assume the free propagator in the form:

$$G^{\alpha\beta}(p_\Delta) = \frac{P^{\alpha\beta}_{3/2}(p_\Delta, M_\Delta)}{p^2_\Delta - M^2_\Delta + iM_\Delta\Gamma_\Delta(p^2_\Delta)} \tag{6.32}$$

$$P^{\alpha\beta}_{3/2}(p_\Delta, M_\Delta) = -(\not{p}_\Delta + M_\Delta)\left(g^{\alpha\beta} - \frac{1}{3}\gamma^\alpha\gamma^\beta - \frac{2}{3}\frac{p^\alpha_\Delta p^\beta_\Delta}{M^2_\Delta} + \frac{1}{3}\frac{p^\alpha_\Delta\gamma^\beta - p^\beta_\Delta\gamma^\alpha}{M_\Delta}\right). \tag{6.33}$$

In the above equation $P^{\alpha\beta}_{3/2}$ is a projection operator on spin-$\frac{3}{2}$ states with p_Δ being the Δ resonance 4-momentum and Γ_Δ the free resonance decay width.

For positive parity spin-$\frac{3}{2}$ particles we can write down a general form of the electroweak excitation vertex:

$$\begin{aligned}
\Gamma^{\alpha\mu}(p,q) &= \left[V^{\alpha\mu}_{3/2} - A^{\alpha\mu}_{3/2}\right]\gamma^5 = \\
&= \left[\frac{C^V_3}{M}(g^{\alpha\mu}\not{q} - q^\alpha\gamma^\mu) + \frac{C^V_4}{M^2}(g^{\alpha\mu}q\cdot(p+q) - q^\alpha(p+q)^\mu) + \right. \\
&+ \left. \frac{C^V_5}{M^2}(g^{\alpha\mu}q\cdot p - q^\alpha p^\mu) + g^{\alpha\mu}C^V_6\right]\gamma^5 + \\
&+ \left[\frac{C^A_3}{M}(g^{\alpha\mu}\not{q} - q^\alpha\gamma^\mu) + \frac{C^A_4}{M^2}(g^{\alpha\mu}q\cdot(p+q) - q^\alpha(p+q)^\mu) + \right. \\
&+ \left. C^A_5 g^{\alpha\mu} + \frac{C^A_6}{M^2}q^\alpha q^\mu\right].
\end{aligned} \tag{6.34}$$

Analogously to nucleon currents we have a vector-axial decomposition into $V^{\alpha\mu}_{3/2}$ and $A^{\alpha\mu}_{3/2}$. The knowledge about inner structure of Δ resonance is hidden within the set of vector and axial form factors, C_i. The next paragraph will be devoted to the discussion of different Δ form factor sets.

6.1.3 Form factors of the $\Delta(1232)$ resonance

The vector form factors can be obtained using pion electroproduction experiments, which give us helicity amplitudes. Helicity amplitudes describe the nucleon-resonance transition depending on the baryonic spins and virtual photon polarization. They are described in more detail in Appendix E.2.1.

There exist a few available parameterizations of Δ resonance form factors. Lalakulich and Paschos proposed (Ref. [140]):

$$\begin{aligned}
C^V_3(Q^2) &= \frac{2.13}{(1+Q^2/M^2_V)^2}\frac{1}{1+Q^2/4M^2_V} \\
C^V_4(Q^2) &= \frac{-1.51}{(1+Q^2/M^2_V)^2}\frac{1}{1+Q^2/4M^2_V} \\
C^V_5(Q^2) &= \frac{0.48}{(1+Q^2/M^2_V)^2}\frac{1}{1+Q^2/0.776M^2_V}
\end{aligned} \tag{6.35}$$

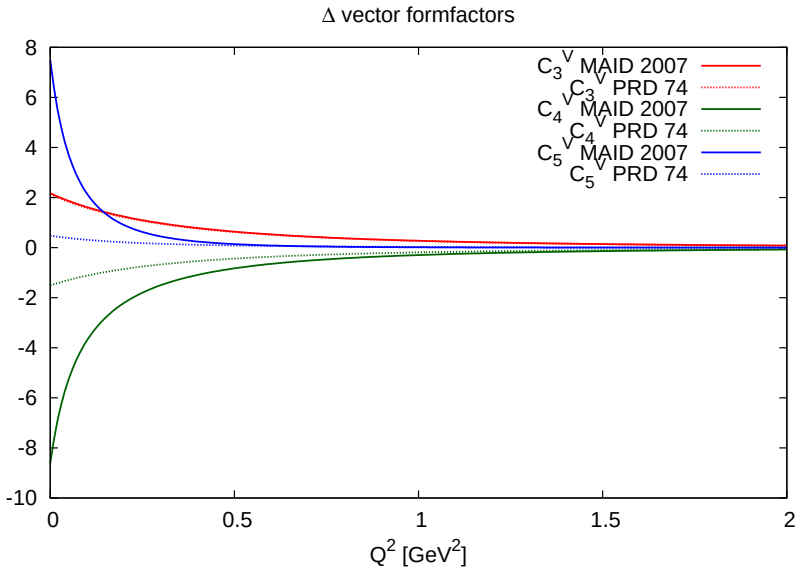

Figure 27: The $\Delta(1232)$ vector form factors from [140] and [50].

with $M_V = 0.84\,\text{GeV}$. This parametrization includes a beyond-dipole correction to the form factor behavior. From the CVC it follows that $C_6^V \equiv 0$. There exist also relatively recent electroproduction analyses, including the MAID2007 paper (Ref. [50]). Formulas describing these form factors can be found in the Appendix E.2. The difference between the form factors is plotted in Fig. 27.

Although the Q^2-dependence of C_4^V and C_5^V is different in both cases, the leading vector form factor C_3^V is the same. The difference in electroproduction coming from switch between those two parameterizations is negligible, which is shown on Fig. 28. The two MAID parameterizations are indistinguishable. This figure shows us also, that the resonant contribution is not enough to describe experimental data.

The extraction of $\Delta(1232)$ electromagnetic form factors depends on particular models of resonance and background, so in particular one would have to do an independent analysis of helicity amplitudes for each model. In order to compare with the authors of Ref. [46], we will use Eq. (6.35).

In the axial part leading contribution comes from $C_5^A(Q^2)$ it is an analogue of the isovector axial form factor of the nucleon. PCAC relates the value of $C_5^A(0)$ with strong f^* coupling constand through off-diagonal Goldberger-Treiman relation (Ref. [28]):

$$C_5^A(0) = \frac{f^*}{\sqrt{2}} \approx 1.2. \tag{6.36}$$

In the standard approach it is assumed, that C_5^A has a dipole Q^2 dependence:

$$C_5^A(Q^2) = \frac{C_5^A(0)}{(1 + Q^2/M_{A\Delta}^2)^2} \tag{6.37}$$

The axial mass parameter $M_{A\Delta}$ is expected to be of the order of $1\,\text{GeV}$. Values of $C_5^A(0)$ and $M_{A\Delta}$ are of great importance for the weak single pion production. They are analysis-dependent, thus we may deviate from the strict Goldberger-Treiman relation given by Eq.

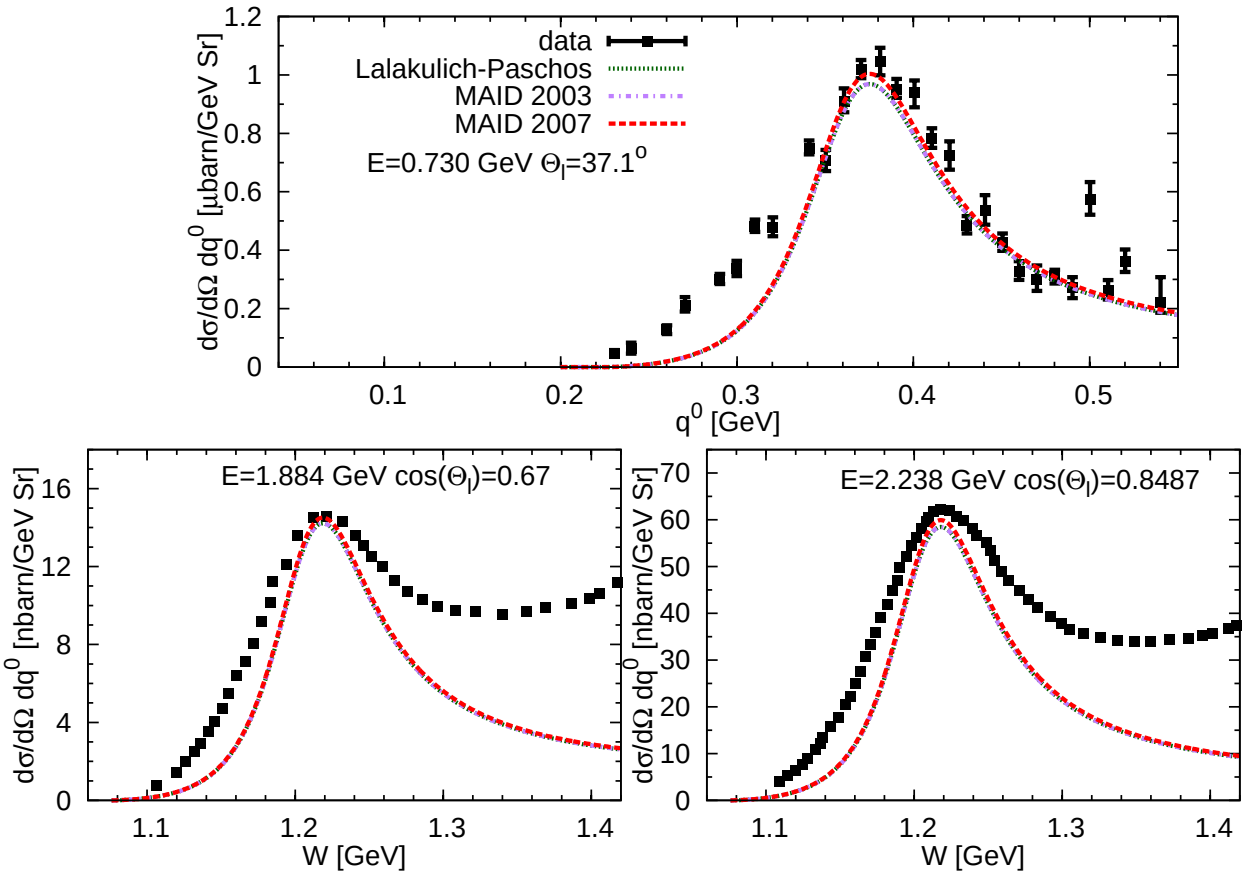

Figure 28: Comparison of the three different sets of Δ resonance vector form factors plotted against inclusive $p(e, e')$ data from [141] (top) and [142] (bottom). Only the resonant contribution is shown. Fine dashed green curve is the Lalakulich-Paschos form factor set, blue/red lines are for the MAID2003/2007 form factor sets. The Q^2 values at peak are from top to bottom and left to right: 0.1 [GeV^2], 1.15 [GeV^2] and 0.95 [GeV^2] respectively.

(6.36). One can also treat both $C_5^A(0)$ and $M_{A\Delta}$ as free fit parameters in order to get the best agreement between theoretical predictions and data. Main source of information about their values comes from neutrino scattering experiments, particularly form the ANL [61] and BNL [60] bubble chamber experiments. This technique is used *e. g.* by the authors of Refs. [46, 47].

The C_6^A form factor is an analogue of the induced pseudoscalar form factor of the nucleon. It can be ralated to the C_5^A via PCAC hypothesis:

$$C_6^A(Q^2) = \frac{M^2}{m_\pi^2 + Q^2} C_5^A(Q^2). \tag{6.38}$$

$C_3^A(Q^2)$ is the axial counterpart of the electric quadrupole (E2) transition form factor G_E^2. It seems to be negligibly small. In our analysis we set $C_3^A = 0$. For C_4^A we use the Adler model (Ref. [143]):

$$C_4^A(Q^2) = -\frac{1}{4} C_5^A(Q^2). \tag{6.39}$$

In this manner we assume the axial contribution to be fully determined by C_5^A. If there

is enough experimental data one can also resign on the Adler relation and treat C_4^A as an independent form factor.

6.1.4 $\Delta(1232)$ Width

In the framework of quantum field theory the $\Delta \to \pi N$ decay width can be obtained from the interaction Lagrangian:

$$\mathcal{L}_{\pi N\Delta} = \frac{f^*}{m_\pi}\overline{\psi}_\mu \boldsymbol{T}^\dagger(\partial^\mu \boldsymbol{\phi})\psi + h.c. \tag{6.40}$$

Detailed calculation shown in Appendix F.2 leads to the following result:

$$\Gamma_\Delta(W) = \frac{1}{12\pi}\left(\frac{f^*}{m_\pi}\right)^2 (k^{cm})^3 \frac{E_N^{cm}+M}{W} \tag{6.41}$$

with k^{cm} being the hadronic center-of-mass pion momentum and E_N^{cm} the nucleon center-of-mass energy[9]. We impose $\Gamma_\Delta(M_\Delta) = 118$ MeV and extract the $\Delta\pi N$ coupling from Eq. 6.41. We have in our calculations $f^* = 2.16$. This is somewhat higher coupling, than usual value of $f^* = 2.14$ used in *e. g.* Ref. [46]. We have performed tests of the full model against some of the existing electroproduction data. It appears, that one can slightly improve performance of the model by using a different expression for the Δ width and propagator. We use the prescription of Ref. [144] for the $R \to a + b$ decays:

$$\begin{aligned}
\Gamma_{R\to ab} &= \Gamma^0_{R\to ab}\frac{\rho_{R\to ab}(W^2)}{\rho_{R\to ab}(M_R^2)} \\
\rho_{ab}(W^2) &= \int dp_a^2 \int dp_b^2 A_a(p_a^2)A_b(p_b^2)\frac{k^{cm}_{R\to ab}}{W}B^2_{R\to ab}(k^{cm}_{R\to ab}, l)F^2_{ab}(W)
\end{aligned} \tag{6.42}$$

with R denoting a hadronic resonance state and a,b- its decay products. In the above equation $A_i(p_i^2)$ stands for either $\delta(p_i^2 - m_i^2)$ for a stable product, or a Breit-Wigner distribution for unstable ones. The $k^{cm}_{R\to ab}$ is the center-of-mass (CMS) momentum of the decay and l-the angular momentum. Blatt-Weisskopf angular momentum functions are given by:

$$\begin{aligned}
B_{R\to ab}(k^{cm}_{R\to ab}, 0) &= 1 \\
B_{R\to ab}(k^{cm}_{R\to ab}, 1) &= \frac{x}{\sqrt{1+x^2}} \\
B_{R\to ab}(k^{cm}_{R\to ab}, 2) &= \frac{x^2}{\sqrt{9+3x^2+x^4}}
\end{aligned} \tag{6.43}$$

with $x = k^{cm}_{R\to ab} \times R$, $R = 1$ [fm]. Additionaly there is also a form factor ([145]):

$$F_{ab}(W) = \frac{\lambda_{ab}^4 + \frac{1}{4}(s_0 - M_R^2)^2}{\lambda_{ab}^4 + (W^2 - \frac{1}{2}(s_0 - M_R^2))^2} \tag{6.44}$$

In the above equation s_0 is the threshold invariant mass for regarded process. For stable products $F_{ab} = 1$. Else we use following cutoffs:

$$\lambda_{ab} = \begin{cases} 0.85GeV & \Delta\rho \text{ channel} \\ 1.6GeV & \text{unstable meson} + \text{stable baryon} \\ 2.0GeV & \text{stable meson} + \text{unstable baryon} \end{cases} \tag{6.45}$$

[9] In the Ref. [46] $\Gamma_\Delta(W) = \frac{1}{6\pi}\left(\frac{f^*}{m_\pi}\right)^2 (k^{cm})^3 \frac{M}{W}$. It gives the the same result at $W = M_\Delta$.

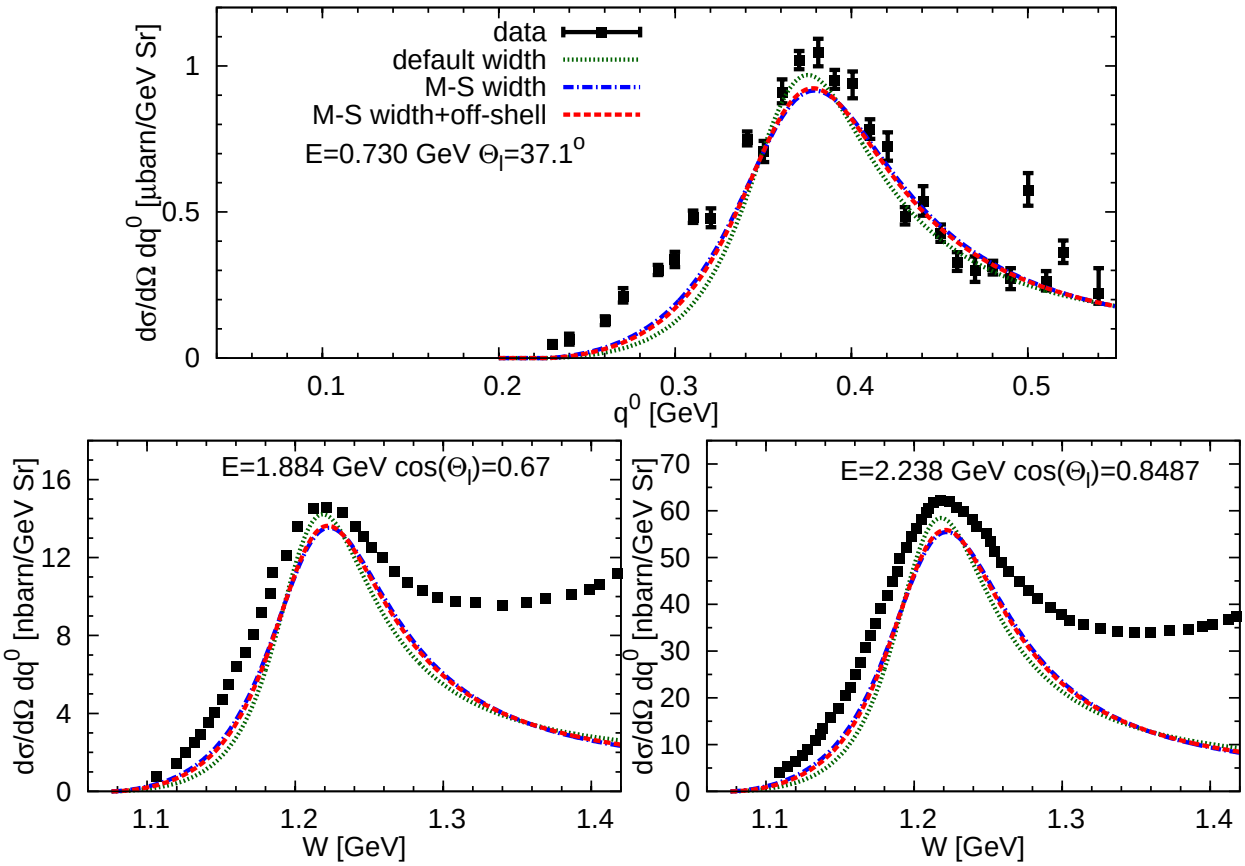

Figure 29: Comparison of the different descriptions of Δ resonance vector form factors plotted against inclusive $p(e, e')$ data from Ref. [141] (top) and Ref. [142] (bottom). Only the resonant contribution is shown. The fine dashed green curve shows calculation for default Δ width and propagator, the blue dashed curve shows calculation for Manley-Saleski Δ width and default propagator and the dashed red curve shows calculation for Manley-Saleski Δ width and off-shell propagator. The Q^2 values at peak are from top to bottom and left to right: 0.1 [GeV^2], 1.15 [GeV^2] and 0.95 [GeV^2] respectively.

For unstable meson decays, like the ρ meson, we use the same set of formulas. Taking into account the above considerations the Δ decay width can be re-expressed as:

$$\begin{aligned} \Gamma_{M-S}(W) &= 118MeV \cdot \frac{\rho_{\Delta\to\pi N}(W)}{\rho_{\Delta\to\pi N}(M_\Delta)} \\ \rho_{\Delta\to\pi N}(W) &= \frac{k_{cm}}{W}\frac{k_{cm}^2 R^2}{1+k_{cm}^2 R^2} \quad R = 1[fm]. \end{aligned} \tag{6.46}$$

The term $\frac{k_{cm}^2 R^2}{1+k_{cm}^2 R^2}$ accounts for the phenomenological knowledge about decay πN system angular momentum $l = 1$, which is absent in the Lagrangian given by Eq. (6.40). In order to stay consistent, after changing the width given by Eq. (6.41) to the one defined in Eq. (6.46) one has to multiply the ΔP term by $\sqrt{\frac{\Gamma_{M-S}(W)}{\Gamma_\Delta(W)}}$. It will compensate for the fact, that our current has a decay vertex defined by Eq. (6.40) in the numerator, which leads to old width, Eq. (6.41). Furthermore, $\Delta(1232)$ is not a stable particle. One can account partially

for the off-shell effects by replacing the propagator in DP term (6.32) by

$$\begin{aligned}\tilde{G}^{\alpha\beta}(p_\Delta) &= \frac{\tilde{P}^{\alpha\beta}_{3/2}(p_\Delta)}{p_\Delta^2 - M_\Delta^2 + iW\Gamma_\Delta(p_\Delta^2)} = -\frac{(\not{p}_\Delta + W)}{p_\Delta^2 - M_\Delta^2 + iW\Gamma\Delta(p_\Delta^2)} \times \\ &\times \quad (g^{\alpha\beta} - \frac{1}{3}\gamma^\alpha\gamma^\beta - \frac{2}{3}\frac{p_\Delta^\alpha p_\Delta^\beta}{W^2} + \frac{1}{3}\frac{p_\Delta^\alpha\gamma^\beta - p_\Delta^\beta\gamma^\alpha}{W}). \end{aligned} \tag{6.47}$$

The effect of such operation is visible in Fig. 29 for resonant contribution. The Manley-Saleski prescription leads to somewhat broader Δ peak, redistributing the strength from the peak to high- and low-W slopes of differential cross section.

6.1.5 Second resonance region

If one considers scattering off a neutron in the ANL energy range, one gets a contribution from the heavier resonances. We need to incorporate the second resonance region, including the positive parity spin-$\frac{1}{2}$ isospin-$\frac{1}{2}$ Roper $P_{11}(1440)$, negative parity spin-$\frac{1}{2}$ isospin-$\frac{1}{2}$ $S_{11}(1535)$ and negative parity spin-$\frac{3}{2}$ isospin-$\frac{1}{2}$ $D_{13}(1520)$ resonances. We have taken their general properties from [50]. They are listed in table (5).

Table 5: Properties of heavier resonances included in our code: pole mass, spin, isospin, parity, total pole width, branching ratio to πN and $F_A(0)$ or $C_5^A(0)$ from [50].

Name	M_R GeV	S	I	P	$\Gamma_0^{tot.}$ GeV	πN branching ratio	$F_A(0)$ or $C_5^A(0)$
$P_{11}(1440)$	1.440	$\frac{1}{2}$	$\frac{1}{2}$	+	0.391	0.69	-0.52
$D_{13}(1520)$	1.520	$\frac{3}{2}$	$\frac{1}{2}$	-	0.124	0.69	-2.15
$S_{11}(1535)$	1.534	$\frac{1}{2}$	$\frac{1}{2}$	-	0.151	0.51	-0.23

In general one should introduce the following currents:

$$\begin{aligned} s^\mu_{P_{11}} &= e^{i\phi_{P_{11}}} C_{2nd} \frac{\sqrt{2} f_{P_{11}}}{m_\pi} \frac{\not{k}\gamma^5(\not{p} + \not{q} + W)}{(p+q)^2 - M^2_{P_{11}} + iW\Gamma_{P_{11}}} \left[V^\mu_{P_{11}}(q) - A^\mu_{P_{11}}(q)\right] \\ s^\mu_{S_{11}} &= e^{i\phi_{S_{11}}} C_{2nd} \frac{\sqrt{2} f_{S_{11}}}{m_\pi} \frac{\not{k}(\not{p} + \not{q} + W)}{(p+q)^2 - M^2_{S_{11}} + iW\Gamma_{S_{11}}} \left[V^\mu_{S_{11}}(q) - A^\mu_{S_{11}}(q)\right] \gamma^5 \\ s^\mu_{D_{13}} &= e^{i\phi_{D_{13}}} C_{2nd} \frac{\sqrt{2} f_{D_{13}}}{m_\pi} \frac{k^\alpha \gamma^5 P_{\alpha\beta}(p+q)\Gamma^{\beta\mu}_{D_{13}}(p,q)}{(p+q)^2 - M^2_{D_{13}} + iW\Gamma_{D_{13}}((p+q)^2)} \\ C_{2nd} &= C_{NP} \end{aligned} \tag{6.48}$$

In the above equations Γ_R stands for total resonance decay widths and $P_{3/2}$ is given by the Eq. (6.47). These resonances have the same isospin Clebsch-Gordan coefficients, as the NP term, because they are all isospin-$\frac{1}{2}$ doublets. All of them have unknown phases $e^{i\phi_R}$ relative to the background terms. They can be established using the Watson's theorem [146]. However, we shall use an approximation, in which none of them interferes with the nonresonant background. This approximation is motivated also by the fact, that all of these resonances have multi-pion decay channels, which would require also higher-order nonresonant terms in order to form a consistent background. One would also have to take into account the ρ, σ and η mesons. Because of the before mentioned approximation in our

calculations the complex phases will be irrelevant. The second resonance region contributes as a separate cross section. For free nucleon scattering case we have:

$$\frac{d\sigma_R}{dE_{l'}d\Omega_{l'}} = \frac{|\boldsymbol{l'}|G_F^2\cos^2(\Theta_C)}{32\pi^2\sqrt{(l\cdot p)^2 - m_l^2M^2}}S(W)|\overline{M}_R|^2 \tag{6.49}$$

with vacuum spectral function of a resonance:

$$S(W) = \frac{W}{\pi}\frac{\Gamma_R(W)}{(W^2 - M_R^2)^2 + W^2\Gamma_R^2(W)}. \tag{6.50}$$

The Γ_R stands here for resonance decay width, which is calculated using Eq. (6.42). The term "spectral function" is used here, because the resonance propagator are dressed in the imaginary parts of self energies coming from all decay channels widths. This relates it to the usual spectral function definition through relations given by Eq. (4.137).

Matrix elements for the resonance excitation reaction are given by:

$$|\overline{M}_R|^2 = L_{\mu\nu}A_R^{\mu\nu}. \tag{6.51}$$

The details of resonance excitation hadronic tensors $A_R^{\mu\nu}$ will be given in the next paragraphs.

$P_{11}(1440)$ and $S_{11}(1535)$ Resonances

The hadronic tensor of spin-$\frac{1}{2}$ resonance has the following form:

$$A_{R_{1/2}}^{\mu\nu}(p,q,k) = \mathrm{Tr}\left[(\not{p} + M)\gamma^0 J_{ccR}^{\mu^\dagger}\gamma^0(\not{p}' + M)J_{ccR}^{\nu}\right]. \tag{6.52}$$

The spin-$\frac{1}{2}$ resonance reduced weak charged current elements can be expressed as:

$$\begin{aligned} J_{ccR}^{\mu} &= \left(\frac{F_{1R}^V}{(M+M_R)^2}\left(q^\mu\not{q} - q^2\gamma^\mu\right) + i\frac{F_{2R}^V}{M+M_R}\sigma^{\mu\alpha}q_\alpha\right)(\mathbb{1}_{4\times4}/\gamma^5) + \\ &- \left(G_A\gamma^\mu + \frac{G_P}{M+M_R}q^\mu\not{q}\right)(\gamma^5/\mathbb{1}_{4\times4}) \end{aligned} \tag{6.53}$$

with M_R being the resonance mass and F_1^V, F_2^V, G_A, G_P the corresponding vector and axial form factors. First and second Dirac matrices in the parentheses stand for positive/negative parity resonances. The vector part of current defined in Eq. (6.53) is by definition conserved: $q_\mu J_V^\mu \equiv 0$. For the P_{11} and S_{11} resonances PCAC is assumed, thus:

$$G_P(Q^2) = \frac{(M_R \pm M)M}{m_\pi^2 + Q^2}G_A(Q^2). \tag{6.54}$$

In the above equation $+/-$ stands for the positive/negative parity resonances. The knowledge about axial form factors in the second and higher resonance region is very poor. The procedure of establishing the values of $F_A(0)$ has been given in details in [147], so we will give only a brief description. First one has to obtain the πNR coupling from the $R \to \pi N$ decay width (details in the Appendix F.1):

$$\Gamma_{R\to N\pi} = \frac{3}{4\pi}\frac{f_R^2}{m_\pi^2}(M_R \pm M)^2\frac{E_N^{cm} \mp M}{M_R}k^{cm}. \tag{6.55}$$

with k^{cm} and E_N^{cm} being the CMS system momentum and energy of nucleon. Upper/lower signs stand for the positive/ negative parity resonances. Then one uses the Goldberger-Treiman relation to obtain F_A:

$$F_A(0) = -\sqrt{2}\frac{f_\pi}{m_\pi} f_R. \tag{6.56}$$

The Q^2-dependence of axial form factor is unknown, so we adapt the same dipole parametrization, as for the nucleon:

$$F_A(Q^2) = \frac{F_A(0)}{(1+Q^2/M_A^2)^2} \tag{6.57}$$

with $M_A = 1$ GeV. For the vector form factor set we use the helicity amplitude based analysis of MAID2007 [50]. See also [147] for more details.

Table 6: Decay channels with decay product angular momenta in the second resonance region.

Resonance	chan. 1	chan 2	chan. 3	chan. 4	chan5
$P_{11}(1440)$	69% πN(l=1)	22% $\pi\Delta$(l=1)	9% σN (l=0)	-	-
$D_{13}(1520)$	59% πN(l=2)	5% $\pi\Delta$(l=0)	21% $\pi\Delta$(l=2)	21% ρN(l=0)	-
$S_{11}(1535)$	51% πN(l=0)	43% ηN(l=0)	3% ρN(l=0)	3% σN(l=1)	1% πP_{11}(l=0)

Decay channels of all considered resonances are listed in table 6. Additionally we simplify the S_{11} decay to the form 51% πN + 49% ηN with η treated as a stable particle. This does not alter the cross section in any significant manner.

$D_{13}(1520)$ **Resonance**

For the D_{13} resonance we have following hadronic tensor element:

$$A^{\mu\nu}_{R_{3/2}}(p,q,k) = \mathrm{Tr}\left[(\not{p}+M)\gamma^0\Gamma^{\alpha\mu^\dagger}\gamma^0 P_{3/2\alpha\beta}(p+q)\Gamma^{\beta\nu}\right]. \tag{6.58}$$

In the above equation $P_{3/2}$ stands for the projection operator defined as in Eq. (6.47). The vertex of a negative parity spin-3/2 resonance has the following form:

$$\begin{aligned}
\Gamma^{\alpha\mu}_{D_{13}}(p,q) &= \left[V^{\alpha\mu}_{3/2} - A^{\alpha\mu}_{3/2}\right] = \\
&= \left[\frac{C_3^V}{M}(g^{\alpha\mu}\not{q} - q^\alpha\gamma^\mu) + \frac{C_4^V}{M^2}(g^{\alpha\mu}q\cdot(p+q) - q^\alpha(p+q)^\mu) + \right. \\
&+ \left. \frac{C_5^V}{M^2}(g^{\alpha\mu}q\cdot p - q^\alpha p^\mu) + g^{\alpha\mu}C_6^V\right] + \\
&+ \left[\frac{C_3^A}{M}(g^{\alpha\mu}\not{q} - q^\alpha\gamma^\mu) + \frac{C_4^A}{M^2}(g^{\alpha\mu}q\cdot(p+q) - q^\alpha(p+q)^\mu) + \right. \\
&+ \left. C_5^A g^{\alpha\mu} + \frac{C_6^A}{M^2}q^\alpha q^\mu\right]\gamma^5
\end{aligned} \tag{6.59}$$

and is analogous to the $\Delta(1232)$ vertex, but with different placement of γ^5 because of opposite parity. For the vector form factors we use again the MAID2007 analysis from Ref.

[50]. The axial part is basically unknown, save for the $C_5^A(0)$ coming from Goldberger-Treiman relation:

$$C_5^A(0) = -\sqrt{2}\frac{f_\pi}{m_\pi} f_{D_{13}}. \tag{6.60}$$

The same dipole ansatz is used for the Q^2-dependence, as in the case of P_{11} and S_{11} (6.57). PCAC is used for C_6^A as in the $\Delta(1232)$ case in Eq. (6.38). C_3^A and C_4^A remain totally unknown, but we assume their contributions are small. Thus we set $C_3^A = C_4^A = 0$. For decay the width we also use Eq. (6.42).

The relevant contribution to our analysis comes from pion production, hence we put in all cases for the spectral function:

$$S(W) = \frac{W}{\pi}\frac{\Gamma_{R\to\pi N}(W)}{(W^2 - M_R^2)^2 + W^2\Gamma_R^2(W)}. \tag{6.61}$$

This way we produce only the total $R \to \pi N$ cross section. The conributions to channels defined in Eqs. (6.2) and (6.3) are obtained by multiplying the cross section by factors $\frac{1}{3}$ and $\frac{2}{3}$ respectively.

6.2 Integration of the SPP cross section on free nucleons

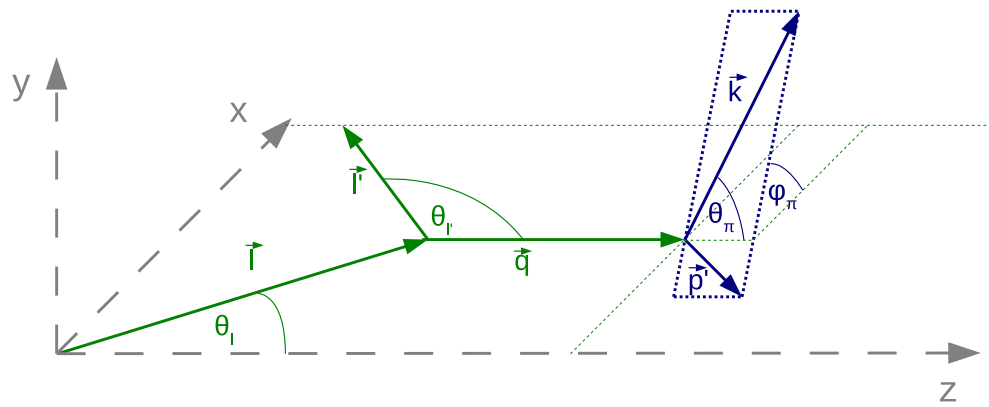

Figure 30: By $\boldsymbol{l}$, $\boldsymbol{l'}$, $\boldsymbol{p'}$ and $\boldsymbol{k}$ we denote the neutrino, muon, final nucleon and pion momenta. We distinguish the lepton scattering plane (green), and final $\pi N'$ plane (blue) with respective rotation angles w.r.t. to leptonic plane.

Calculation of SPP cross section on free nucleons is the most simple case. We will work in a reference frame depicted in Fig. 30, where the initial nucleon is at rest.

We have two possible approaches to the integral in Eq. (6.17): either use the delta function to integrate it in the pion momentum or in the pion angle. The fastest way is to perform the integration in $\cos(\Theta(\boldsymbol{k}, \boldsymbol{p}+\boldsymbol{q})) = \mu$.

$$\int d\Omega_\pi \int_0^\infty \frac{\boldsymbol{k}^2 d|k|}{E_\pi(k)E_N(p')} F(k,p,q)\delta(E(p') + E_\pi(k) - M - q^0) =$$
$$= \int_0^{2\pi} d\phi_\pi \int_{-1}^{1} d\mu \int_0^\infty \frac{\boldsymbol{k}^2 d|k|}{E_\pi(k)E_N(p')} \delta(\sqrt{(\boldsymbol{p}+\boldsymbol{q})^2 - 2|\boldsymbol{p}+\boldsymbol{q}||\boldsymbol{k}|\mu + \boldsymbol{k}^2 + M^2} + E_\pi(k) - M - q^0)$$
$$F(k,p,q). \tag{6.62}$$

Let us denote $\boldsymbol{p}+\boldsymbol{q}=\boldsymbol{a}$, $q^0+M=a^0$. The function under the Dirac Delta can be re-expressed in our variables:

$$\begin{aligned}
\delta(\sqrt{\boldsymbol{a}^2-2|\boldsymbol{a}||\boldsymbol{k}|\mu+\boldsymbol{k}^2+M^2}+E_\pi(k)-a^0) &= \frac{E_N(p')}{|\boldsymbol{a}||\boldsymbol{k}|}\delta(\mu-\mu^0) \\
\mu_0 &= \frac{2E_\pi a^0+M^2-W^2-m_\pi^2}{2|\boldsymbol{k}||\boldsymbol{a}|}; \\
W^2 &= (p+q)^2=a_\mu^2. \qquad (6.63)
\end{aligned}$$

The integral will have the form:

$$\int_0^{2\pi}d\phi_\pi\int_{-1}^{1}d\mu\int_{k_{min}}^{k^{max}}\frac{|k|d|k|}{E_\pi(k)|\boldsymbol{a}|}F(k,p,q)\delta(\mu-\mu^0)=\int_0^{2\pi}d\phi_\pi\int_{E_{min}}^{E^{max}}\frac{dE_\pi}{|\boldsymbol{a}|}F(k,p,q). \qquad (6.64)$$

The integration limits in pion energy can be established just like in the case of quasielastic scattering, i.e. from the condition $\mu_0^2\leq 1$. There are two solutions:

$$E_{min/max}=\frac{a^0(W^2+m_\pi^2-M^2)\mp|a|\sqrt{W^4+M^4+m_\pi^4-2(W^2m_\pi^2+W^2M^2+M^2m_\pi^2)}}{2W^2}. \qquad (6.65)$$

An additional condition is coming from $W^2\geq W_{min}^2=(M+m_\pi)^2$. In the laboratory frame the nucleon is at rest, thus here $\boldsymbol{a}=\boldsymbol{q}$ and the pionic angle is measured with respect to the momentum transfer direction (z-axis). From a general form of the hadronic tensor and this type of cross section one can show, that the dependence over the remaining pionic angle is as follows:

$$\frac{d^5\sigma}{d\Omega' dE' d\Omega_\pi}=\frac{|\boldsymbol{l}'|}{|\boldsymbol{l}|}\frac{G_F^2\cos^2(\Theta_C)}{4\pi^2}(A+B\cos(\phi_\pi)+C\cos(2\phi_\pi)+D\sin(\phi_\pi)+E\sin(2\phi_\pi)). \qquad (6.66)$$

Thus the integral over ϕ_π may be trivialized to a sum over four points $\int_0^{2\pi}d\phi_\pi F(\phi_\pi)=\frac{\pi}{2}(F(0)+F(\pi/2)+F(\pi)+F(3/2\pi))$. In a collinear frame (nucleon momentum going along the momentum transfer axis) one can even extract the part independent on this angle. In the case of $\boldsymbol{p}\parallel\boldsymbol{q}\parallel\hat{z}$ and leptons moving in the $x-z$ plane one has to substitute:

$$\begin{aligned}
L_{\mu\nu}A^{\mu\nu} &\rightarrow L^{00}A^{00}+L^{33}A^{33}-L^{03}A^{03}-L^{30}A^{30}+ \\
&+ \frac{1}{2}(L^{11}+L^{22})(A^{11}+A^{22})+L^{21}A^{21}+L^{12}A^{12} \qquad (6.67)
\end{aligned}$$

and the whole integral simplifies to $\int_0^{2\pi}d\phi_\pi F(\phi_\pi)=2\pi\tilde{F}(0)$ where the tilde stands for a function with contraction re-defined as in Eq. (6.67). In numerical computations it saves a lot of CPU time. The proof of Eq. (6.67) can be done only by means of direct calculation, which we have placed it in the Appendix G. In general this trick could be applied for scattering off nuclei by applying boost to the hadronic CMS, rotating the momentum transfer to point along the z-axis and rotating the lepton scattering plane to the x-z plane. Notice, that when one integrates over the nucleon azimuthal angle ϕ_n, our re-defined contraction from Eq. (6.67) after the mentioned boost and rotations does not depend on this angle as well. This could allow us to drop two integrations. Unfortunately, the De Forest prescription, which alters the energy transfer (4.45), makes it impossible to use common boost and rotation arguments for the leptonic and hadronic systems without breaking the momentum

conservation as well and leading to uncontrollable error. The above mentioned numerical simplification can be done only for free nucleons.

In order to handle complicated Dirac and Lorentz structure algebra, we have created a set of numerical procedures in C++, which make the programs easy to write and read. They basic classes and templates together with program functionalities have been described in Appendix I. They are used throughout this whole chapter.

6.2.1 Results for free nucleon: pion electroproduction

We shall start the discussion of the effects of different Δ resonance descriptions on the full model. We will switch between the decay widths given by Eq. (6.41) and Eq. (6.46) as well as the "on-shell" (Eq. (6.32) and "off-shell" (Eq. (6.47) propagators. Since for the $C\Delta P$ (Eq. (6.21)) term we have $p_\Delta^2 = (p-k)^2 < (M+m_\pi)^2$ this term has always zero width and we need to modify only the ΔP (Eq. (6.20)) contribution. The effects can ce seen in the

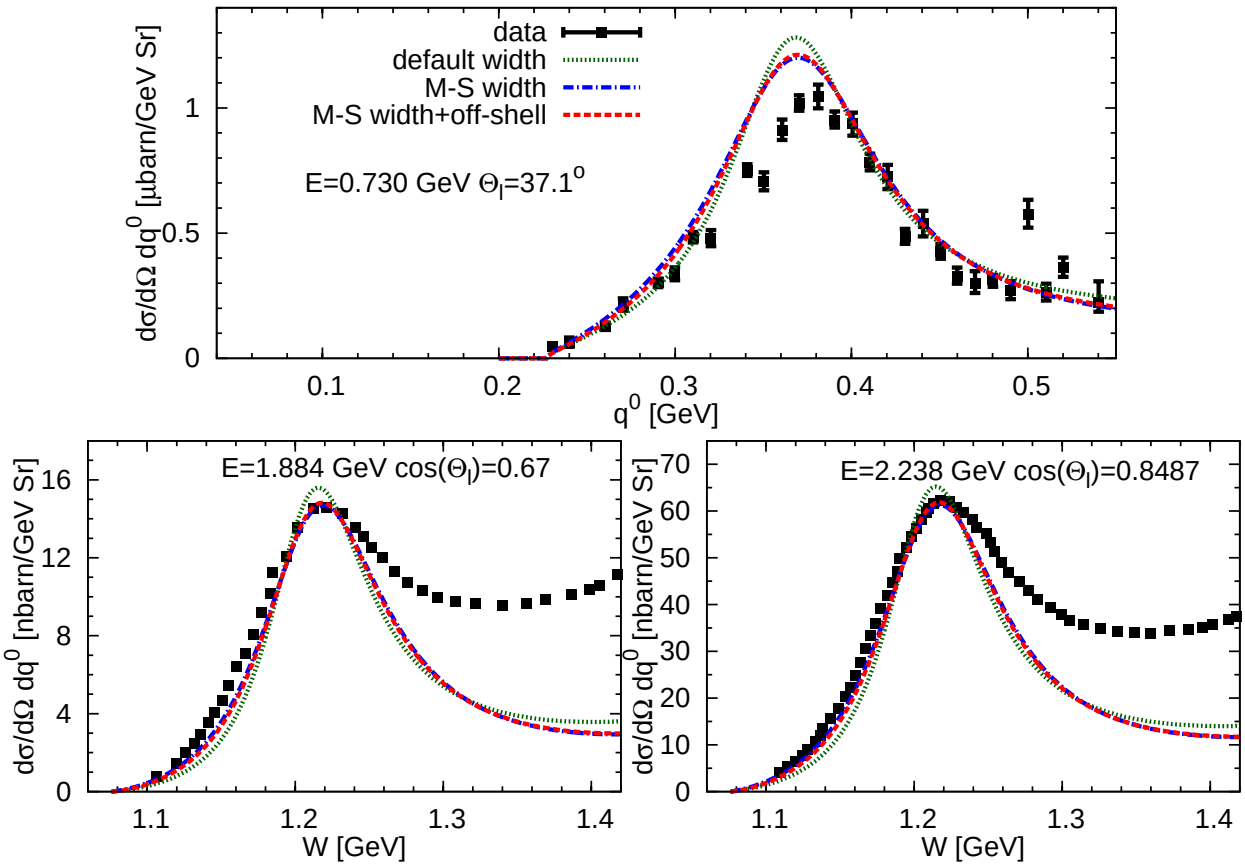

Figure 31: Comparison of the different descriptions of Δ resonance vector form factors plotted against pion electroproduction data from Ref. [141] (top) and Ref. [142] (bottom) for full HNV model. The fine dashed green curve shows calculation for default Δ width and propagator, the blue dashed curve shows calculation for Manley-Saleski Δ width and default propagator and the dashed red curve shows calculation for Manley-Saleski Δ width and off-shell propagator. The Q^2 values at peak are from top to bottom and left to right: 0.1 [GeV^2], 1.15 [GeV^2] and 0.95 [GeV^2] respectively.

Fig. 31. Impact of all the mentioned Δ resonance modifications is rather moderate, however

the Manley-Saleski width seems to give slightly better agreement with the data. In order to stay consistent with Ref. [127] we will always use the off-shell prescription whenever the M-S width is in use. Comparison of this figure to Fig. 29 shows us, that the nonresonant background is necessary in order to get a reasonable agreement with the data. The HNV model seems to badly underestimate experimental data for higher energies, which can be both a result of SPP modeling deficiencies or lack of other dynamical mechanisms including possible multi-pion production contribution for $W > 1200$ GeV and second resonance region contribution which is not accounted for in the HNV model.

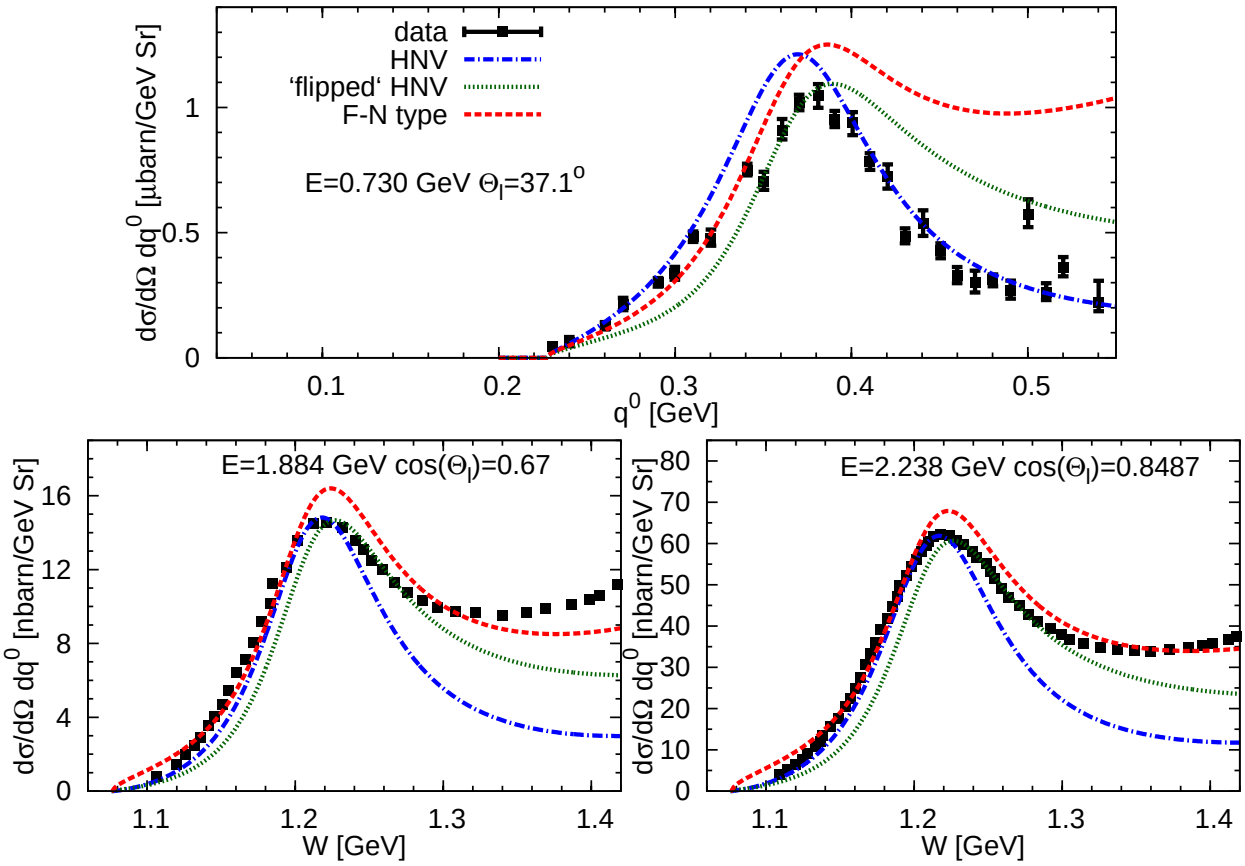

Figure 32: Comparison of HNV , HNV with different Δ diagrams sign ("flipped" HNV) and F-N type nonresonant backgroung models with inclusive $p(e, e')$ data from Ref. [141] (top) and Ref. [142] (bottom). The Q^2 values at peak are from top to bottom and left to right: 0.1 [GeV^2], 1.15 [GeV^2] and 0.95 [GeV^2] respectively.

For the presumably optimal description of Δ (Eqs. (6.46,6.47)) we have compared the HNV and F-N type background models. Such a direct comparison of these models has never been done before. Results are shown in Fig. 32. F-N type prescription works well for higher Q^2 and lepton energies, but fails to describe the data for $E_e = 730$ MeV. This fact alone makes this model useless at T2K energies and renders it less reliable, than HNV. The HNV model seems to work reasonably well for lower energies, but underestimates the high-energy data. In all SPP models there is a strong dependence on relative Δ-background terms interference sign. In order to illustrate this effect we have also plotted the predictions of "flipped" HNV model with an extra minus sign put "by hand" between the ΔP and $C\Delta P$ terms(Eqs. (6.20-6.21)) and the rest of the diagrams (Eqs. (6.22-6.24)). The resulting cross

section (blue dash-dotted line in Fig. 32) differs at large with the original HNV prediction and resembles very closely the shape of Fogli-Nardulli model predicions. It has the same problem at lowest electron energy and Q^2 as F-N model but seems to work better for higher energy and Q^2 values. The agreement with data below the Δ peak is worse, but gets better in the high-W tail. This is an indication, that all resonance-background interferences need a very careful treatment. In a consistent approach one would have to perform a multipole expansion of all pion production amplitudes and use Watson's theorem to unitarize the model. The result is a complex phase between Δ and background, which depends both on Q^2 and W.

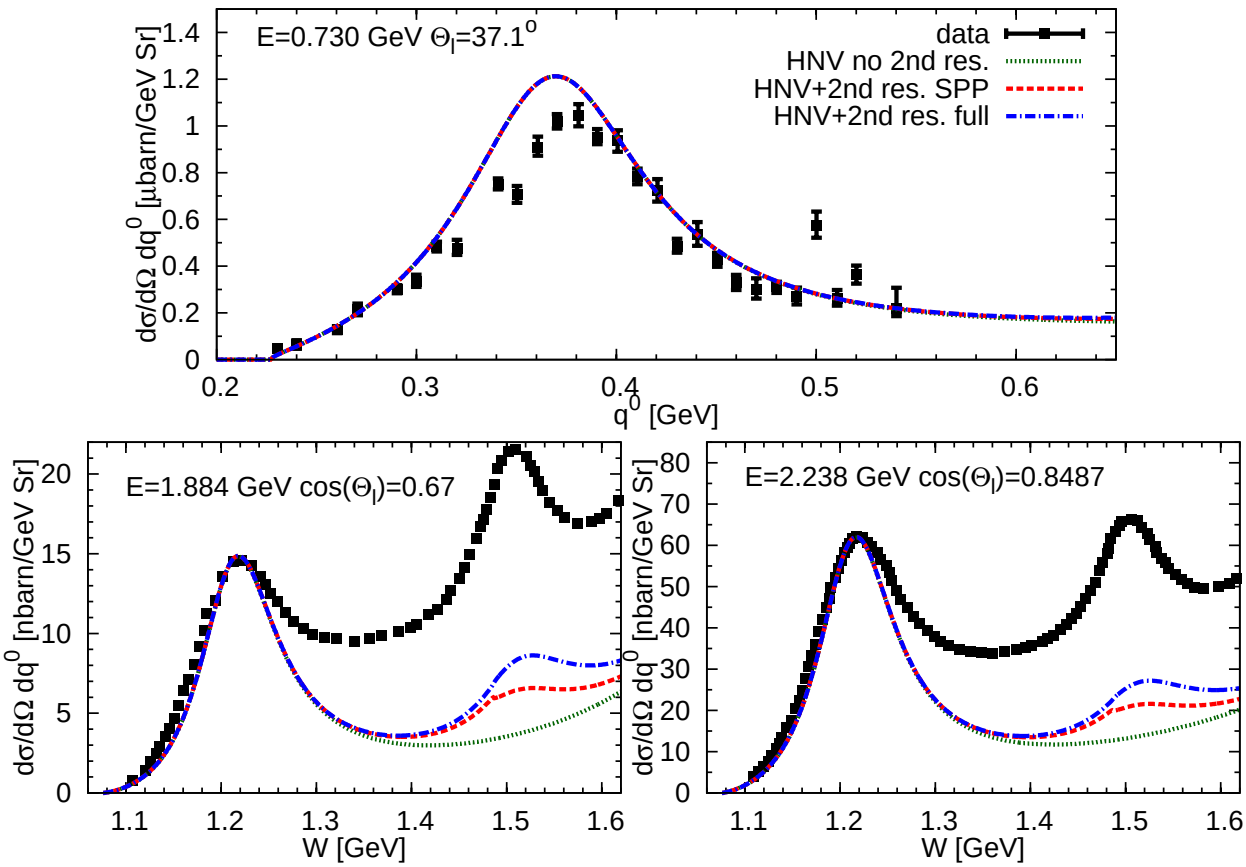

Figure 33: Comparison of HNV SPP, HNV SPP with second resonance region included and total inelastic cross section including all heavy resonance decay channels with inclusive $p(e, e')$ data from Ref. [141] (top) and Ref. [142] (bottom).

Inclusion of the second resonance region in the form of a sum of separate resonant cross sections gives a rather moderate effect, as one can see in the Fig. 33, where we extended the plot ranges to higher invariant mass values. Negligence of the resonance-background interference of S_{11}, P_{11} and D_{13} as well as two-pion production diagrams leads to a bad underestimation of data near the second resonance peak. The second resonance region contribution to SPP can be neglected for lepton energies below 1 GeV or invariant masses up to $W \approx 1.4$ GeV. The HNV model can not explain measured inelastic cross section. This is expected as it lacks higher order pion production terms, heavier meson contributions, resonances with $M_R > 1.6$ GeV etc. Theoretical cross section at the second resonance peak is far below data even after including all heavy resonance decay channels going beyond SPP

(dash-dotted blue curve). We need to make a remark about the sudden "twist" in the red dashed curve at $W \approx 1.48$ GeV. It has a probable explanation in opening of one of the resonance decay channels, which enter the denominator, but not the numerator of SPP resonance spectral function given by Eq. (6.61). We do not see it on the inclusive plot, where all the widths enter both numerator and denominator.

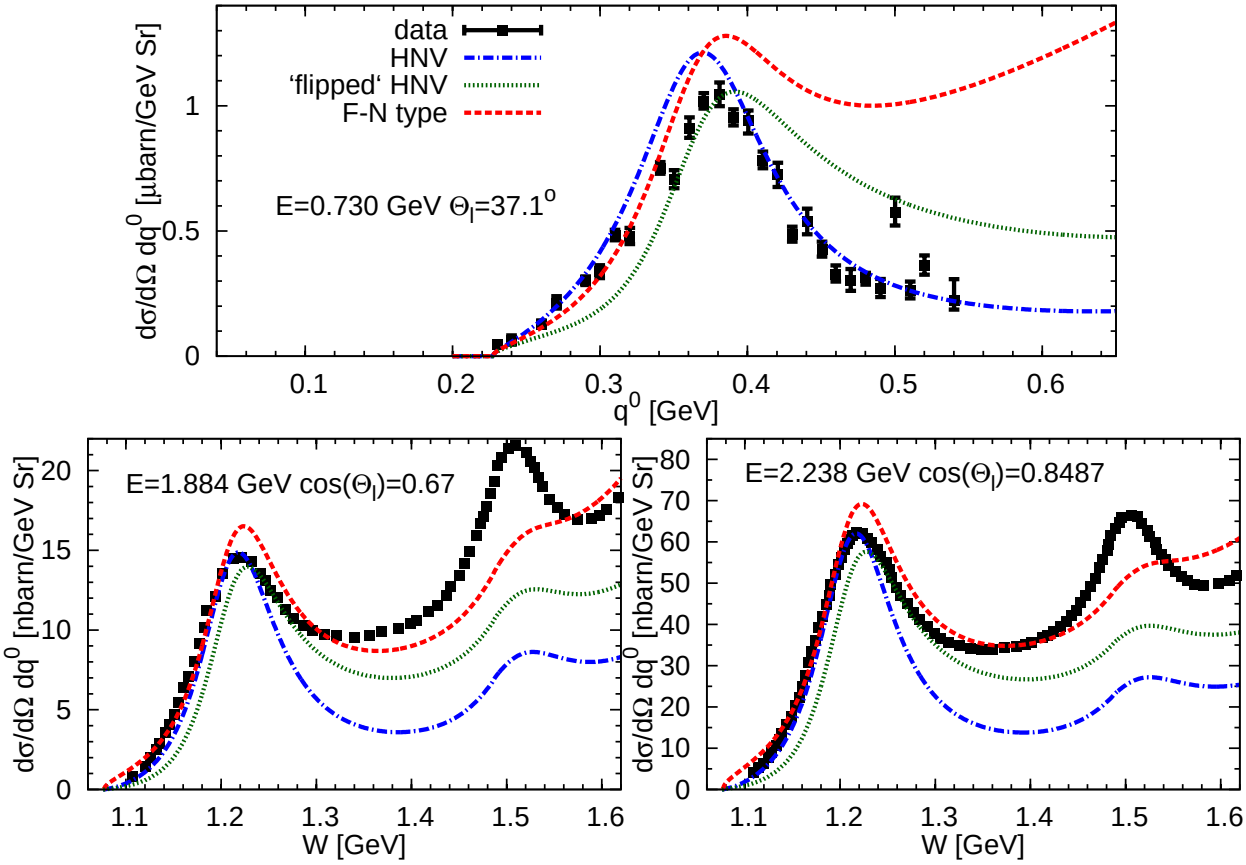

Figure 34: Comparison of HNV, HNV with different Δ diagrams sign ("flipped" HNV) and F-N type models plus second resonance region with inclusive $p(e, e')$ data from Ref. [141] (top) and Ref. [142] (bottom). Second resonance region inclusive cross section included.

As a final remark we would like to compare again the predictions of HNV model, Fogli-Nardulli model and "flipped" HNV model extended to higher invariant mass region. This has been done in Fig. 34. As we see, none of these models fits the data perfectly. At higher electron energies best results are obtained with the F-N model, but such high SPP cross section has to be discarded due to a large number of inelastic channels opening at high W. Actually, none of these models should give meaningful predictions for lepton energies above 1.5 GeV due to effective field theory limitations mentioned in section 6.1.1. Thus we find the agreement between F-N model and high-W data surprising. The behavior of HNV and its "flipped" version seem to be more realistic, as they give more space for the DIS cross section. Another noteworthy fact is that the simplified second resonance region model introduced in section 6.1.5 does not reproduce well the strength of experimental second resonance peak.

6.2.2 Results for free nucleon: neutrino bubble chamber experiments

As we have mentioned before, the axial properties of Δ resonance are studied mainly using data ANL [61] and BNL [60] bubble chamber experiments. In these experiments muon neu-

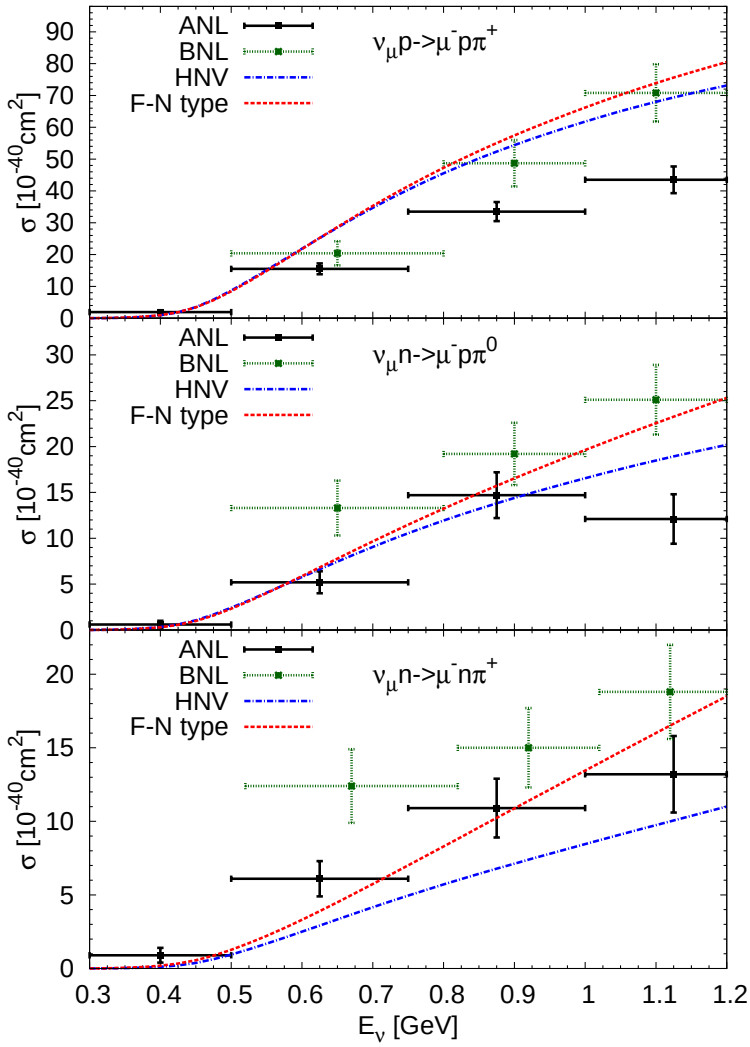

Figure 35: Total cross section predictions of HNV and F-N type models on free nucleon compared todata from Ref. [61] and Ref. [148] without invariant mass cuts. Default values $C_5^A(0) = 1.2$ and $M_{A\Delta} = 1.05$ GeV as well as $f^* = 2.14$ coupling constant from Ref. [46] are used.

trinos were scattered off deuteron target in order to measure charged current SPP process. Because of possible nonresonant contributions most of the ANL data has been published with a cut on maximum $N\pi$ invariant mass. For the case of scattering off free protons and neutrons we have made a comparison of theoretical total cross section predictions to ANL and BNL experimental data (Fig. 35). In order to stay consistent with the original HNV paper (Ref. [46]) we will use here $f^* = 2.14$, on-shell Δ propagator given by Eq. (6.32) as well as beyond-dipole axial form factor (only in this section):

$$C_5^A(Q^2) = \frac{C_5^A(0)}{(1 + Q^2/M_{A\Delta}^2)^2(1 + Q^2/(3M_{A\Delta}^2))}. \tag{6.68}$$

In the $p\pi^+$ channel both F-N type and HNV models predict cross sections slightly too large for ANL data with default values of $C_5^A(0) = 1.2$ and $M_{A\Delta} = 1.05$. Comparison with BNL yields better agreement We need to remember, that ANL experiment has a large flux uncertainty of bout 20% and that data are taken on deuteron, which slightly reduces all cross sections. In the $p\pi^0$ channel both models seem to give a rather good agreement with data. In the $n\pi^+$ channel HNV model fall visibly below data points, but F-N type seems to agree better with measured cross sections. We need to remember, that this comparison is made for $free$ nucleons and $default$ Δ axial form factor.

There exist additional Q^2-related observables provided by ANL, which are distributions of events in each of the three interaction channels. We need to remember, that the above mentioned observables are biased by additional ANL kinematic cuts and possible deuteron effects. In order to investigate the impact of nuclear effects and possible cuts we need to develop a MC method of cross-section integration on ^2H target.

6.3 SPP on deuteron: neutrino bubble chamber experiments

We shall test the F-N type and HNV SPP models against the ANL data using one of the most simple models of deuteron, showing the impact of nuclear effects on neutrino-nucleus cross section. The triple-differential cross section with respect to final lepton angle and energy can be expressed in the following form:

$$\frac{d^3\sigma}{dE_{l'}d\Omega_{l'}} = 4\pi G_F^2 \cos^2(\Theta_C)\frac{|\boldsymbol{l'}|}{|\boldsymbol{l}|}\int\frac{d^3k}{(2\pi)^3 2E_\pi}L_{\mu\nu}W^{\mu\nu}. \tag{6.69}$$

The nuclear tensor is defined as:

$$W^{\mu\nu} = \frac{1}{2}\overline{\sum_i}\frac{1}{v_{rel.}}\int\frac{d^3p'}{(2\pi)^3}\frac{\delta^{(4)}(p'+k-p-q)}{4E(p)E(p')}\sum_{s_{N'}}\langle N'\pi\left|j^\mu_{cc+}(0)\right|N\rangle^*\left\langle N'\pi\left|j^\nu_{cc+}(0)\right|N\right\rangle \tag{6.70}$$

and it describes transitions between the initial and final (pion+nucleon) hadronic states. In the above equation we define the relative neutrino-target nucleon velocity as:

$$v_{rel.} = \frac{\sqrt{(l\cdot p)^2}}{EE_p} = \left|\frac{(EE_p - \mathbf{l}\cdot\mathbf{p})}{EE_p}\right| = \left|1 - \frac{\mathbf{l}\cdot\mathbf{p}}{EE_p}\right|. \tag{6.71}$$

We sum over the final nucleon states and average over the initial ones. In our approach the deuteron effects are approximated by the nucleon motion and binding energy. In the case of deuteron we integrate the target nucleon momentum:

$$\overline{\sum_i} \equiv \frac{1}{2}\sum_{s_N}\int d^3p f(p). \tag{6.72}$$

We assume that the proton momentum is distributed according to the square of the deuteron wave function

$$f(p) \equiv |\phi(p)|^2, \int d^3p f(p) = 1. \tag{6.73}$$

This approach is different to the RFG model, because we integrate over the large nucleon momentum range with weight proportional to deuteron wave function, rather than over a fixed Fermi sea. It is also different from LFG, which is a weighted integral over infinite

sets of Fermi seas with Fermi momenta proportional to local nuclear matter density. In deuteron we do not include Pauli blocking as well. There exist several deuteron potential parameterizations (*e.g.* Hulthen [149], Paris [150], Bonn [151]). Because the differences in integrated cross sections are minor, we choose to use only the one from [150], which is also used by the authors of Ref. [152]. Furthermore, we want to introduce binding energy effects. We start with the process:

$$\nu(l) + d(P) \to \mu^-(l') + N'(p') + S(s) + \pi(k), \tag{6.74}$$

P denotes the deuteron four-momentum, p, s, and p', s are the target nucleon and spectator momenta before and after interaction. In other words, the second nucleon is treated here as a spectator. We consider the deuteron at rest:

$$P = (M_D, 0), \tag{6.75}$$

where M_D is the deuteron mass. The conservation of the energy and momentum gives the following constraint

$$l + P = l' + p' + s + k, \tag{6.76}$$

and consequently

$$\vec{l} = \vec{l'} + \vec{p'} + \vec{s} + \vec{k} \tag{6.77}$$

$$E_l + M_D = E_{l'} + E_{N'}(p') + E_S(s) + E_\pi(k). \tag{6.78}$$

The lack of FSI effects in this computation implies

$$\vec{p} + \vec{s} = 0. \tag{6.79}$$

On the other hand we have:

$$\vec{l} + \vec{p} = \vec{l'} + \vec{p'} + \vec{k} \tag{6.80}$$

$$E_l + E_N(p) = E_{l'} + E_{N'}(p') + E_\pi(k) + B(p), E_N(p) = \sqrt{M^2 + \vec{p}^2} \tag{6.81}$$

where B is the binding energy:

$$B(p) = E_N(p) + E_S(s) - M_D = 2E_N(p) - M_D. \tag{6.82}$$

We shall use the De Forest prescription [113]. We will introduce the 4-momentum transfer $\tilde{q}$, treating the hadronic part as if p was an on-shell nucleon momentum:

$$\tilde{q} = p' - p = (E_{N'}(p') - E_N(p), \vec{q}) = (q^0 - B(p), \vec{q}). \tag{6.83}$$

And consequently substitute:

$$W^{\mu\nu}(p, q, k) \to \tilde{W}^{\mu\nu}(p, \tilde{q}, k) \tag{6.84}$$

in the cross section. This requires a substitution $q \to \tilde{q}$ everywhere in Eq. (6.70).

The contribution coming from second resonance region is readily done by the same means as for the rest of the model *i. e.* :

$$\frac{d\sigma_R^{deuter}}{dE_{l'}d\Omega_{l'}} = \int d^3p f(p) \frac{|\boldsymbol{l'}| G_F^2 \cos^2(\Theta_C)}{32\pi^2\sqrt{(l\cdot p)^2 - m_l^2 M^2}} S(\tilde{W}) |\overline{\tilde{M}}_R|^2 \tag{6.85}$$

with $|\overline{\tilde{M}}_R|^2$ standing for Eq. (6.51) with the substitution $q \to \tilde{q}$ in $A_R^{\mu\nu}$ and $\tilde{W} \equiv \sqrt{(p+\tilde{q})^2}$.

In the case of deuteron we set approximately $q^0_{min} = 0$ while calculating ANL flux-averaged cross-section. The triple-differential cross sections with respect to the final lepton energy and angle have been defined in Eq. (6.69). First of all one can use the 4-momentum conserving δ-function to perform the d^3p' integral. We are left with:

$$\left\langle \frac{d\sigma}{dQ^2} \right\rangle_{ANL} = \int dE_\nu \frac{w(E_\nu)}{N} \int_{q^0_{min}}^{E_\nu - m_\mu} dq^0 \frac{G_F^2 \cos^2(\Theta_C)}{512\pi^4 E_\nu^2} \int d^3p \frac{f(p)}{v_{rel.}} \int \frac{d^3k}{E_\pi(k)} \frac{1}{E(p)E(p')} L_{\mu\nu} A^{\mu\nu}(p,q,k) \delta(p^0 + \tilde{q}^0 - k^0 - p'^0) \tag{6.86}$$

with the hadronic tensor $A^{\mu\nu}$ defined in Eq. (6.15). Approach to the solution for Eq. (6.86) depends on whether we want to calculate cross sections on a free nucleon at rest or on the deuteron. Here the cross section formula (6.86) reads:

$$\left\langle \frac{d\sigma}{dQ^2} \right\rangle_{ANL} = \int dE_\nu \frac{w(E_\nu)}{N} \int_0^{E_\nu - m_\mu} dq^0 \frac{G_F^2 \cos^2(\Theta_C)}{512\pi^4 E_\nu^2} \int d^3p \frac{f(p)}{v_{rel.}} \int \frac{d^3k}{E_\pi(k)} \frac{1}{E(p)E(p')} L_{\mu\nu} A^{\mu\nu}(p,\tilde{q},k) \delta(p^0 + \tilde{q}^0 - k^0 - p'^0) \tag{6.87}$$

with $\tilde{q}$ defined in Eq. (6.83). We will not boost the particles to nucleon rest frame, where one could in general use Eq. (6.67) to get rid of the $d\phi_\pi$ and $d\phi_N$, neither to the πN system center-of-mass frame. The reason is that ANL experiment includes several kinematical cuts and correction coefficients, listed in Tab. 1 of [61]. In general all of these cuts can be expressed as multiplicative coefficients, but we can do some of them in a more explicit manner. In particular we want to incorporate following conditions in the computations:

1. Spectator nucleon momentum s can not exceed 0.35 [GeV/c].
2. In channels (6.2) and (6.3) the neutron-to-neutrino momentum ratio p_n/p_ν has to be smaller, than 0.9.
3. In channels (6.2) and (6.3) the neutron-neutrino angle $\Theta_{n\nu}$ has to be smaller, than 150°.
4. In channels (6.2) and (6.3) the pion-muon angle $\Theta_{\pi\mu}$ has to be bigger, than 10°.

First of these conditions is straightforward to include. In deuteron model without FSI the spectator always has momentum opposite to target nucleon. The latter three give additional constraints on nucleon and pion phase spaces. Unfortunately, together with beforementioned De Forest prescription shortcomings, this makes Eq. (6.67) impossible to apply here. In other words, we need to perform all 7 integrals in Eq. (6.87). The traditional Gaussian measure numerical integral used in the case of scattering off free nucleon is too slow for deuteron calculation. One would have to calculate $\mathcal{O}(10^7)$ points. Thus we shall use the Vegas Monte Carlo integration algorithm implementation from GNU Scientific Library (GSL) [153]. It allows to perform multidimensional integrals over a pre-defined hypercube. One has to optimize the integrated function, so most of the points will be sampled within the kinematical limits. We can simplify our calculation in only one way: by performing rotation

to the system with $\boldsymbol{p}+\boldsymbol{q} \parallel \hat{z}$. We shall use the Dirac delta to establish the outgoing pion momentum to $\tilde{k}_\pi$:

$$\left\langle \frac{d\sigma}{dQ^2} \right\rangle_{ANL} = \int_{E_{min}}^{E_{max}} dE_\nu \frac{w(E_\nu)}{N} \int_0^{E_\nu - m_\mu} dq^0 \frac{G_F^2 \cos^2(\Theta_C)}{512\pi^4 E_\nu^2} \int_0^{p_{cut}} dp \int_{-1}^{1} d\cos(\Theta_n) \int_0^{2\pi} d\phi_n \frac{f(p)}{v_{rel.} E(p)}$$
$$\int_{-1}^{1} d\cos(\Theta_\pi^{(r)}) \int_0^{2\pi} d\phi_\pi^{(r)} \frac{\tilde{k}_\pi^2}{|\tilde{k}_\pi a^0 - |\boldsymbol{a}| \tilde{E}_\pi \cos(\Theta_\pi^{(r)})|} L_{\mu\nu}^{(r)} A^{\mu\nu(r)}. \tag{6.88}$$

In the above equation we have defined $\boldsymbol{a} \equiv \boldsymbol{p}+\boldsymbol{q}$ and $a^0 \equiv \tilde{q}^0 + E(p)$. The index (r) means,

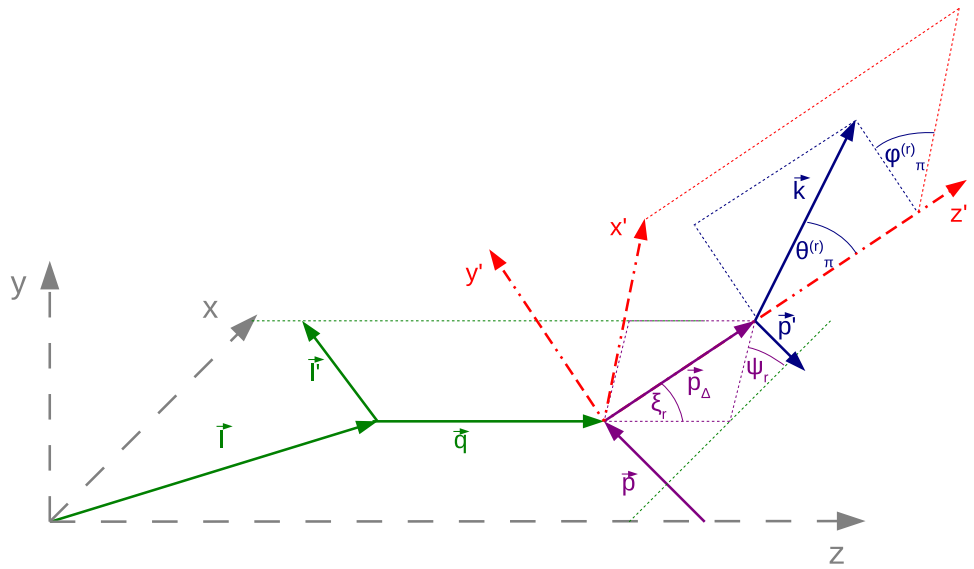

Figure 36: Kinematics and coordinate system for SPP on nucleon for frame rotated w.r.t the one defined in Fig. 25.

that we have rotated the inner integral coordinate system, so that $\boldsymbol{p}+\boldsymbol{q} \parallel \hat{z}$, as shown in Fig. 36. This rotation acts on the spacial coordinates of all 4-vectors and is performed by a matrix $\mathrm{A}^{(\mathrm{r})}$:

$$\boldsymbol{v}^{(r)} = \mathrm{A}^{(\mathrm{r})} \boldsymbol{v}; \;\; \mathrm{A}^{(\mathrm{r})} \equiv \begin{pmatrix} \cos(\xi_r)\cos(\psi_r) & \cos(\xi_r)\sin(\psi_r) & -\sin(\xi_r) \\ -\sin(\psi_r) & \cos(\psi_r) & 0 \\ \sin(\xi_r)\cos(\psi_r) & \sin(\xi_r)\sin(\psi_r) & \cos(\xi_r) \end{pmatrix} \tag{6.89}$$

with the rotation angles defined as:

$$\begin{aligned} \cos(\xi_r) &= \frac{a^z}{|\boldsymbol{a}|} \\ \sin(\xi_r) &= \sqrt{1-\cos^2(\xi_r)} \\ \cos(\psi_r) &= \frac{a^x}{|\boldsymbol{a}|\sin(\xi_r)} \\ \sin(\psi_r) &= \frac{a^y}{|\boldsymbol{a}|\sin(\xi_r)}. \end{aligned} \tag{6.90}$$

Within this system one may easily establish the pion momentum, $\tilde{k}$, by solving the equation:

$$E(\boldsymbol{a}^{(r)} - \boldsymbol{k}^{(r)}) + E_\pi(\boldsymbol{k}^{(r)}) = a^0 \tag{6.91}$$

which leds to:

$$|\boldsymbol{k}|^2 - |\boldsymbol{k}|\frac{|\boldsymbol{a}|^2\cos(\Theta_\pi^{(r)})(s+m_\pi^2-M^2)}{a_0^2-|\boldsymbol{a}^2|\cos^2(\Theta_\pi^{(r)})} - \frac{\lambda(s,m_\pi^2,M^2)}{4(a_0^2-|\boldsymbol{a}^2|\cos^2(\Theta_\pi^{(r)}))} = 0 \tag{6.92}$$

where we have dropped the rotation indices, because the rotation does not change the vector's norms. The invariant mass $s = a_0^2 - |\boldsymbol{a}|^2$ and

$$\lambda(a,b,c) = a^2+b^2+c^2-2(ab+bc+ca). \tag{6.93}$$

There may be two solutions to Eq. (6.92), but only one is physical (positive).

The Vegas integration algorithm integrates over fixed hypercubes. This means we need to put some modifications into Eq. (6.88).

1. The upper limit on energy transfer is approximated by $E_\nu - m_\mu$. We substitute:

$$\begin{aligned} q^0 &\rightarrow x\times(E_\nu - m_\mu);\ x\in[0,1] \\ dq^0 &= (E_\nu - m_\mu)dx \end{aligned} \tag{6.94}$$

2. There is a threshold condition for invariant mass $\tilde{W} > W_{thr.} = M + m_\pi$. For given $\tilde{q}^\mu$ and p^μ the biggest value of $\tilde{W}$ appears, when $\boldsymbol{p}$ and $\boldsymbol{q}$ point in the opposite directions:

$$\tilde{W}^2_{max} = (\tilde{q}^0 + E(p))^2 - \boldsymbol{p}^2 - \boldsymbol{q}^2 + 2|\boldsymbol{p}||\boldsymbol{q}|. \tag{6.95}$$

Solution for $\tilde{W}^2_{max} > W^2_{thr.}$ yields following condition for minimal nucleon momentum:

$$\begin{aligned} p_{min} &= max\left[0, \frac{|\boldsymbol{q}|((q^0+M_D)^2+M^2-W^2_{thr.})+\sqrt{d}}{2(q^0+M_D)^2}\right] \\ d &= ((q^0+M_D)^2+M^2-W^2_{thr.})^2-4(q^0+M_D)^2M^2)((q^0+M_D)^2+\boldsymbol{q}^2). \end{aligned} \tag{6.96}$$

Additionally there is another condition for maximal allowed nucleon momentum reulting from the condition $\tilde{q}^0 > 0$. This gives us following relation:

$$p_{max} = min\left[p_{cut}, \sqrt{(q^0+M_D)^2/4 - M^2}\right] \tag{6.97}$$

which leads to following variable switch:

$$\begin{aligned} p &\rightarrow y\times(p_{max}-p_{min})+p_{min};\ y\in[0,1] \\ dp &= (p_{max}-p_{min})dy \end{aligned} \tag{6.98}$$

with p_{min} and p_{max} defined in Eqs. (6.96, 6.97).

3. For any given set of $(\tilde{q}^\mu, |\boldsymbol{p}|)$ one has $\tilde{W}\in[W_{thr.}, W_{cut}]$, where $W_{cut} = 1.4$ GeV. This condition imposes limits on the nucleon azimuthal angle:

$$\begin{aligned} \cos(\Theta_n)_{min} &= max\left[-1, \frac{M^2+2E(p)\tilde{q}^0-\tilde{Q}^2-W^2_{cut}}{2|\boldsymbol{p}||\boldsymbol{q}|}\right] \\ \cos(\Theta_n)_{max} &= max\left[-1, \frac{M^2+2E(p)\tilde{q}^0-\tilde{Q}^2-W^2_{thr.}}{2|\boldsymbol{p}||\boldsymbol{q}|}\right] \end{aligned} \tag{6.99}$$

and allows us to change one more variable in our integral:

$$\begin{aligned} \cos(\Theta_n) &\rightarrow z\times(\cos(\Theta_n)_{max}-\cos(\Theta_n)_{min})+\cos(\Theta_n)_{min};\ z\in[0,1] \\ d\cos(\Theta_n) &= (\cos(\Theta_n)_{max}-\cos(\Theta_n)_{min})dz. \end{aligned} \tag{6.100}$$

With the variable changes defined in Eqs. (6.94), (6.98) and (6.100) integral needed for cross section calculation (6.88) becomes:

$$\left\langle \frac{d\sigma}{dQ^2} \right\rangle_{ANL} = \int dE_\nu \frac{w(E_\nu)}{N} \int_0^1 dx (E_\nu - m_\mu) \frac{G_F^2 \cos^2(\Theta_C)}{512\pi^4 E_\nu^2} \int_0^1 dy (p_{max} - p_{min}) \int_0^1 dz (\cos(\Theta_n)_{max} - \cos(\Theta_n)_{min}) \int_0^{2\pi} d\phi_n \frac{f(p)}{v_{rel.} E(p)} \int_{-1}^1 d\cos(\Theta_\pi^{(r)}) \int_0^{2\pi} d\phi_\pi^{(r)} \frac{\tilde{k}_\pi^2}{\tilde{k}_\pi a^0 - |\boldsymbol{a}| \tilde{E}_\pi \cos(\Theta_\pi^{(r)})|} L_{\mu\nu}^{(r)} A^{\mu\nu(r)}. \tag{6.101}$$

Using the GSL MC algorithms one can perform this integration on $\mathcal{O}(10^5)$ points, which is a huge improvement comparing to standard numerical integration methods.

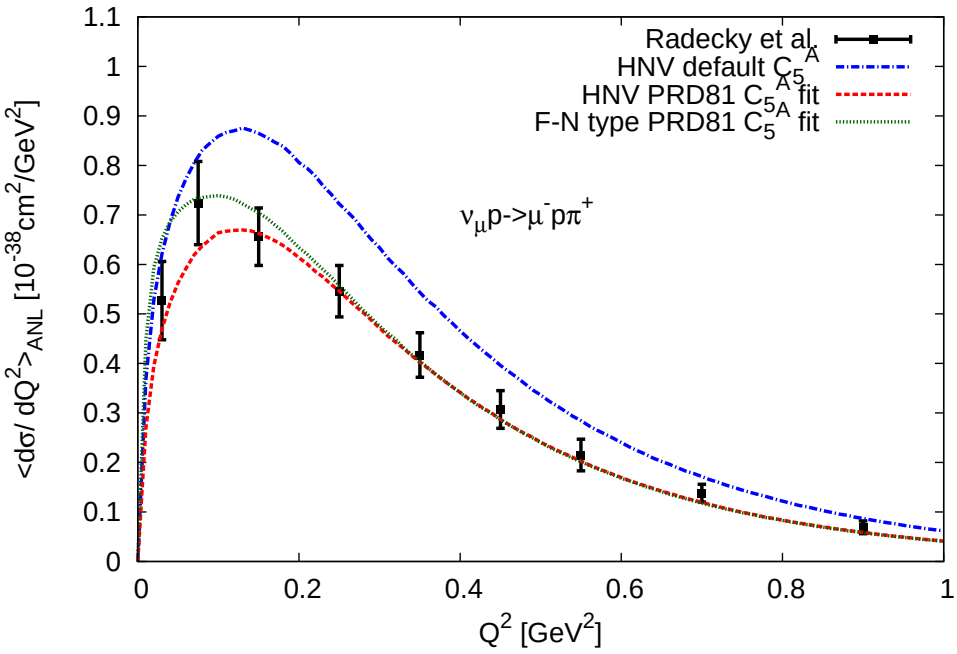

Figure 37: Comparison of HNV model predictions for $C_5^A(0) = 1.2$ and $M_{A\Delta} = 1.05$ GeV to HNV and F-N type predictions with best-fit C_5^A from Ref. [152]) on deuteron. For consistency with Ref. [152] $f^* = 2.2$ coupling constant is used. The cross section data are taken from Ref. [61].

We will make now the comparison to data using the results and conventions from Ref. [152] ($F^* = 2.2$ and C_5^A takes again dipole form from Eq. (6.37)). We will start with $d\sigma/dQ^2$ plotted in Fig. 37. Authors of Ref. [152] have performed a fit to $p\pi^+$ channel data. They obtained $C_5^A(0) = 1.0 \pm 0.11$ and $M_{A\Delta} = 0.93 \pm 0.07$ GeV. After applying the fitted values of $C_5^A(0)$ and $M_{A\Delta}$ HNV model gives almost perfect agreement with experimental data. Our result for F-N type is almost the same as for HNV, save for $Q^2 < 0.25$ GeV^2, where the F-N type model gives unphysical results (shown for $Q^2 = 0.1$ GeV^2 for electron scattering). One has to remember, that ANL predicts total cross sections systematically smaller by $\sim$30% from BNL results in all channels and has a flux uncertainty of around 20% (not shown on the plot). Taking this into account we can assume, that the default C_5^A parameters are still in a rather good agreement with data and safe to use.

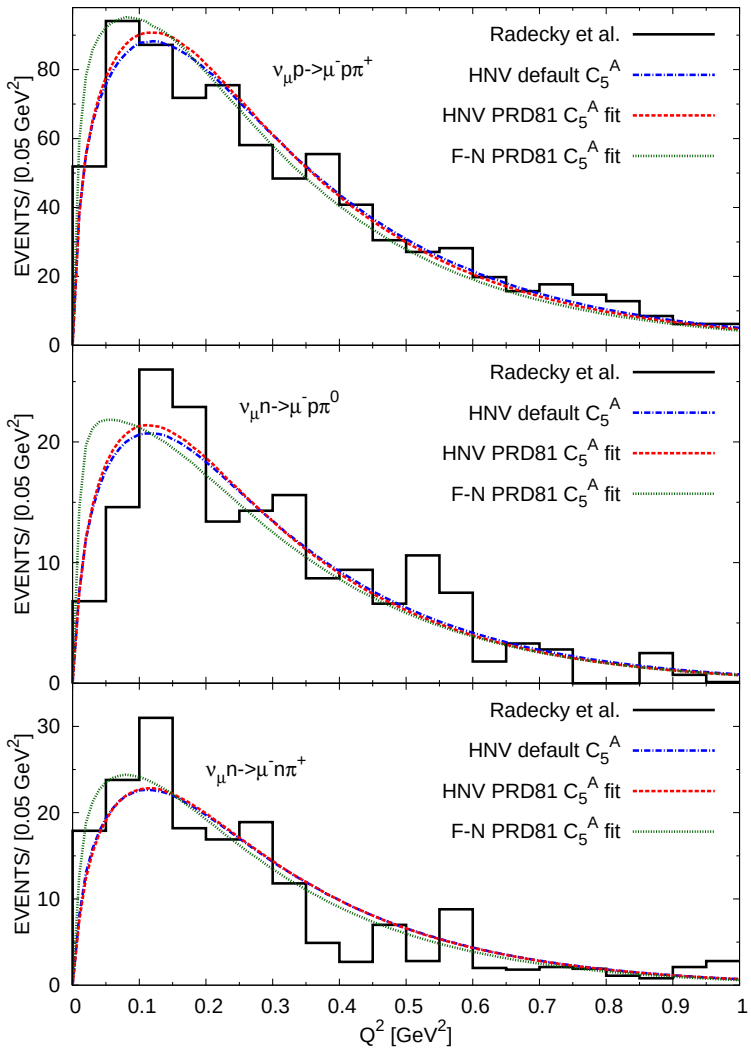

Figure 38: Comparison of HNV and F-N type model results for deuteron target and best fit valuses ($C_5^A(0) = 1.0$, $M_{A\Delta} = 0.93$ GeV) from Ref. [152] area-normalized to number of ANL events in each physical channel with data from Ref. [61].

For deuteron scattering with imposed ANL kinematic cuts we have made comparison to ANL Q^2 event distributions. In Fig. 38 we show the effects of changing parameters in $C_5^A(Q^2)$ and switching between Fogli-Nardulli type and HNV models. Biggest difference in normalized cross section is made by switching to F-N type model. Changes of C_5^A parameterization seems to give negligible results here.

We need to underline here, that all fits so far have been performed in the dominant $\nu_\mu p \to \mu^- p \pi^+$ channel and inclusion of the rest of available data might change the fitted parameters with respect to what has been calculated in Ref. [152].

6.3.1 Summary of SPP on free nucleon and deuteron targets

We have performed basic qualitative tests of the two SPP models using ANL data. Combining these results with the knowledge from previous section about pion electroproduction data we conclude, that both HNV and Fogli-Nardulli type models have their advantages and disadvantages.

The first model works well for relatively low-Q^2 values and has better theoretical foundations in a chiral effective field theory, thus it includes more nonresonant amplitudes, than F-N type. The inclusive cross section for higher invariant mass values seems to be too low, but on the other hand it leaves some space for more inelastic channels. Unfortunately, this model does not reproduce the proportions between cross sections measured in different channels by ANL and BNL experiments, which is a quite serious disadvantage. In neutrino oscillation experiments one wold like to have a realistic prediction of pion production in all channels, as the charged pions and neutral pions produce different types of backgrounds to the oscillation signal.

All ANL channels are reproduced simultaneously in the Fogli-Nardulli type model, but the low-Q^2 behavior observed in electron scattering data is unphysical. For higher Q^2 and invariant mass values this model reproduces the electron scattering data well. However, one has to notice, that for $W \gtrsim 1.4$ GeV we need space for cross section coming from channels more inelastic, than SPP. We have shown in the inclusive electron scattering case, that F-N type leaves almost no place for these channels, as it diverges badly with growing W.

Both models lack on unitarization, which would introduce a dynamical phase between the resonant and background contributions. This kind of phase may be very important, as the toy example of HNV model with flipped relative sign between Δ and background amplitudes has shown behavior different from the original HNV and closer to the one of Fogli-Nardulli model. For the neutrino scattering off atomic nuclei we choose to use the HNV model, because we will work in lower energy region $E_\nu \leq 1$ GeV where low-Q^2 contribution becomes important.

Axial coupling of the Δ resonance is still an open question, because the values have been fitted only in the $\nu_\mu p \to \mu^- p \pi^+$ channel in a way, which seems to reproduce only the ANL cross section. This cross section has an extra 20% normalization uncertainty. and total ANL cross sections are much smaller from those reported by BNL. Nuclear model uncertainties introduce a systematic bias in all observables. In order to make a conclusive fit of Δ axial properties to data one would have to incorporate realistic nuclear effects and use information from all SPP channels. Thus we find it rather safe to use $C_5^A(0) = 1.19$ and $M_{A\Delta} = 1.05$ GeV.

6.4 SPP on atomic nuclei

The theoretical approach presented in this chapter is based on the general scheme described in Ref. [70] and includes our results from Ref. [15]. The basic cross section formula for the electromagnetic or weak charged-current lepton inclusive differential cross section is described by Eq. (4.1). For the atomic nucleus model we will use the local density approximation with $\rho(\boldsymbol{r})$ being the nuclear matter density. We took the harmonic oscillator density profiles from Ref. [114] (4.61) with corrections to parameters a and R calculated in Ref. [115]. These parameters are slightly different for protons and neutrons. The local Fermi momentum is calculated from relation $k_F^N(\boldsymbol{r}) = (3\pi^2\rho(\boldsymbol{r})^N)^{\frac{1}{3}}$. Authors of [70] subtract Fermi kinetic energy from nucleons inside medium $E(p) \to E(p) - T_F$. In this manner they account for the binding effects.

The cross section can be re-expressed in terms of the gauge boson self-energy in nuclear medium, it is readily done by a substitution:

$$L_{\mu\nu} W^{\mu\nu}(\rho(\boldsymbol{r})) = -\frac{1}{\pi} \Im \left[L_{\mu\nu} \Pi^{\mu\nu}(q, \boldsymbol{r}) \right]. \tag{6.102}$$

The polarization tensor $\Pi^{\mu\nu}$ has a dimension of (energy)^3. After multiplying it by an appropriate external couplings and performing the spatial d^3r integration one gets a representation of the gauge boson self-energy. It can be evaluated by adding contributions from Feynman diagrams representing various processes, with nucleon loops having momentum cutoffs given by local Fermi momentum

A dominant SPP part is in the many body language denoted as $1p1h1\pi$ (contributions from $2p2h1\pi$ and more complicated final states is assumed to be small): there is one pion and one nucleon-hole pair ($1p1h$) in the final state. The corresponding contribution to polarization tensor can be represented as:

$$\begin{aligned} -i\Pi^{\mu\nu}_{1p1h1\pi} &= \sum_{iso}\int d^3r \int\frac{d^4p}{(2\pi)^4}\int\frac{d^4k}{(2\pi)^4} iD_\pi(k) \\ & iG_N(p)iG_{N'}(p+q-k)\mathrm{Tr}\left[A^{\mu\nu}_{1p1h1\pi}(p,q,k)\right]. \end{aligned} \tag{6.103}$$

The hadronic tensor $A^{\mu\nu}_{1p1h1\pi}$ is defined as in Eq. (6.15).

In Eq. (6.103) G_N denotes the nucleon propagator:

$$G_N(p,\boldsymbol{r}) = \frac{1}{p^0+E(p)+i\epsilon}\left(\frac{n_N(\boldsymbol{p},\boldsymbol{r})}{p^0-E(p)-i\epsilon}+\frac{1-n_N(\boldsymbol{p},\boldsymbol{r})}{p^0-E(p)+i\epsilon}\right) \tag{6.104}$$

with $n_N(\boldsymbol{p},\boldsymbol{r})$ being the occupation numbers for nucleon of isospin N. In the FG model $n_N(\boldsymbol{p},\boldsymbol{r})$ is a Heaviside step function $\Theta(|\boldsymbol{p}|-k_F^N(\boldsymbol{r}))$. Since we are working always within the LFG framework from now on we will remove the $\boldsymbol{r}$ index from notation in order to make the equations more compact. From the same reason we will not write down explicit sums over isospins. The pion propagator is defined as follows:

$$D_\pi(k) = \frac{1}{k^2-m_\pi^2+i\epsilon}. \tag{6.105}$$

The $\langle N'(p',s')\pi(k)\left|j^\mu_{cc}\right|N(p,s)\rangle$ are transition amplitudes between initial nucleon state with spin s and four-momentum p and final state containing pion with four-momentum k and nucleon with four-momentum $p=p+q-k$ and spin s'. We shall insert the explicit forms of particle propagators into Eq. (6.103):

$$\begin{aligned} -i\Pi^{\mu\nu}_{1p1h1\pi} &= -i\sum_{iso}\int d^3r\int\frac{d^4p}{(2\pi)^4}\int\frac{d^4k}{(2\pi)^4}\frac{1}{k^0-E_\pi(k)+i\epsilon}\frac{1}{k^0+E_\pi(k)-i\epsilon} \\ & \frac{1}{p^0+E(p)+i\epsilon}\left(\frac{n_N(p)}{p^0-E(p)-i\epsilon}+\frac{1-n_N(p)}{p^0-E(p)+i\epsilon}\right) \\ & \frac{1}{p^0+q^0-k^0+E(p')+i\epsilon}\left(\frac{n_{N'}(p')}{p^0+q^0-k^0-E(p')-i\epsilon}+\right. \\ + & \left.\frac{1-n_{N'}(p')}{p^0+q^0-k^0-E(p')+i\epsilon}\right)\mathrm{Tr}\left[A^{\mu\nu}_{1p1h1\pi}(p,q,k)\right]. \end{aligned} \tag{6.106}$$

First we put the outgoing pion on the mass shell and integrate over k^0:

$$\begin{aligned}\Pi^{\mu\nu}_{1p1h1\pi} &= -i\sum_{iso}\int d^3r\int\frac{d^4p}{(2\pi)^4}\int\frac{d^3k}{(2\pi)^3}\frac{1}{2E_\pi(k)}\\ &\quad \frac{1}{p^0+E(p)+i\epsilon}\left(\frac{n_N(p)}{p^0-E(p)-i\epsilon}+\frac{1-n_N(p)}{p^0-E(p)+i\epsilon}\right)\\ &\quad \frac{1}{p^0+q^0-E_\pi+E(p')+i\epsilon}\left(\frac{n_{N'}(p')}{p^0+q^0-E_\pi-E(p')-i\epsilon}+\right.\\ &+ \left.\frac{1-n_{N'}(p')}{p^0+q^0-E_\pi-E(p')+i\epsilon}\right)\mathrm{Tr}\left[A^{\mu\nu}_{1p1h1\pi}(p,q,k)\right]. \end{aligned} \tag{6.107}$$

Now we integrate over p^0 putting the final nucleon state on-shell:

$$\begin{aligned}\Pi^{\mu\nu}_{1p1h1\pi} &= \sum_{iso}\int d^3r\int\frac{d^3p}{(2\pi)^3}\int\frac{d^3k}{(2\pi)^3}\frac{1}{2E_\pi(k)}\\ &\quad \left(\frac{1}{2E(p)(E(p)+q^0-E_\pi+E(p')+i\epsilon)}\frac{n_N(p)(1-n_{N'}(p'))}{E(p)+q^0-E_\pi-E(p')+i\epsilon}\right.\\ &+ \left.\frac{1}{2E(p')(E(p')-q^0+E_\pi+E(p)+i\epsilon)}\frac{n_{N'}(p')(1-n_N(p))}{E(p')-q^0+E_\pi-E(p)+i\epsilon}\right)\times\\ &\times \mathrm{Tr}\left[A^{\mu\nu}_{1p1h1\pi}(p,q,k)\right]. \end{aligned} \tag{6.108}$$

Now we can evaluate the expression needed in the cross section:

$$\begin{aligned}-\frac{1}{\pi}\Im\left(\Pi^{\mu\nu}_{1p1h1\pi}L_{\mu\nu}\right) &= \sum_{iso}\int d^3r\int\frac{d^3p}{(2\pi)^3}\int\frac{d^3k}{(2\pi)^3}\frac{1}{8E_\pi(k)E(p)E(p')}\\ &\quad [n_N(p)(1-n_{N'}(p'))+n_{N'}(p')(1-n_N(p))]\\ &\quad \delta(E(p')-q^0+E_\pi-E(p))\mathrm{Tr}\left[A^{\mu\nu}_{1p1h1\pi}(p,q,k)\right]L_{\mu\nu}. \end{aligned} \tag{6.109}$$

In the above equation one has to take into account also the non-perturbative medium modifications of hadron properties. The leading effects will be discussed briefly in the next paragraph.

6.4.1 Δ self-energy in nuclear matter

The free resonance decay width gets decreased because of Pauli blocking. We do not take into the account additional information on $N\pi$ angular momentum, which is absent in the free Lagrangian, and assume a uniform distribution of decay pions in the Δ rest frame. We calculate all CMS variables according to Eq. (F.7). Boost from CMS to laboratory frame is realized by $B^{\mu\nu}_{p^0_\Delta,\boldsymbol{p}_\Delta}$:

$$B^{\mu\nu}_{p^0_\Delta,\boldsymbol{p}_\Delta} = \left(\begin{array}{c|c} \frac{p^0_\Delta}{W} & -\frac{p^j_\Delta}{W} \\ \frac{p^i_\Delta}{W} & \delta^{ij}+\frac{p^i_\Delta p^j_\Delta}{W(p^0_\Delta+W)} \end{array}\right). \tag{6.110}$$

We have taken into account, that Δ is not an on-mass-shell particle here. Thus one has to substitute the usual relation $p^2_\Delta = M^2_\Delta$ by the *C.M.S.* invariant mass $p^2_\Delta = s = (p+q)^2$.

To check, whether it is a properly defined Lorentz matrix, one can simply try to boost $p^\mu_\Delta = (p^0_\Delta, \boldsymbol{p}_\Delta)$ hence and forth. First let us perform a boost to the CMS with $B^{\mu\nu}_{p^0_\Delta,-\boldsymbol{p}_\Delta}$:

$$\begin{aligned} B^{\mu\nu}_{p^0_\Delta,-\boldsymbol{p}_\Delta} p^\mu_\Delta &= \left(\frac{p^{0^2}_\Delta - \boldsymbol{p}^2_\Delta}{W}, -\frac{p^0_\Delta \boldsymbol{p}_\Delta}{W} + \boldsymbol{p}_\Delta + \frac{\boldsymbol{p}_\Delta \boldsymbol{p}^2_\Delta}{W(W+p^0_\Delta)} \right) = \\ &= \left(W, \frac{\boldsymbol{p}_\Delta (p^2_\Delta + p^0_\Delta W - p^0_\Delta W + W^2 - p^{0^2}_\Delta)}{W(p^0_\Delta + W)} \right) = (W, 0). \end{aligned} \tag{6.111}$$

The boost from rest frame is trivial if one uses $B_{p^0_\Delta,\boldsymbol{p}_\Delta}$. It implies, that

$$B_{-\boldsymbol{p}_\Delta}(|\boldsymbol{p}_\Delta|) B_{\boldsymbol{p}_\Delta}(|\boldsymbol{p}_\Delta|) = id. \tag{6.112}$$

With the definition of boost tensor (6.110) we find the LAB final nucleon energy:

$$E(p') = \frac{p^0_\Delta E^*_N + |\boldsymbol{p}_\Delta||\boldsymbol{k}^*| \cos(\Theta^*_N)}{W}. \tag{6.113}$$

Under the assumption of spherically symmetric Δ decay in CMS the Pauli blocking factor is a pure phase-space factor. It is calculated to be:

$$F(p^0_\Delta, |\boldsymbol{p}_\Delta|, E_F) = \frac{p^0_\Delta E^*_N + |\boldsymbol{p}_\Delta||\boldsymbol{k}^*| - E_F W}{|\boldsymbol{p}_\Delta||\boldsymbol{k}^*|} \tag{6.114}$$

and

$$\Gamma^{vac} \to \tilde{\Gamma} = F(p^0_\Delta, |\boldsymbol{p}_\Delta|, E_F)\Gamma^{vac}(s). \tag{6.115}$$

Inside nucleus other Δ decay channels are opened: the two- and three-nucleon absorption. The net effect is an overall increase of the Δ width.

$$\begin{aligned} \Gamma^{vac.}_\Delta(s) &\to 2(\frac{1}{2}\tilde{\Gamma}_\Delta + i\Sigma^{matter}_\Delta) = \\ &= \tilde{\Gamma}_\Delta - 2(\Im\Sigma_{1p1h1\pi} + \Im\Sigma_{2p2h} + \Im\Sigma_{3p3h}) + 2i\Re\Sigma_\Delta \end{aligned} \tag{6.116}$$

In [58] Oset parameterized this width as a functions of either the incoming pion kinetic energy $x = \frac{T_\pi}{m_\pi}$ or the real photon energy and the local density of nuclear matter. We use this approach in our computations. It is necessary to *translate* the Oset results obtained in the kinematical situations of real photon or pion scattering to the situation of virtual boson interaction. It was assumed that the Oset functions:

$$\begin{aligned} -\Im\Sigma_{1p1h1\pi} &= C_{1p1h1\pi} \left(\frac{\rho}{\rho_0}\right)^\alpha \\ -\Im\Sigma_{2p2h} &= C_{2p2h} \left(\frac{\rho}{\rho_0}\right)^\beta \\ -\Im\Sigma_{3p3h} &= C_{3p3h} \left(\frac{\rho}{\rho_0}\right)^\gamma \\ \rho_0 &= 0.17\ [\mathrm{fm}^{-3}] \end{aligned} \tag{6.117}$$

(all C_x and α, β, γ are the functions of photon energy or pion kinetic energy) are in a good approximation the functions of the average invariant hadronic system mass. The relations:

$$\langle W^2 \rangle = \begin{cases} M^2 + 2E_\gamma \langle E_N(\rho_N) \rangle & \gamma \\ M^2 + 2E_\pi \langle E_N(\rho_N) \rangle + m_\pi^2 & \pi \end{cases} \tag{6.118}$$

together with $W^2 = (p_N + q)^2$ allow us to *translate* the virtual boson into one of the available parameterizations. The numerical values for the real photon scattering have been given in the following table: From these few values one has to get a well-defined behavior of self-energies.

ω MeV	$C_{1p1h1\pi}$ MeV	C_{2p2h} MeV	C_{3p3h} MeV	α	β
100	0	12.9	0	1	0.31
200	5.5	19.0	3.7	0.93	0.66
300	11.7	16.6	16.5	0.47	0.79
400	14.5	15.1	21.2	0.40	0.85
500	5.4	12.0	12.5	0.47	0.89

The algorithm interpolates the values between given points. There are some additional assumptions: $C_i(0) = 0$, because for photons with zero energy there are no possible physical processes. Furthermore there were some available plots in [58], which allowed us to establish more realistic thresholds. The density dependence coefficients $\alpha, \beta, \gamma = 2\beta$ are assumed to be constant for photon energies below 100 MeV.

The real part of self-energy is yet another challenge. It has been discussed for example in Ref. [154] for the case of electron scattering. The authors say, that the real part of Δ self-energy can be parametrized by a simple linear function of incident real photon energy and local density:

$$\Re\Sigma_\Delta \approx (-70\text{MeV} + 0.113 E_\gamma \text{MeV}) \frac{\rho}{\rho_0}. \tag{6.119}$$

There are some additional effects coming from the Δh RPA resummations. In the case of electron scattering one can account for the RPA sum just by replacing the real part of self-energy by:

$$\Re\Sigma_\Delta \to \Re\Sigma_\Delta + \frac{4}{9}(f_{\pi N\Delta}/f_{\pi NN})^2 V_t \rho. \tag{6.120}$$

The nucleon-nucleon longitudinal and transverse potentials have a few parametrizations. The simplest one assumes explicit π and ρ-meson exchanges.

$$\begin{aligned} V_l &= \frac{f_{\pi NN}^2}{m_\pi^2} \left[\boldsymbol{q}^2 D_\pi(q) F_\pi(q)^2 + g' \right] \\ V_t &= \frac{f_{\pi NN}^2}{m_\pi^2} \left[\boldsymbol{q}^2 D_\rho(q) F_\rho(q)^2 C_\rho + g' \right]. \end{aligned} \tag{6.121}$$

In the above equations $D_x = \frac{1}{m_x^2 - q^2}$ are the standard propagators of π and ρ mesons ($m_\pi \approx$ 138 MeV, $m_\rho \approx 776$ MeV), $F_x = \frac{\Lambda_x^2 - m_x^2}{\Lambda_x^2 - q^2}$ are the phenomenological virtual meson form factors with $\Lambda_\pi = 1.25 GeV$ and $\Lambda_\rho = 2.5 GeV$. The modification of ρ meson interaction coupling is taken into account in the $C_\rho = 2.2$. There is also a Landau-Migdal factor $g' \approx 0.65$

responsible for the short range correlations. In the Ref. [154] there are some refinements of this interaction model, replacing g' with an effective meson exchange effect.

$$\begin{aligned} V_l &= \frac{f_{\pi NN}^2}{m_\pi^2}\Big[\boldsymbol{q}^2(D_\pi(q)F_\pi(q)^2 - \tilde{D}_\pi(q)\tilde{F}_\pi(q)^2) + \\ &- \frac{1}{3}\boldsymbol{q_c}^2(\tilde{D}_\pi(q)\tilde{F}_\pi(q)^2 + 2\tilde{D}_\rho(q)\tilde{F}_\rho(q)^2 C_\rho)\Big] \\ V_t &= \frac{f_{\pi NN}^2}{m_\pi^2}\Big[\boldsymbol{q}^2 C_\rho(D_\rho(q)F_\rho(q)^2 - \tilde{D}_\rho(q)\tilde{F}_\rho(q)^2) \\ &- \frac{1}{3}\boldsymbol{q_c}^2(\tilde{D}_\pi(q)\tilde{F}_\pi(q)^2 + 2\tilde{D}_\rho(q)\tilde{F}_\rho(q)^2 C_\rho)\Big]. \end{aligned} \tag{6.122}$$

In the case of neutrino interaction one can perform the same trick, but now the time-like components and space-like components of the polarization tensor are renormalized in a different manner. Time-like part gets the longitudinal part of potential instead.

In our calculations we chose a more simple, but widely accepted approximation. For the real part of self-energy we use the same prescription as in [52], [53], [56] and [57]:

$$\Re(\Sigma_\Delta) \approx 40\frac{\rho(r)}{\rho(0)}\ \text{MeV}. \tag{6.123}$$

This prescription neglects different renormalizations of the longitudinal and transverse Δ response functions in the nuclear medium, but for our purpose it is sufficient.

The main problem in using these prescriptions in model of [46] comes from the fact that Σ_Δ is calculated using nonperturbative effects not included in tree-level diagrams of Eqs. (6.20-6.26). All of them contain simple single pion interaction vertex. Thus we modify only the widths in denominators of ΔP diagram by substituting:

$$\begin{aligned} &\frac{1}{p_\Delta^2 - M_\Delta^2 + iM_\Delta\Gamma^{vac.}(s)} \rightarrow \\ \rightarrow &\frac{1}{p_\Delta^2 - M_\Delta^2 + iM_\Delta\left[\tilde{\Gamma} - 2(\Im\Sigma_\Delta - i\Re\Sigma_\Delta)\right]}. \end{aligned} \tag{6.124}$$

The many-body correction to the SPP through Δ resonance $\Im\Sigma_{1p1h1\pi}$ and cross sections for multinucleon channels connected to $\Im\Sigma_{2p2h}$ and $\Im\Sigma_{3p3h}$ can be accounted for by changing the $|\Delta P|^2$ contribution (6.20). It can be done by replacing it by the full Δ resonance production cross section. The polarization tensor describing production of the Δ resonance can be derived in a straightforward manner:

$$\begin{aligned} -i\Pi_{\Delta h}^{\mu\nu} &= \int d^3r \sum_{iso} C_{iso} \int \frac{d^4p}{(2\pi)^4} i \frac{1}{p^0 + E(p) + i\epsilon}\left[\frac{n_N(p)}{p^0 - E(p) - i\epsilon} + \frac{1 - n_N(p)}{p^0 - E(p) + i\epsilon}\right] \\ & i\frac{\mathrm{Tr}\left[\gamma^0\Gamma^{\alpha\mu\dagger}\gamma^0 P_{\alpha\beta}^{3/2}(p_\Delta)\Gamma^{\beta\nu}(\not{p} + M)\right]}{p_\Delta^2 - M_\Delta^2 + iM_\Delta\Gamma_\Delta}. \end{aligned} \tag{6.125}$$

As for the isospin dependence in C_{iso}: for electrons proton and neutron get the same factor of 1; for neutrinos/antineutrinos protons/neutrons get a factor of 3 because of the Clebsch-Gordan $\sqrt{3}$ in the weak Δ excitation vertex. The decays of Δ resonance into pion-nucleon

pair are then calculated for different charge states using Clebsch-Gordan coefficients of $\Delta \to \pi N$ reactions. The pionless process depends only on the isospins in primary Δ excitation vertex. Here only the direct diagram gives rise to the physical process:

$$\Pi^{\mu\nu}_{\Delta h} = \int d^3r \sum_{iso} C_{iso} \int \frac{d^3p}{(2\pi)^3} \frac{n_N(p)}{2E(p)} \frac{\mathrm{Tr}\left[\gamma^0 \Gamma^{\alpha\mu\dagger} \gamma^0 P^{3/2}_{\alpha\beta}(p_\Delta) \Gamma^{\beta\nu} (\not{p} + M)\right]}{p_\Delta^2 - M_\Delta^2 + i M_\Delta \Gamma_\Delta}. \quad (6.126)$$

Because Oset's model is totally nonrelativistic, we do a little expansion in the denominator of the Δ-propagator, assuming $\frac{1}{2}(W + M_\Delta) \approx M_\Delta$ ($W^2 \equiv p_\Delta^2$):

$$\Pi^{\mu\nu}_{\Delta h} \approx \int d^3r \sum_{iso} C_{iso} \int \frac{d^3p}{(2\pi)^3} \frac{n_N(p)}{2E(p)} \frac{\mathrm{Tr}\left[\gamma^0 \Gamma^{\alpha\mu\dagger} \gamma^0 P^{3/2}_{\alpha\beta}(p_\Delta) \Gamma^{\beta\nu} (\not{p} + M)\right]}{(M_\Delta + W)(W - M_\Delta + i\frac{1}{2}\Gamma_\Delta)}. \quad (6.127)$$

We can insert the self-energy parts. As for the imaginary product neeed for cross section:

$$-\frac{1}{\pi} \Im \Pi^{\mu\nu}_{\Delta h} L_{\mu\nu} \approx \int \frac{r^2 dr}{4\pi^3} \sum_{iso} C_{iso} \int d^3p \frac{n_N(p)(\frac{1}{2}\tilde{\Gamma} - \Im\Sigma_\Delta)}{E(p)(M_\Delta + W)} \frac{\mathrm{Tr}\left[\gamma^0 \Gamma^{\alpha\mu\dagger} \gamma^0 P^{3/2}_{\alpha\beta}(p_\Delta) \Gamma^{\beta\nu} (\not{p} + M)\right] L_{\mu\nu}}{(W - (M_\Delta + \Re\Sigma_\Delta))^2 + (\frac{1}{2}\tilde{\Gamma} - \Im\Sigma_\Delta)^2}. \quad (6.128)$$

The cross section in electron scattering is then:

$$\frac{d^3\sigma}{dE' d\Omega'} \approx \frac{\alpha^2 |\boldsymbol{l}'|}{2\pi^3 Q^4 |\boldsymbol{l}|} \int dr r^2 \sum_{iso} C_{iso} \int d^3p \frac{n_N(p)(\frac{1}{2}\tilde{\Gamma} - \Im\Sigma_\Delta)}{E(p)(M_\Delta + W)} \cdot \frac{\mathrm{Tr}\left[\gamma^0 \Gamma^{\alpha\mu\dagger} \gamma^0 P^{3/2}_{\alpha\beta}(p_\Delta) \Gamma^{\beta\nu} (\not{p} + M)\right] L_{\mu\nu}}{(W - (M_\Delta + \Re\Sigma_\Delta))^2 + (\frac{1}{2}\tilde{\Gamma} - \Im\Sigma_\Delta)^2} \quad (6.129)$$

and in νCC scattering:

$$\frac{d^3\sigma}{dE' d\Omega'} \approx \frac{G_F^2 \cos^2(\Theta_C) |\boldsymbol{l}'|}{16\pi^5 |\boldsymbol{l}|} \int dr r^2 \sum_{iso} C_{iso} \int d^3p \frac{n_N(p)(\frac{1}{2}\tilde{\Gamma} - \Im\Sigma_\Delta)}{E(p)(M_\Delta + W)} \cdot \frac{\mathrm{Tr}\left[\gamma^0 \Gamma^{\alpha\mu\dagger} \gamma^0 P^{3/2}_{\alpha\beta}(p_\Delta) \Gamma^{\beta\nu} (\not{p} + M)\right] L_{\mu\nu}}{(W - (M_\Delta + \Re\Sigma_\Delta))^2 + (\frac{1}{2}\tilde{\Gamma} - \Im\Sigma_\Delta)^2}. \quad (6.130)$$

With Eqs. (6.109) and (6.129), (6.130)) we are ready to evaluate all the necessary SPP cross sections on atomic nuclei.

6.4.2 Numerical procedures

We shall discuss now the integration procedures used in our calculations of SPP cross section on atomic nuclei. We shall focus on the approximation done by the authors of Ref. [70] in order to estimate the Eq. (6.109). The full integration of cross section within LDA (as given in Eq. (6.109)) even with an assumption of spherically symmetric nuclear matter distribution and on-shell nucleons would require performing six nested integrals. For a small

$\mathcal{O}(10)$ number of integration points in each of them we would need to evaluate $\mathcal{O}(10^6)$ points in the numerical integration procedure to obtain just one point in the triple-differential cross section. Thus the authors of Ref. [70] assumed the nucleon momentum to be an average one in local Fermi sea, $\langle|\boldsymbol{p}|\rangle = \sqrt{\frac{3}{5}}k_F^N(\boldsymbol{r})$. Furthermore $\boldsymbol{p}$ is assumed to be orthogonal to the $(\boldsymbol{q},\boldsymbol{k})$ plane.

$$\begin{aligned}
-\frac{1}{\pi}\Im\left(\Pi^{\mu\nu}_{1p1h1\pi}L_{\mu\nu}\right) \approx & \sum_{iso}\int d^3r\int\frac{d^3k}{(2\pi)^3}\frac{1}{2E_\pi(k)}\mathrm{Tr}\left[A^{\mu\nu}_{1p1h1\pi}(\langle p\rangle,q,k)\right]L_{\mu\nu} \\
& \int\frac{d^3p}{(2\pi)^3}\frac{[n_N(p)(1-n_{N'}(p'))+n_{N'}(p')(1-n_N(p))]}{4E(p)E(p')} \\
& \delta(E(p')-q^0+E_\pi-E(p)) \qquad (6.131)
\end{aligned}$$

Within this approximation the number of nested integrals is reduced by 2 (6.131). The integral over d^3p can now be performed analytically, giving a result proportional to the Lindhard function. There are severe shortcomings of this approximation and we loose a lot of precision. One example is the threshold behavior of the pion production cross section. The hadronic tensor is described by an *averaged* invariant pion-nucleon mass. Thus the physically meaningful tensor is obtained, when

$$\langle W^2\rangle = M^2 + 2\langle E_N\rangle q^0 + q_\mu^2 \geq (M+m_\pi)^2. \qquad (6.132)$$

The above mentioned condition is important for nucleon pole diagram, for which an unphysical W^2 may give rise to a singularity at $(\langle p\rangle + q)^2 = M^2$. This requires an additional cutoff in the acceptable kinematics, which sometimes moves up the threshold for pion production process in an artificial way.

Taking into account, that the pion may carry a charge and the nucleus atomic number can be changed, one can establish the threshold corrected energy transfer (as for the quasielastic peak):

$$\tilde{q}^0 = q^0 - Q_{corr} + \Delta_{E_F}, \Delta_{E_F} \equiv E_F^N - E_F^{N'}. \qquad (6.133)$$

In this way one accounts for the difference of rest masses of isotopes by subtracting the rest mass difference $Q_{corr.}$ and different Fermi levels of protons and neutrons. We substitute $q^0 \to \tilde{q}^0$ everywhere in the hadronic part of the polarization tensor. The $\tilde{q}^0$ is also used to calculate the effective W^2 in Eq. 6.132. The integration limit in pion energy is

$$E_\pi \in (m_\pi, \tilde{q}^0). \qquad (6.134)$$

When the pion energy is given, one can also establish the limit in the angular integration. It is the limit, in which the Lindhard function $U(\tilde{q}-k, E_F)$ is nonzero. One has to solve the condition, that the lower limit in the nucleon energy integration, given by Eq. (4.81), is smaller, than E_{FN} for q^μ replaced with $q^\mu - k^\mu$ (or $E_{FN'}$ and $-(q^\mu - k^\mu)$ for the exchange bubble). The limiting cases are:

$$E_{\min} = \mp\frac{1}{2}(\tilde{q}^0 - E_\pi) \pm \frac{1}{2}|\boldsymbol{q}-\boldsymbol{k}|\sqrt{1-\frac{4M^2}{(\tilde{q}-k)^2}} = E_{FN/N'} \qquad (6.135)$$

for direct/exchange diagrams. In the isospin symmetric nuclei, like ^{12}C, the exchange part of cross section given by the terms with $n_{N'}(p')(1-n_N(p))$ is negligibly small and thus we neglect it. Let us denote $a^0 = \tilde{q}^0 - E_\pi$, $\boldsymbol{q}-\boldsymbol{k}=\boldsymbol{a}$. We find:

$$\begin{aligned} E_{FN} &= -\frac{1}{2}a^0 + \frac{1}{2}|\boldsymbol{a}|\sqrt{1-\frac{4M^2}{a_\mu^2}} \\ (2E_{FN}+a^0)^2 &= \boldsymbol{a}^2\left(1-\frac{4M^2}{a_\mu^2}\right) \\ 0 &= (\boldsymbol{a}^2)^2+\boldsymbol{a}^2(4M^2-(a^0)^2-(2E_{FN}+a^0)^2)+(a^0)^2(2E_{FN}+a^0)^2. \end{aligned} \tag{6.136}$$

The above quadratic equation has two solutions for $\boldsymbol{a}^2$:

$$\begin{aligned} \boldsymbol{a}^2_{min/max} &= \frac{(a^0)^2+(2E_F+a^0)^2-4M^2 \mp \sqrt{\Delta}}{2} \\ \Delta &= 16M^4+(a^0)^4+(2E_F+a^0)^4-2((2E_F+a^0)^2(a^0)^2+ \\ &+ 4(a^0)^2M^2+4M^2(2E_F+a^0)^2. \end{aligned} \tag{6.137}$$

It is easy to verify, that both of these solutions are positive. They give limitations for the pionic angle from the condition:

$$\boldsymbol{a}^2_{min/max} = \boldsymbol{q}^2+\boldsymbol{k}^2-2|q||k|cos(\Theta_{max/min}). \tag{6.138}$$

In the program there is an additional failsafe to check, whether these solutions are in $[-1,1]$ range. The code distinguishes all isospin channels and treats them separately due to difference in Fermi levels and changes in the nucleus charge. Details can be found in Appendix I.

$$\begin{aligned} -\frac{1}{\pi}\Im\left(\Pi^{\mu\nu}_{1p1h1\pi}L_{\mu\nu}\right) &\approx \frac{1}{256\pi^5}\sum_{iso}\int d^3r\int_{m_\pi}^{\tilde{q}^0}kdE_\pi\int_{\cos(\Theta_{min})}^{\cos(\Theta_{max})}d\cos(\Theta_\pi)\int_0^{2\pi}d\phi_\pi\frac{1}{|\boldsymbol{q}-\boldsymbol{k}|} \\ &(E_{FN}-E_{min}(q-k,k'_F))\,\mathrm{Tr}\left[A^{\mu\nu}_{1p1h1\pi}(\langle p\rangle,q,k)\right]L_{\mu\nu}. \end{aligned} \tag{6.139}$$

In the case of electron scattering the cross section will be:

$$\begin{aligned} \frac{d^3\sigma}{dE'd\Omega'} &\approx \frac{\alpha^2}{32\pi^4Q^4}\frac{|\boldsymbol{l'}|}{|\boldsymbol{l}|}\sum_{iso}\int drr^2\int_{m_\pi}^{\tilde{q}^0}kdE_\pi\int_{\cos(\Theta_{min})}^{\cos(\Theta_{max})}d\cos(\Theta_\pi)\int_0^{2\pi}d\phi_\pi\frac{1}{|\boldsymbol{q}-\boldsymbol{k}|} \\ &(E_{FN}-E_{min}(q-k,k'_F))\,\mathrm{Tr}\left[A^{\mu\nu}_{1p1h1\pi}(\langle p\rangle,q,k)\right]L_{\mu\nu} \end{aligned} \tag{6.140}$$

and in the case of νCC process:

$$\begin{aligned} \frac{d^3\sigma}{dE'd\Omega'} &\approx \frac{G_F^2\cos^2(\Theta_C)}{256\pi^6}\frac{|\boldsymbol{l'}|}{|\boldsymbol{l}|}\sum_{iso}\int drr^2\int_{m_\pi}^{\tilde{q}^0}kdE_\pi\int_{\cos(\Theta_{min})}^{\cos(\Theta_{max})}d\cos(\Theta_\pi)\int_0^{2\pi}d\phi_\pi\frac{1}{|\boldsymbol{q}-\boldsymbol{k}|} \\ &(E_{FN}-E_{min}(q-k,k'_F))\,\mathrm{Tr}\left[A^{\mu\nu}_{1p1h1\pi}(\langle p\rangle,q,k)\right]L_{\mu\nu}\ (\nu CC) \end{aligned} \tag{6.141}$$

with the nucleon energy $E(p)=\sqrt{\boldsymbol{p}^2+M^2}$ and the final pion energy $E_\pi(k)=\sqrt{\boldsymbol{k}^2+m_\pi^2}$.

However, the six dimensional integration can be calculated using Monte Carlo techniques. There exist several available algorithms for that. We have chosen the Vegas algorithm implemented in GNU Scientific Library for C/C++ compilers [153]. It is efficient enough to

compute 8-dimensional total cross section integration in a reasonable time using only $\mathcal{O}(10^5)$ points. This solves the threshold problem caused by averaged hadronic tensor with averaged W^2. One has to first analyze the equation (6.109). Simple manipulations lead to:

$$-\frac{1}{\pi}\Im\left(\Pi^{\mu\nu}_{1p1h1\pi}L_{\mu\nu}\right) = \sum_{iso}\frac{1}{512\pi^6}\int d^3r\int_{p_{min}}^{k_F(r)}\frac{p^2dp}{E(p)}\int_{\cos(\Theta_p)_{min}}^{\cos(\Theta_p)_{max}}d\cos(\Theta_p)\int_0^{2\pi}d\phi_p\int_0^{2\pi}d\phi_\pi^{(r)}\int_{\cos(\Theta_\pi^{(r)})_{min}}^{\cos(\Theta_\pi^{(r)})_{max}}d\cos(\Theta_\pi^{(r)})$$
$$\frac{\tilde{k}_\pi^2}{|\tilde{k}_\pi a^0 - |\boldsymbol{a}|\tilde{E}_\pi\cos(\Theta_\pi^{(r)})|}\mathrm{Tr}\left[A^{(r)\mu\nu}_{1p1h1\pi}(p,q,k)\right]L^{(r)}_{\mu\nu}. \tag{6.142}$$

In the above equation we have defined $\boldsymbol{a}\equiv\boldsymbol{p}+\boldsymbol{q}$ and $a^0\equiv\tilde{q}^0+E(p)$. The index (r) means, that we have rotated the inner integral coordinate system, so that $\boldsymbol{p}+\boldsymbol{q}\parallel\hat{z}$. This rotation acts on the spacial coordinates of all 4-vectors and is performed by the matrix defined in Eq. (6.89). The outgoing pion momentum is again established from the Eq. (6.92).

The Pauli blocking is imposed on the level of MC integration by discarding points with $E(p')<E_F(r)$. Thus we sample the pion laboratory angle in the limits $\cos(\Theta_\pi^{(r)})_{min}=-1$ and $\cos(\Theta_\pi^{(r)})_{max}=1$. Additionally, there are limits for the nucleon momentum p and cosine of the nucleon angle $\cos(\Theta_p)$ in the LAB frame. Firstly, we check, whether for the given $\tilde{q}^0$ and $|\boldsymbol{q}|$ one can reach the pion production threshold:

$$s=(p+\tilde{q})^2=(E(p)+\tilde{q}^0)^2-(\boldsymbol{p}+\boldsymbol{q})^2>s_{thr.}=(M+m_\pi)^2. \tag{6.143}$$

We solve the above problem for minimal value of p having assumed $\boldsymbol{p}$ antiparallel to $\boldsymbol{q}$ (this angle maximizes s). The minimal allowed nucleon momentum p_{min} is sought from the positive solution to quadratic equation resulting from Eq. (6.143):

$$\frac{\tilde{Q}^2}{\tilde{q}_0^2}\boldsymbol{p}^2+|\boldsymbol{q}|\frac{\tilde{Q}^2+s_{thr.}-M^2}{\tilde{q}_0^2}|\boldsymbol{p}|+\frac{(\tilde{Q}^2+s_{thr.}-M^2)^2}{\tilde{q}_0^2}-M^2=0. \tag{6.144}$$

Next it is checked, whether $p_{min}<k_F(r)$. This results in an information, whether one can reach the pion production threshold for given $\tilde{q}^0$, $|\boldsymbol{q}|$ and nuclear matter density. The momentum sampling is made always in a $[0,1]$ range, where momentum is calculated from formula

$$p=p_{min}+(k_F(r)-p_{min})\cdot x;\ x\in[0,1]. \tag{6.145}$$

Another limit is then calculated for $\cos(\Theta_p)$ for given $\tilde{q}^0$, $|\boldsymbol{q}|$ and $|\boldsymbol{p}|$. One solves Eq. (6.143), this time for $\cos(\Theta_p)_{max}$:

$$\cos(\Theta_p)_{max}=min\left(\frac{M^2+2E(p)\tilde{q}^0-\tilde{Q}^2-s_{thr.}}{2|\boldsymbol{p}||\boldsymbol{q}|},1\right). \tag{6.146}$$

Then angular sampling is made always in a $[0,1]$ range, where $\cos(\Theta_p)$ is calculated from formula

$$\cos(\Theta_p)=-1+(\cos(\Theta_p)_{max}+1)\cdot x;\ x\in[0,1]. \tag{6.147}$$

We have plotted the SPP model comparisons for the case of electron scattering in Fig. 39. The SPP process in nuclear matter does not reproduce the total Delta peak cross section,

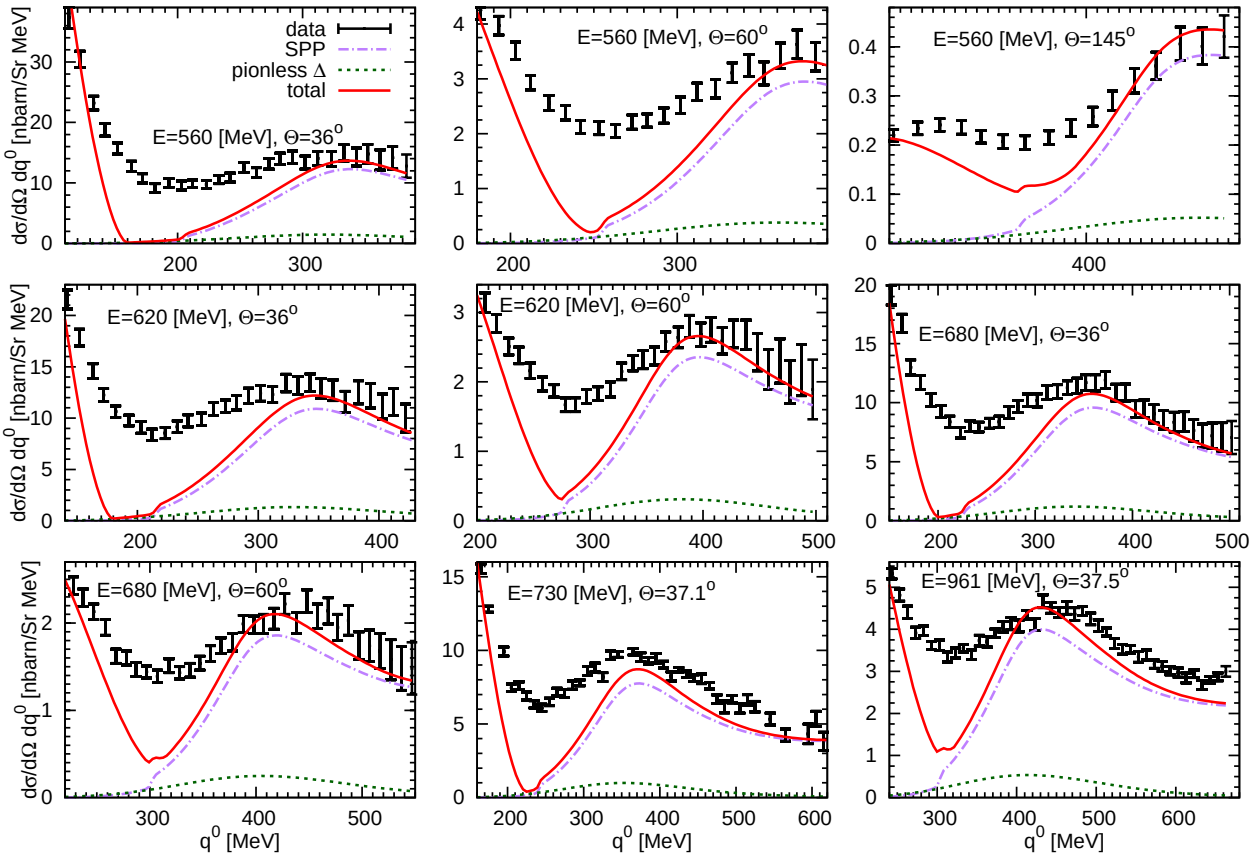

Figure 39: Comparison of theoretical double-differential cross section prediction for electron scattering off carbon. Dashed green line is the pionless Δ contribution, purple dash-dotted line is the SPP contribution calculated using approximation given by Eq. (6.131), solid red line is the total inclusive cross section, including local Fermi gas QE contribution shown separately in Fig. 14. Data for inclusive $^{12}C(e,e')$ process (black points with error bars) taken from Ref. [117] (electron energy up to 680 MeV), Ref. [118] (electron energy 730 MeV) and Ref. [119] (electron energy 961 MeV).

but after adding the pionless Δ *npnh* contribution the overall agreement with data seems to be satisfactory. The situation in "dip" region between QE and Δ peaks is different, we lack most of the experimental cross section there. One would have to add at least *npnh* mechanisms beyond the pionless Δ decays to attempt to achieve agreement with inclusive data. The approximation from Eq. (6.131) together with approximate real part of Δ self-energy (Eq. (6.123)) seems to work well giving a good strength and position of SPP peak, albeit we can clearly see the artificial threshold of full SPP model contribution, which appears as a sudden "kink" in the curve. The small low-q^0 SPP tail is comes from the resonant contribution given by separate equation (6.129).

In order to show the difference between the exact calculation and the approximation adopted in Eq. (6.131) we calculated a sample double-differential electron neutrino cross section off carbon. The results are shown in Fig. 40 for neutrinos (top) and for antineutrinos (bottom). The curves calculated using Eq. (6.131) are quite different from those calculated without approximations (although the approximation seemed to work well in the case of electron scattering).

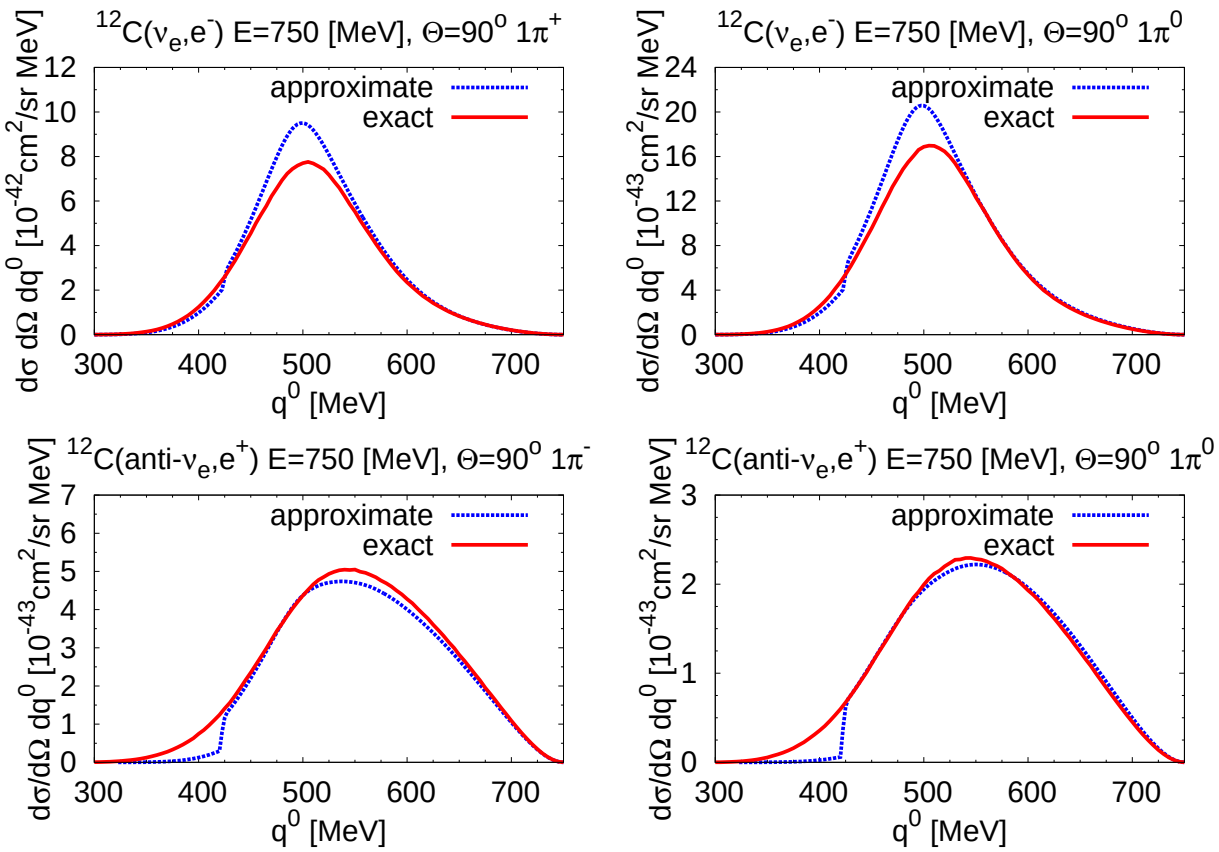

Figure 40: Difference between the exact cross section calculation from this thesis and approximations used in [70].

For total cross section both approaches: exact and approximate give similar results, as one can see in the Fig. 41. In the case of antineutrino charged pion production there is a systematic difference between our calculation and approximated results, but it is rather small. Thus we find the approximation (6.131) sufficient on the level of total cross sections. In what follows we will always use the exact calculations.

6.4.3 Results

Importance of background terms

Fig. 42 shows importance of background terms for pion production on a set of 6 free protons and 6 free neutrons. The curves describe ratios of cross sections coming from only Delta pole diagram to the cross section calculated with all the background diagrams (and the interference terms) included in computations.

We see that especially for the low neutrino energies, below 500 [MeV], the background contribution is very important. The background terms are more relevant for antineutrinos than for neutrinos and for the π^0 production than for a charged pion production.

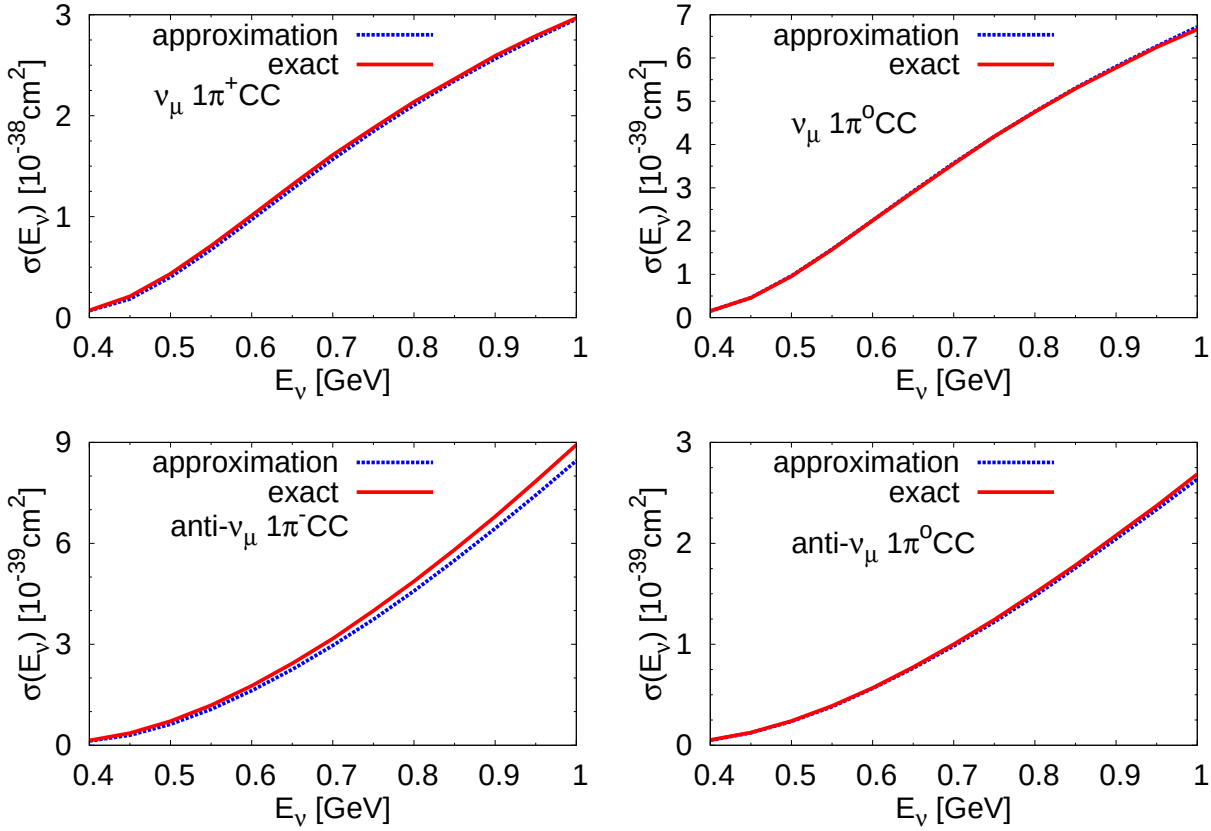

Figure 41: Difference between exact cross section calculation from this thesis and approximations used in [70].

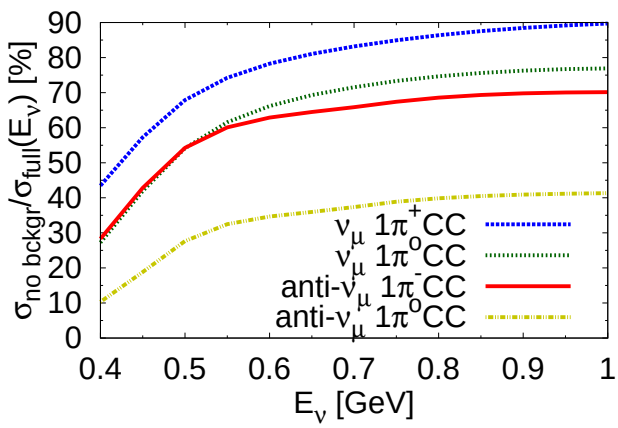

Figure 42: Ratios of the total cross sections for ν_μ and $\overline{\nu}_\mu$ SPP reactions on carbon calculated with a model without the background terms to the predictions of full model of this thesis.

Importance of in-medium effects

Fig. 43 shows an impact of the in-medium effects on the pion production. We plotted a relative modification of the free nucleon cross section (six free protons and neutrons but

with the background contribution included) caused by the in-medium effects. In almost all of the cases the in-medium effects lead to a significant decrease of the total cross section. For the electron (anti)-neutrinos, where energy 400 [MeV] is far from the SPP reaction threshold, we see an almost constant reduction of the cross section on the level of $30-40\%$. There is an interesting difference in shapes between the curves for electron neutrinos and antineutrinos, see Fig. 43. The latter exhibits a smooth drop of in-medium reduction with growing neutrino energy. In the case of muon neutrinos and antineutrinos near the pion production threshold ($E_\nu < 0.5$ [GeV]) the cross section is less affected by nuclear effects. For π^+ production channel and $E_\nu = 0.4$ [GeV] it even seems to be slightly enhanced. This happens due to the nucleon Fermi motion which dominates other effects in that kinematical region. This is not the case for π^0 production by antineutrinos. There exists a correlation between the nonresonant background contribution and the cross section reduction due to in-medium effects. Shapes of the reduction ratios in neutrino π^0 and antineutrino π^- channels are almost the same, so is the background contribution shown in Fig. 42. In general, the more cross section comes from background and interference terms, the smaller is the near threshold effect. For the larger muon neutrino/antineutrino energies $E > 0.6$ [GeV] we see again an almost uniform reduction of the cross section of the order of 30%.

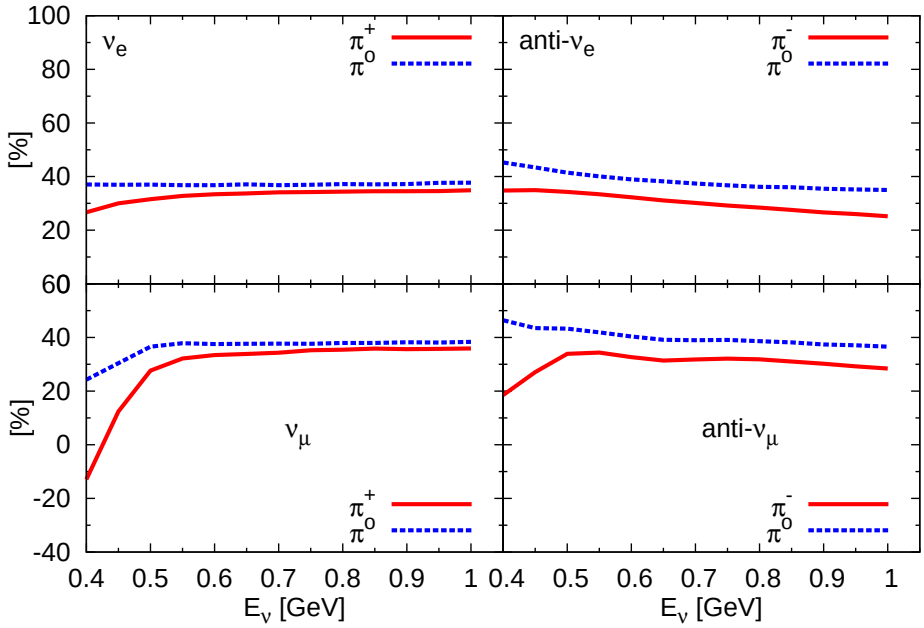

Figure 43: Impact of nuclear effects on SPP off ^{12}C. Plots show $(\sigma_{free}-\sigma_{medium})/\sigma_{free}\times 100\%$

Similar studies were done in [56, 57], where LFG-based model of carbon nucleus has been used with the same parameterization of Δ self-energy, but without nonresonant terms. In [155] global RFG and relativistic plane-wave impulse approximation (RPWIA) with realistic bound-state wave functions calculated in Walecka $\sigma-\omega$ model were studied. For the medium modifications of Δ resonance global density $\rho = 0.75\rho_0$ is applied, leading to a constant increase in the Δ mass and self-energy estimated to be 30 and 40 [MeV] correspondingly. Within the Δ dominance model the calculations were performed for carbon and iron targets and muon neutrinos. RFG and RPWIA models lead to very similar results. Without the Δ

in-medium effects, RFG and RPWIA total SPP cross sections are reduced by 50% or more at 400 MeV and about 15% at 1 GeV with respect to the free proton cross section. There seems to be no near-threshold cross section enhancement due to the Fermi motion. The Δ in-medium effects (in the adopted approximation of the constant nuclear density) lead to the further reduction of SPP cross section in carbon (about 45% at $E_\nu = 800$ [MeV]).

Total cross sections

We compared predictions from our model with the recent MiniBooNE pion production data. MiniBooNE, unlike K2K, published their results in a form of absolutely normalized cross section and not as a ratio to CC inclusive cross sections. We performed calculations with our model of the total SPP cross sections on CH_2. A direct comparison with the data is not straightforward because MiniBooNE reported the cross sections for pions in the final state after leaving nucleus (in a case of neutrino-carbon scattering) with all the FSI effects included. The pion FSI effects can be evaluated within a cascade models like those implemented in Monte Carlo event generators. Our model is not yet an ingredient of any MC generator and we decided to estimate an impact of FSI effects using the results of MC comparison study published in Ref. [156]. We approximate the relevant probabilities as:

$$P(\pi^0 \to \pi^0) = 67\%, P(\pi^0 \to \pi^+) = 5\% \tag{6.148}$$

$$P(\pi^+ \to \pi^+) = 69\%, P(\pi^+ \to \pi^0) = 5\%. \tag{6.149}$$

The results for the cross section with and without FSI are plotted in Fig. 44.

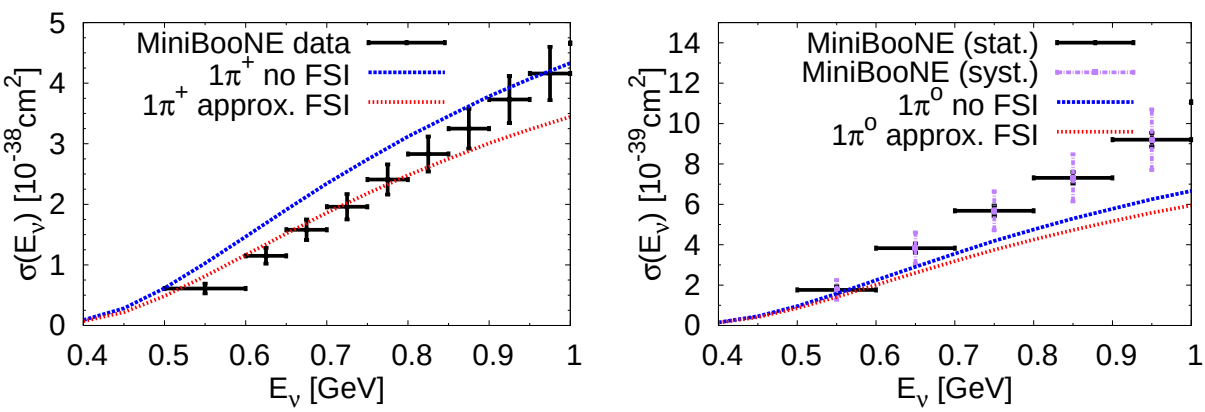

Figure 44: Charged and neutral pion production cross sections on CH_2 for the full model of this thesis. The data is taken from Ref. [65] and [66].

For charged pion production we obtained a quite good agreement with the data up to the neutrino energy of around 0.8 [GeV]. In the case of charged-current π^0 production both free and in-medium cross sections calculated with our model are too small, and the discrepancy becomes larger with increasing neutrino energy. FSI introduce large modifications for the π^+ channel. In the π^0 channel an effect of absorption of π^0 is partially compensated by a fraction of initial π^+ events, that end up as π^0 due to the charge exchange reaction inside nucleus.

The MiniBooNE SPP data were also analyzed by the Giessen group using GiBUU - a code for hadron transport in nuclear matter based on the semiclassical Boltzmann-Uehling-Uhlenbeck equation [157]. The Giessen SPP model covers larger kinematical region and includes contributions from heavier resonances. In its most recent version the model uses both ANL and BNL data fit to Δ excitation transition form factors and treats them as lower and upper bounds for SPP [158]. The nonresonant background is included in a phenomenological fashion and the pion production cross section is a incoherent sum of two contributions:

$$d\sigma_{SPP} = d\sigma_{res} + d\sigma_{nonres} \tag{6.150}$$

where the first one comes from the excitation of resonances with invariant masses W <2 [GeV] and the second one from a nonresonant background and resonance-background interference terms. The vector part of the background is found as a fit to the difference between experimental and theoretical resonant contribution to electron SPP on nucleons. The axial and axial-vector part of the background are assumed to have the same functional form and are scaled by a constant factor in order to get an agreement with the low energy SPP data. Nuclear effects include a momentum dependent potential for initial state nucleons and spectral functions for final state hadrons (including resonances). The Δ spectral functions includes the same in-medium effects as those incorporated in the model discussed in this thesis.

Fig. 12 from Ref. [158] allows for a comparison with an impact of consequtive nuclear effects on the pion production rate. Fermi motion and Pauli blocking make the Δh excitation cross section smaller by $\sim$ 5%. A further 5-8% reduction of the cross section is introduced by Δ self-energy. Finally, due to pionless decay modes, the pion production is reduced by extra 15-20%. Ref. [158] shows predictions for SPP cross sections for energies up to 2 [GeV] and it is clearly seen that in the range discussed in this thesis ($E_\nu \leq 1$ [GeV]) a contribution from heavier resonances is negligible.

Interesting are comparisons of the GiBUU model with the MiniBooNE CC pion production data. For the π^+ production the computations based on BNL-fitted form factors are slightly below the data (including errorbars) and the difference is largest at neutrino energies of 1-1.5 [GeV]. In the case of π^0 production the situation is slightly better and except from a region of about 1 [GeV] the predictions agree with the data, again including errorbars. ANL-fitted form factors produce predictions which fall far apart from the MiniBooNE data points.

A good review of the discrepancies between different theoretical SPP calculations and experimental data (as well as of other types of neutrino-nucleus interactions) can be found in Ref. [45].

Ratios of muon to electron (anti-) neutrino cross sections

In the neutrino oscillation appearance experiments it is very important to calculate precisely the ratios of muon and electron neutrino cross sections. Even in a presence of a near detector and with full understanding of initial muon neutrino flux a good knowledge of the ratios (and their dependence on the neutrino energy) is crucial for a correct identification of the oscillation signal.

In Fig. 45 we see that the ratios calculated with the complete model are slowly increasing functions of the neutrino energy. In the case of antineutrinos there is a small difference

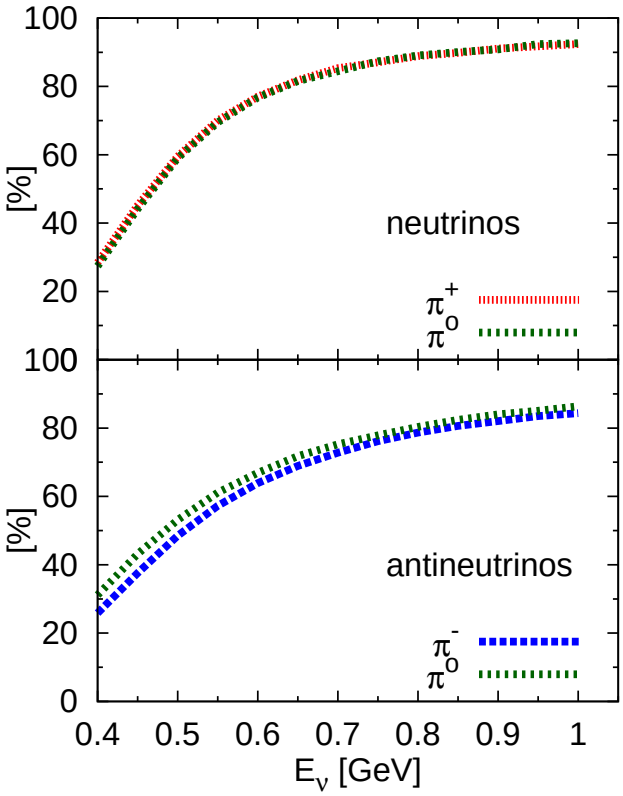

Figure 45: Ratios of muon to electron (anti) neutrino total SPP cross sections on ^{12}C for the full model of this thesis.

between the π^- and π^0 production: in the first case the ratio is slightly lower. On the contrary, we obtain almost the same ratios for π^+ and π^0 production by neutrinos.

It is important to know how well the ratios are calculated when simpler models of SPP are used, which is often a case in MC event generators.

Fig. 46 shows an impact of the background terms on the π^0 production ratios. We compared two situations: the full model and the model without background contributions. We see that the results are significantly different only in the case of antineutrinos. For lower neutrino energies using a purely resonant SPP mechanism one obtains much smaller ratios. For the neutrinos these differences are negligible. The resonant contribution ratio is very close to the one plotted in Ref. [52] for the sum of neutrino and antineutrino cross sections in a similar model.

Fig 47 shows an effect of the Δ self-energy on the ratios. We compared two situations: the full model and the model without the Δ self-energy. We see that the negligence of the Δ self-energy has almost no effect on the considered observable. We conclude, that in order to evaluate well the anti-muon to anti-electron neutrino cross section ratio it is important to include the nonresonant background, but not necessarly the Δ self-energy.

We also investigated a possible impact on predictions from the model coming from alternative descriptions of the Δ resonance vacuum width to Eq. (6.46) and Δ propagator to Eq. (6.47).

On the level of total cross sections the difference between two $\Delta\pi N$ decay descriptions

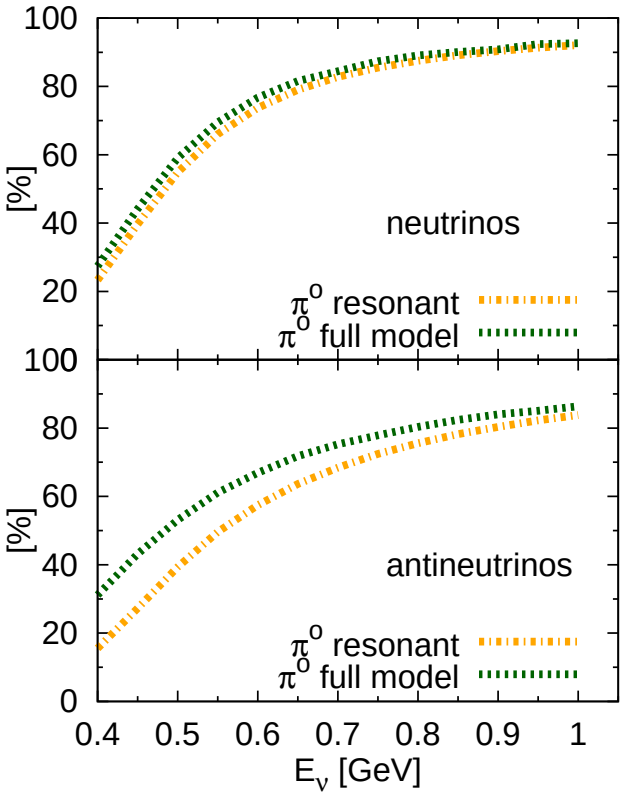

Figure 46: Ratios of muon to electron (anti-) neutrino total SPP cross sections on ^{12}C for the full model of this thesis and for the resonant SPP only (without the background terms).

is negligible. This is illustrated in the Fig. 48 where we plot again the muon to electron (anti-) neutrino total π^0 production cross section ratios and we compare the default and the Manley-Saleski Δ description.

In the work of Barbero *et al.* [51] the nonresonant background is described in a way quite similar to Ref. [46] (ρ and ω meson diagrams were used instead of PP contribution). The authors of [51] have pointed out, that the standard Rarita-Schwinger spin-3/2 projection operator used in Eqs. (6.32) and (6.47) should be replaced by a more consistent approach. In this treatment one demands invariance under the contact transformations of Rarita-Schwinger fields, eliminating the spurious spin-1/2 degree of freedom in the on-shell Rarita-Schwinger propagator. One can then introduce a set of *reduced* Feynman rules ([159]), which include a *reduced* Δ propagator, different from Eqs. (6.32), (6.47). The effect of switching between the reduced and Rarita-Schwinger propagators on the pion production in a model containing nonresonant background can be as large as 30% (depending on the pion production channel). Reduced Δ propagator leads to a better agreement with ANL and BNL data in Ref. [51], than in Ref. [46]. Moreover, in [160] the authors show, that Delta resonance itself should be included on the level of consistent chiral perturbation theory. Using the next-to-leading order in "δ expansion" one reproduces the pion electroproduction data fairly well and finds the same dependence of Delta multipole form factors on pion mass, as in lattice QCD. It is worthy to mention, that using the reduced propagator has significant impact only in models containing background terms. In Ref. [155] the similar changes to Δ

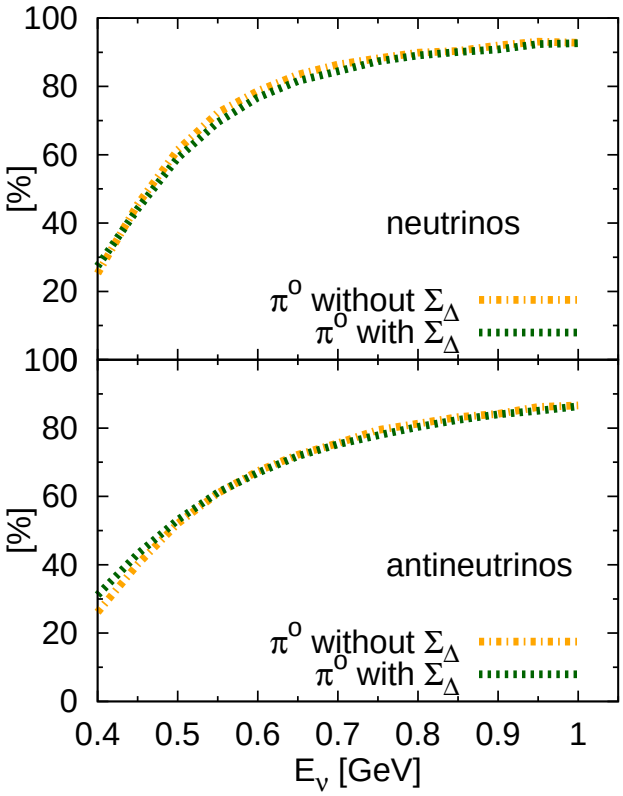

Figure 47: Ratios of muon to electron (anti) neutrino total SPP cross sections on ^{12}C for the full model of this thesis with and without the Δ self-energy Σ_Δ.

propagator following Pascalutsa [161] have been made in a Δ-dominance model, leading to negligible changes in the resonant SPP.

Finally, we investigated also how much does the numerical approximation in Eq. 6.131 affect muon to electron neutrino cross section ratios. This is illustrated in Fig. 49, where we have plotted $\overline{\nu}_\mu/\overline{\nu}_e$ $1\pi^0 CC$ cross section ratios. Differences are present only for energies $E_\nu < 550$ [MeV] and at $E_\nu = 500$ [MeV] it is about 4%.

Pionless Δ decays

An interesting feature of our model is that there exists a contribution to the cross section coming from pionless Δ decays. This is a part of the MEC cross section which has recently attracted a lot of attention ([107, 91, 92]). There is a lot of evidence that the MEC mechanism is responsible for a large CCQE axial mass measurement reported by the MiniBooNE collaboration [11]. Theoretical microscopic computations always include pionless Δ decays as a part of the calculated effect. Some MC event generators (NEUT, NUANCE) assume a constant fraction of the pionless Δ decays and we find it interesting to check how well this assumption is satisfied in our model.

The fractions of the pionless decays and their dependence on the neutrino energy and species are shown in Fig. 50. There is no difference between neutrinos and antineutrinos, because we include only the $np - nh$ mechanism coming from the resonant diagrams. The

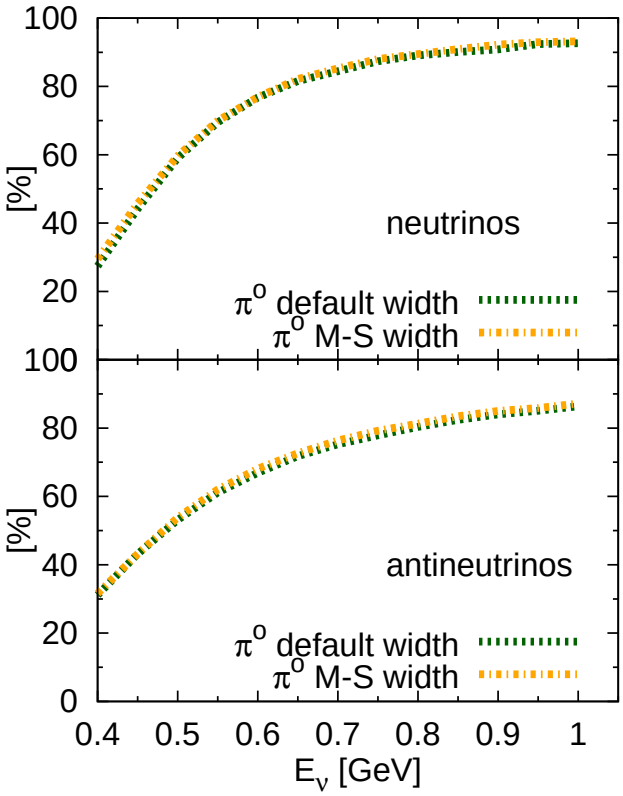

Figure 48: Ratios of muon to electron (anti) neutrino total SPP cross sections on ^{12}C for the full model of this thesis with Δ width described by Eqs. (F.15) and (6.46).

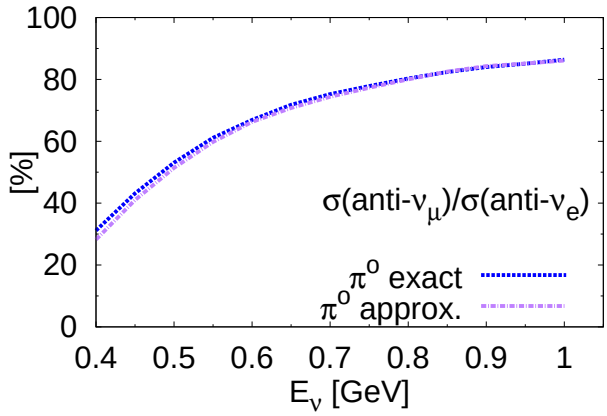

Figure 49: Ratios of $\overline{\nu}_\mu$ to $\overline{\nu}_e$ neutrino CCπ^0 SPP cross sections on ^{12}C calculated with the full model of this thesis and with approximations used in Ref. [46].

fraction of pionless Δ decays is very large for the energies below 500 [MeV]. For the larger energies it exhibits a smooth energy dependence, dropping down to 20% at $E_\nu = 1$ [GeV]. It is clear that for experiments with a large fraction of neutrinos with energies below 1 [GeV] one can not consider the investigated quantity to be constant.

The total pionless Δ decay cross section may be treated as a lower bound for the $np-nh$

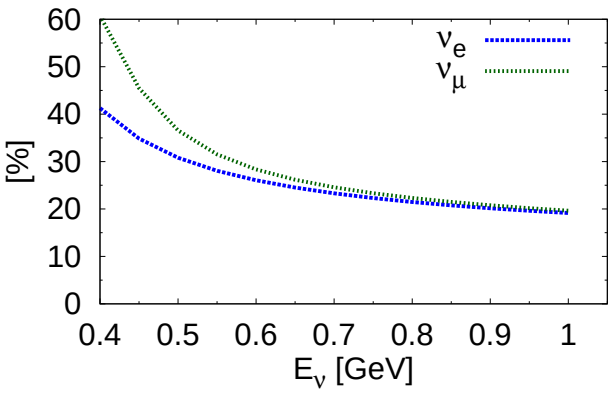

Figure 50: Fraction of the pionless Δ decays to the resonant SPP production cross section $(\sigma_{pionless\ \Delta})/\sigma_{SPP\ res.} \times 100\%$ in ^{12}C for ν_e and ν_μ.

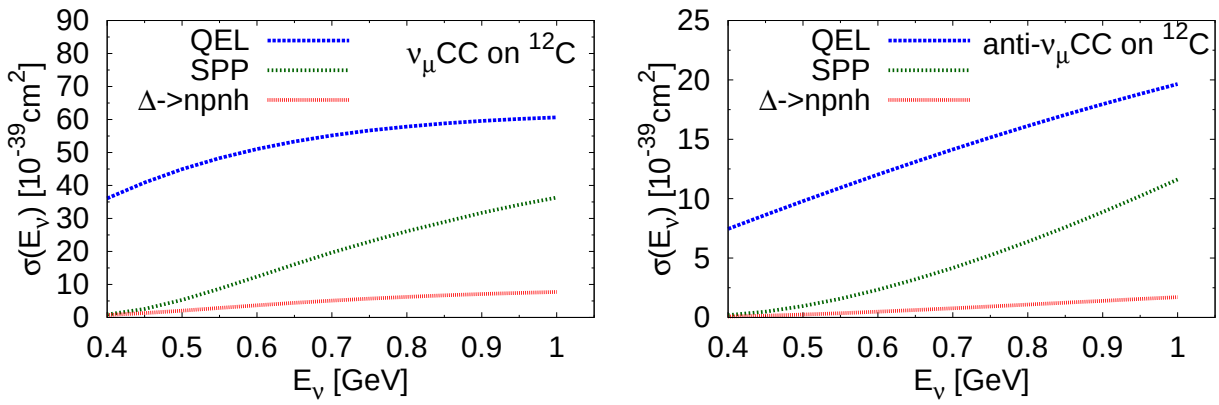

Figure 51: Total CC cross sections on ^{12}C for: quasielastic scattering, SPP, and pionless Δ decay.

contribution. One has to keep in mind, that there are many other sources of $np-nh$ final states, which can be built from diagrams in Fig. 26 but are not considered in this thesis. The total cross section coming from $\Delta \to np-nh$ decays can be seen in Fig. 51. The CCQE contribution has been calculated with NuWro neutrino event generator [41] within the spectral function approach [39] and $M_A = 1.05$ [GeV]. The $np-nh$ contribution coming from pionless Δ decays may seem small compared to CCQE and SPP cross sections (around 10-15% of the first), but at $E_\nu = 1$ [GeV] it accounts for about 60% of the $np-nh$ cross section in the model of Nieves et al [70] (at $E_\nu = 750$ [MeV] the fraction is even larger and amounts to 64%).

6.5 Summary and conclusions from SPP on atomic nuclei

We have investigated in detail the model of single pion production on nuclei based on an effective field theory. The nuclear model includes local Fermi gas effects, Pauli blocking and Δ in-medium self-energy. Contributions from heavier resonances are neglected, thus

the model is expected to reproduce well the data in the energy region $E_\nu \leq 1$ [GeV]. We use an open-source MC integration algorithm, which allows us to avoid many numerical approximations present in Ref. [70].

We have analyzed in detail the ratio of muon to electron neutrino cross sections for pion production because this is an important theoretical input in neutrino oscillation appearance experiments.

The inclusion of nonresonant background has a non-negligible impact on the analyzed observables. It is more pronounced in the antineutrino channels, where the background terms play a major role in the considered neutrino energy region. The muon to electron neutrino cross section ratios for neutrinos do not depend on the final state pion charge, whereas for the antineutrinos we predict a small splitting between the π^- and π^0 channels. This splitting seems to originate from the nonresonant background terms, which give rise to a large fraction of cross section in the antineutrino π^0 production modes (sometimes the cross section is more, than doubled by including the background terms!).

We showed that these ratios are almost independent on the nuclear effect modeling details, like the self-energy of Δ resonance or numerical integration approximations proposed in Ref. [70]. Neither do they depend on the Δ free decay width model changes between the one resulting from relativistic decay width Eq. (F.15) to the one used in Manley-Saleski analysis Eq. (6.46), which incorporates the angular momentum of the decaying hadronic system.

We have also found, that one cannot treat the pionless Δ decay fraction as a constant number for neutrino interactions below 1 [GeV]. This is an important information, since the pionless Δ decay seems to give rise to more than half of the $2p2h$ cross section (by comparing to our implementation of IFC model in NuWro in chapter 7).

Using an estimate of FSI effects based on [156], we obtained a reasonable agreement with the MiniBooNE CCπ^+ production data but the model underestimates CCπ^0 cross section. The same problems appear in most of the before mentioned theoretical models and it is likely that something important is missing. Perhaps one needs a better description of the Δ resonance, see *e. g.* Refs. [51] and [161], which focus on more consistent treatment of the Δ propagator. This can be also a problem of nuclear effect description, as the HNV model with default values of Δ axial coupling $C_5^A(0) = 1.19$ and $M_{A\Delta} = 1.05$ GeV used as a basis in these calculations tends to overestimate the ANL data for calculations on free nucleons.

One should also try to investigate other models of nonresonant background, *e. g.* Ref. [51], because Ref. [46] does not seem to reproduce all isospin channels equally well. This is pronounced in the $\nu_\mu n \to \mu^- p \pi^0$ channel.

In our model the in-medium Δ spectral function was included only in the ΔP diagram and the pure background contribution (36 out of 49 combinations from Eqs. (6.20-6.26)) is not affected by the presence of nuclear matter. In the Δ-background interference terms (12 combinations) the in-medium effects enter only through ΔP diagram, thus are included only partially. A conclusive verification of the model predictions can be done only by evaluating the nonperturbative in-medium effects for all the genuine amplitudes (28 independent terms). This is a very difficult task to achieve. Because of that we are unable to conclude whether the resulting reduction of the cross section is a genuine physical effect or rather an artifact of the adopted approximations.

Another possible explanation of the existing disagreement with the data is that there is a large $1\pi 2p2h$ contribution (analogous to $2p2h$ enhancing CCQE-like cross section) neglected in the computations. In Ref. [158] there is an interesting comment that the data/theoretical

computations comparison for pion photoproduction on carbon suggest that the data are underestimated (at $E_\gamma = 500$ MeV by around 20%) and a possible explanation is the neglected $1\pi 2p2h$ contribution. Very recently authors of Ref. [162] have shown, that this dynamical channel may be very important for SPP on atomic nuclei, contributing a large fraction of single pion production cross section measured by MiniBooNE.

All the consistent $2p2h$ models are constructed basing on the SPP diagrams with virtual pions connected to nucleons. Thus it seems crucial to have a good SPP model in order to build also a consistent two-nucleon current theory and estimate the multinucleon contamination of CCQE-like data samples.

7 Meson exchange currents

In this section we will discuss the last dynamical neutrino interaction channel included in our considerations, which may give rise to systematic errors in accelerator neutrino oscillation experiments: the Meson Exchange Currents. Since w did not perform the full calculation regarding MEC we will discuss the present MEC models and their implementation in NuWro MC generator. The IFIC MEC model has been implemented there on an effective level using data tables provided by collaborators working in IFIC. In the last section we will also show an idea how to proceed with MEC calculations and discuss possible approximations and divergences in some of the contributions.

7.1 General idea beyond the chosen MEC models

7.1.1 IFIC model

This model has been introduced in Ref. [70]. Main idea behind this model is firstly to take all the diagrams corresponding to SPP (Fig. 26) in HNV model [46] and attach the pions to another paticle-hole loop. Feynman diagram connected to that process can be seen in

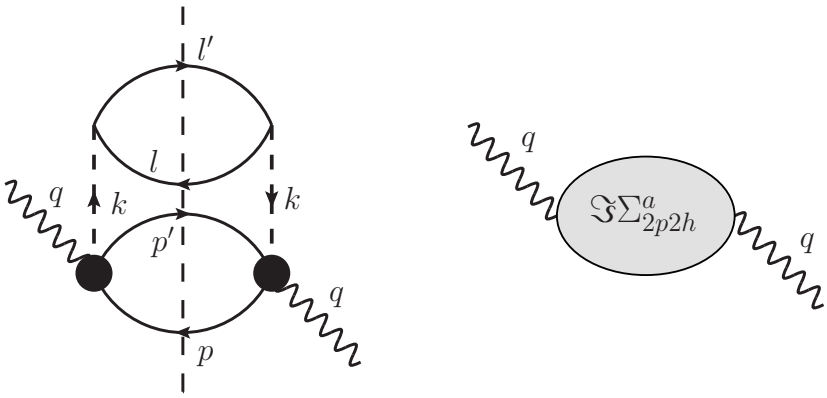

Figure 52: First type of 2p2h contribution with all external bosons connected to the same nucleon loop (we depict the gauge boson self-energy coming from nuclear system excitation).

Fig. 52, where the black circles correspond to any of the vertices depicted in Fig. 26. If one puts the intermediate nucleon loops on shell, then the diagram will produce a genuine $2p2h$ excitation. Both loops are calculated at given nuclear matter density from LFG distribution. Second class of diagrams taken into account have the external gauge bosons enter different nucleon loops, as depicted in Fig. 53. In addition to these "bare" LFG contributions, several refinements connected to nuclear medium effects are applied. We will point them ot briefly:

- Virtual pion connecting both nucleon loops is iterated through an infinite RPA series of nucleon-hole and Δ-hole excitations in both classes of diagrams.
- One-pion exchange interaction piece is replaced by a more realistic longitudinal nucleon-nucleon potential from Eq. (6.121)
- The diagrams from Fig. 52, which have two ΔP vertices are replaced by the in-medium Δ excitation given by Eq. (6.130).

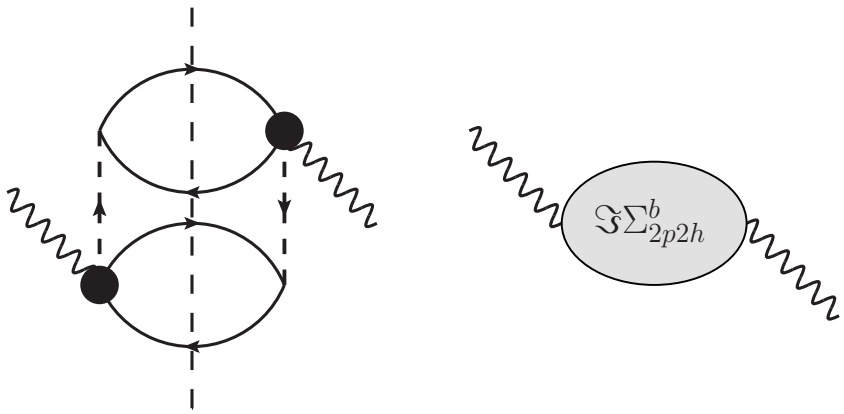

Figure 53: Second type of 2p2h contribution with all external bosons connected to separate nucleon loops (we depict the gauge boson self-energy coming from nuclear system excitation).

- Additional terms driven by the ρ-meson exchange are introduced with the topology of Fig. 52. They are generated from following interaction Lagrangians:

$$\begin{aligned}\mathcal{L}_{NN\rho} &= \frac{f_{\pi NN}}{m_\pi}\sqrt{C_\rho}\bar{\psi}\sigma_{\mu\nu}\partial^\mu\boldsymbol{\tau}\boldsymbol{\rho}^\nu\psi \\ \mathcal{L}_{N\rho\Delta} &= -i\frac{f^a st}{m_\pi}\sqrt{C_\rho}\bar{\psi}_\nu\gamma^5\gamma^\mu\boldsymbol{T}^\dagger(\partial_\mu\boldsymbol{\rho}_\nu - \partial_\nu\boldsymbol{\rho}_\mu)\psi + h.c. \end{aligned} \tag{7.1}$$

  with $C_\rho = 2$ and $\boldsymbol{\rho}$-the ρ-meson field isospin triplet. Other fields as well as the isospin operators are explained in Appendix A.2 and A.3. Coupling constants can be found in section 6.1.1.

- In the above contributions they replace the ρ-meson propagators by transverse nucleon-nucleon potential from Eq. (6.121).

Additionally, one encounters divergences in the $2p2h$ part, which will be explained in more details together with main calculation steps and approximations from Ref. [70] in section 7.3.

7.1.2 Transverse Enhancement Model

Besides the before mentioned microscopic MEC models, there exists an effective approach, proposed in Ref. [94]. It is based on an assumption coming from theoretical calculations, which for electron scattering give the strongest effects of MEC in the transverse response function. Thus one can expect the difference between the measured cross section and theoretical QE and SPP process in electron scattering from QE to Δ peaks to come from two-body currents. They find a ratio function in the transverse response:

$$\mathcal{R}_T = \frac{QE_{transverse} + TE}{QE_{transverse}} \tag{7.2}$$

with $QE_{transverse}$ being the theoretical transverse QE response and TE the transverse excess, which is defined as a difference between experimental data and sum of theoretical quasielastic

and inelastic SPP processes. The authors of Ref. [94] find in a good approximation:

$$\mathcal{R}_T(Q^2) \quad = \quad 1 + AQ^2 e^{-Q^2/B} \tag{7.3}$$

with best fit values $A = 6.0$ GeV^{-2} and $B = 0.34$ GeV^2. Error bands for these parameters are $A \in [5.3, 6.7]$ GeV^{-2} and $B \in [0.33, 0.35]$ GeV^2 and the fitting has been done for carbon nucleus only. Authors of Ref. [94] assume, that the difference (7.2) can be effectively parameterized by a modification of proton and neutron magnetic form factors for quasielastic scattering, which give rise to the transverse response function (4.24). The modification is parameterized as follows:

$$G_M^{TE(p/n)}(Q^2) \quad = \quad R_T^{\frac{1}{2}}(Q^2) G_M^{(p/n)free}(Q^2)$$

where the whole modification is assigned to free proton and neutron form factors. Thus in their approximation:

$$\sigma^{MEC} \quad = \quad \sigma_{QE}^{TE} - \sigma_{QE}. \tag{7.4}$$

For electron scattering this solution gives a relatively simple prescription to account for the MEC effects. The drawback is that all MEC effects are put into QE kinematic region and that one can not construct realistic MC predictions for outgoing nucleons in that model. It also misses any modifications of the nucleon axial current, which may be important for the proper treatment of neutrino CC-driven MEC. It is remarkable, that an early attempt of incorporating two-body currents into nucleon form factors can be found in [73].

7.2 NuWro implementation

T2K collaboration shows a big interest in MEC models. The concern about MEC effects in neutrino oscillation analysis has motivated the Wroclaw group to implement various MEC in NuWro. The first two models were the Lyon group model and TEM. Later on we have been given access to IFIC model. Due to courtesy of Juan Nieves we have obtained the double-differential cross section tables, $d^2\sigma/dT_\mu d\cos(\theta_\mu)$, for the inclusive $^{12}C(\nu_\mu, \mu^-)$ process coming from his MEC model. The data set has spanned 40 neutrino energies between 0.155 GeV and 3 GeV. For each energy it spanned 40 values of muon kinetic energy T_μ and 40 values of $\cos(\theta_\mu)$. The points were place according to Gaussian quadratures in each variable, giving 64000 independent cross section values. Recently, we have also been given analogous tables with more uniform binning for electron neutrinos and for oxygen and carbon separately thanks to Peter Sinclair and Panos Stamoulis from T2K collaboration.

We have used them to implement MEC in an effective way in NuWro. The MEC event algorithm looks as follows:

1. Pick a neutrino energy E_ν from a beam profile.
2. Randomly pick the final muon kinetic energy and production angle w.r.t to beam in the allowed kinematical range.
3. Set the event's weight by interpolating the differential cross section from fixed data set

4. Try to pick two nucleons from LFG momentum distribution according to algorithm from Ref. [106] until the sum of 4-momenta of nucleons p_1^μ and p_2^μ and momentum transfer q^μ satisfies $(p_1 + p_2 + q)^2 > 4M^2$ (final nucleons on-shell condition). If one fails after N samplings, then the weight is set to 0.

5. Accept/discard event.

Since the cross section data have uneven binning one had to store them in an appropriately ordered manner. The angular binning in $\cos(\theta_\mu)$ have 40 repeatable values, the binning in T_μ has changed with energy (1600 independent values of T_μ). We decided to store the data points sorted with respect to energy, then angle, and then muon kinetic energy in separate tables for each variable:

1. Table 1 with 40 neutrino energies.

2. Table 2 with 40 angles.

3. Table 3 with 1600 kinetic energies (E_ν grows each 40 steps).

4. Table 4 with 64000 differential cross secton values, energy grows each 1600 steps, angle each 40 steps and kinetic energy changes from step to step.

For each event generated by NuWro characterized by $(E_\nu^{ev.}, \cos(\theta_\mu)^{ev.}, T_\mu^{ev.})$ the program performs a search:

1. Position of nearest $E_\nu^{data} < E_\nu^{ev.}$ from Table 1.

2. Position of nearest $\cos(\theta_\mu)^{data} < \cos(\theta_\mu)^{ev.}$ from Table 2.

3. Positions of nearest $T_\mu^{data} < T_\mu^{ev.}$ for nearest $E_\nu^{data} < E_\nu^{ev.}$ and $T_\mu^{data} < T_\mu^{ev.}$ for nearest $E_\nu^{data} > E_\nu^{ev.}$ from Table 3. Two values are needed because of T_μ binning changes with E_ν.

In this manner one closes the event coordinates in a data "box", as shown in Fig. 54. The

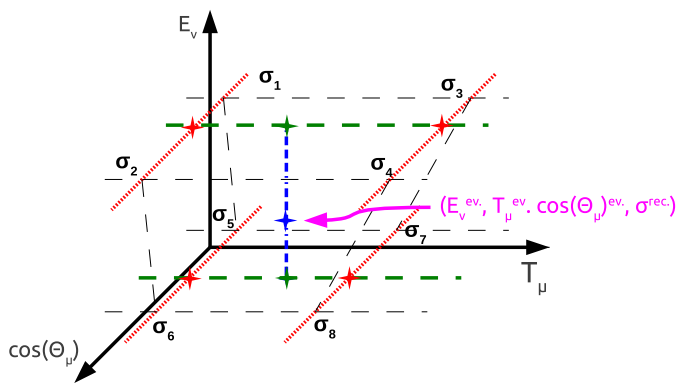

Figure 54: The "box" of nearest data points with event inside.

vertices of the box are IFIC model data points with cross section values $\sigma_1 ... \sigma_8$. Then we do linear interpolation, first along the edges of the cube spanning along $\cos(\theta_\mu)$ (red lines in Fig. 54). In this manner we get the interpolated values describing the cross section on

vertices of trapezoid placed in the plane of constant $\cos(\theta_\mu)$ of given event (red stars in Fig. 54). Then we interpolate again along the trapezoid edges along T_μ (green lines) getting two points on the line at the coordinates ($\cos(\theta_\mu), T_\mu$) of the given event (green stars). In the end we interpolate these values of the cross section along E_ν to get the linearly interpolated cross section $\sigma_{rec.}$ at $(\cos(\theta_\mu), T_\mu, E_\nu)$ of the given event (marked by a blue star).

This algorithm is a generalization of the linear interpolation between data points to the three-dimensional case.

The nucleon sampling algorithm of Ref. [106] has been used to implement the TEM and Lyon models in NuWro. The scheme of the procedure is following:

- Two nucleons are selected from the LFG momentum distribution
- Four momentum of the hadronic system is calculated by adding four momenta of selected nucleons and energy and momentum transfered by the inter acting neutrino
- If the hadronic invariant mass is physical, Lorentz boost to the hadronic center of mass system is done.
- Two nucleons are selected isotropically in the hadronic center of mass system
- They are boosted back to the laboratory frame.

In order to account for the binding effects the initial nucleons are placed in a potential well of the depth V=8 MeV+E_F. Then:

- Fermi energy is subtracted from each initial state nucleon.
- For each nucleon in the final state (in the LAB frame) the energy is reduced by the amount of 8 MeV adjusting its momentum so that they remains on-shell.

Problem with nucleon sampling arises because of the interpolation accuracy and some details of the IFIC model. IFIC model gives nonzero cross section outside region, where one can find p_1 and p_2 satisfying $(q + p_1 + p_2)^2 > 4M_N^2$. Fortunately, only negligible amount of the cross section is stored in that region (less, than 10^{-3} of the total cross section). No simple analytic solution for a sampling cut was found. Thus we allow up to N samplings of nucleon pairs (default N=100). If for a given event we fail to find the nucleon pair in N checks, we set the event weight to 0 (event gets discarded). In order to see, which muon kinematic region is affected by this procedure, we have calculated number of test events with nonzero interpolated cross section for $E_\nu = 750$ MeV (average T2K energy) and carbon target for both N=100 and N=1000. These regions are shown in Fig. 55. Although it seems, that there is a difference between the excluded regions for different sampling cutoffs, the effect on the total cross section is negligible. But the effect on NuWro speed is quite large, so we set N=100 by default.

In order to compare all available MEC models we have plotted the total cross sections for TEM, Martini and IFIC models together with SF CCQE cross section for carbon. They are plotted in Fig. 56. Below neutrino energy of 1 GeV the biggest cross section is predicted by the TEM model, the smallest by IFIC model. Both Lyon and TEM models seem to saturate, whereas the IFIC model predicts a constant growth in energy. One has too keep in mind, that the IFIC and Lyon MEC models are not reliable at E_ν >1.5 GeV due to

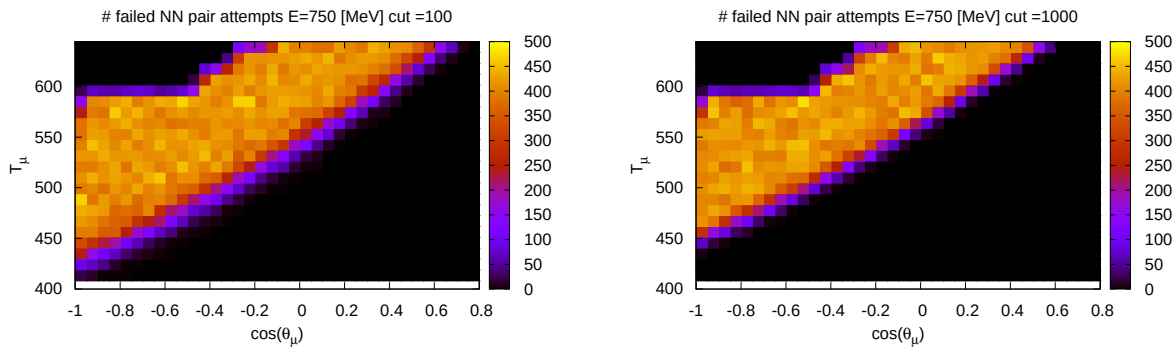

Figure 55: Plots showing, in how many test events we have failed to sample nucleon pair in 100 and 1000 allowed samplings in spite of nonzero interpolated cross section. Average number of test event/bin is 415, thus the region with around 400 failures of test event is excluded.

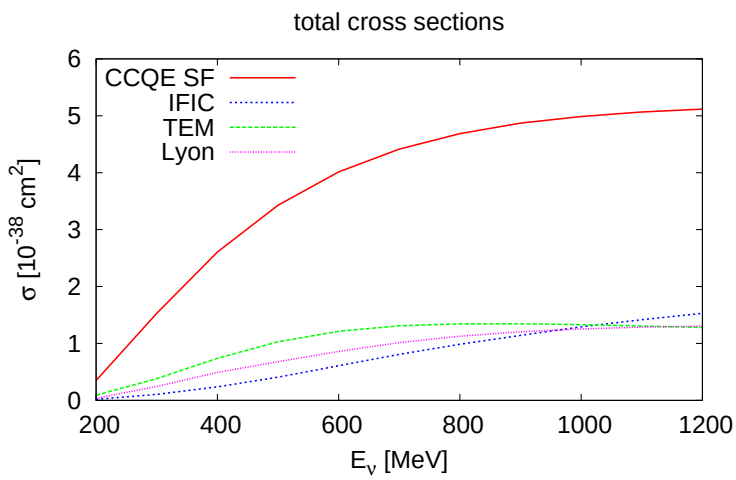

Figure 56: Total cross sections for different MEC models.

limited applicability of the underlying effective field theory and openings of other hadron production channels (multi-π, $npnhm\pi$, K, etc.).

Double-differential cross sections for all three MEC models implemented in NuWro are shown in the Fig. 57. Main features of the shapes of cross sections coming from Lyon and IFIC models are quite similar. They exhibit a double-peaked structure. It can be deducted from the fact, that a large part of the MEC in Lyon and IFIC models comes from the pionless Δ decays and is peaked at different hadronic invariant mass region, than parts constructed on other amplitudes. The TEM model is totally different due to simplified kinematics (scattering off a nucleon at rest).

We have also investigated the energy reconstruction in the case of pure MEC events. We have produced a large sample (20 million) of IFIC model MEC events using the MiniBooNE ν_μ beam. We calculated the reconstructed neutrino energy according to Eq. (2.33). We have used $E_b = 34$ MeV, which is averaged binding energy of Carbon. For chosen values of $E_{rec.} = 500 \pm 10$ MeV, 750 ± 10 MeV and 1000 ± 10 MeV we have created a distribution

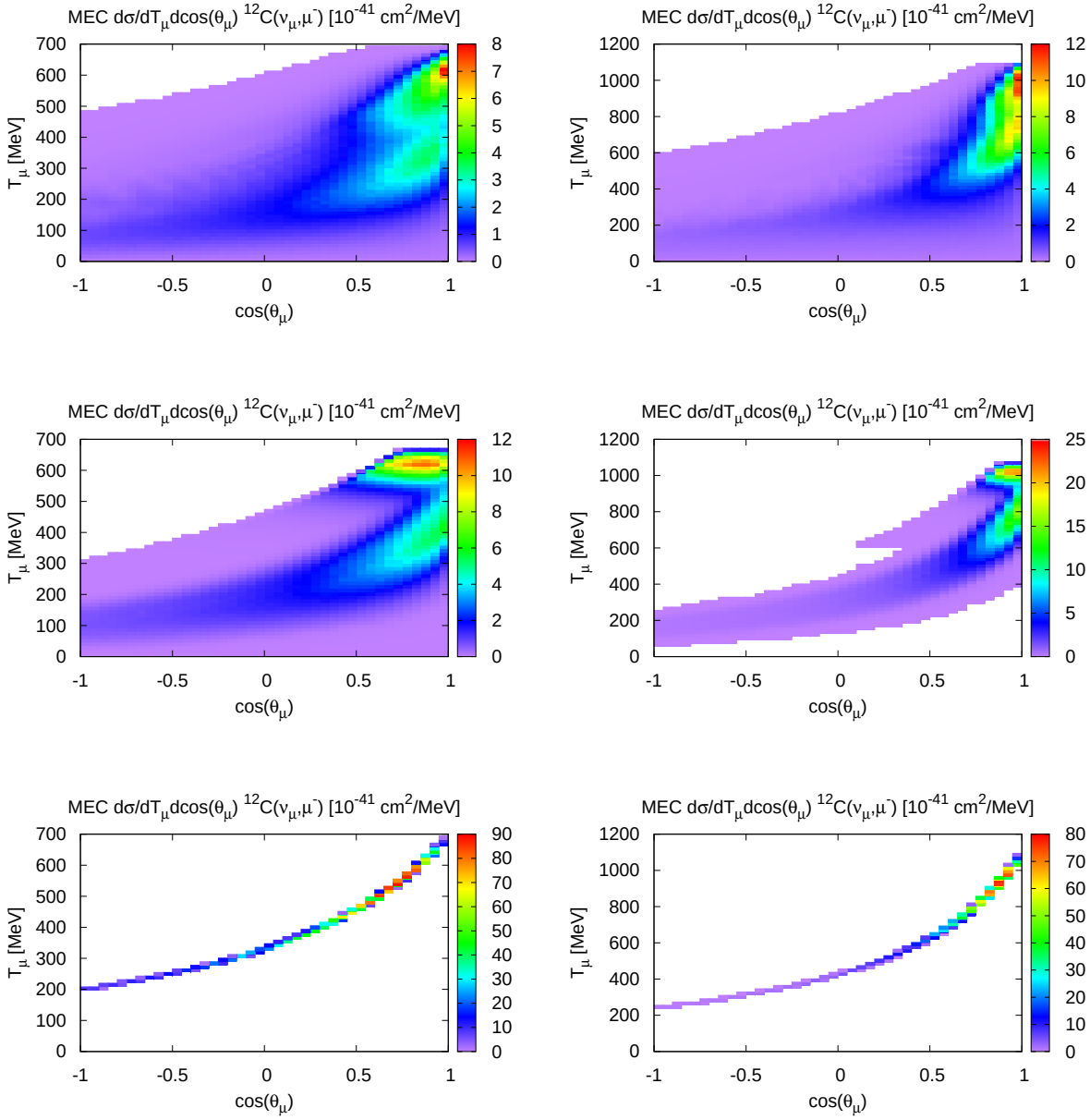

Figure 57: Sample double differential MEC cross sections for muon neutrino on carbon. Top row: IFIC model, middle row: Lyon model, bottom row: TEM model. First column: E_ν =800 MeV, second column: E_ν =1200 MeV.

of true neutrino energies, which contribute to each of the reconstructed energy values. The result is shown in Fig. 58. As one can see, the reconstructed energy is poorly correlated with the true neutrino energy, there is a strong shift toward higher energies. This shift corresponds to the fact, that large factor of the MEC events comes from pionless Δ decays, which correspond to energy shift of almost 300 MeV. The clear double-peaked structure of true energy spectrum is not seen in the original paper regarding energy reconstruction in IFIC model in Ref. [97]. In order to compare the neutrino energy reconstruction bias coming from the above mentioned MEC models we have also evaluated the spectrum of reconstructed energies for fixed $E_\nu = 1200$ MeV. The results calculated for three 5 000 000

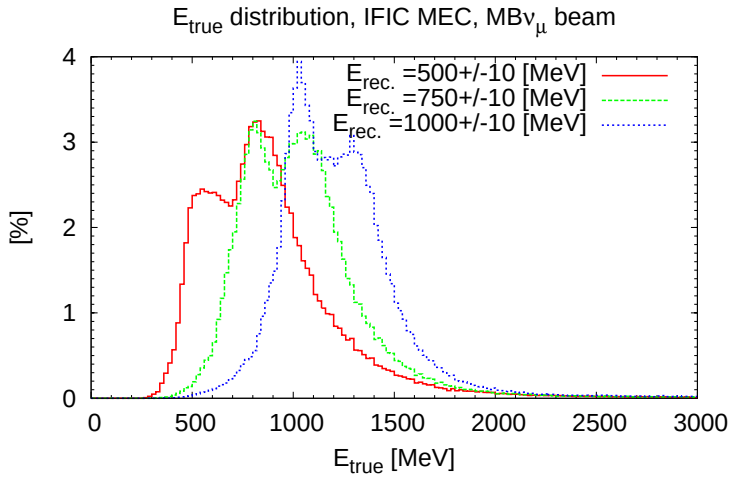

Figure 58: Energy reconstruction quality for IFIC MEC events and MiniBoonE ν_μ beam.

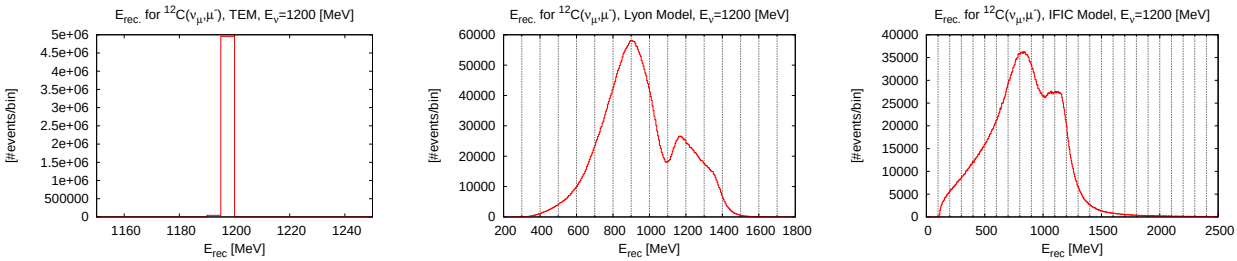

Figure 59: Distributions of reconstructed neutrino energy spectrum for MEC samples calculated using NuWro and true E_ν =1200 MeV.

MEC event samples are shown in Fig. 59 for 5 MeV neutrino energy bin width. The TEM energy reconstruction seems to fit the true neutrino energy almost perfectly. This is an expected result, since we calculate the TEM MEC cross section on a nucleon at rest. The Lyon and IFIC models both display a clear double peaked structure coming from pionless Δ decays included in both models. Both of them tend to underestimate the true neutrino energy. This results from the fact, that in the Eq. (2.33) we assume a single target nucleon at rest and in MEC events the energy and momentum transfer has to excite two nucleons in the final state.

The implementation of Lyon and IFIC models in NuWro has drawn a lot of attention of T2K collaboration. Currently we are providing them with pure MEC data samples calculated within both models. They are going to be included in the T2K oscillation analysis and used to callibrate and solve issues with the IFIC MEC model implementation in NEUT. The issues of double-peaked structure, proper nucleon pair isospin proportions (currently we use 60% p-n and 40% nn pairs) and consistent treatment of PDD are under strong debate on T2K Neutrino Interaction Working Group (NIWG) meetings. Probably the biggest challenge is the proper nucleon isospin structure of IFIC MEC model can be extracted only by the means of full model implementation. The PDD treatment is an issue of NEUT implementation.

7.3 From SPP to MEC in IFIC model

We shall discuss here the main computational problems related to the IFIC model with possible divergencies. We start with an example calculation of one of the MEC contributions. The first contribution to 2p2h excitations in the IFIC model is constructed by puting a particle-hole loop on the SPP diagram (Eqs. (6.20-6.26), taking the pion off-shell (all bosons connected on the same loop, see Fig. 52):

$$\begin{aligned}
-i\Pi^{\mu\nu(a)}_{2p2h} &= i^8 \sum_{iso} C_{iso} \int d^3r \int \frac{d^4k}{(2\pi)^4} \int \frac{d^4p}{(2\pi)^4} G(p,N)G(p',N')D_\pi(k)^2 \frac{f_\pi^2}{m_\pi^2} \\
&\quad \mathrm{Tr}\left[(\not{p}+M)\gamma^0 s^{\mu\dagger}\gamma^0(\not{p}'+M)s^\nu\right] \\
&\quad \int \frac{d^4l}{(2\pi)^4} G(l,N'')G(l',N''')\mathrm{Tr}\left[(\not{l}+M)\gamma^5\not{k}(\not{l}'+M)\gamma^5\not{k}\right]
\end{aligned} \tag{7.5}$$

with the 4-momentum conservation defined as:

$$\begin{aligned}
p' &= p+q-k \\
l' &= l+k.
\end{aligned} \tag{7.6}$$

by Dirac Delta functions obtained from each pair of nucleon propagators. The trace over pionic loop:

$$\begin{aligned}
\mathrm{Tr}\left[(\not{l}+M)\gamma^5\not{k}(\not{l}'+M)\gamma^5\not{k}\right] &= 4\left[2(l\cdot k)(l'\cdot k) - l\cdot l'k^2 - M^2k^2\right] = \\
&= 4\left[2(l\cdot k)^2 + k^2((l\cdot k - 2M^2)\right].
\end{aligned} \tag{7.7}$$

We make an assumption, that nucleons in the second loop are on-shell:

$$M^2 = l^2 = l'^2 = (l+k)^2 = M^2 + 2l\cdot k + k^2 \rightarrow l\cdot k = -\frac{k^2}{2}. \tag{7.8}$$

Thus the identity:

$$\mathrm{Tr}\left[(\not{l}+M)\gamma^5\not{k}(\not{l}'+M)\gamma^5\not{k}\right] = -8M^2k^2 \tag{7.9}$$

lets us define:

$$\begin{aligned}
i\mathcal{I}_1 &= \int \frac{d^4l}{(2\pi)^4} G(l,N'')G(l',N''')\mathrm{Tr}\left[(\not{l}+M)\gamma^5\not{k}(\not{l}'+M)\gamma^5\not{k}\right] \\
&= -\frac{8M^2k^2}{(2\pi)^4}\int d^4l \frac{1}{l^0+k^0+E(l')+i\epsilon}\frac{1}{l^0+E(l)+i\epsilon}\left(\frac{n_{N''}(l)}{l^0-E(l)-i\epsilon}+\frac{1-n_{N''}(l)}{l^0-E(l)+i\epsilon}\right) \\
&\quad \left(\frac{n_{N'''}(l')}{l^0+k^0-E(l')-i\epsilon}+\frac{1-n_{N'''}(l')}{l^0+k^0-E(l+k)+i\epsilon}\right) = \\
&= -i\frac{M^2k^2}{\pi^3}\int d^3l \left[\frac{n_{N''}(l)(1-n_{N'''}(l+k))}{(E(l)+E(l+k)+k^0+i\epsilon)2E(l)(E(l)+k^0-E(l')+i\epsilon)} + \right. \\
&+ \left. \frac{n_{N'''}(l+k)(1-n_{N''}(l))}{(2E(l+k))(E(l+k)-k^0+E(l)+i\epsilon)(E(l+k)-k^0-E(l)+i\epsilon)}\right].
\end{aligned} \tag{7.10}$$

One can easily identify the remaining integral as a Lindhard function. Having the 1p1h calculation previously done, we can calculate the imaginary part of $\mathcal{I}_1$ in the RFG model:

$$\begin{aligned}
i\Im\mathcal{I}_1 &= i\frac{M^2k^2}{4\pi^2}\int \frac{d^3l}{E(l)E(l+k)}\left[\Theta(k''_F-|l|)\Theta(|l+k|-k'''_F)+\Theta(k'''_F-|l+k|)\Theta(|l|-k''_F)\right] \\
&\quad \delta(E(l+k)-E(l)-k^0).
\end{aligned} \tag{7.11}$$

The same steps, as for the $1p1h$ excitation lead us to the result:

$$
\begin{aligned}
i\Im\mathcal{I}_1 &= i\frac{M^2k^2}{2\pi|k|}\Big[(E_F^{''}-E_{min}(k^\mu,E_F^{'''}))\Theta(E_F^{''}-E_{min}(k^\mu,E_F^{'''}))+\\
&+ (k^\mu\to -k^\mu, E_F^{''}\leftrightarrow E_F^{'''})\Big]. \qquad (7.12)
\end{aligned}
$$

This result is proportional to the definition of a Lindhard function from Ref. [163]

$$
\Im\mathcal{I}_1 = -k^2\Im U_R(k,p_F^{''},p_F^{'''}). \qquad (7.13)
$$

The 2p2h polarization tensor can be re-written in a more convenient form:

$$
\begin{aligned}
\Pi_{2p2h}^{\mu\nu(a)} &= i\sum_{iso}C_{iso}\int d^3r\int\frac{d^4k}{(2\pi)^4}D_\pi(k)^2\frac{f_\pi^2}{m_\pi^2}i\mathcal{I}_1(k)i\mathcal{I}_2^{\mu\nu}(q-k)\\
\mathcal{I}_2^{\mu\nu}(q-k) &= \int d^3r\int\frac{d^3p}{(2\pi)^3}\left(\frac{1}{2E(p)(E(p)+q^0-k^0+E(p')+i\epsilon)}\frac{n_N(p)(1-n_{N'}(p'))}{E(p)+q^0-k^0-E(p')+i\epsilon}\right.\\
&+ \left.\frac{1}{2E(p')(E(p')-q^0+k^0+E(p)+i\epsilon)}\frac{n_{N'}(p')(1-n_N(p))}{E(p')-q^0+k^0-E(p)+i\epsilon}\right)\times\\
&\times \mathrm{Tr}\left[A_{1p1h1\pi}^{\mu\nu}(p,q,k)\right]. \qquad (7.14)
\end{aligned}
$$

Here the problem is again separated into a form of braid of $1p1h1\pi$ excitation, but with virtual pion and a Lindhard function depending on the virtual pion 4-momentum.

$$
\Pi_{2p2h}^{\mu\nu(a)} = i\sum_{iso}C_{iso}\int d^3r\int\frac{d^4k}{(2\pi)^4}D_\pi(k)^2\frac{f_\pi^2}{m_\pi^2}k^2U_R(k,k_F^{''},k_F^{'''})\mathcal{I}_2^{\mu\nu}(q-k). \qquad (7.15)
$$

The imaginary part corresponding to the $2p2h$ excitation:

$$
\begin{aligned}
-\frac{1}{\pi}\Im(\Pi_{2p2h}^{\mu\nu(a)}L_{\mu\nu}) &= -\frac{1}{\pi}\sum_{iso}C_{iso}\int d^3r\int\frac{d^4k}{(2\pi)^4}D_\pi(k)^2\frac{f_\pi^2}{m_\pi^2}k^2\Im U_R(k,k_F^{''},k_F^{'''})\times\\
&\times \Im(\mathcal{I}_2^{\mu\nu}(q-k)L_{\mu\nu}). \qquad (7.16)
\end{aligned}
$$

The biggest numerical problem is there in the integral:

$$
\begin{aligned}
\Im(\mathcal{I}_2^{\mu\nu}(q-k)L_{\mu\nu}) &= -\pi\int\frac{d^3p}{(2\pi)^3}\frac{1}{4E(p)E(p')}\left(\Theta(p_F-|\boldsymbol{p}|)\Theta(|\boldsymbol{p'}|-k_F')+\right.\\
&+ \left.\Theta(p_F'-|\boldsymbol{p'}|)\Theta(|\boldsymbol{p}|-k_F)\right)\delta(E(p')-E(p)-q^0+k^0)\times\\
&\times \mathrm{Tr}\left[A_{1p1h1\pi}^{\mu\nu}(p,q,k)\right]L_{\mu\nu}. \qquad (7.17)
\end{aligned}
$$

One can check that together with the LDA integration one would have to perform a 7-dimensional numerical integration. Here we can use again an approximation proposed in Ref. [70]: one puts an averaged nucleon momentum in the hadronic tensor. Thus:

$$
\begin{aligned}
\Im(\mathcal{I}_2^{\mu\nu}(q-k)L_{\mu\nu}) &= -\pi\int\frac{d^3p}{(2\pi)^3}\frac{1}{4E(p)E(p')}\left(\Theta(k_F-|\boldsymbol{p}|)\Theta(|\boldsymbol{p'}|-k_F')+\right.\\
&+ \left.\Theta(k_F'-|\boldsymbol{p'}|)\Theta(|\boldsymbol{p}|-k_F)\right)\delta(E(p')-E(p)-q^0+k^0)\times\\
&\times \mathrm{Tr}\left[A_{1p1h1\pi}^{\mu\nu}(<p>,q,k)\right]L_{\mu\nu} =\\
&= \frac{1}{8M^2}\Im U_R(q-k,k_F,k_F')\mathrm{Tr}\left[A_{1p1h1\pi}^{\mu\nu}(<p>,q,k)\right]L_{\mu\nu}. \qquad (7.18)
\end{aligned}
$$

Within this approximation the calculated $2p2h$ contribution has the form:

$$
\begin{aligned}
-\frac{1}{\pi}\Im(\Pi^{\mu\nu(a)}_{2p2h}L_{\mu\nu}) &= -\frac{1}{\pi}\sum_{iso}C_{iso}\int d^3r\int\frac{d^4k}{(2\pi)^4}D_\pi(k)^2\frac{f_\pi^2}{m_\pi^2}k^2\Im U_R(k,k''_F,k'''_F)\times \\
&\times \frac{1}{8M^2}\Im U_R(q-k,k_F,k'_F)\mathrm{Tr}\left[A^{\mu\nu}_{1p1h1\pi}(<p>,q,k)\right]L_{\mu\nu} = \\
&= \frac{1}{128\pi^5}\frac{1}{M^2}\frac{f^2_{\pi NN}}{m_\pi^2}\sum_{iso}C_{iso}\int d^3r\int d^4kD_\pi(k)^2(-k^2)\Im U_R(k,k''_F,k'''_F)\times \\
&\times \Im U_R(q-k,k_F,k'_F)\mathrm{Tr}\left[A^{\mu\nu}_{1p1h1\pi}(<p>,q,k)\right]L_{\mu\nu} = \\
&= \frac{M^2}{512\pi^7}\frac{f^2_{\pi NN}}{m_\pi^2}\sum_{iso}C_{iso}\int d^3r\int d^4kD_\pi(k)^2(-k^2)\frac{1}{|q||q-k|}\times \\
&\times [(E_F-E_{min}(q-k,E'_F))+(E'_F-E_{min}(k-q,E_F))]\times \\
&\times [(E''_F-E_{min}(k,E'''_F))+(E'''_F-E_{min}(-k,E''_F))]\times \qquad (7.19)\\
&\times \mathrm{Tr}\left[A^{\mu\nu}_{1p1h1\pi}(<p>,q,k)\right]L_{\mu\nu}.
\end{aligned}
$$

And the cross sections:

$$
\begin{aligned}
\frac{d^3\sigma}{dE'd\Omega'} &= \frac{\alpha^2|\boldsymbol{l'}|}{16\pi^4Q^4|\boldsymbol{l}|M^2}\frac{f^2_{\pi NN}}{m_\pi^2}\int drr^2\sum_{iso}C_{iso}\int d^4kD_\pi(k)^2(-k^2)\Im U_R(k,k''_F,k'''_F)\times \\
&\times \Im U_R(q-k,k_F,k'_F)\mathrm{Tr}\left[A^{\mu\nu}_{1p1h1\pi}(<p>,q,k)\right]L_{\mu\nu} = \\
&= \frac{\alpha^2|\boldsymbol{l'}|M^2}{64\pi^6Q^4|\boldsymbol{l}|}\frac{f^2_{\pi NN}}{m_\pi^2}\int drr^2\sum_{iso}C_{iso}\int d^4kD_\pi(k)^2(-k^2)\frac{1}{|q||q-k|}\times \\
&\times [(E_F-E_{min}(q-k,E'_F))+(E'_F-E_{min}(k-q,E_F))]\times \\
&\times [(E''_F-E_{min}(k,E'''_F))+(E'''_F-E_{min}(-k,E''_F))]\times \\
&\times \mathrm{Tr}\left[A^{\mu\nu}_{1p1h1\pi}(<p>,q,k)\right]L_{\mu\nu}\ \text{(electrons)} \qquad (7.20)
\end{aligned}
$$

$$
\begin{aligned}
\frac{d^3\sigma}{dE'd\Omega'} &= \frac{G_F^2\cos^2(\Theta_C)|\boldsymbol{l'}|}{128\pi^6|\boldsymbol{l}|M^2}\frac{f^2_{\pi NN}}{m_\pi^2}\int drr^2\sum_{iso}C_{iso}\int d^4kD_\pi(k)^2(-k^2)\Im U_R(k,k''_F,k'''_F)\times \\
&\times \Im U_R(q-k,k_F,k'_F)\mathrm{Tr}\left[A^{\mu\nu}_{1p1h1\pi}(<p>,q,k)\right]L_{\mu\nu} = \\
&= \frac{G_F^2\cos^2(\Theta_C)|\boldsymbol{l'}|M^2}{512\pi^7|\boldsymbol{l}|}\frac{f^2_{\pi NN}}{m_\pi^2}\int drr^2\sum_{iso}C_{iso}\int d^4kD_\pi(k)^2(-k^2)\frac{1}{|q||q-k|}\times \\
&\times [(E_F-E_{min}(q-k,E'_F))+(E'_F-E_{min}(k-q,E_F))]\times \\
&\times [(E''_F-E_{min}(k,E'''_F))+(E'''_F-E_{min}(-k,E''_F))]\times \\
&\times \mathrm{Tr}\left[A^{\mu\nu}_{1p1h1\pi}(<p>,q,k)\right]L_{\mu\nu}\ \nu CC. \qquad (7.21)
\end{aligned}
$$

As for the isospin dependence we will have $2\Im U_R(k,n,p)/2\Im U_R(k,p,n)$ for $2p2h$ interactions driven by π^+/π^- or $\Im U_R(k,n,n)+\Im U_R(k,p,p)$ for interactions driven by π^0. Rest of the isospin dependencies is hidden in $A^{\mu\nu}_{1p1h1\pi}$. The above approximation needs, however, a "small" modification. Let us take a look at the diagram in the figure 60. For a virtual pion there exists a possibility, that the intermediate nucleon goes on shell, leading to a singular contribution in the integral. This singularity is physical, because the real nucleon can excite another particle-hole pair in the Fermi sea with infinite probability. One has to account

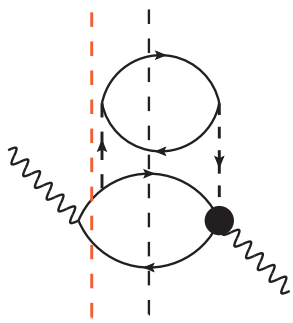

Figure 60: Alternative cut in the Nucleon Pole contribution.

in for the fact, that particle-hole pairs have finite lifetime and nucleons leave nucleus in finite time. Real nucleus is localized, it is not an infinite Fermi sea. As in the $1p1h1\pi$ part, one could assume the average nucleon momentum perpendicular to the (q, k) plane. But then one would randomly hit the pole or get close to it, disturbing the numerical stability. Better idea is to take the averaged momentum in one of the planes, like the (x, z) plane, and integrate over the angle between nucleon momentum and momentum transfer. One can then locate the pole by solving $(\langle p\rangle + q)^2_\mu = M^2$:

$$\begin{aligned} \langle p\rangle^2 + q^2 + 2\langle p\rangle \cdot q &= M^2 = M^2 + q^2 + 2\langle E\rangle q^0 - 2\langle |p|\rangle |q|\mu \\ \mu &= \frac{2\langle E\rangle q^0 + q^2}{2\langle |p|\rangle |q|}. \end{aligned} \tag{7.22}$$

Then one substitutes either ([70])

$$(\langle p\rangle + q)^2_\mu - M^2 + i\epsilon \to (\langle p\rangle + q)^2_\mu - M^2 + iM\Gamma_N \tag{7.23}$$

with averaged in-medium nucleon self energy $\Gamma_N \approx 10MeV$ or one can direcly relate this quantity to the averaged nucleon time of flight inside a nucleus through the relation ([164]):

$$\int_{-T/2}^{T/2} dt e^{i(p^0 - E(p))t}\Theta(t) = \frac{1}{p^0 - E(p) + i\epsilon} \tag{7.24}$$

in the limit $T \to \infty$ and $\epsilon \to 0$. For an on-shell particle $p^0 = E(p)$ and

$$\frac{T}{2} = \frac{1}{\epsilon}. \tag{7.25}$$

Authors of [164] assume, that nucleons move approximately at the speed of light from the center on nucleus. They claim, that:

$$\epsilon \approx \frac{2\hbar}{T} \approx \frac{2\hbar c}{R} \tag{7.26}$$

and this gives for Carbon $\epsilon \approx 200MeV$. Both approaches give slightly different answers to the question how to solve the nucleon pole puzzle and need to be tested thoroughly. The strategy is as follows:

1. Find the pole.

2. Give a width to the propagator using either Eq. (7.23) or Eq. (7.26).

3. Put a lot of integration points in $\cos(\Theta_N) \pm \delta$ around the pole, fewer outside. Find how sensitive it is to the choice of δ and n.o. points. Substitute in Eq. (7.20) and Eq. (7.21):

$$A^{\mu\nu}_{1p1h1\pi}(< p >, q, k) \rightarrow \frac{1}{2}\int_{-1}^{1} d\mu A^{\mu\nu}_{1p1h1\pi}(< p >, \mu, q, k). \tag{7.27}$$

Another difficulty may occur in the crossed correlation diagram, if:

$$\begin{aligned} \langle p\rangle^2 + k^2 - 2\langle p\rangle \cdot k &= M^2 = M^2 + k^2 - 2\langle E\rangle k^0 + 2\langle |p|\rangle |k|\mu \\ \mu &= \frac{2\langle E\rangle k^0 - k^2}{2\langle |p|\rangle |k|}. \end{aligned} \tag{7.28}$$

This will lead to another divergence, which needs to be removed in the same manner, as the direct Nucleon Pole diagram.
There is also a slight problem in the integration limits. In the $2p2h$ dynamics one needs to put two Lindhard functions on shell simultaneously. This requires:

$$\begin{aligned} 1)k^2_\mu &< 0 \rightarrow k^0 < |\boldsymbol{k}| \\ 2)E &> -\frac{1}{2}\left((q^0 - k^0) - |\boldsymbol{q} - \boldsymbol{k}|\right)\sqrt{1 - \frac{4M^2}{(q-k)^2_\mu}} \\ 3)F &> -\frac{1}{2}\left(k^0 - |\boldsymbol{k}|\right)\sqrt{1 - \frac{4M^2}{k^2_\mu}} \end{aligned} \tag{7.29}$$

with E and F being the Fermi energies of final nucleon state in the first and secon loop respectively. Solution of the above mentioned problems and theoretical computation of $2p2h$ excitations is current work in progress in our group. Independent numerical code describing the MEC mechanism will be a valuable tool to test different ideas and descriptions of this dynamical channel.

8 Conclusions

In this thesis we have explored multiple lepton-nucleus interaction models based on effective field theories from free nucleon target, through simple deuteron model up to (local) Fermi gas picture with nonperturbative medium modifications of Δ resonance properties as well as effects of nuclear spectral function in quasielastic neutrino cross section measurement. By comparisons to available data we could see, that all of them work in a very limited interaction energy range for lepton energies between ~ 500 and 1200 MeV and within impulse approximation applicability regime, *i. e.* for momentum transfers above $\sim$400 MeV.

We have shown that all physical observables in lepton-nucleus scattering are highly dependent on the treatment of nuclear effects.

Perhaps the most important interaction process for accelerator oscillation experiments is the quasielastic scattering. In our paper [14] we have performed an nucleon axial mass fit to MiniBooNE data in which we have used spectral function formalism to model CCQE process. We have shown, that both theoretical and experimental understanding of CCQE process has serious deficiencies. If we assume that MiniBooNE data from [11] concern purely quasielastic process, we need to accept that the leading parameter describing nucleon axial coupling dependence on Q^2 is completely different for free nucleons and atomic nuclei by about 30% and 5 standard deviations, excluding theoretical PCAC-based computations as well. This is a strong indication, that we need more, than CCQE and (multiple) pion production assumed by MiniBooNE collaboration in order to understand experimental data. Later on an analogous experimental fit has been made by IFIC group in Ref. [92], where they have applied their model of multinucleon excitations. The outcome of their fit to MiniBooNE data (with the same definition of probability measure, as in our paper) is in full agreement with PCAC-based computations and old deuterium experiments. This has triggered a still ongoing discussion of *npnh* channel impact on neutrino oscillation measurements. Recently three independent models have been introduced to our MC generator, NuWro. The IFIC model has been implemented on an effective level and used to produced event saples, which enter the current T2K systematic error analysis. T2K is working on its own implementation of *npnh* dynamics in NEUT. we have also used NuWro in order to compare the *npnh* cross sections resulting from three different models (TEM, IFIC and Lyon models), showing they differ at large both in total cross section as well as in the reconstructed neutrino energy spectrum.

The second most important process from the point of view of T2K is SPP. We performed extensive tests of two theoretical models: HNV from Ref. [46] and Fogli-Nardulli from Ref. [48]. The inclusive electron-proton data show, that HNV model gives more realistic predictions for low Q^2, but seems to lack some cross section for higher W. Fogli-Nardulli model on the contrary shows too large cross sections both for low Q^2 values and very large W, but it can reproduce the proportions between ANL neutrinoproduction cross sections, which can not be done with default HNV model. Electron scattering tests using HNV model with different sign between Δ and background terms suggest, that maybe one can improve it with proper unitarization, as it gives cross section shapes closer to that of Fogli-Nardulli. Nevertheless, one can not explain the pion production data without a model of nonresonant background.

Separate problem concerns the axial Δ coupling, which is determined at large by $C_5^A(Q^2)$ form factor. In contrary to neutrino scattering, where the value of axial coupling at $Q^2 = 0$ can be determined with high accuracy from neutron β-decay experiments, there is no no

such precise information about Δ. From the Goldberger-Treiman relation one can establish $C_5^A(0) \sim 1.15 - 1.2$, but it is only an approximate PCAC-based solution. Extraction of its true value as well as the Q^2 dependence of C_5^A is strongly biased by nuclear effects, as in the case of quasielastic scattering and nucleon axial mass problem. The fits to ANL data for free nucleon from Ref. [46] and on deuteron from Ref. [152] seem to prefer different values of $C_5^A(0)$ and resonant axial mass $M_{A\Delta}$. Furthermore, our results for HNV model SPP cross section on carbon from Ref. [15] underestimate the MiniBooNE data for values of $C_5^A(0) = 1.19$ and $M_{A\Delta}$, which lead to bad overestimation of ANL cross sections both on free nucleon and deuterium targets. Possible explanation may lie within the $2p2h1\pi$ mechanism, which has been studied by the authors of Ref. [162], who claim it may give rise to a large fraction of MiniBooNE SPP cross section. In our paper we also found out, that the muon to electron neutrino cross section ration depend on inclusion of nonresonant background, but are independent on nuclear effects. On the contrary, the total cross section depends at large on the inclusion of Δ self-energy in nuclear matter. The resulting fraction of pionless Δ decays depends on neutrino energy if one considers the $E_\nu \leq$ GeV region, which is different from what is used in present MC generators (constant fraction of 20% pionless Δ decays). We found out as well, that thee pionless Δ decays into *npnh* states contribute a large fraction to IFIC model MEC cross section and are presumably responsible for the double-peaked structure in the reconstructed neutrino energy spectrum for MEC events. Nevertheless, the pionless Δ decay does not lead to any substantial improvement of the double-differential cross section in the dip region between quasielastic, and Δ peaks, as we have shown for the inclusive $^{12}C(e, e')$ scattering.

All of the above mentioned dynamics have been implemented in a C++ codes, which are capable of returning diferent cross sections for free nucleon, deuteron and nucleus (in LFG approximation) targets and can be used for further research of leptonic interactions on hadronic targets, including *npnh* dynamics, whose implementation is being currently worked on. Results may be further used for the improvement of MC simulations in NuWro as well as other generators.

As a final conclusion we need to state, that we are still missing a truly unified approach to the QE, SPP and MEC dynamics for lepton energies under consideration. All of the mentioned models have their deficiencies and fail to describe either some of the SPP channels or interactions in kinematical range at the verge of applicability of impulse approximation. Further improvements, like unitarization of HNV model together with simultaneous fits of $C_5^A(Q^2)$ to all ANL channels or inclusion of nucleon correlations in MEC are needed. Thus we believe the lepton-nucleus interaction modeling will be a constant work-in-progress for a long period of time and ay lead to interesting discoveries in the field of both nuclear and particle physics.

Appendix

A Units, physical constants and conventions

In this thesis we use the HEP unit system. One puts for the Plank constant and velocity of light $\hbar = c = 1$. Thus the relations between time, length, energy and momentum units are following:

$$[\text{energy}] = [\text{momentum}] = [\text{length}]^{-1} = [\text{time}]^{-1}. \tag{A.1}$$

The natural energy scale is either "electronvolt", eV, (elementary electron charge $\times$ 1 Volt) or inversed femtometer fm^{-1} (1 [fm]= 10^{-15} [m]). From practical energy scale reasons we use rather MeV=10^6eV or GeV=10^9eV. These units are related by simple formula:

$$197.3269631(49) MeV \times fm \approx \hbar c = 1. \tag{A.2}$$

For example, most common hadron masses used in this dissertation are listed in Tab. 7.

Table 7: Hadronic masses

Symbol	Value GeV	Hadron name
m_π	$\frac{1}{3}(m_{\pi^0} + m_{\pi^+} + m_{\pi^-})$=0.13804	pion
m_ρ	0.770	ρ meson
M	$\frac{1}{2}(M_p + M_n)$=0.93892	nucleon
M_Δ	1.232	$\Delta(1232)$ resonance

A.1 Metric and four-vectors

Real metric $g^{\mu\nu} = \text{diag}(+,-,-,-)$ is used. The four-vectors are used in the following convention:

$$\begin{aligned} x^\mu &= (x^0, \boldsymbol{x}) \text{ contravariant} \\ x_\mu &= (x^0, -\boldsymbol{x}) \text{ covariant.} \end{aligned} \tag{A.3}$$

so that $x_\mu = g_{\mu\nu} x^\nu$ and vice-versa. This defines the four-vector contraction:

$$x^\mu x_\mu = x_0^2 - \boldsymbol{x}^2. \tag{A.4}$$

We define the four-derivative operators as:

$$\begin{aligned} \partial^\mu &= \frac{\partial}{\partial_\mu} = (\frac{\partial}{\partial_t}, -\boldsymbol{\nabla}) \text{ contravariant} \\ \partial_\mu &= \frac{\partial}{\partial^\mu} = (\frac{\partial}{\partial_t}, \boldsymbol{\nabla}) \text{ covariant.} \end{aligned} \tag{A.5}$$

Contraction of both derivatives gives the D'Alembertian:

$$\partial_\mu \partial^\mu = \Box = \frac{\partial^2}{\partial_t^2} - \Delta;\ \Delta = \boldsymbol{\nabla}^2. \tag{A.6}$$

For all on-shell particles with mass m and momentum $\boldsymbol{p}$ we have following relation for four-momentum:

$$p^\mu = (E(\boldsymbol{p}), \boldsymbol{p}) = (\sqrt{\boldsymbol{p}^2 + m^2}, \boldsymbol{p}) \tag{A.7}$$

so that $p^\mu p_\mu = m^2$.

A.2 Isospin operators and transitions

This section is devoted to the isospin operator algebra and transition currents.

A.2.1 Nucleons

Nucleon fields form a $SU(2)$ isospin doublet. Their isospin wave functions are eigenvectors of the $\frac{\tau_3}{2}$ matrix belonging to the Pauli matrices:

$$\tau_1 = \begin{pmatrix} 0 & 1 \\ 1 & 0 \end{pmatrix}; \ \tau_2 = \begin{pmatrix} 0 & -i \\ i & 0 \end{pmatrix}; \ \tau_3 = \begin{pmatrix} 1 & 0 \\ 0 & -1 \end{pmatrix}. \tag{A.8}$$

They obey the following commutation relation:

$$\left[\frac{\tau_i}{2}, \frac{\tau_j}{2}\right] = i\epsilon_{ijk}\frac{\tau_k}{2} \tag{A.9}$$

Proton and neutron correspond to the isospin eigenvalues of $\frac{1}{2}$ and $-\frac{1}{2}$:

$$\begin{aligned} \frac{1}{2}\tau_3 \left|p\right\rangle &= \frac{1}{2}\tau_3 \begin{pmatrix} 1 \\ 0 \end{pmatrix} = \frac{1}{2}\left|p\right\rangle \\ \frac{1}{2}\tau_3 \left|n\right\rangle &= \frac{1}{2}\tau_3 \begin{pmatrix} 0 \\ 1 \end{pmatrix} = -\frac{1}{2}\left|n\right\rangle . \end{aligned} \tag{A.10}$$

From the above definitions one obtains following charge operator:

$$\boldsymbol{Q} = \frac{1}{2}(\mathbb{1} + \tau_3). \tag{A.11}$$

This equation can be realted to the more general Gell-Mann-Nishijima relation for hadrons:

$$\boldsymbol{Q} = I_3 + \frac{1}{2}(B + S + C + B' + T) \tag{A.12}$$

with I_3 being the isospin's third component, B- the baryon number (counterpart of hypercharge), (S, C, B', T)- the strangeness, charm, bottomness and topness (related to heavy quark components of hadrons). As one can see, the nucleon has baryon number $B = 1$. For isospin-changing reactions one defines also the isospin raising/lowering operators:

$$\begin{aligned} \tau_+ &= \frac{1}{2}(\tau_1 + i\tau_2) = \begin{pmatrix} 0 & 1 \\ 0 & 0 \end{pmatrix} \\ \tau_- &= \frac{1}{2}(\tau_1 - i\tau_2) = \begin{pmatrix} 0 & 0 \\ 1 & 0 \end{pmatrix} \end{aligned} \tag{A.13}$$

which act on the nucleon wave functions in the following way:

$$\tau_+ \left|p\right\rangle = 0; \ \tau_- \left|p\right\rangle = \left|n\right\rangle ; \ \tau_+ \left|n\right\rangle = \left|p\right\rangle ; \ \tau_- \left|n\right\rangle = 0. \tag{A.14}$$

Useful (anti)commutation relations for the isospin ladder operators are:

$$\begin{aligned} (\tau_\pm)^2 &= 0; \ [\tau_+, \tau_-] = \tau_3; \ \{\tau_+, \tau_-\} = \mathbb{1}; [\tau_3, \tau_+] = 2\tau_+; \\ \{\tau_3, \tau_+\} &= 0; [\tau_3, \tau_-] = -2\tau_-; \ \{\tau_3, \tau_-\} = 0 \end{aligned} \tag{A.15}$$

They are useful in all calculations regarding multiple isospin interchange vertices. The above considerations are true for all isospin-1/2 fields.

A.2.2 Pions

Pions fields π^+, π^- and π^0 form an isospin-1 $SU(2)$ triplet. A convenient choice of isospin wave functions is:

$$\left|\pi^+\right\rangle \equiv \begin{pmatrix} 1 \\ 0 \\ 0 \end{pmatrix}; \left|\pi^0\right\rangle \equiv \begin{pmatrix} 0 \\ 1 \\ 0 \end{pmatrix}; \left|\pi^-\right\rangle \equiv \begin{pmatrix} 0 \\ 0 \\ 1 \end{pmatrix}. \tag{A.16}$$

Their transformations are realized by the following $SU(2)$ Lie matrix algebra representation:

$$t_1 = \frac{1}{\sqrt{2}} \begin{pmatrix} 0 & 1 & 0 \\ 1 & 0 & 1 \\ 0 & 1 & 0 \end{pmatrix}; \; t_2 = \frac{i}{\sqrt{2}} \begin{pmatrix} 0 & -1 & 0 \\ 1 & 0 & -1 \\ 0 & 1 & 0 \end{pmatrix}; \; t_3 = \begin{pmatrix} 1 & 0 & 0 \\ 0 & 0 & 0 \\ 0 & 0 & -1 \end{pmatrix} \tag{A.17}$$

which obeys standard $SU(2)$ commutation relations:

$$[t_i, t_j] = i\epsilon_{ijk} t_k. \tag{A.18}$$

All pion charge eigenstates are eigenvectors of t_3,*i. e.* :

$$t_3 \left|\pi^\lambda\right\rangle = \lambda \left|\pi^\lambda\right\rangle \tag{A.19}$$

with $\lambda = -1, 0, 1$ for $|\pi^-\rangle$, $|\pi^0\rangle$ and $|\pi^+\rangle$ respectively. The charge operator for pions is t_3 and their baryon number is zero (Eq. (A.12)). The ladder operators are constructed in a standard way:

$$t_+ = (t_1 + it_2) = \sqrt{2} \begin{pmatrix} 0 & 1 & 0 \\ 0 & 0 & 1 \\ 0 & 0 & 0 \end{pmatrix}; \; t_- = (t_1 - it_2) = \sqrt{2} \begin{pmatrix} 0 & 0 & 0 \\ 1 & 0 & 0 \\ 0 & 1 & 0 \end{pmatrix}. \tag{A.20}$$

so that:

$$t_+ \left|\pi^\lambda\right\rangle = \sqrt{2} \left|\pi^{\lambda+1}\right\rangle; \; t_+ \left|\pi^+\right\rangle = 0; \; t_- \left|\pi^\lambda\right\rangle = \sqrt{2} \left|\pi^{\lambda-1}\right\rangle; \; t_- \left|\pi^-\right\rangle = 0 \tag{A.21}$$

according to the ladder operator relations for total isospin j:

$$\begin{aligned} J_\pm \left|j, m\right\rangle &= \sqrt{(j \mp m)(j \pm m + 1)} \left|j, m \pm 1\right\rangle \\ J_3 \left|j, m\right\rangle &= m \left|j, m\right\rangle; \; m \in [-j, j]. \end{aligned} \tag{A.22}$$

These relations produce the Clebsch-Gordan coefficients. The ladder operators obey the following commutation relations:

$$[t_+, t_-] = \sqrt{2} t^3; \; [t_3, t_+] = \sqrt{2} t_+; \; [t_3, t_-] = -\sqrt{2} t_-. \tag{A.23}$$

Pionic fields are usually defined in Cartesian isospin coordinates:

$$\boldsymbol{\phi} = (\phi_1, \phi_2, \phi_3). \tag{A.24}$$

They are linked to the charged field states through following relations:

$$\pi^\pm = \frac{1}{\sqrt{2}} (\phi_1 \pm i\phi_2); \; \pi^0 = \phi_3. \tag{A.25}$$

the physical interpretation of these fields is that $\pi^{\pm}$ create $|\pi^{\pm}\rangle$ or annihilate $|\pi^{\mp}\rangle$. It is useful to introduce the product of cartesian pion fields with vector of nucleon isospin matrices:

$$\boldsymbol{\tau} \cdot \boldsymbol{\phi} = \sqrt{2}(\tau_+\pi^- + \tau_-\pi^+) + \tau_3\pi^0 \tag{A.26}$$

which can be found in pion-nucleon interaction vertices. We would also like to introduce the product of isospin matrix vector with $SU(2)$ gauge field triplet $\boldsymbol{A}^{\mu}$, which is helpful in the establishment of isospin coefficients for $W^{\pm}N$ and γN vertices:

$$\begin{aligned} \boldsymbol{\tau} \cdot \boldsymbol{A}_{\mu} &= \sqrt{2}(\tau_+ W^-_{\mu} + \tau_- W^+_{\mu}) + \tau_3 A^3_{\mu} \\ W^{\pm\mu} &= \frac{1}{\sqrt{2}}(A^{\mu}_1 \pm i A^{\mu}_2). \end{aligned} \tag{A.27}$$

A.2.3 Δ resonance

The $\Delta(1232)$ resonance isospin-3/2 states form an $SU(2)$ quartet $(\Delta^{++}, \Delta^{+}, \Delta^{0}, \Delta^{-})$. We choose the isospinor basis to be:

$$|\Delta^{++}\rangle \equiv \begin{pmatrix} 1 \\ 0 \\ 0 \\ 0 \end{pmatrix}; \ |\Delta^{+}\rangle \equiv \begin{pmatrix} 0 \\ 1 \\ 0 \\ 0 \end{pmatrix}; \ |\Delta^{0}\rangle \equiv \begin{pmatrix} 0 \\ 0 \\ 1 \\ 0 \end{pmatrix}; \ |\Delta^{-}\rangle \equiv \begin{pmatrix} 0 \\ 0 \\ 0 \\ 1 \end{pmatrix}. \tag{A.28}$$

There exists also a Lie algebra of matrices $\boldsymbol{\Theta} = (\Theta_1, \Theta_2, \Theta_3)$, such that $\Theta_3 |3/2, \lambda_{\Delta}\rangle = \lambda_{\Delta} |3/2, \lambda_{\Delta}\rangle$ with $\lambda_{\Delta} \in (-3/2, -1/2, 1/2, 3/2)$. The explicit form of this representation is following:

$$\Theta_1 = \frac{1}{\sqrt{2}} \begin{pmatrix} 0 & \sqrt{3} & 0 & 0 \\ \sqrt{3} & 0 & 2 & 0 \\ 0 & 2 & 0 & \sqrt{3} \\ 0 & 0 & \sqrt{3} & 0 \end{pmatrix}; \ \Theta_2 = \frac{i}{\sqrt{2}} \begin{pmatrix} 0 & -\sqrt{3} & 0 & 0 \\ \sqrt{3} & 0 & -2 & 0 \\ 0 & 2 & 0 & -\sqrt{3} \\ 0 & 0 & \sqrt{3} & 0 \end{pmatrix};$$

$$\Theta_3 = \frac{1}{2} \begin{pmatrix} 3 & 0 & 0 & 0 \\ 0 & 1 & 0 & 0 \\ 0 & 0 & -1 & 0 \\ 0 & 0 & 0 & -3 \end{pmatrix}. \tag{A.29}$$

Again, the commutation relation is:

$$[\Theta_i, \Theta_j] = i\epsilon_{ijk}\Theta_k. \tag{A.30}$$

We define the Δ charge operator as:

$$\boldsymbol{Q_{\Delta}} = \frac{1}{2}\mathbb{1} + \Theta_3 \tag{A.31}$$

The Gell-Mann-Nishijima relation (A.12) helps to establish Δ baryon number $B = 1$. The ladder operators are defined as:

$$\begin{aligned} \Theta_+ &= \Theta_1 + i\Theta_2; \ ; \Theta_- = \Theta_1 - i\Theta_2; \\ \Theta_+ |\Delta^-\rangle &= \sqrt{3}\,|\Delta^0\rangle; \ \Theta_+ |\Delta^0\rangle = 2\,|\Delta^+\rangle; \ \Theta_+ |\Delta^+\rangle = \sqrt{3}\,|\Delta^{++}\rangle; \ \Theta_+ |\Delta^{++}\rangle = 0; \\ \Theta_- |\Delta^{++}\rangle &= \sqrt{3}\,|\Delta^+\rangle; \ \Theta_- |\Delta^+\rangle = 2\,|\Delta^0\rangle; \ \Theta_- |\Delta^0\rangle = \sqrt{3}\,|\Delta^-\rangle; \ \Theta_- |\Delta^-\rangle = 0 \end{aligned} \tag{A.32}$$

For the isospin-1/2 to isospin-3/2 state transitions one introduces matrices $\boldsymbol{T}^\dagger$. They are by the following relation:

$$\left\langle \frac{3}{2}, \lambda_\Delta \left| \boldsymbol{T}^\dagger \right| \frac{1}{2}, \lambda_N \right\rangle \equiv \sum_\lambda \left\langle \frac{3}{2}, \lambda_\Delta \left| T^\dagger_\lambda \right| \frac{1}{2}, \lambda_N \right\rangle \boldsymbol{e}^*_{\boldsymbol{\lambda}};\ \lambda = -1, 0, 1 \tag{A.33}$$

where we introduce the set of orthonormal spherical isospin-1 vectors:

$$\boldsymbol{e}_{\boldsymbol{\pm 1}} \equiv \mp \frac{1}{\sqrt{2}} \begin{pmatrix} 1 \\ \pm i \\ 0 \end{pmatrix}; \boldsymbol{e}_{\boldsymbol{0}} \equiv \begin{pmatrix} 0 \\ 0 \\ 1 \end{pmatrix}. \tag{A.34}$$

The Clebsch-Gordan coefficients, which enter the product of the isospin-1 and isospin-1/2 representations intto the isospin-3/2 representation enter through:

$$\left\langle \frac{3}{2}, \lambda_\Delta \left| T^\dagger_\lambda \right| \frac{1}{2}, \lambda_N \right\rangle = \left\langle \frac{3}{2}, \lambda_\Delta | 1, \lambda; \frac{1}{2}, \lambda_N \right\rangle. \tag{A.35}$$

The ladder operator algebra, which creates a Δ states from nucleons through pion/gauge boson absorption is following:

$$T^\dagger_\pm \equiv \mp \frac{T^\dagger_1 \pm i T^\dagger_2}{\sqrt{2}};\ T^\dagger_0 = T^\dagger_3. \tag{A.36}$$

The $T^\dagger_+$ operator corresponds to a process, where Δ state is created by absorption of positively charged particle (*e. g.* $\pi+$ or W^+) on nucleon, $T^\dagger_-$ enters the absorption of negative charge on nucleon and $T^\dagger_0$ corresponds to Δ production by a neutral field on nucleon. Useful relation is obtained by inserting a complete set of Δ states between T_i and $T^\dagger_j$:

$$\sum_{\lambda_\Delta} T_i | \frac{3}{2}, \lambda_\Delta \rangle \langle \frac{3}{2}, \lambda_\Delta | T^\dagger_j = \frac{2}{3}\delta_{ij} - \frac{i}{3}\epsilon_{ijk}\sigma_k \tag{A.37}$$

which allows to establish:

$$\begin{aligned}
\sum_{\lambda_\Delta} T_+ | \frac{3}{2}, \lambda_\Delta \rangle \langle \frac{3}{2}, \lambda_\Delta | T^\dagger_+ &= \frac{2}{3}\mathbb{1} + \frac{1}{3}\tau_3 \\
\sum_{\lambda_\Delta} T_+ | \frac{3}{2}, \lambda_\Delta \rangle \langle \frac{3}{2}, \lambda_\Delta | T^\dagger_- &= 0 \\
\sum_{\lambda_\Delta} T_+ | \frac{3}{2}, \lambda_\Delta \rangle \langle \frac{3}{2}, \lambda_\Delta | T^\dagger_3 &= \frac{\sqrt{2}}{3}\tau^-; \\
\sum_{\lambda_\Delta} T_- | \frac{3}{2}, \lambda_\Delta \rangle \langle \frac{3}{2}, \lambda_\Delta | T^\dagger_+ &= 0 \\
\sum_{\lambda_\Delta} T_- | \frac{3}{2}, \lambda_\Delta \rangle \langle \frac{3}{2}, \lambda_\Delta | T^\dagger_- &= \frac{2}{3}\mathbb{1} - \frac{1}{3}\tau_3 \\
\sum_{\lambda_\Delta} T_- | \frac{3}{2}, \lambda_\Delta \rangle \langle \frac{3}{2}, \lambda_\Delta | T^\dagger_3 &= \frac{\sqrt{2}}{3}\tau^+
\end{aligned}$$

$$
\begin{aligned}
\sum_{\lambda_\Delta} T_3 |\frac{3}{2}, \lambda_\Delta\rangle\langle\frac{3}{2}, \lambda_\Delta| T_+^\dagger &= \frac{\sqrt{2}}{3}\tau^+ \\
\sum_{\lambda_\Delta} T_3 |\frac{3}{2}, \lambda_\Delta\rangle\langle\frac{3}{2}, \lambda_\Delta| T_-^\dagger &= \frac{\sqrt{2}}{3}\tau^- \\
\sum_{\lambda_\Delta} T_3 |\frac{3}{2}, \lambda_\Delta\rangle\langle\frac{3}{2}, \lambda_\Delta| T_3^\dagger &= \frac{2}{3}\mathbb{1}.
\end{aligned} \tag{A.38}
$$

The above relations are useful in all calculations of isospin coefficients in pion electro- and neutrinoproduction through intermediate Δ states.

Very common are products of pion fields with the isospin transition matrix vectors:

$$
\begin{aligned}
\boldsymbol{T}^\dagger \cdot \boldsymbol{\phi} &= T_-^\dagger \pi^+ - T_+^\dagger \pi^- + T_3^\dagger \pi^0 \\
\boldsymbol{T} \cdot \boldsymbol{\phi} &= T_- \pi^- - T_+ \pi^+ + T_3 \pi^0
\end{aligned} \tag{A.39}
$$

which occur in all $\pi N\Delta$ vertices. Anoter useful relations come from the product of $SU(2)$ gauge fields with the isospin transition matrix vectors:

$$
\begin{aligned}
\boldsymbol{T}^\dagger \cdot \boldsymbol{A}_\mu &= T_-^\dagger W_\mu^+ - T_+^\dagger W_\mu^- + T_3^\dagger A_\mu^3 \\
\boldsymbol{T} \cdot \boldsymbol{A}_\mu &= T_- W_\mu^- - T_+ W_\mu^+ + T_3 A_\mu^3
\end{aligned} \tag{A.40}
$$

which occur in all $W^\pm N\Delta$ and $\gamma N\Delta$ vertices.

A.2.4 Electromagnetic and weak CC isospin transitions

It is assumed, that the isovector part of the current for nucleon and resonance excitations has the usual vector-axial decomposition:

$$
\boldsymbol{\mathcal{J}}^\mu = \boldsymbol{\mathcal{V}}^\mu - \boldsymbol{\mathcal{A}}^\mu. \tag{A.41}
$$

The decomposition into isospin elements is following:

$$
\boldsymbol{\mathcal{V}}^\mu - \boldsymbol{\mathcal{A}}^\mu = (V^\mu - A^\mu)\boldsymbol{\Upsilon}. \tag{A.42}
$$

The operators Υ_i are either $\frac{\tau_i}{2}$ for nucleon-nucleon and nucleon-isospin-1/2 resonance or $-\sqrt{\frac{3}{2}}T_i^\dagger$ for the nucleon-isospin-3/2 resonance. The factor $\sqrt{\frac{3}{2}}$ is commonly chosen, so that the electromagnetic excitation of Δ resonance does not carry any isospin coefficients.

Electromagnetic and charged current excitations of isospin-1/2 baryons

In the case of isospin-1/2 baryons (nucleons and resonances) the electromagnetic transition needs a hypercharge current as in section 3.1:

$$
\mathcal{V}_Y^\mu = \mathbb{1} V_Y^\mu. \tag{A.43}
$$

The electromagnetic excitation matrix element for protons/positively charged resonances becomes:

$$
\begin{aligned}
\langle R^+/p\,|\mathcal{J}_{EM}^\mu|\,p\rangle &= \left\langle R^+/p \left| \mathcal{V}_3^\mu + \frac{1}{2}\mathcal{V}_Y^\mu \right| p \right\rangle = \left\langle R^+/p \left| V_3^\mu \frac{\tau_3}{2} + \frac{1}{2}\mathbb{1} V_Y^\mu \right| p \right\rangle = \\
&= \frac{V_3^\mu + V_Y^\mu}{2} = V_p^\mu
\end{aligned} \tag{A.44}
$$

and for nthe neutrons/neutral resonances:

$$\begin{aligned}\left\langle R^0/n\,|\mathcal{J}^\mu_{EM}|\,n\right\rangle &= \left\langle R^0/n\left|\mathcal{V}^\mu_3+\frac{1}{2}\mathcal{V}^\mu_Y\right|n\right\rangle = \left\langle R^0/n\left|V^\mu_3\frac{\tau_3}{2}+\frac{1}{2}\mathbb{1}V^\mu_Y\right|n\right\rangle = \\ &= \frac{-V^\mu_3+V^\mu_Y}{2} = V^\mu_n. \end{aligned} \tag{A.45}$$

In this manner we obtain relations between the isovector and hypercharge transitions and usual vector currents:

$$\begin{aligned} V^\mu &= V^\mu_p - V^\mu_n \\ V^\mu_Y &= V^\mu_p + V^\mu_n. \end{aligned} \tag{A.46}$$

The transition current elements with form factors for nucleons are given in Eq. (3.19) and for the isospin-1/2 resonances in Eq. (6.53).

The weak charge current matrix elements are:

$$\begin{aligned}\left\langle R^+/p\,|\mathcal{J}^\mu_{CC}|\,n\right\rangle &= \left\langle R^+/p\,|\mathcal{V}^\mu_1+i\mathcal{V}^\mu_1|\,n\right\rangle = \left\langle R^+/p\,|V^\mu\tau_+|\,n\right\rangle = \\ &= V^\mu. \end{aligned} \tag{A.47}$$

By comparison to Eq. (A.46) one finds, that both for nucleons and isospin-1/2 resonances the vector form factors satisfy $\mathcal{F}^V_i = \mathcal{F}^+_i - \mathcal{F}^0_i$. This proves the relation between nucleon weak and electromagnetic form factors, $F^V_i = F^p_i - F^n_i$.

The axial part of weak charged current can be obtained by the same means, as the vector part:

$$\begin{aligned}\left\langle R^+/p\,|\mathcal{A}^\mu_{CC}|\,n\right\rangle &= \left\langle R^+/p\,|\mathcal{A}^\mu_1+i\mathcal{A}^\mu_1|\,n\right\rangle = \left\langle R^+/p\,|A^\mu\tau_+|\,n\right\rangle = \\ &= A^\mu. \end{aligned} \tag{A.48}$$

Throughout this dissertation we keep only the pseudovector form factor of nucleons and resonances, $\mathcal{G}_A(Q^2)$.

Electromagnetic and charged current excitations of isospin-3/2 baryons

In the case of isospin-3/2 baryons (in this dissertation- the $\Delta(1232)$ isobar) the electromagnetic transition from an isospin-1/2 state is purely isovector. The electromagnetic excitation matrix element is defined as:

$$\begin{aligned}\left\langle \Delta^+\,|\mathcal{J}^\mu_{EM}|\,p\right\rangle &= -\sqrt{\frac{3}{2}}\left\langle \frac{3}{2},\frac{1}{2}|1,0;\frac{1}{2},\frac{1}{2}\right\rangle V^\mu = -V^\mu \\ \left\langle \Delta^0\,|\mathcal{J}^\mu_{EM}|\,n\right\rangle &= -\sqrt{\frac{3}{2}}\left\langle \frac{3}{2},\frac{1}{2}|1,0;\frac{1}{2},-\frac{1}{2}\right\rangle V^\mu = -V^\mu \end{aligned} \tag{A.49}$$

with the minus sign being a popular convention (Ref. [165]).

The weak charge current matrix elements for Δ^{++} and proton are:

$$\begin{aligned}\left\langle \Delta^{++}\,|\mathcal{J}^\mu_{CC}|\,p\right\rangle &= \left\langle \Delta^{++}\,|\mathcal{V}^\mu_1+i\mathcal{V}^\mu_1|\,p\right\rangle = \left\langle \Delta^{++}\left|-\sqrt{2}(-\sqrt{\frac{3}{2}})T^\dagger_+\right|p\right\rangle V^\mu \\ &= \sqrt{3}\left\langle \frac{3}{2},\frac{3}{2}|1,1;\frac{1}{2},\frac{1}{2}\right\rangle V^\mu = \sqrt{3}V^\mu \end{aligned} \tag{A.50}$$

and, analogously, for the neutron:

$$\left\langle \Delta^+ \left| \mathcal{J}^\mu_{CC} \right| n \right\rangle = \sqrt{3} \left\langle \frac{3}{2}, \frac{3}{2} | 1, 1; \frac{1}{2}, -\frac{1}{2} \right\rangle V^\mu = V^\mu. \tag{A.51}$$

From Eqs. (A.49) and (A.50) it follows, that for all isospin-3/2 baryons $\mathcal{F}_i^V = -\mathcal{F}_i^N$ and that the form factors of Δ^{++} state have to be multiplied by a factor of $\sqrt{3}$. We use a convention, where electromagnetic and weak vector form factors of the Δ resonance are the same, but we include the above relations in the form of multiplicative factor for resonant pion production in tables (3) and (4).

The axial part of weak charged current can be obtained by the same means, as the vector part, and thus:

$$\begin{aligned} \left\langle \Delta^{++} \left| \mathcal{A}^\mu_{CC} \right| p \right\rangle &= \sqrt{3} A^\mu \\ \left\langle \Delta^+ \left| \mathcal{A}^\mu_{CC} \right| n \right\rangle &= A^\mu. \end{aligned} \tag{A.52}$$

This leads to a common factor of $\sqrt{3}$ in the weak excitation vertex of Δ^{++} states.

A.3 Free fields

A.3.1 Free-pion field

Pionic fields form an isospin triplet. In the cartesian coordinates we denote these fields as $\boldsymbol{\phi} = (\phi_1, \phi_2, \phi_3)$. One defines the free-pion Lagrangian as:

$$\mathcal{L} = \frac{1}{2} \partial_\mu \boldsymbol{\phi} \cdot \partial^\mu \boldsymbol{\phi} - \frac{1}{2} m_\pi^2 \boldsymbol{\phi} \cdot \boldsymbol{\phi}. \tag{A.53}$$

We assume here the pion masses to be equal. We can re-express it using the charged pion fields π^λ defined in Eq. (A.25):

$$\mathcal{L} = \frac{1}{2} \partial_\mu \pi^0 \cdot \partial^\mu \pi^0 - \frac{1}{2} m_\pi^2 (\pi^0)^2 + \partial_\mu (\pi^+)^\dagger \cdot \partial^\mu \pi^+ - m_\pi^2 |\pi^+|^2 \partial_\mu (\pi^-)^\dagger \cdot \partial^\mu \pi^- + m_\pi^2 |\pi^-|^2 \tag{A.54}$$

The Euler-Lagrange equation for free pion field is the Klein-Gordon equation:

$$(\Box + m_\pi^2) \pi_\lambda(x) = 0. \tag{A.55}$$

The plane-wave quantized pion field is defined as:

$$\pi_\lambda(x) = \int \frac{d^3 k}{(2\pi)^3 2 E_\pi(k)} [a_{-\lambda}(k) e^{-ikx} + a^\dagger_\lambda(k) e^{ikx}] \tag{A.56}$$

with $E_\pi(k) = \sqrt{m_\pi^2 + \boldsymbol{k}^2}$. The charged pion creation/annihilation operators obey the following commutation ralations:

$$[a_\lambda(k), a^\dagger_{\lambda'}(k')] = 2 E_\pi(k) \delta_{\lambda,\lambda'} (2\pi)^3 \delta^3(\boldsymbol{k} - \boldsymbol{k'}). \tag{A.57}$$

Thus the pion field π^+ can either create the $|\pi^+\rangle$ state or annihilate the $|pi^-\rangle$ state and vice versa.

Alternatively, one can express the pionic fields in terms of the cartesian isospin basis using following relations:

$$\begin{aligned} a_{\pm}^{\dagger} &= \frac{1}{\sqrt{2}}(a_1^{\dagger} \pm i a_2^{\dagger}) \\ a_{\pm} &= \frac{1}{\sqrt{2}}(a_1 \mp i a_2) \\ a_0^{\dagger} &= a_3^{\dagger} \\ a_0 &= a_3 \end{aligned} \tag{A.58}$$

which can be useful in some computations.

A.3.2 Free Dirac fields and Dirac matrices

The free Dirac Lagrangian is:

$$\mathcal{L} = \overline{\psi}(x)(i\partial\!\!\!/ - M)\psi(x). \tag{A.59}$$

The Feynman slash operator is defined as $\partial\!\!\!/ \equiv \gamma^{\mu}\partial_{\mu}$. The convention of Dirac matrices is following:

$$\gamma^0 = \begin{pmatrix} \mathbb{1} & 0 \\ 0 & -\mathbb{1} \end{pmatrix}; \ \boldsymbol{\gamma} = \begin{pmatrix} 0 & -\boldsymbol{\sigma} \\ \boldsymbol{\sigma} & 0 \end{pmatrix} \tag{A.60}$$

with usual Pauli matrix representation:

$$\sigma_1 = \begin{pmatrix} 0 & 1 \\ 1 & 0 \end{pmatrix}; \ \sigma_2 = \begin{pmatrix} 0 & -i \\ i & 0 \end{pmatrix}; \ \sigma_3 = \begin{pmatrix} 1 & 0 \\ 0 & -1 \end{pmatrix}. \tag{A.61}$$

The Dirac matrices obey following anticommutation relation:

$$\{\gamma^{\mu}, \gamma^{\nu}\} = 2g^{\mu\nu} \tag{A.62}$$

Free Dirac field equation of motion

$$(i\partial\!\!\!/ - M)\psi(x) = 0 \tag{A.63}$$

has the general solution:

$$\psi(x) = \sum_s \int \frac{d^3p}{\sqrt{(2\pi)^3}} \frac{1}{\sqrt{2p^0}} \left[a_s(p) u_s(\boldsymbol{p}) e^{-ipx} + b_s^{\dagger}(p) v_s(\boldsymbol{p}) e^{ipx} \right]. \tag{A.64}$$

Dirac spinors are solutions to the following momentum-representation equation:

$$\begin{aligned} (ip\!\!\!/ - M)u_s(\boldsymbol{p}) &= 0 \\ (ip\!\!\!/ + M)v_s(\boldsymbol{p}) &= 0. \end{aligned} \tag{A.65}$$

In our convention:

$$\begin{aligned} u_s(\boldsymbol{p}) &\equiv \sqrt{E(p)+M} \begin{pmatrix} \chi_s \\ \frac{\boldsymbol{\sigma p}}{E(p)+M}\chi_s \end{pmatrix} \\ v_s(\boldsymbol{p}) &\equiv \sqrt{E(p)+M} \begin{pmatrix} \frac{\boldsymbol{\sigma p}}{E(p)+M}\chi_s \\ \chi_s \end{pmatrix} \end{aligned} \tag{A.66}$$

with χ_2 being a two-component spinor. They are normalized as follows:

$$\begin{aligned}\overline{u}_s(\boldsymbol{p})u_{s'}(\boldsymbol{p}) &= -\overline{v}_s(\boldsymbol{p})v_s(\boldsymbol{p}) = 2M\delta_{s,s'} \\ u_s^\dagger(\boldsymbol{p})u_{s'}(\boldsymbol{p}) &= v_s^\dagger(\boldsymbol{p})v_s(\boldsymbol{p}) = 2E(p)\delta_{s,s'}.\end{aligned} \tag{A.67}$$

They are also orthogonal to each other, *i. e.* :

$$\overline{u}_s(\boldsymbol{p})v_{s'}(\boldsymbol{p}) = \overline{v}_s(\boldsymbol{p})u_{s'}(\boldsymbol{p}) = 0. \tag{A.68}$$

This normalization convention is rather unusual, but it makes the notation more compact.

Dirac field operators anticommute according to:

$$\begin{aligned}\{a_s(p), a_{s'}^\dagger(p')\} = \{b_s(p), b_{s'}^\dagger(p')\} &= (2\pi)^3\delta^{(3)}(\boldsymbol{p}-\boldsymbol{p'})\delta_{s,s'} \\ \{a_s(p), b_{s'}^\dagger(p')\} = \{b_s(p), a_{s'}^\dagger(p')\} &= 0.\end{aligned} \tag{A.69}$$

In our convention the positive and negative energy state projection operators are projection operator is:

$$\begin{aligned}P_+ &= \tfrac{1}{\sqrt{2m}}\textstyle\sum_s u_s(\boldsymbol{p})\overline{u}_s(\boldsymbol{p}) = \frac{1}{\sqrt{2m}}(\not{p}+m) \\ P_- &= \tfrac{1}{\sqrt{2m}}\textstyle\sum_s v_s(\boldsymbol{p})\overline{v}_s(\boldsymbol{p}) = \frac{1}{\sqrt{2m}}(\not{p}-m)\end{aligned} \tag{A.70}$$

with usual 4-vector short notation $\not{p} \equiv \gamma^\mu p_\mu$.

There are additional matrices in the Dirac algebra. We define:

$$\gamma^5 \equiv i\gamma^0\gamma^1\gamma^2\gamma^3. \tag{A.71}$$

It has following properties:

$$\begin{aligned}(\gamma^5)^\dagger &= \gamma^5 \\ (\gamma^5)^2 &= \gamma^5 \\ \{\gamma^5, \gamma^\mu\} &= 0\end{aligned} \tag{A.72}$$

and in our basis it is antidiagonal:

$$\gamma^5 = \begin{pmatrix} 0 & \mathbb{1} \\ \mathbb{1} & 0 \end{pmatrix}. \tag{A.73}$$

The full four-dimensional Dirac algebra can be represented by following matrices corresponding to different types of objects:

$$\begin{aligned}\mathbb{1} &\quad \text{scalar} \\ \gamma^5 &\quad \text{pseudo}-\text{scalar} \\ \gamma^\mu &\quad \text{vector} \\ \gamma^5\gamma^\mu &\quad \text{pseudo}-\text{vector} \\ \sigma^{\mu\nu} = \frac{i}{2}[\gamma^\mu, \gamma^\nu] &\quad \text{tensor.}\end{aligned} \tag{A.74}$$

In total, there are 16 independent elements.

A.4 Free Rarita-Schwinger fields

The sin-3/2 fields are solutions to the Rarita-Schwinger equation:

$$(i\partial\!\!\!/ - M)\psi_\mu(x) = 0. \tag{A.75}$$

Additional constraints are needed in order to eliminate unphysical sin-3/2→spin-1/2 spontaneous transitions (*i. e.* direct spin-1/2 to spin-3/2 coupling terms):

$$\begin{aligned} \gamma^\mu \psi_\mu(x) &= 0 \\ \partial^\mu \psi_\mu(x) &= 0. \end{aligned} \tag{A.76}$$

The additional two equations remove the spin-1/2 degree of freedom from Rarita-Schwinger field. We focus here on the positive-energy solutions, which satisfy following momentum-representation set of equations:

$$\begin{aligned} (p\!\!\!/ - M)u_\mu(p,s) &= 0 \\ \gamma^\mu u_\mu(p,s) &= 0 \\ p^\mu u_\mu(p,s) &= 0. \end{aligned} \tag{A.77}$$

The spinors $u_\mu(p,s)$ can be constructed by combining Dirac spinors $u_s(\boldsymbol{p})$ with spin-1 vectors $e^\mu(p)$. We have defined $u_s(\boldsymbol{p})$ in Eq. (A.66). The spin-1 vector corresponding to a given polarization in particle rest frame is defined as:

$$e^\mu_\lambda(0) \equiv (0, \boldsymbol{e}_\lambda). \tag{A.78}$$

The polariztion eigenstates of vectors are defined in the seme way, as the e^*_λ for the isospin in Eq. (A.34). One can boost the vector to any frame by using the boost tensor from Eq. (6.110) with $W = M$. The result is:

$$e^\mu_\lambda(p) \equiv \left(\frac{\boldsymbol{e_\lambda} \cdot \boldsymbol{p}}{M}, \boldsymbol{e}_\lambda + \boldsymbol{p}\frac{\boldsymbol{e_\lambda} \cdot \boldsymbol{p}}{M(p^0 + M)} \right). \tag{A.79}$$

now one can construct the Rarita-Schwinger spinor by combining the Dirac and vector fields:

$$u^\mu(p, s_\Delta) = \sum_{\lambda,s} \left\langle 1, \lambda; \frac{1}{2}, s | \frac{3}{2}, s_\Delta \right\rangle e^\mu_\lambda(p) u_s(\boldsymbol{p}). \tag{A.80}$$

Sum of RS spinors gives $2M\times$ the positive energy spin-3/2 projection operator:

$$\sum_s \psi_\alpha(p,s)\overline{\psi}_\beta(p,s) = P^{3/2}_{\alpha\beta}(p) = -(p\!\!\!/ + M)(g_{\alpha\beta} - \frac{1}{3}\gamma_\alpha\gamma_\beta - \frac{2}{3}\frac{p_\alpha p_\beta}{M^2} + \frac{p_\alpha\gamma_\beta - p_\beta\gamma_\alpha}{M^2}) \tag{A.81}$$

The above formula holds strictly only for on-shell Rarita-Schwinger fields. If one wants to use the expression consistent with Ref. [127] one has to substitute $M_R \to W$ everywhere in Eq. (A.81).

B Neutrino-nucleus cross section derivation

We would like to discuss briefly scattering of a neutrino $|\nu(\boldsymbol{l},-)\rangle$ with four-momentum l and negative chirality (and helicity, since here we approximate the neutrinos to be massless) off an atomic nucleus $|i\rangle$ with four-momentum P_i producing a charged lepton $\langle l_-(\boldsymbol{l'},s')|$ with four-momentum momentum l' and spin s' and final nuclear system $\langle P_f|$ with total four-momentum P_f. The most general differential cross section is:

$$d\sigma = (2\pi)^4 u_{\nu,i}^{-1}|M_{\alpha\beta}^2|\delta^{(4)}(l+P_i-l'+P_f)\frac{d^3l'}{(2\pi)^3}\frac{d^3P_f}{(2\pi)^3}. \tag{B.1}$$

In the above formula $M_{\alpha\beta}$ denotes the transition matrix element between initial $|\nu(\boldsymbol{l},s),i\rangle$ and final $\langle l_-(\boldsymbol{l'},s'),f|$ states and $u_{\nu,i}$ is the flux parameter (relative velocity) of incoming neutrino:

$$u_{\nu,i} = \frac{\sqrt{(l\cdot P_i)^2}}{E_\nu E_i} \tag{B.2}$$

with initial nucleus energy E_i. We define tha scattering matrix element as:

$$S_{\alpha\beta} = \langle\alpha|\beta\rangle = \langle l_-(\boldsymbol{l'},s'),f|\nu(\boldsymbol{l},s),i\rangle = -2\pi i\delta^{(4)}(l+P_i-l'-P_f)M_{\alpha\beta}. \tag{B.3}$$

Within one-boson and Fermi approximations the above matrix element is reduced to current-current interaction:

$$\begin{aligned} S_{\alpha\beta} &= -2\pi i\frac{G_F\cos(\Theta_c)}{\sqrt{2}}\delta^{(4)}(l+P_i-l'-P_f)\frac{1}{\sqrt{2E_\nu}}\frac{1}{\sqrt{2E_{l'}}}\bar{l}_-(\boldsymbol{l'},s')\gamma_\mu(1-\gamma^5)\nu(\boldsymbol{l},-)\times \\ &\times \left\langle f\left|\int d^3x e^{i\boldsymbol{qx}}\mathcal{J}^\mu(\boldsymbol{x})\right|i\right\rangle \end{aligned} \tag{B.4}$$

where we have introduced a general transition current operator $\mathcal{J}^\mu(\boldsymbol{x})$ between initial and final nuclear system states. It can, in general, contain multinucleon currents, create new particles in the final state etc. In our definition we take out the common Cabibbo angle factor out of weak currents connected to $W^\pm$ interaction vertex. The desired transition matrix element reads:

$$\begin{aligned} M_{\alpha\beta} &= \frac{G_F\cos(\Theta_c)}{\sqrt{2}}\frac{1}{\sqrt{2E_\nu}}\frac{1}{\sqrt{2E_{l'}}}\bar{l}_-(\boldsymbol{l'},s')\gamma_\mu(1-\gamma^5)\nu(\boldsymbol{l},-)\times \\ &\times \left\langle f\left|\int d^3x e^{i\boldsymbol{qx}}\mathcal{J}^\mu(\boldsymbol{x})\right|i\right\rangle. \end{aligned} \tag{B.5}$$

We want to calculate unpolarized cross sections for lepton scattering with no distict initial hadronic configuration, thus:

$$\begin{aligned} d^3\sigma &= \frac{G_F^2\cos^2(\Theta_C)}{4\pi^2}\frac{d^3l'}{8E_\nu E_l'}\sum_{s'}\overline{\sum_i}\sum_f\delta(E_\nu+P_i-E_{l'}-P_f)\frac{E_\nu E_i}{\sqrt{(l\cdot P_i)^2}}\times \\ &\times (\bar{l}_-(\boldsymbol{l'},s')\gamma_\mu(1-\gamma^5)\nu(\boldsymbol{l},-))(\bar{l}_-(\boldsymbol{l'},s')\gamma_\nu(1-\gamma^5)\nu(\boldsymbol{l},-))^*\times \\ &\times \left\langle f\left|\int d^3x e^{i\boldsymbol{qx}}\mathcal{J}^\mu(\boldsymbol{x})\right|i\right\rangle\left\langle f\left|\int d^3x e^{i\boldsymbol{qx}}\mathcal{J}^\nu(\boldsymbol{x})\right|i\right\rangle^* \\ &= \frac{G_F^2\cos^2(\Theta_C)}{4\pi^2}L_{\mu\nu}W^{\mu\nu}\frac{d^3l'}{\sqrt{(l'\cdot P_i)^2}E_l'} \end{aligned}$$

where we have introduced the leptonic tensor:

$$L_{\mu\nu} \equiv \frac{1}{8}\mathrm{Tr}[(\not{l}' + m_x)\gamma_\mu(1 \mp \gamma^5)(\not{l} + m_{\nu_x})\gamma_n u(1 \mp \gamma^5)] \approx \tag{B.6}$$

$$\approx l_\mu l'_\nu + l'_\mu l_\nu - g_{\mu\nu} l l' \pm i\epsilon_{\mu\nu\alpha\beta} l'^\alpha l^\beta \tag{B.7}$$

with approximation for massless neutrinos, and nuclear tensor:

$$W^{\mu\nu} \equiv \overline{\sum_i}\sum_f \delta(E_i + q^0 - E_f)\left\langle f \left| \int d^3x e^{i\boldsymbol{qx}} \hat{J}^\mu(\boldsymbol{x}) \right| i \right\rangle \left(\left\langle f \left| \int d^3y e^{i\boldsymbol{qy}} \hat{J}^\nu(\boldsymbol{y}) \right| i \right\rangle \right)^* E_i. \tag{B.8}$$

With these definitions a straightforward manipulation yields:

$$\frac{d\sigma}{dE_{l'} d\Omega'} = \frac{G_F^2 \cos^2(\Theta_C)}{4\pi^2} \frac{|\boldsymbol{l'}|}{\sqrt{(l \cdot P_i)^2}} L_{\mu\nu} W^{\mu\nu}.$$

The same formula can be obtained for electrons, by substituting weak CC interaction factors with appropriate electromagnetic counterparts and averaging over initial electron spins.

C Nucleon propagator in the Fermi gas model

We would like to calculate the nucleon propagator in the Fermi gas model:

$$
\begin{aligned}
iG^{(0)RFG}_{\alpha\beta}(x'-x) &= \left\langle 0 \left| T\left\{\psi_\alpha(x')\bar{\psi}_\beta(x)\right\}\right| 0\right\rangle = \\
&= \left\langle 0 \left|\psi_\alpha(x')\bar{\psi}_\beta(x)\right| 0\right\rangle\theta(t'-t) - \left\langle 0 \left|\bar{\psi}_\beta(x)\psi_\alpha(x')\right| 0\right\rangle\theta(t-t') = \\
&= \frac{1}{\Omega}\sum_{\substack{\boldsymbol{k}\boldsymbol{k'}\\ ss'}} \frac{1}{2\sqrt{E(\boldsymbol{k})E(\boldsymbol{k'})}}\Big\{\langle 0\|\Big[a_{\boldsymbol{k}s}u_{s\alpha}(\boldsymbol{k})e^{-ikx'} + b^\dagger_{\boldsymbol{k},s}v_{s\alpha}(\boldsymbol{k})e^{ikx'}\Big] \\
&\quad \Big[a^\dagger_{\boldsymbol{k'}s'}\overline{u}_{s'\beta}(\boldsymbol{k'})e^{ik'x} + b_{\boldsymbol{k'},s'}\overline{v}_{s'\beta}(\boldsymbol{k'})e^{-ik'x}\Big]\|0\rangle\,\theta(t'-t) + \\
&\quad - \langle 0\|\Big[a^\dagger_{\boldsymbol{k'}s'}\overline{u}_{s'\beta}(\boldsymbol{k'})e^{ik'x} + b_{\boldsymbol{k'},s'}\overline{v}_{s'\beta}(\boldsymbol{k'})e^{-ik'x}\Big] \\
&\quad \Big[a_{\boldsymbol{k}s}u_{s\alpha}(\boldsymbol{k})e^{-ikx'} + b^\dagger_{\boldsymbol{k},s}v_{s\alpha}(\boldsymbol{k})e^{ikx'}\Big]\|0\rangle\,\theta(t-t')\Big\}. \qquad \text{(C.1)}
\end{aligned}
$$

Now we will make a remark about possible generalization of the model. An assumption can be made about the contractions of the creation and annihilation operators in the nuclear ground state:

$$
\begin{aligned}
\left\langle 0 \left| a^\dagger_{\boldsymbol{k},s}a_{\boldsymbol{k'}s'}\right| 0\right\rangle &= \langle 0\left|\hat{n}_{\boldsymbol{k},s}\right| 0\rangle\,\delta_{\boldsymbol{k}\boldsymbol{k'}}\delta_{ss'} = n(\boldsymbol{k},s)\delta_{\boldsymbol{k}\boldsymbol{k'}}\delta_{ss'} \\
\left\langle 0 \left| a_{\boldsymbol{k},s}a^\dagger_{\boldsymbol{k'}s'}\right| 0\right\rangle &= \left\langle 0 \left|\left\{a^\dagger_{\boldsymbol{k},s}, a_{\boldsymbol{k'}s'}\right\} - a^\dagger_{\boldsymbol{k},s}a_{\boldsymbol{k'}s'}\right| 0\right\rangle = \delta_{\boldsymbol{k}\boldsymbol{k'}}\delta_{ss'}(1-n(\boldsymbol{k},s)). \qquad \text{(C.2)}
\end{aligned}
$$

The notation allows for a possible non uniform density. The quantity $n(\boldsymbol{k},s)$ is the occupation number and for the Fermi Gas is equal to $\Theta(k_F - |\boldsymbol{k}|)$. This generalization is useful for the local Fermi gas models. Occupation number is used as a weight for integrations over the nucleon momenta. However in what follows we always assume the density to be simply $\Theta(k_f - |\boldsymbol{k}|)$.

$$
\begin{aligned}
iG^{(0)RFG}_{\alpha\beta}(x'-x) &= \frac{1}{\Omega}\sum_{\boldsymbol{k}s}\frac{1}{2E(\boldsymbol{k})}\Big\{u_{s\alpha}(\boldsymbol{k})\overline{u}_{s\beta}(\boldsymbol{k})(1-\Theta(k_F-|\boldsymbol{k}|))e^{ik(x-x')}\Theta(t'-t)+ \\
&\quad -u_{s\alpha}(\boldsymbol{k})\overline{u}_{s\beta}(\boldsymbol{k})\Theta(k_F-|\boldsymbol{k}|)e^{ik(x-x')}\Theta(t-t') + \\
&\quad - v_{s\alpha}(\boldsymbol{k})\overline{v}_{s\beta}(\boldsymbol{k})e^{-ik(x-x')}\Theta(t-t')\Big\}. \qquad \text{(C.3)}
\end{aligned}
$$

Existence of the Fermi sea of nucleons affects only the particle part of the Green function, which is what one would expect. Again, we use Θ function integral representation:

$$
\Theta(x) = \int\frac{dk^0}{2\pi i}\frac{e^{ik^0x}}{k^0-i\varepsilon} = -\int\frac{dk^0}{2\pi i}\frac{e^{-ik^0x}}{k^0+i\varepsilon} = \Theta(x)^*. \qquad \text{(C.4)}
$$

These identities allow us to show the pole structure of the propagator:

$$
\begin{aligned}
iG^{(0)RFG}_{\alpha\beta}(x'-x) &= \frac{i}{\Omega}\sum_{\boldsymbol{k}s}\frac{1}{2E(\boldsymbol{k})}u_{s\alpha}(\boldsymbol{k})\overline{u}_{s\beta}(\boldsymbol{k})\Theta(|\boldsymbol{k}|-k_F)e^{-ik(x'-x)}\int\frac{dk^0}{(2\pi)}\frac{e^{-ik^0(t'-t)}}{k^0+i\varepsilon}+ \\
&+ \frac{i}{\Omega}\sum_{\boldsymbol{k}s}\frac{1}{2E(\boldsymbol{k})}u_{s\alpha}(\boldsymbol{k})\overline{u}_{s\beta}(\boldsymbol{k})\Theta(k_F-|\boldsymbol{k}|)e^{-ik(x'-x)}\int\frac{dk^0}{(2\pi)}\frac{e^{-ik^0(t'-t)}}{k^0-i\varepsilon}+ \\
&+ \frac{i}{\Omega}\sum_{\boldsymbol{k}s}\frac{1}{2E(\boldsymbol{k})}v_{s\alpha}(\boldsymbol{k}.)\overline{v}_{s\beta}(\boldsymbol{k})e^{-ik(x-x')}\int\frac{dk^0}{(2\pi)}\frac{e^{-ik^0(t'-t)}}{k^0-i\varepsilon}. \qquad \text{(C.5)}
\end{aligned}
$$

For simplicity we split the propagator in particle and antiparticle part and switch to the infinite space:

$$
\begin{aligned}
iG^{(0)\,RFG}_{\alpha\beta\,\text{part.}}(x'-x) &= i\sum_s \int \frac{d^3k}{(2\pi)^3}\frac{1}{2E(\boldsymbol{k})}\int\frac{dk^0}{(2\pi)} \\
& \quad u_{s\alpha}(\boldsymbol{k})\overline{u}_{s\beta}(\boldsymbol{k})\Theta(|\boldsymbol{k}|-k_F)e^{-ik(x'-x)}\frac{e^{-ik^0(t'-t)}}{k^0+i\varepsilon}+ \\
&+ i\sum_s \int \frac{d^3k}{(2\pi)^3}\frac{1}{2E(\boldsymbol{k})}\int\frac{dk^0}{(2\pi)} \\
& \quad u_{s\alpha}(\boldsymbol{k})\overline{u}_{s\beta}(\boldsymbol{k})\Theta(k_F-|\boldsymbol{k}|)e^{-ik(x'-x)}\frac{e^{-ik^0(t'-t)}}{k^0-i\varepsilon}
\end{aligned}
\tag{C.6}
$$

We change variable $k^0 \to \tilde{k^0} = E(\boldsymbol{k}) + k^0$ and obtain:

$$
\begin{aligned}
G^{(0)\,RFG}_{\alpha\beta\,\text{part.}}(x'-x) &= \int\frac{d^3k d\tilde{k^0}}{(2\pi)^4}\frac{1}{2E(\boldsymbol{k})}e^{i\tilde{k^0}(t-t')}e^{-i\boldsymbol{k}(\boldsymbol{x}-\boldsymbol{x'})}\frac{(\not{K}+M)_{\alpha\beta}}{2E(\boldsymbol{k})} \\
& \quad \left(\frac{1-\Theta(k_F-|\boldsymbol{k}|)}{\tilde{k^0}-E(\boldsymbol{k})+i\varepsilon}+\frac{\Theta(k_F-|\boldsymbol{k}|)}{\tilde{k^0}-E(\boldsymbol{k})-i\varepsilon}\right)= \\
&= \int\frac{d^4k}{(2\pi)^4}e^{ik(x-x')}\frac{(\not{K}+M)_{\alpha\beta}}{2E(\boldsymbol{k})} \\
& \quad \left(\frac{1-\Theta(k_F-|\boldsymbol{k}|)}{k_0-E(\boldsymbol{k})+i\varepsilon}+\frac{\Theta(k_F-|\boldsymbol{k}|)}{k_0-E(\boldsymbol{k})-i\varepsilon}\right),
\end{aligned}
\tag{C.7}
$$

where:

$$
\not{K} \equiv \gamma^0 E(\boldsymbol{k}) - \boldsymbol{\gamma}\cdot\boldsymbol{k}. \tag{C.8}
$$

We stress that k^0 is present only in the exponential and in the denominators.

The similar steps are repeated in order to obtain the antiparticle part of the propagator:

$$
\begin{aligned}
G^{(0)\,RFG}_{\alpha\beta\,\text{a-part.}}(x'-x) &= \sum_s \int\frac{d^3k}{(2\pi)^3}\int\frac{dk^0}{(2\pi)}\frac{v_{s\alpha}(\boldsymbol{k})\overline{v}_{s\beta}(\boldsymbol{k})}{2E(\boldsymbol{k})}\frac{e^{-ik(x-x')}e^{-ik^0(t'-t)}}{k^0-i\varepsilon}= \\
&= \sum_s \int\frac{d^3k}{(2\pi)^3}\int\frac{dk^0}{(2\pi)}\frac{v_{s\alpha}(\boldsymbol{k})\overline{v}_{s\beta}(\boldsymbol{k})}{2E(\boldsymbol{k})}\frac{e^{i\boldsymbol{k}(\boldsymbol{x}-\boldsymbol{x'})}e^{i(k^0-E(\boldsymbol{k}))(t-t')}}{k^0-i\varepsilon}= \\
&= \sum_s \int\frac{d^3k}{(2\pi)^3}\int\frac{dk^0}{(2\pi)}\frac{v_{s\alpha}(-\boldsymbol{k})\overline{v}_{s\beta}(-\boldsymbol{k})}{2E(\boldsymbol{k})}\frac{e^{-i\boldsymbol{k}(\boldsymbol{x}-\boldsymbol{x'})}e^{i(k^0-E(\boldsymbol{k}))(t-t')}}{k^0-i\varepsilon}= \\
&= \sum_s \int\frac{d^3k}{(2\pi)^3}\int\frac{d\tilde{k}^0}{(2\pi)}\frac{v_{s\alpha}(-\boldsymbol{k})\overline{v}_{s\beta}(-\boldsymbol{k})}{2E(\boldsymbol{k})}\frac{e^{-i\boldsymbol{k}(\boldsymbol{x}-\boldsymbol{x'})}e^{i\tilde{k}^0(t-t')}}{\tilde{k}^0+E(\boldsymbol{k})-i\varepsilon}= \\
&= -\int\frac{d^4k}{(2\pi)^4}e^{ik(x-x')}\frac{(\tilde{\not{K}}+M)_{\alpha\beta}}{2E(\boldsymbol{k})}\frac{1}{k_0+E(\boldsymbol{k})-i\varepsilon}
\end{aligned}
\tag{C.9}
$$

where

$$\tilde{\not{K}} \equiv -\gamma^0 E(\boldsymbol{k}) - \boldsymbol{\gamma} \cdot \boldsymbol{k}.$$

The full Feynman propagator for RFG model can be written as:

$$G^{(0)RFG}_{\alpha\beta}(p) = \frac{1}{2E(\boldsymbol{p})} \left\{ (\not{P} + M)_{\alpha\beta} \left[\frac{(1 - \Theta(k_F - |\boldsymbol{p}|))}{p_0 - E(\boldsymbol{p}) + i\varepsilon} + \frac{\Theta(k_F - |\boldsymbol{p}|)}{p_0 - E(\boldsymbol{p}) - i\varepsilon} \right] + \right.$$
$$\left. - \left(\tilde{\not{P}} + M \right)_{\alpha\beta} \frac{1}{p_0 + E(\boldsymbol{p}) - i\varepsilon} \right\}. \quad \text{(C.10)}$$

In some applications it is useful to use the expression for the propagator with explicit summations over spin variables:

$$G^{(0)RFG}_{\alpha\beta}(p) = \frac{1}{2E(\boldsymbol{p})} \left\{ \sum_{s'} u_{s'\alpha}(\boldsymbol{p}) \overline{u}_{s'\beta}(\boldsymbol{p}) \left[\frac{(1 - \Theta(k_F - |\boldsymbol{p}|))}{p_0 - E(\boldsymbol{p}) + i\varepsilon} + \frac{\Theta(k_F - |\boldsymbol{p}|)}{p_0 - E(\boldsymbol{p}) - i\varepsilon} \right] + \right.$$
$$\left. + \frac{1}{p_0 + E(\boldsymbol{p}) - i\varepsilon} \sum_{s'} v_{s'\alpha}(-\boldsymbol{p}) \overline{v}_{s'\beta}(-\boldsymbol{p}) \right\}. \text{(C.11)}$$

D Electron QE cross section from the direct contraction of leptonic and hadronic tensors

In this paragraph we shall show, how one can obtain the same electron RFG cross sections as for the Rosenbluth separation (4.24) by directly contracting the leptonic and RFG electron polarization (4.83) tensors. It's a good exercise to show the extent equivalence of both descriptions in electron scattering with De Forest prescription for binding energy. The general double-differential cross section formula reads:

$$\frac{d\sigma}{d\Omega dE'} = \frac{2\alpha^2 E'}{q_\alpha^4 E}\left(\frac{-1}{\pi}\Im L_{\mu\nu}\Pi^{\mu\nu}\right). \tag{D.1}$$

The only required quantity is the contraction $L_{\mu\nu}\Pi^{\mu\nu}$. For simplicity it is assumed, that there is no binding energy and the gauge invariance is conserved. The parts of hadronic tensor $A^{\mu\nu}$ proportional to q^μ simply drop out. Thus one has to introduce De Forest binding after contracting both tensors in order to have equivalent expression to Rosenbluth procedure.

$$L_{\mu\nu}A^{\mu\nu} = (l_\mu l'_\nu + l_\nu l'_\mu - g_{\mu\nu}(l\cdot l' - m^2))\left(2p^\mu p^\nu\left(F_1^2 - \frac{q_\alpha^2}{4M^2}F_2^2\right) + \frac{1}{2}q_\alpha^2 g^{\mu\nu}(F_1+F_2)^2\right). \tag{D.2}$$

the above formula can be further simplified using $l\cdot l' = l^2 - l\cdot q$ and $l\cdot q = \frac{q_\mu^2}{2}$

$$\begin{aligned} L_{\mu\nu}A^{\mu\nu} &= (2l_\mu l_\nu - l_\nu q_\alpha - l_\mu q_\nu + g_{\mu\nu}\frac{q_\alpha^2}{2})(2p^\mu p^\nu\left(F_1^2 - \frac{q_\alpha^2}{4M^2}F_2^2\right) + \frac{q_\alpha^2}{2}g^{\mu\nu}(F_1+F_2)^2) \\ &= (4(p\cdot l)^2 - 4p\cdot l p\cdot q + p^2 q_\alpha^2)\left(F_1^2 - \frac{q_\alpha^2}{4M^2}F_2^2\right) + \frac{q_\alpha^2}{2}(2l^2 - 2l\cdot q + 2q_\alpha^2)(F_1+F_2)^2 \\ &= \left[4(p\cdot l)^2 + 2q_\alpha^2(p\cdot l) + M^2 q_\alpha^2\right]\left(F_1^2 - \frac{q_\alpha^2}{4M^2}F_2^2\right) + \frac{1}{2}q_\alpha^4(F_1+F_2)^2. \end{aligned} \tag{D.3}$$

The only "troublesome" part is the contraction $p\cdot l$.

$$p\cdot l = E(p)E - \boldsymbol{pl}. \tag{D.4}$$

In the spherical coordinates:

$$\begin{aligned} \boldsymbol{p} &= p(\sin\Theta_p\sin\phi_p, \sin\Theta_p\cos\phi_p, \cos\Theta_p) \\ \boldsymbol{l} &= l(\sin\Theta_l\sin\phi_l, \sin\Theta_l\cos\phi_l, \cos\Theta_l). \end{aligned} \tag{D.5}$$

The laboratory coordinates and angle ϕ_l can be chosen arbitrarily, let's assume it's 0. The angle Θ_l is defined by the relation:

$$l'^2 = (l-q)^2 = l^2 - 2Eq^0 + 2lq\cos\Theta_l + q_\alpha^2 \to \cos\Theta_l = \frac{2Eq^0 - q_\alpha^2}{2lq} \approx \frac{2Eq^0 - q_\alpha^2}{2Eq}. \tag{D.6}$$

And $\cos\Theta_p = \mu_0$. Thus:

$$
\begin{aligned}
p\cdot l &= E\cdot p(\sin\Theta_l\sin\Theta_p\cos\phi_p + \cos\Theta_l\cos\Theta_p) = \\
&= E(p)E - E(p)E\frac{q^0}{|\boldsymbol{q}|}\cos\Theta_l - \frac{q_\alpha^2}{2|\boldsymbol{q}|}E\cos\Theta_l - pE\sin\Theta_p\sin\Theta_l\cos\phi_p = \\
&= EE(p)(1-\frac{q^0}{|\boldsymbol{q}|}\cos\Theta_l) - \frac{q_\alpha^2}{2q}E\cos\Theta_l - pE\sin\Theta_p\sin\Theta_l\cos\phi_p \\
(p\cdot l)^2 &= E^2E(p)^2(1-\frac{q^0}{q}\cos\Theta_l)^2 + \frac{q_\alpha^4}{4\boldsymbol{q}^2}E^2\cos^2\Theta_l + p^2E^2\sin^2\Theta_p\sin^2\Theta_l\cos^2\phi_p + \\
&- E^2E(p)\frac{q_\alpha^2}{|\boldsymbol{q}|}\cos\Theta_l(1-\frac{q^0}{|\boldsymbol{q}|}\cos\Theta_l) + (\ldots)\cos\phi_p = \\
&= E^2E(p)^2(1-\frac{q^0}{|\boldsymbol{q}|}\cos\Theta_l)^2 + \frac{q_\alpha^4}{4\boldsymbol{q}^2}E^2\cos^2\Theta_l + E^2E(p)^2\sin^2\Theta_l\cos^2\phi_p + \\
&- M^2E^2\sin^2\Theta_l\cos^2\phi_p - E^2\frac{(2q^0E(p)+q_\mu^2)^2}{4\boldsymbol{q}^2}\sin^2\Theta_l\cos^2\phi_p + \\
&- E^2E(p)\frac{q_\alpha^2}{|\boldsymbol{q}|}\cos\Theta_l(1-\frac{q^0}{|\boldsymbol{q}|}\cos\Theta_l) + (\ldots)\cos\phi_p = \\
&= E^2E(p)^2\left((1-\frac{q^0}{|\boldsymbol{q}|}\cos\Theta_l)^2 - \frac{q_\alpha^2}{\boldsymbol{q}^2}\sin^2\Theta_l\cos^2\phi_p\right) + \\
&- E(p)\frac{q_\alpha^2E^2}{|\boldsymbol{q}|}\left(\cos\Theta_l(1-\frac{q^0}{|\boldsymbol{q}|}\cos\Theta_l) + \frac{q^0}{|\boldsymbol{q}|}\sin^2\Theta_l\cos^2\phi_p\right) + \\
&+ \left(\frac{q_\alpha^4}{4\boldsymbol{q}^2}E^2(\cos^2\Theta_l - \sin^2\Theta_l\cos^2\phi_p) - M^2E^2\sin^2\Theta_l\cos^2\phi_p\right) + (\ldots)\cos\phi_p. \qquad \text{(D.7)}
\end{aligned}
$$

Here we neglect everything $\propto \cos\phi_p$, because it will drop out in the integration.

$$
\begin{aligned}
L_{\mu\nu}A^{\mu\nu} = &= \Bigg[4E^2E(p)^2\left((1-\frac{q^0}{|\boldsymbol{q}|}\cos\Theta_l)^2 - \frac{q_\alpha^2}{\boldsymbol{q}^2}\sin^2\Theta_l\cos^2\phi_p\right) + \\
&- 4E(p)\frac{q_\alpha^2E^2}{|\boldsymbol{q}|}\left(\cos\Theta_l(1-\frac{q^0}{|\boldsymbol{q}|}\cos\Theta_l) + \frac{q^0}{|\boldsymbol{q}|}\sin^2\Theta_l\cos^2\phi_p\right) + \\
&+ \left(\frac{q_\alpha^4}{\boldsymbol{q}^2}E^2(\cos^2\Theta_l - \sin^2\Theta_l\cos^2\phi_p) - 4M^2E^2\sin^2\Theta_l\cos^2\phi_p\right) + \\
&+ 2q_\alpha^2EE(p)(1-\frac{q^0}{|\boldsymbol{q}|}\cos\Theta_l) - \frac{q_\alpha^4}{|\boldsymbol{q}|}E\cos\Theta_l + M^2q_\alpha^2 + (\ldots)\cos\phi_p\Bigg] \\
&\left(F_1^2 - \frac{q_\alpha^2}{4M^2}F_2^2\right) + \frac{1}{2}q_\alpha^4(F_1+F_2)^2. \qquad \text{(D.8)}
\end{aligned}
$$

In the cross section one shall have:

$$
\begin{aligned}
\frac{-1}{\pi}\Im L_{\mu\nu}\Pi^{\mu\nu} &= \frac{\Omega}{4\pi^2|\boldsymbol{q}|}\int_0^{2\pi}\frac{d\phi}{2\pi}\int_{E_{min}}^{E_F} dE(p)L_{\mu\nu}A^{\mu\nu} = \\
&= \frac{\Omega}{4\pi^2|\boldsymbol{q}|}\left\{\left[\frac{4}{3}E^2E(p)^3\left((1-\frac{q^0}{|\boldsymbol{q}|}\cos\Theta_l)^2-\frac{q_\alpha^2}{2\boldsymbol{q}^2}\sin^2\Theta_l\right)+\right.\right. \\
&- 2E(p)^2\frac{q_\alpha^2E^2}{|\boldsymbol{q}|}\left(\cos\Theta_l(1-\frac{q^0}{|\boldsymbol{q}|}\cos\Theta_l)+\frac{q^0}{2|\boldsymbol{q}|}\sin^2\Theta_l\right)+ \\
&+ E(p)\left(\frac{q_\alpha^4}{\boldsymbol{q}^2}E^2(\cos^2\Theta_l-\frac{1}{2}\sin^2\Theta_l)-2M^2E^2\sin^2\Theta_l-\frac{q_\alpha^4}{|\boldsymbol{q}|}E\cos\Theta_l+M^2q_\alpha^2\right)+ \\
&+ \left.\left.q_\alpha^2EE(p)^2(1-\frac{q^0}{|\boldsymbol{q}|}\cos\Theta_l)\right]\left(F_1^2-\frac{q_\alpha^2}{4M^2}F_2^2\right)+\frac{1}{2}q_\alpha^4(F_1+F_2)^2E(p)\right\}_{E_{min}}^{E_F}. \quad \text{(D.9)}
\end{aligned}
$$

This cross section is independent on the momentum transfer direction. The global FG case (per nucleon):

$$
\begin{aligned}
\frac{d\sigma}{d\Omega dE'} &= \frac{3\alpha^2E'}{2q_\alpha^4E}\frac{1}{k_F^3|\boldsymbol{q}|}\left\{\left[\frac{4}{3}E^2E(p)^3\left((1-\frac{q^0}{|\boldsymbol{q}|}\cos\Theta_l)^2-\frac{q_\alpha^2}{2\boldsymbol{q}^2}\sin^2\Theta_l\right)+\right.\right. \\
&- 2E(p)^2\frac{q_\alpha^2E^2}{|\boldsymbol{q}|}\left(\cos\Theta_l(1-\frac{q^0}{|\boldsymbol{q}|}\cos\Theta_l)+\frac{q^0}{2|\boldsymbol{q}|}\sin^2\Theta_l\right)+ \\
&+ E(p)\left(\frac{q_\alpha^4}{\boldsymbol{q}^2}E^2(\cos^2\Theta_l-\frac{1}{2}\sin^2\Theta_l)-2M^2E^2\sin^2\Theta_l-\frac{q_\alpha^4}{|\boldsymbol{q}|}E\cos\Theta_l+M^2q_\alpha^2\right)+ \\
&+ \left.\left.q_\alpha^2EE(p)^2(1-\frac{q^0}{|\boldsymbol{q}|}\cos\Theta_l)\right]\left(F_1^2-\frac{q_\alpha^2}{4M^2}F_2^2\right)+\frac{1}{2}q_\alpha^4(F_1+F_2)^2E(p)\right\}_{E_{min}}^{E_F}. \quad \text{(D.10)}
\end{aligned}
$$

The case of the LFG (per all protons/neutrons):

$$
\begin{aligned}
\frac{d\sigma}{d\Omega dE'} &= \frac{2\alpha^2E'}{q_\alpha^4E}\frac{1}{\pi|\boldsymbol{q}|}\int r^2dr\left\{\left[\frac{4}{3}E^2E(p)^3\left((1-\frac{q^0}{|\boldsymbol{q}|}\cos\Theta_l)^2-\frac{q_\alpha^2}{2\boldsymbol{q}^2}\sin^2\Theta_l\right)+\right.\right. \\
&- 2E(p)^2\frac{q_\alpha^2E^2}{|\boldsymbol{q}|}\left(\cos\Theta_l(1-\frac{q^0}{|\boldsymbol{q}|}\cos\Theta_l)+\frac{q^0}{2|\boldsymbol{q}|}\sin^2\Theta_l\right)+ \\
&+ E(p)\left(\frac{q_\alpha^4}{\boldsymbol{q}^2}E^2(\cos^2\Theta_l-\frac{1}{2}\sin^2\Theta_l)-2M^2E^2\sin^2\Theta_l-\frac{q_\alpha^4}{|\boldsymbol{q}|}E\cos\Theta_l+M^2q_\alpha^2\right)+ \\
&+ \left.\left.q_\alpha^2EE(p)^2(1-\frac{q^0}{|\boldsymbol{q}|}\cos\Theta_l)\right]\left(F_1^2-\frac{q_\alpha^2}{4M^2}F_2^2\right)+\frac{1}{2}q_\alpha^4(F_1+F_2)^2E(p)\right\}_{E_{min}(r)}^{E_F(r)} \quad \text{(D.11)}
\end{aligned}
$$

As one can see, both the direct calculation as well as the Rosenbluth separation (Eqs. (4.89), (4.90)) give the same results.

E Alternative vector and axial form factor sets

E.1 Nucleon form factors

The isospin symmetry relates the vector form factors to the electromagnetic ones:

$$F_i^V(Q^2) = F_i^p(Q^2) - F_i^n(Q^2). \tag{E.1}$$

For the electromagnetic form factors we use the parameterization of Galster *et al.*, Ref. [166]:

$$\begin{aligned}
F_1^N(Q^2) &= \frac{G_E^N(Q^2) + \tau G_M^N(Q^2)}{1+\tau} \\
F_2^N(Q^2) &= \frac{G_M^N(Q^2) - G_E^N(Q^2)}{1+\tau} \\
G_E^p(Q^2) &= \frac{G_M^p(Q^2)}{\mu_p} = \frac{G_M^n(Q^2)}{\mu_n} = \\
&= -(1+\lambda_n\tau)\frac{G_E^n(Q^2)}{\mu_n\tau} = \frac{1}{(1+\frac{Q^2}{M_D^2})^2}
\end{aligned} \tag{E.2}$$

with $\mu_p = 2.792.847$, $\mu_n = 1.913043$, $\lambda_n = 5.6$, $\tau = \frac{Q^2}{4M^2}$ and $M_D = 0.843$ GeV. We assume the axial nucleon form factor in a dipole form:

$$G_A(Q^2) = \frac{g_A}{(1+\frac{Q^2}{M_A^2})^2};\ M_A = 1.05GeV \tag{E.3}$$

with $g_A = 1.267$.

In the ANL fits we use a different set of form factors. The electric and magnetic form factors of nucleons follow the parametrization of Alberico *et al.*, Ref. [167], (instead of Galster *et al.*, Ref. [166] used in Ref. [46]):

$$\begin{aligned}
G_E^p(Q^2) &= \frac{1-0.19\tau}{1+11.12\tau+15.16\tau^2+21.25\tau^3} \\
G_M^p(Q^2) &= \frac{\mu_p(1+1.09\tau)}{1+12.31\tau+25.57\tau^2+30.61\tau^3} \\
G_E^n(Q^2) &= 0.10\left(\frac{1}{(1+0.43Q^2/[\mathrm{GeV}^2])^2} - \frac{1}{(1+2.83Q^2/[\mathrm{GeV}^2])^2}\right) \\
G_M^n(Q^2) &= \frac{\mu_n(1+8.28\tau)}{1+21.30\tau+77\tau^2+238\tau^3}.
\end{aligned} \tag{E.4}$$

We use $\mu_p = 2.792847$ and $\mu_n = -1.913043$.

E.2 Alternative sets of $\Delta(1232)$ form factors

E.2.1 Vector form factors

In this thesis we use the vector form factors from Ref. [140], which are defined in Eq. (6.35). There exist a few more parameterizations, which we will briefly discuss.

The set of electromagnetic Δ form factors can be extracted from measured "helicity amplitudes". We adopt use their definition from Appendix E of Ref. [127] together with all conventions and simplifications mentioned there (*i. e.* no W-dependence). More details can be also found *e. g.* in Refs. [168]. There are three commonly used helicity amplitudes describing the transition from spin $+1/2$ state of the nucleon N to spin $+3/2$ state of the resonance R with positive photon polarization ($A^N_{3/2}$), transition from spin -1/2 state of the nucleon N to spin 1/2 state of the resonance R with positive photon polarization ($A^N_{1/2}$) and transition from spin 1/2 state of the nucleon N to spin 1/2 state of the resonance R with positive photon polarization ($S^N_{1/2}$). They are defined in the CMS and have following form:

$$\begin{aligned}
A^N_{3/2} &= \sqrt{\frac{2\pi\alpha}{k_R}} \left\langle R; J_z = 3/2 \left| x^\mu_+ J^{EM}_\mu \right| N; J_z = 1/2 \right\rangle \zeta \\
A^N_{1/2} &= \sqrt{\frac{2\pi\alpha}{k_R}} \left\langle R; J_z = 1/2 \left| x^\mu_+ J^{EM}_\mu \right| N; J_z = -1/2 \right\rangle \zeta \\
S^N_{1/2} &= -\sqrt{\frac{2\pi\alpha}{k_R}} \frac{|\boldsymbol{q}|}{\sqrt{Q^2}} \left\langle R; J_z = 1/2 \left| x^\mu_l J^{EM}_\mu \right| N; J_z = -1/2 \right\rangle \zeta
\end{aligned} \tag{E.5}$$

with $k_R = \frac{W^2 - M^2}{2W}$ and photon polarization projection operators x^i_μ defined as in Eq. (4.19). The ralative phase ζ comes from possible phase between πNN and πNR couplings and in many cases one can set $\zeta \approx 1$ (see Appendix F.1 of Ref. [127]). The relation between positive-parity spin-, isospin- 3/2 resonance electromagnetic form factors and helicity amplitudes for initial proton and neutron states is calculated to be:

$$\begin{aligned}
A^{p/n}_{1/2} &= \sqrt{\frac{\pi\alpha}{3M} \frac{(M_R - M)^2 + Q^2}{M_R^2 - M^2}} \left[\frac{C_3^{p/n}}{M} \frac{M^2 + MM_R + Q^2}{M_R} - \frac{C_4^{p/n}}{M^2} \frac{M_R^2 - M^2 - Q^2}{2} \right. \\
&- \left. \frac{C_4^{p/n}}{M^2} \frac{M_R^2 - M^2 + Q^2}{2} \right] \\
A^{p/n}_{3/2} &= \sqrt{\frac{\pi\alpha}{M} \frac{(M_R - M)^2 + Q^2}{M_R^2 - M^2}} \left[\frac{C_3^{p/n}}{M} (M + M_R) + \frac{C_4^{p/n}}{M^2} \frac{M_R^2 - M^2 - Q^2}{2} \right. \\
&+ \left. \frac{C_4^{p/n}}{M^2} \frac{M_R^2 - M^2 + Q^2}{2} \right] \\
S^{p/n}_{1/2} &= \sqrt{\frac{\pi\alpha}{6M} \frac{(M_R - M)^2 + Q^2}{M_R^2 - M^2}} \frac{\sqrt{[(M_R - M)^2 + Q^2][(M_R + M)^2 + Q^2]}}{M_R^2} \times \\
&\times \left[\frac{C_3^{p/n}}{M} M_R + \frac{C_4^{p/n}}{M_N^2} M_R^2 + \frac{C_5^{p/n}}{M^2} \frac{M_R^2 + M^2 + Q^2}{2} \right].
\end{aligned} \tag{E.6}$$

We denote the resonance pole mass as M_R. Here $M_R = M_\Delta$ and for the $\Delta(1232)$ resonance both p and n amplitudes and form factors are the same, *i. e.* $A^p_{1/2} = A^n_{1/2} = A_{1/2}$, $A^p_{3/2} = A^n_{3/2} = A_{3/2}$ and $S^p_{1/2} = S^n_{1/2} = S_{1/2}$.

The MAID2007 analysis from Ref. [50] relates the helicity amplitudes to the electric G_E,

magnetic G_M and Coulomb G_C form factors:

$$\begin{aligned} G_M(Q^2) &= -c_\Delta(A_{1/2}+\sqrt{3}A_{3/2}) = 2c_\Delta A_M^\Delta(M_\Delta,Q^2) \\ G_E(Q^2) &= c_\Delta(A_{1/2}-\frac{1}{\sqrt{3}}A_{3/2}) = -2c_\Delta A_E^\Delta(M_\Delta,Q^2) \\ G_C(Q^2) &= 2\sqrt{2}c_\Delta\frac{M_\Delta}{k_\Delta}S_{1/2} = -4c_\Delta\frac{M_\Delta}{k_\Delta}A_C^\Delta(M_\Delta,Q^2) \end{aligned} \tag{E.7}$$

with:

$$c_\Delta = \sqrt{\frac{M^3 k_\Delta^W}{4\pi\alpha k_\Delta^2 M_\Delta}} \tag{E.8}$$

and:

$$k = \sqrt{\left(\frac{W^2-M^2-Q^2}{2W}+Q^2\right)};\ k_\Delta = k(M_\Delta,Q^2);\ k_\Delta^W = k(M_\Delta,0). \tag{E.9}$$

The amplitudes A_i^Δ have been given in Ref. [50] a phenomenological parametrization resulting from available experimental data:

$$A_i^\Delta(W,Q^2) = A_i^0(1+\beta_i Q^{2n_i})\frac{k}{k_W}e^{-\gamma_i Q^2}G_D(Q^2) \tag{E.10}$$

where the dpole form factor $G_D(Q^2) = (1+Q^2/M_V^2)^{-2}$ is calculated with $M_V^2 = 0.71$ [GeV^2]. The newest MAID2007 analysis uses For the Coulomb amplitude slightly different parametrization:

$$A_S^\Delta(W,Q^2) = A_S^0\frac{1+\beta_i Q^2}{1+4.9\tau}\frac{k^2}{k_\Delta k_W}e^{-\gamma_i Q^2}G_D(Q^2) \tag{E.11}$$

where τ s defined as in Eq. (E.2). All coefficients are listed in the Tab. 8. Using this

Table 8: Parametrization coefficients of Eqs. (E.10) and (E.11) for the MAID2003/2007 analysis.

	M	E	S	Model
A_i^0	300	-6.50	-19.50	2003
	300	-6.37	-12.40	2007
β_i	0	-0.306	0.017	2003
	0.01	-0.021	0.12	2007
γ_i	0.21	0.21	0.21	2003
	0.23	0.16	0.23	2007
n_i	1	1	3	2003
	1	1	-	2007

parametrization and Eqs. (E.6-E.11) with $W = M_\Delta$ one can calculate all vector form factors $C_i^V(Q^2)$ of the $\Delta(1232)$ resonance used in MAID.

It is worthy to mention here, that some groups in their recent papers (*e. g.* Ref. [57]) sometimes use an old parametrization of Δ electromagnetic form factors from Ref. [165]:

$$\begin{aligned} C_3^V(Q^2) &= 2.05 G_D(Q^2) \\ C_4^V(Q^2) &= -\frac{M}{M_\Delta} C_3^V(Q^2) \\ C_5^V(Q^2) &= 0. \end{aligned} \tag{E.12}$$

Existence of so many form factor parameterizations may lead to confusion. The extraction procedure from experimental pion electroproduction data depends on the model of nonresonant background. All data are in fact sum of the resonant and nonresonant contributions. In order to stay completely consistent one should do separate form factor extraction for each proposed model of the Δ resonance and background. Fortunately, most of the available form factor parameterizations differ in a rather negligible way in cross section computation, which is apparent in Fig. 28.

E.2.2 Axial form factors

The leading axial form factor is C_5^A. Authors of Refs. [46] and [170] use the parametrization from Ref. [171]:

$$C_5^A(Q^2) = \frac{C_5^A(0)}{(1+Q^2/M_{A\Delta}^2)^2} \frac{1}{(1+Q^2/(3M_{A\Delta}^2))^2} \tag{E.13}$$

wwhere the behavior of C_5^A is determined by two parameters: $C_5^A(0)$ and $M_{A\Delta}$. From Goldberger-Treiman relations one has $C_5^A(0) \approx 1.15 \sim 1.2$. The default $M_{A\Delta} \approx 1.05$ GeV is expected to be of the same order as axial nucleon mas. After performing fits to the $\pi^+ p$ ANL channel the authors of Ref. [46] obtained $C_5^A(0) 0.867 \pm 0.075$ and $M_{A\Delta} = 0.985 \pm 0.082$. These differences are very significant. Due to large uncertainty on these values we adopt simple dipole approximation:

$$C_5^A(Q^2) = \frac{C_5^A(0)}{(1+Q^2/M_{A\Delta}^2)^2}. \tag{E.14}$$

The group of authors of Ref. [57]) sometimes use parametrization from Ref. [165]:

$$C_i^A(Q^2) = \frac{C_i^A(0)}{(1+Q^2/M_{A\Delta}^2)^2} \left(1 - \frac{a_i Q^2}{1+b_i Q^2}\right) \tag{E.15}$$

with $C_3^A(0) = a_3 = b_3 = 0$, $C_5^A(0) = 1.2$, $C_4^A(0) = -\frac{1}{4} C_5^A(0)$ and $a_4 = a_5 = -1.21$ [GeV^{-2}] and $b_4 = b_5 = 2$ [GeV^2]. They also adopt $M_{A\Delta} = 1.05$ GeV.

F Resonance decay widths

In this section we shall calculate the basic decay widths of spin-1/2 and spin-3/2 resonances into a pion-nucleon pair.

F.1 Spin 1/2 resosnace decay

The Lagranagian of $N^*N\pi$ interaction is as follows:

$$\mathcal{L} = \frac{f_R}{m_\pi}\overline{\psi}_R(x)\left\{\begin{array}{c}\gamma^\mu\gamma_5\\ \gamma^\mu\end{array}\right\}\boldsymbol{t}\partial_\mu\boldsymbol{\phi}(x)\psi_N(x) + h.c. \tag{F.1}$$

The upper/lower components describe the interaction vertex of positive/negative parity resonance. The isospin transition matrix $\boldsymbol{t} = \boldsymbol{\tau}$ for isospin-1/2 resonance and $\boldsymbol{t} = \boldsymbol{T}^\dagger$ for isospin-3/2 resonance. One can use it to evaluate the matrix element of $N^* \to N\pi$ decay:

$$S_{fi} = -i\frac{1}{\sqrt{4E_NE_R}}\frac{1}{(2\pi)^3}\overline{u}_{s_N}(\boldsymbol{p'})\not{k}(\gamma_5)u_{s_R}(\boldsymbol{p})C^{iso}_{t_R,t_N,t_\pi} \times (2\pi)^4\delta^4(p'+q-p). \tag{F.2}$$

The isospin coefficients for isospin-1/2 resonances are $C^{iso} = \sqrt{2}$ for charged pion interaction and $C^{iso} = \pm 1$ for the neutral pion interaction with a proton(+)/neutron(-). One can readily evaluate the $|M_{fi}|^2$ for unpolarized decay measurement into any pion:

$$\begin{aligned}|M_{fi}|^2 &= \frac{f_R^2}{m_\pi^2}\frac{1}{4E_NE_R}\frac{1}{2}\sum_{s_R,s_N}\sum_{\{t_N,t_\pi\}}(C^{iso}_{t_R,t_N,t_\pi})^2|\overline{u}_{s_N}(\boldsymbol{p'})\not{k}(\gamma_5)u_{s_R}(\boldsymbol{p})\not{k}(\gamma_5)|^2 = \\ &= \frac{3}{2}\frac{f_R^2}{m_\pi^2}\frac{1}{4E_NE_R}\mathrm{Tr}\left[(\not{p}'+M)\not{k}(\gamma_5)(\not{p}+W)\not{k}(\gamma_5)\right].\end{aligned} \tag{F.3}$$

We take into account, that the resonance state has an invariant mass $W = \sqrt{p^2}$. It is worthy to notice, that for the isospin-3/2 spin-1/2 resonances it is enough to substitute the factor of 3 with the factor of 1 (isospin factors are $\pm\sqrt{\frac{2}{3}}$ for $\pi^\mp$ and $\sqrt{\frac{1}{3}}$ for π^0).The Dirac trace is quick to evaluate:

$$\begin{aligned}\mathrm{Tr}\left[\ldots\right] &= 4\left[2p\cdot kp'\cdot k - k^2p\cdot p' \mp k^2WM\right] = \\ &= 4\left[p\cdot k((p'+q)^2 - p'^2 - k^2) - k^2p\cdot p' \mp k^2WM\right] = \\ &= 4\left[(W^2-M^2-m_\pi^2)p\cdot k - m_\pi^2(p\cdot p' \pm WM)\right]..\end{aligned} \tag{F.4}$$

The upper/lower sign in the last term is for the positive/negative parity resonance We are ready to calculate the width:

$$\begin{aligned}\Gamma_{N^*\to N\pi} &= \frac{3}{2}\frac{f_R^2}{m_\pi^2}\int\frac{d^3p'}{(2\pi)^3}\int\frac{d^3k}{(2\pi)^3 2E_\pi}\frac{[(W^2-M^2-m_\pi^2)p\cdot k - m_\pi^2(p\cdot p'\pm WM)]}{E_NE_R} \\ &\quad (2\pi)^4\delta^{(4)}(p'+k-p) = \\ &= \frac{3}{16\pi^2}\frac{f_R^2}{m_\pi^2}\int d^3k\frac{[(W^2-M^2-m_\pi^2)p\cdot k - m_\pi^2(p\cdot p'\pm WM)]}{E_NE_RE_\pi}\delta(E_N+E_\pi-W)\end{aligned} \tag{F.5}$$

It is convenient to move to the resonance rest frame and assume it is an off-shell particle. All CMS variables will be denoted by "cm". Thus $E_R^{cm} = W$, $p\cdot k = WE_\pi^{cm}$, $p\cdot p' = WE_N^{cm}$

and $E^{cm}_{\pi/N} = \sqrt{k^{cm} + m_\pi^2/M^2}$. Thus:

$$\begin{aligned}\Gamma^{cm}_{N^{cm}\to N\pi} &= \frac{3}{4\pi}\frac{f_R^2}{m_\pi^2}\int k^2 dk \frac{[(W^2-M^2-m_\pi^2)E^{cm}_\pi - m_\pi^2(E^{cm}_N \pm M)]}{E^{cm}_N E^{cm}_\pi} \cdot \\ &\cdot \quad \delta(E^{cm}_N + E^{cm}_\pi - W). \end{aligned} \tag{F.6}$$

Now one has to switch the integration variables in the δ function:

$$\begin{aligned}\delta(E^{cm}_N + E^{cm}_\pi - W) &= \frac{E^{cm}_\pi E^{cm}_N}{kW}\delta(k-k^{cm}) \\ k^{cm} &= \left[\frac{W^4+M^4+m_\pi^4-2(W^2M^2+W^2m_\pi^2+M^2m_\pi^2)}{4W^2}\right]^{1/2} \\ E^{cm}_\pi &= \frac{W^2+m_\pi^2-M^2}{2W} \\ E^{cm}_N &= \frac{W^2+M^2-m_\pi^2}{2W}. \end{aligned} \tag{F.7}$$

Thus the width is given by:

$$\Gamma^{cm}_{N^{cm}\to N\pi} = \frac{3}{4\pi}\frac{f_R^2}{m_\pi^2}\frac{k^{cm}}{W}\left[(W^2-M^2-m_\pi^2)E^{cm}_\pi - m_\pi^2 W(E^{cm}_N \pm M)\right]. \tag{F.8}$$

We can further simplify this expression:

$$\begin{aligned}\Gamma^{cm}_{N^{cm}\to N\pi} &= \frac{3}{4\pi}\frac{f_R^2}{m_\pi^2}\frac{k^{cm}}{W^2}\left[\frac{(W^2-M^2-m_\pi^2)(W^2+m_\pi^2-M^2)}{2} - m_\pi^2\left(\frac{(W^2+M^2-m_\pi^2)}{2} \pm WM\right)\right] = \\ &= \frac{3}{8\pi}\frac{f_R^2}{m_\pi^2}\frac{k^{cm}}{W^2}\left[(W^2-M^2)^2 - m_\pi^2(W\pm M)^2)\right]. \end{aligned} \tag{F.9}$$

The couplings f_r can be obtained from the experimental total decay width Γ^{tot} and πN branching ratio r at the peak ($W = M_R$):

$$r\Gamma^{tot} = \; = \frac{3}{8\pi}\frac{f_R^2}{m_\pi^2}\frac{k^{cm}}{M_R^2}\left[(M_R^2-M^2)^2 - m_\pi^2(M_R \pm M)^2\right]. \tag{F.10}$$

It is consistent with Ref. [147]. The above formulas are useful in all numerical calculations.

F.2 Spin 3/2 resosnace decay

The Lagranagian of $RN\pi$ interaction is as follows:

$$\mathcal{L} = \frac{f_R}{m_\pi}\overline{\psi}_\mu(x)\left\{\begin{array}{c}\mathbf{1}_{4\times4}\\ \gamma_5\end{array}\right\}\boldsymbol{t}\partial^\mu\boldsymbol{\phi}(x)\psi_N(x) + h.c. \tag{F.11}$$

In the expressions for decay width almost all isospin factors, normalizations etc. will remain the same. There will be only one difference:

$$\mathrm{Tr}\left[(\not{p}' + M)\not{k}(\gamma_5)(\not{p} + W)\not{k}(\gamma_5)\right] \;\to\; (-)\frac{1}{2}\mathrm{Tr}\left[(\not{p}' + M)k^\alpha(\gamma_5)P_{\alpha\beta}k^\beta(\gamma_5)\right]. \tag{F.12}$$

The additional $\frac{1}{2}$ comes from the average over spin-3/2 resonance states (4 possible spin projections). It is a straightforward task to evaluate it:

$$\begin{aligned}
(-)\mathrm{Tr}\left[(\not{p}'+M)k^{\alpha}(\gamma_5)P_{\alpha\beta}(p)k^{\beta}(\gamma_5)\right] &= -(+)\mathrm{Tr}\left[(\not{p}'+M)(\gamma_5)(\not{p}+W)\right. \\
&\quad \left.(k^2-\frac{1}{3}\not{k}\not{k}-\frac{2}{3}\frac{(p\cdot k)^2}{W^2})(\gamma_5)\right] = \\
&= (-)\frac{2}{3}\left(m_\pi^2-\frac{(p\cdot k)^2}{W^2}\right)\mathrm{Tr}\left[(\not{p}'+M)(\mp\not{p}-W)\right] = \\
&= \frac{8}{3}\left(\frac{(p\cdot k)^2}{W^2}-m_\pi^2\right)(p\cdot p'\pm WM). \qquad \text{(F.13)}
\end{aligned}$$

Again, we shall move to the resonance CMS system:

$$(-)\mathrm{Tr}\left[(\not{p}'+M)k^{\alpha}(\gamma_5)P_{\alpha\beta}(p)k^{\beta}(\gamma_5)\right] = \frac{8}{3}\left(\frac{(WE_\pi^{cm})^2}{W^2}-m_\pi^2\right)W(E_N^{cm}\pm M). \quad \text{(F.14)}$$

For the spin-3/2 resonance decay width we shall get:

$$\Gamma^{cm}_{N^{cm}\to N\pi} = \frac{3/1}{12\pi}\frac{f_R^2}{m_\pi^2}\frac{k^{cm3}(E_N^{cm}\pm M)}{W}. \qquad \text{(F.15)}$$

which covers the isospin-1/2 / isospin-3/2 and positive/negative parity cases. Again, at $W = M_R$:

$$r\Gamma^{tot} = \frac{3/1}{12\pi}\frac{f_R^2}{m_\pi^2}\frac{k^{cm3}}{M_R}(E_N^{cm}\pm M). \qquad \text{(F.16)}$$

G SPP hadronic and leptonic tensors contraction simplification.

We would like to prove the Eq. (6.67). First let us write down the contraction of hadronic and leptonic tensors:

$$\begin{aligned} L_{\mu\nu}A^{\mu\nu} &= L^{00}A^{00} + L^{11}A^{11} + L^{22}A^{22} + L^{33}A^{33} + L^{12}A^{12} + L^{23}A^{23} + L^{31}A^{31} + \\ &+ L^{21}A^{21} + L^{32}A^{32} + L^{13}A^{13} - L^{01}A^{01} - L^{02}A^{02} - L^{03}A^{03} + \\ &- L^{10}A^{10} - L^{20}A^{20} - L^{30}A^{30}. \end{aligned} \tag{G.1}$$

Now we need the most general form of the hadronic tensor for SPP process. It can be constructed out of parity conserving (PC)/parity violating (PV) symmetric (s)/antisymmetric (a) components. We may use all 4-vectors describing our system: p^μ, q^μ and k^μ. We write down 19 linearly independent components:

$$\begin{aligned} A^{\mu\nu} &= A_s^{\mu\nu} + A_a^{\mu\nu} = A_s^{\mu\nu\,(PC)} + A_s^{\mu\nu\,(PV)} + A_a^{\mu\nu\,(PC)} + A_a^{\mu\nu\,(PV)} \\ A_s^{\mu\nu\,(PC)} &= A_1 g^{\mu\nu} + A_2 p^\mu p^\nu + A_3 q^\mu q^\nu + A_4 k^\mu k^\nu + \\ &+ A_5(p^\mu q^\nu + p^\nu q^\mu) + A_6(q^\mu k^\nu + q^\nu k^\mu) + A_7(k^\mu p^\nu + k^\nu p^\mu) \\ A_s^{\mu\nu\,(PV)} &= A_8(p^\mu \epsilon^{\nu\alpha\beta\gamma} p_\alpha q_\beta k_\gamma + p^\nu \epsilon^{\mu\alpha\beta\gamma} p_\alpha q_\beta k_\gamma) + A_9(q^\mu \epsilon^{\nu\alpha\beta\gamma} p_\alpha q_\beta k_\gamma + q^\nu \epsilon^{\mu\alpha\beta\gamma} p_\alpha q_\beta k_\gamma) + \\ &+ A_{10}(k^\mu \epsilon^{\nu\alpha\beta\gamma} p_\alpha q_\beta k_\gamma + k^\nu \epsilon^{\mu\alpha\beta\gamma} p_\alpha q_\beta k_\gamma) \\ A_a^{\mu\nu\,(PC)} &= A_{11}(p^\mu q^\nu - p^\nu q^\mu) + A_{12}(q^\mu k^\nu - q^\nu k^\mu) + A_{13}(k^\mu p^\nu - k^\nu p^\mu) \\ A_a^{\mu\nu\,(PV)} &= A_{14}\epsilon^{\mu\nu\alpha\beta} p_\alpha q_\beta + A_{15}\epsilon^{\mu\nu\alpha\beta} q_\alpha k_\beta + A_{16}\epsilon^{\mu\nu\alpha\beta} k_\alpha p_\beta + \\ &+ A_{17}(p^\mu \epsilon^{\nu\alpha\beta\gamma} p_\alpha q_\beta k_\gamma - p^\nu \epsilon^{\mu\alpha\beta\gamma} p_\alpha q_\beta k_\gamma) + A_{18}(q^\mu \epsilon^{\nu\alpha\beta\gamma} p_\alpha q_\beta k_\gamma - q^\nu \epsilon^{\mu\alpha\beta\gamma} p_\alpha q_\beta k_\gamma) + \\ &+ A_{19}(k^\mu \epsilon^{\nu\alpha\beta\gamma} p_\alpha q_\beta k_\gamma - k^\nu \epsilon^{\mu\alpha\beta\gamma} p_\alpha q_\beta k_\gamma). \end{aligned} \tag{G.2}$$

Now we shall evaluate the contraction element-by-element. Notice, that the only dependence on ϕ_π comes from the k^1 and k^2 components and that $p^1 = p^2 = q^1 = q^2 = 0$. The "diagonal" elements:

$$\begin{aligned} L^{00}A^{00} &= L^{00}(A_1 + A_2 p_0^2 + A_3 q_0^2 + A_4 k_0^2 + 2A_5 p^0 q^0 + 2A_6 q^0 k^0 + 2A_7 k^0 p^0) \\ L^{11}A^{11} &= L^{11}(-A_1 + A_4 (k^1)^2 + 2A_{10} k^1 (q^0 p^3 k^2 - q^3 p^0 k^2)) \\ L^{22}A^{22} &= L^{22}(-A_1 + A_4 (k^2)^2 + 2A_{10} k^2 (q^3 p^0 k^1 - q^0 p^3 k^1)) \\ L^{33}A^{33} &= L^{33}(-A_1 + A_2 (p^3)^2 + A_3 (q^3)^2 + A_4 (k^3)^2 + 2A_5 p^3 q^3 + 2A_6 q^3 k^3 + 2A_7 k^3 p^3). \end{aligned} \tag{G.3}$$

In the above equations components 00 and 33 are manifestly ϕ_π-independent. The problem lies within the 11 and 22 components, which contain both the ϕ_π-dependent and ϕ_π-independent terms. We need to recall, that we need the inclusive cross section and that in spherical coordinates:

$$\begin{aligned} k^1 &= k \sin(\Theta_\pi)\cos(\phi_\pi) \\ k^2 &= k \sin(\Theta_\pi)\sin(\phi_\pi). \end{aligned} \tag{G.4}$$

In order to keep only the part, which does not disappear after performing $\int d\phi_\pi$, one can substitute

$$L^{11}A^{11} + L^{22}A^{22} \to \frac{1}{2}(L^{11} + L^{22})(A^{11} + A^{22}) = \frac{1}{2}(L^{11} + L^{22})(-2A_1 + A_4 k^2 \sin^2(\Theta_\pi)). \tag{G.5}$$

which is equivalent to what we get after the $\int d\phi_\pi$:

$$\frac{1}{2\pi}\int_0^{2\pi} d\phi_\pi (L^{11}A^{11} + L^{22}A^{22}) = (L^{11}+L^{22})(-A_1 + \frac{1}{2}A_4 \boldsymbol{k}^2 \sin^2(\Theta_\pi)). \tag{G.6}$$

The "vector-vector" off-diagonal part with 12 and 21 components:

$$\begin{aligned}
L^{12}A^{12} &= L^{12}\left[A_4 k^1 k^2 + A_{10}(k^1\epsilon^{2\alpha\beta 1}p_\alpha q_\beta k_1 + k^2\epsilon^{1\alpha\beta 2}p_\alpha q_\beta k_2) + A_{14}\epsilon^{12\alpha\beta}p_\alpha q_\beta + \right.\\
&+ \left. A_{15}\epsilon^{12\alpha\beta}q_\alpha k_\beta + A_{16}\epsilon^{12\alpha\beta}k_\alpha p_\beta + A_{19}(k^1\epsilon^{2\alpha\beta 1}p_\alpha q_\beta k_1 - k^2\epsilon^{1\alpha\beta 2}p_\alpha q_\beta k_2)\right]\\
L^{21}A^{21} &= L^{21}\left[A_4 k^2 k^1 + A_{10}(k^2\epsilon^{1\alpha\beta 2}p_\alpha q_\beta k_2 + k^1\epsilon^{2\alpha\beta 1}p_\alpha q_\beta k_1) + A_{14}\epsilon^{21\alpha\beta}p_\alpha q_\beta + \right.\\
&+ \left. A_{15}\epsilon^{21\alpha\beta}q_\alpha k_\beta + A_{16}\epsilon^{21\alpha\beta}k_\alpha p_\beta + A_{19}(k^2\epsilon^{1\alpha\beta 2}p_\alpha q_\beta k_2 - k^1\epsilon^{2\alpha\beta 1}p_\alpha q_\beta k_1)\right].
\end{aligned} \tag{G.7}$$

As one can see, the $L^{12}A^{12}$ and $L^{21}A^{21}$ separately contain both desired and undesired components. Here we will make a use of the fact, that scattering takes place in the $x-z$ plane. Hence the y-components of neutrino and lepton momenta are zero and $L^{12} = -L^{21}$. Thus the contributions from symmetric part of $A^{\mu\nu}$ will cancel out, leaving us only with non-vanishing terms:

$$\begin{aligned}
L^{12}A^{12} + L^{21}A^{21} &= 2L^{12}\left[A_{14}\epsilon^{12\alpha\beta}p_\alpha q_\beta + A_{15}\epsilon^{12\alpha\beta}q_\alpha k_\beta + A_{16}\epsilon^{12\alpha\beta}k_\alpha p_\beta + \right.\\
&+ \left. A_{19}((k^2)^2\epsilon^{1\alpha\beta 2}p_\alpha q_\beta - (k^1)^2\epsilon^{2\alpha\beta 1}p_\alpha q_\beta)\right] =\\
&= 2L^{12}\left[A_{14}\epsilon^{12\alpha\beta}p_\alpha q_\beta + A_{15}\epsilon^{12\alpha\beta}q_\alpha k_\beta + A_{16}\epsilon^{12\alpha\beta}k_\alpha p_\beta + \right.\\
&+ \left. A_{19}\boldsymbol{k}^2\sin^2(\Theta_\pi)\epsilon^{12\alpha\beta}p_\alpha q_\beta\right].
\end{aligned} \tag{G.8}$$

Notice, that in the electron scattering case and in our special frame of reference $L^{12} = L^{21} = 0$ and there is no problem at all.

The "vector-vector" off-diagonal part with $13-31$ and $23-32$ components:

$$\begin{aligned}
L^{13}A^{13} &= L^{13}\left[A_4 k^1 k^3 + (A_6 - A_{12})q^3 k^1 + (A_7 + A_{13})p^3 k^1 + \right.\\
&+ (A_8 - A_{17})p^3\epsilon^{1\alpha\beta 2}p_\alpha q_\beta k_2 + (A_9 - A_{18})q^3\epsilon^{1\alpha\beta 2}p_\alpha q_\beta k_2 +\\
&+ \left.(A_{10} + A_{19})k^1\epsilon^{3\alpha\beta 1}p_\alpha q_\beta k_1 + A_{15}\epsilon^{1302}q_0 k_2 + A_{16}\epsilon^{1320}k_2 p_0\right]\\
L^{31}A^{31} &= L^{31}\left[A_4 k^3 k^1 + (A_6 + A_{12})q^3 k^1 + (A_7 - A_{13})p^3 k^1 + \right.\\
&+ (A_8 + A_{17})p^3\epsilon^{1\alpha\beta 2}p_\alpha q_\beta k_2 + (A_9 + A_{18})q^3\epsilon^{1\alpha\beta 2}p_\alpha q_\beta k_2 +\\
&+ \left.(A_{10} - A_{19})k^1\epsilon^{3\alpha\beta 1}p_\alpha q_\beta k_1 + A_{15}\epsilon^{3102}q_0 k_2 + A_{16}\epsilon^{3120}k_2 p_0\right]
\end{aligned} \tag{G.9}$$

$$\begin{aligned}
L^{23}A^{23} &= L^{23}\left[A_4 k^2 k^3 + (A_6 - A_{12})q^3 k^2 + (A_7 + A_{13})p^3 k^2 + \right.\\
&+ (A_8 - A_{17})p^3\epsilon^{2\alpha\beta 1}p_\alpha q_\beta k_1 + (A_9 - A_{18})q^3\epsilon^{2\alpha\beta 1}p_\alpha q_\beta k_1 +\\
&+ \left.(A_{10} + A_{19})k^2\epsilon^{3\alpha\beta 1}p_\alpha q_\beta k^1 + A_{15}\epsilon^{2301}q_0 k_1 + A_{16}\epsilon^{2310}k_1 p_0\right]\\
L^{32}A^{32} &= L^{32}\left[A_4 k^3 k^2 + (A_6 + A_{12})q^3 k^2 + (A_7 - A_{13})p^3 k^2 + \right.\\
&+ (A_8 + A_{17})p^3\epsilon^{2\alpha\beta 1}p_\alpha q_\beta k_1 + (A_9 + A_{18})q^3\epsilon^{2\alpha\beta 1}p_\alpha q_\beta k_1 +\\
&+ \left.(A_{10} - A_{19})k^2\epsilon^{3\alpha\beta 1}p_\alpha q_\beta k^1 + A_{15}\epsilon^{3201}q_0 k_1 + A_{16}\epsilon^{3210}k_1 p_0\right].
\end{aligned} \tag{G.10}$$

None of the above terms will survive the integration, thus they do not enter to Eq. (6.67).

The same applies for the $01-10$ and $02-20$ components:

$$\begin{aligned}
L^{01}A^{01} &= L^{01}\big[A_4k^0k^1+(A_6+A_{12})q^0k^1+(A_7-A_{13})p^0k^1+\\
&+ (A_8+A_{17})p^0\epsilon^{1\alpha\beta 2}p_\alpha q_\beta k_2+(A_9+A_{18})q^0\epsilon^{1\alpha\beta 2}p_\alpha q_\beta k_2+\\
&+ (A_{10}-A_{19})k^1\epsilon^{0\alpha\beta 1}p_\alpha q_\beta k_1+A_{15}\epsilon^{0132}q_3k_2+A_{16}\epsilon^{0123}k_2p_3\big]\\
L^{10}A^{10} &= L^{10}\big[A_4k^1k^0+(A_6-A_{12})q^0k^1+(A_7+A_{13})p^0k^1+\\
&+ (A_8-A_{17})p^0\epsilon^{1\alpha\beta 2}p_\alpha q_\beta k_2+(A_9-A_{18})q^0\epsilon^{1\alpha\beta 2}p_\alpha q_\beta k_2+\\
&+ (A_{10}+A_{19})k^1\epsilon^{0\alpha\beta 1}p_\alpha q_\beta k_1+A_{15}\epsilon^{1032}q_3k_2+A_{16}\epsilon^{1023}k_2p_3\big]
\end{aligned} \tag{G.11}$$

$$\begin{aligned}
L^{02}A^{02} &= L^{02}\big[A_4k^0k^2+(A_6+A_{12})q^0k^2+(A_7-A_{13})p^0k^2+\\
&+ (A_8+A_{17})p^0\epsilon^{2\alpha\beta 1}p_\alpha q_\beta k_1+(A_9+A_{18})q^0\epsilon^{2\alpha\beta 1}p_\alpha q_\beta k_1+\\
&+ (A_{10}-A_{19})k^2\epsilon^{0\alpha\beta 2}p_\alpha q_\beta k_2+A_{15}\epsilon^{0231}q_3k_1+A_{16}\epsilon^{0213}k_1p_3\big]\\
L^{20}A^{20} &= L^{20}\big[A_4k^2k^0+(A_6-A_{12})q^0k^2+(A_7+A_{13})p^0k^2+\\
&+ (A_8-A_{17})p^0\epsilon^{2\alpha\beta 1}p_\alpha q_\beta k_1+(A_9-A_{18})q^0\epsilon^{2\alpha\beta 1}p_\alpha q_\beta k_1+\\
&+ (A_{10}+A_{19})k^2\epsilon^{0\alpha\beta 2}p_\alpha q_\beta k_2+A_{15}\epsilon^{2031}q_3k_1+A_{16}\epsilon^{2013}k_1p_3\big]\,.
\end{aligned} \tag{G.12}$$

The last part, which gives contribution to Eq. (6.67) comes from the $03-30$ components

$$\begin{aligned}
L^{03}A^{03} &= L^{03}\big[A_2p^0p^3+A_3q^0q^3+A_4k^0k^3+\\
&+ A_5(p^0q^3+p^3q^0)+A_6(q^0k^3+q^3k^0)+A_7(k^0p^3+k^3p^0)+\\
&+ A_{11}(p^0q^3-p^3q^0)+A_{12}(q^0k^3-q^3k^0)+A_{13}(k^0p^3-k^3p^0)\big]\\
L^{30}A^{30} &= L^{30}\big[A_2p^3p^0+A_0q^3q^0+A_4k^3k^0+\\
&+ A_5(p^3q^0+p^0q^3)+A_6(q^3k^0+q^0k^3)+A_7(k^3p^0+k^0p^3)+\\
&+ A_{11}(p^3q^0-p^0q^3)+A_{12}(q^3k^0-q^0k^3)+A_{13}(k^3p^0-k^0p^3)\big]
\end{aligned} \tag{G.13}$$

which ends the proof of Eq. (6.67). Notice, that we can actually drop the antisymmetric contributions from $A_{11}-A_{13}$, since in our special reference frame $L_{03}=L_{30}$ (antisymmetric part of $L_{\mu\nu}$ vanishes).

H Vector current conservation in HNV model

The Δ excitation vertex we use conserves CVC by construction, thus CVC is conserved in Eq. (6.20) and Eq. (6.21) automatically (*i. e.* $q_\mu \Gamma^{\alpha\mu\,(V)} = 0$ as long as we choose $C_6^V = 0$). We would like to address the question of vector current conservation of background terms given by Eqs. (6.22-6.25). For simplicity let us drop the overall $-i\frac{g_A}{\sqrt{2}f_\pi}$ factor. We shall start with contraction of vector pion production current to four momentum transfer q^μ. Here we willconstantly make use of the on-shell condition for nucleons and pions, *i. e.* :

$$\begin{aligned} p^2 = p'^2 &= M^2 \\ k^2 &= m_\pi^2 \\ \not{p} u_s(\boldsymbol{p}) &= M u_s(\boldsymbol{p}) \\ \overline{u}_{s'}(\boldsymbol{p'})\not{p'} &= M \overline{u}_s(\boldsymbol{p}) \end{aligned} \tag{H.1}$$

Let us start with the nucleon pole diagram:

$$q_\mu \overline{u}_{s'}(\boldsymbol{p'}) s_{NP}^{\mu(V)} u_s(\boldsymbol{p}) \;\propto\; C_{NP} q_\mu \overline{u}_{s'}(\boldsymbol{p'}) \not{k} \gamma^5 \frac{(\not{p}+\not{q}+M)}{(p+q)^2-M^2}(F_1^V \gamma^\mu + i\sigma^{\mu\alpha} q_\alpha \frac{F_2^V}{2M}) u_s(\boldsymbol{p}). \tag{H.2}$$

We remember, that $k = p + q - p'$. Thus:

$$\begin{aligned} q_\mu \overline{u}_{s'}(\boldsymbol{p'}) s_{NP}^{\mu(V)} u_s(\boldsymbol{p}) &\propto C_{NP} F_1^V \overline{u}_{s'}(\boldsymbol{p'})(\not{p}+\not{q}-\not{p}')\gamma^5 \frac{(\not{p}+\not{q}+M)}{(p+q)^2-M^2}\not{q} u_s(\boldsymbol{p}) = \\ &= C_{NP} F_1^V \overline{u}_{s'}(\boldsymbol{p'})(\not{p}+\not{q}-M)\gamma^5 \frac{(\not{p}+\not{q}+M)}{(p+q)^2-M^2}\not{q} u_s(\boldsymbol{p}) = \\ &= -C_{NP} F_1^V \overline{u}_{s'}(\boldsymbol{p'})\gamma^5 \frac{(\not{p}+\not{q}+M)^2}{(p+q)^2-M^2}\not{q} u_s(\boldsymbol{p}) = \\ &= C_{NP} F_1^V \overline{u}_{s'}(\boldsymbol{p'})\gamma^5 \frac{(M^2+2pq+q^2)^2\not{q}+2M\not{p}\not{q}+2Mq^2+M^2\not{q}}{(q(2p+q)} u_s(\boldsymbol{p}) = \\ &= C_{NP} F_1^V \overline{u}_{s'}(\boldsymbol{p'})\gamma^5 \frac{q(2p+q)\not{q}+2M^2\not{q}+2Mq^2+4Mpq-2M\not{q}\not{p}}{(q(2p+q)} u_s(\boldsymbol{p}) = \\ &= C_{NP} F_1^V \overline{u}_{s'}(\boldsymbol{p'})(\not{q}-2M)\gamma^5 u_s(\boldsymbol{p}). \end{aligned} \tag{H.3}$$

As one can see, this term alone breaks the CVC. But CVC should be conserved by the full HNV model, not separate contributions. We continue our calculation:

$$\begin{aligned} q_\mu \overline{u}_{s'}(\boldsymbol{p'}) s_{CNP}^{\mu(V)} u_s(\boldsymbol{p}) &\propto C_{CNP} F_1^V \overline{u}_{s'}(\boldsymbol{p'})\not{q} \frac{(\not{p}'-\not{q}+M)}{(p'-q)^2-M^2}\not{k}\gamma^5 \overline{u}_s(\boldsymbol{p}) = \\ &= C_{CNP} F_1^V \overline{u}_{s'}(\boldsymbol{p'})\not{q} \frac{(\not{p}'-\not{q}+M)}{(p'-q)^2-M^2}(\not{p}+\not{q}-\not{p}')\gamma^5 \overline{u}_s(\boldsymbol{p}) \\ &= -C_{CNP} F_1^V \overline{u}_{s'}(\boldsymbol{p'})\not{q} \frac{(\not{p}'-\not{q}+M)^2}{(p'-q)^2-M^2}\gamma^5 \overline{u}_s(\boldsymbol{p}) \\ &= -C_{CNP} F_1^V \overline{u}_{s'}(\boldsymbol{p'}) \frac{2\not{q}M^2+q(q-2p')\not{q}-2M\not{q}-2Mq(q-2p)}{q(q-2p)}\gamma^5 \overline{u}_s(\boldsymbol{p}) = \\ &= C_{CNP} F_1^V \overline{u}_{s'}(\boldsymbol{p'})(2M-\not{q})\gamma^5 u_s(\boldsymbol{p}). \end{aligned} \tag{H.4}$$

Analogously by using consequently Eq. (H.1):

$$\begin{aligned} q_\mu \overline{u}_{s'}(\boldsymbol{p'}) s^{\mu(V)}_{CT} u_s(\boldsymbol{p}) &\propto C_{CT} F^V_{CT} \overline{u}_{s'}(\boldsymbol{p'}) \not{q} \gamma^5 u_s(\boldsymbol{p}) \\ q_\mu \overline{u}_{s'}(\boldsymbol{p'}) s^{\mu(V)}_{PIF} u_s(\boldsymbol{p}) &\propto -2M C_{PIF} F^V_{PIF} \overline{u}_{s'}(\boldsymbol{p'}) \gamma^5 u_s(\boldsymbol{p}) \end{aligned} \tag{H.5}$$

We now sum up all the divergencies up in neutrino interaction channels using coefficients from Tab. 4 and Tab. 3:

$$\begin{aligned} \nu_l + p \to l^- + \pi^+ + p \text{ and } \overline{\nu}_l + n \to l^+ + \pi^- + n: \; q_\mu \overline{u}_{s'}(\boldsymbol{p'}) s^{\mu(V)}_{SUM} u_s(\boldsymbol{p}) \propto \\ \propto \overline{u}_{s'}(\boldsymbol{p'}) \left[(2M - \not{q}) \gamma^5 F^V_1 + F^V_{CT} \not{q} \gamma^5 - 2M F^V_{PIF} \gamma^5 \right] u_s(\boldsymbol{p}) \end{aligned} \tag{H.6}$$

$$\begin{aligned} \nu_l + n \to l^- + \pi^0 + p: \; q_\mu \overline{u}_{s'}(\boldsymbol{p'}) s^{\mu(V)}_{SUM} u_s(\boldsymbol{p}) \propto \\ \propto \overline{u}_{s'}(\boldsymbol{p'}) \left[-\frac{2}{\sqrt{2}} (2M - \not{q}) \gamma^5 F^V_1 - \sqrt{2} F^V_{CT} \not{q} \gamma^5 + \sqrt{2} 2M F^V_{PIF} \gamma^5 \right] u_s(\boldsymbol{p}) \end{aligned} \tag{H.7}$$

$$\begin{aligned} \nu_l + n \to l^- + \pi^+ + n \text{ and } \overline{\nu}_l + p \to l^+ + \pi^- + p: \; q_\mu \overline{u}_{s'}(\boldsymbol{p'}) s^{\mu(V)}_{SUM} u_s(\boldsymbol{p}) \propto \\ \propto \overline{u}_{s'}(\boldsymbol{p'}) \left[-(2M - \not{q}) \gamma^5 F^V_1 - F^V_{CT} \not{q} \gamma^5 + 2M F^V_{PIF} \gamma^5 \right] u_s(\boldsymbol{p}) \end{aligned} \tag{H.8}$$

$$\begin{aligned} \overline{\nu}_l + p \to l^+ + \pi^0 + n: \; q_\mu \overline{u}_{s'}(\boldsymbol{p'}) s^{\mu(V)}_{SUM} u_s(\boldsymbol{p}) \propto \\ \propto \overline{u}_{s'}(\boldsymbol{p'}) \left[\frac{2}{\sqrt{2}} (2M - \not{q}) \gamma^5 F^V_1 + \sqrt{2} F^V_{CT} \not{q} \gamma^5 - \sqrt{2} 2M F^V_{PIF} \gamma^5 \right] u_s(\boldsymbol{p}) \end{aligned} \tag{H.9}$$

$$\begin{aligned} \gamma + p \to \pi^0 + p: \; q_\mu \overline{u}_{s'}(\boldsymbol{p'}) s^{\mu(V)}_{SUM} u_s(\boldsymbol{p}) \propto \\ \propto \overline{u}_{s'}(\boldsymbol{p'}) \left[-\sqrt{\frac{1}{2}} (2M - \not{q}) \gamma^5 F^p_1 + \sqrt{\frac{1}{2}} (2M - \not{q}) \gamma^5 F^p_1 \right] u_s(\boldsymbol{p}) \end{aligned} \tag{H.10}$$

$$\begin{aligned} \gamma + p \to \pi^+ + n: \; q_\mu \overline{u}_{s'}(\boldsymbol{p'}) s^{\mu(V)}_{SUM} u_s(\boldsymbol{p}) \propto \\ \propto \overline{u}_{s'}(\boldsymbol{p'}) \left[-(2M - \not{q}) \gamma^5 F^p_1 + (2M - \not{q}) \gamma^5 F^n_1 - F^V_{CT} \not{q} \gamma^5 + 2M F^V_{PIF} \gamma^5 \right] u_s(\boldsymbol{p}) \end{aligned} \tag{H.11}$$

$$\begin{aligned} \gamma + n \to \pi^- + p: \; q_\mu \overline{u}_{s'}(\boldsymbol{p'}) s^{\mu(V)}_{SUM} u_s(\boldsymbol{p}) \propto \\ \propto \overline{u}_{s'}(\boldsymbol{p'}) \left[-(2M - \not{q}) \gamma^5 F^n_1 + (2M - \not{q}) \gamma^5 F^p_1 + F^V_{CT} \not{q} \gamma^5 - 2M F^V_{PIF} \gamma^5 \right] u_s(\boldsymbol{p}) \end{aligned} \tag{H.12}$$

$$\begin{aligned} \gamma + n \to \pi^0 + n: \; q_\mu \overline{u}_{s'}(\boldsymbol{p'}) s^{\mu(V)}_{SUM} u_s(\boldsymbol{p}) \propto \\ \propto \overline{u}_{s'}(\boldsymbol{p'}) \left[\sqrt{\frac{1}{2}} (2M - \not{q}) \gamma^5 F^n_1 - \sqrt{\frac{1}{2}} (2M - \not{q}) \gamma^5 F^n_1 \right] u_s(\boldsymbol{p}) \end{aligned} \tag{H.13}$$

As one can see, the vector current conservation can be imposed simultaneously in neutrino and electron scattering, if we set $F^V_{CT} = F^V_{PIF} = F^p_1 - F^n_1 = F^V_1$. This is also the reason that if we introduce the virtual pion form factor F_π to the PIF term, one has to introduce it automatically to NP, CNP and CT terms.

I Numerical procedures

In order to handle the complex Lorentz and Dirac structures in the model of [46] we have developed a numerical $C++$ library. Its flexibility allows to incorporate different dynamical models on the level of Lorentz vectors and tensors in an efficient and clear manner. It's basic classes, templates and numerical procedures are listed below:

1. Class DM This is a class of 4x4 complex matrices. It is used for calculations related to complex algebra. List of functions:

   (a) Constructor DM(unsigned int i). It creates matrices: $i = 0, 1, 2, 3 \to \gamma^\mu$, $i = 4 \to \mathbf{1}_{4\times4}$, $i = 5 \to \gamma^5$, otherwise $\mathbf{0}_{4\times4}$. Currently only the Dirac representation is used.

   (b) The access operator (unsigned i, unsigned j) returns a complex number from i-th row and j-th column

   (c) Overloaded operators +, -, +=, -= designed for addition/subtraction of two matrices or real/complex numbers on the diagonal.

   (d) Overloaded operators * and *= to multiply the matrix A by the matrix B ($A*B$) or to multiply matrix A by a real/complex number.

   (e) Overloaded operator & = for left-hand-side multiplication of the matrix A by the matrix B ($A = B * A$).

   (f) Overloaded / and /= operators for the division of matrix by a number.

   (g) Function double Trace() returns the real part of the trace.

   (h) Function complex<double> CTrace() returns the complex trace.

   (i) Function void hermit() performs hermitian conjugate on the matrix.

   (j) Function void transp() transposes the matrix.

2. Template D4V<class T> is used for all operations on Lorentz 4-vectors of the type double, complex and DM.

   (a) The constructor D4V(T t0,T t1, T t2, T t3) creates a 4-vector.

   (b) Overloaded operator = to copy/assign 4-vectors.

   (c) Overloaded access operator () (unsigned j) to the j-th element of the vector.

   (d) Overloaded operators +, -, +=, -= to add 4-vectors <u>of the same type</u>.

   (e) Overloaded T operator * returns $a_\mu b^\mu = a^0 b^0 - \boldsymbol{a} \cdot \boldsymbol{b}$. Works with different types of 4-vectors, example $\gamma^\mu \cdot p^\mu = \not{p}$. Warning! Not all combinations allowed, for example D4V<double>*D4V<complex> produces an error.

   (f) Overloaded operator *= multiplies a 4-vector by a number or matrix. The general rule is to never multiply a less complex type by a more complex one. For example D4V<complex>*=double works fine, but not the other way around.

   (g) Overloaded operator & = for the left-handed multiplication of a vector by a matrix.

   (h) Function void hermit() performs a hermitian conjugate of 4-vector elements (only DM type!).

3. Template D4T<class T> This template is used to operate on the Lorentz second rank tensors of the type T.

   (a) Constructors

      i. D4T(const D4V<T> & t,const D4V<T> & u) creates a $t^\mu \otimes u^\nu$ tensor.

      ii. D4T(const T & t00,const T & t01, const T & t02, const T & t03, const T & t10,const T & t11, const T & t12, const T & t13, const T & t20,const T & t21, const T & t22, const T & t23, const T & t30,const T & t31, const T & t32, const T & t33) creates an arbitrary tensor.

   (b) Overloaded operator =. Assigning D4T< complex> to D4T<double> or D4T<DM> to D4T<double> not allowed!

   (c) Overloaded access operator (unsigned int i, unsigned int j).

   (d) Overloaded access operator (unsigned i) for the i-th row. It returns a 4-vector D4V<T>.

   (e) Function void transp() transposes a tensor.

   (f) Function inline void Add(D4V<T1> v1, D4V<T2> v2) adds a tensor product to the tensor. Adding D4T< complex> to D4T<double> or D4T<DM> to D4T<double> not allowed!

   (g) Function inline void Replace(D4V<T1> v1, D4V<T2> v2) replaces the current tensor with a $v_1^\mu \otimes v_2^\nu$ tensor product. Replacing D4T<double> by D4T<complex> or D4T<complex> to D4T<DM> not allowed!

   (h) Overloaded operators +, -, +=, -= add two tensors <u>of the same type</u>.

   (i) Overloaded operator *:

      i. For the two tensors it creates a tensor $C^{\mu\nu} = A^\mu_\alpha B^{\alpha\nu}$.

      ii. For the multiplication of v^μ by $A^{\mu\nu}$ creates a vector $u^\mu = v^\alpha A^\mu_\alpha$.

      iii. Allows to multiply the whole tensor by a number or matrix. The same limitation as for 4-vectors!

   (j) Overloaded operator *=:

      i. For two tensors it performs: $A^{\mu\nu} = A^\mu_\alpha B^{\alpha\nu}$.

      ii. Multiplies the whole tensor by a number or matrix.

   (k) Overloaded operator & =

      i. For two tensors it performs: $A^{\mu\nu} = B^\mu_\alpha A^{\alpha\nu}$.

      ii. Multiplies the whole tensor by a matrix M from the left $A^{\mu\nu} = M \cdot A^{\mu\nu}$.

   (l) Function inline D4T< std::complex<double> > CT(const D4T<DM> & D) returns complex tensor $C^{\mu\nu} = \mathrm{Tr}[A^{\mu\nu}]$.

   (m) Function inline D4T Ants(const D4T<T> & t) returns antisymmetrized tensor $-\epsilon^{\mu\nu\alpha\beta} t_{\alpha\beta}$.

   (n) Function inline void AddAnts(const D4V<double> & u,const D4V<double> & v) adds $-\epsilon^{\mu\nu\alpha\beta} u_\alpha v_\beta$ to a tensor.

   (o) Function inline T contraction(const D4T<T> & t1,const D4T<T> & t2) returns the contraction $t1_{\mu\nu} t2^{\mu\nu}$.

(p) Function inline T contrd(const D4T<T> & t1,const D4T<double> & t2) returns the tensor contraction $t1_{\mu\nu}t2^{\mu\nu}$ with the second tensor being of the type double.

(q) Function inline T contrd(const D4T<T> & t1,const D4T<double> & t2) returns the tensor contraction $t1_{\mu\nu}t2^{\mu\nu}$ with the second tensor being of the type complex.

(r) Function inline void transp() transposes the tensor.

(s) Function inline void hermit() transposes the tensor and Hermitian conjugates its elements (type DM only!).

These classes are used to construct all codes from the free nucleon case to full atomic nucleus.

I.1 Basic code functionalities for scattering off free nucleon and deuteron

We have put cross section calculation both for scattering off free nucleon and deuteron into one program. The main global variables are:

- `chan`

  chooses the interaction channel:

  1. $\nu_l p \to l^- p \pi^+$
  2. $\nu_l n \to l^- p \pi^0$
  3. $\nu_l n \to l^- n \pi^+$

- `dyn`

  chooses dynamical model. Set to 1 for resonant process only and 8 for full $\Delta+$ background calculation.

- `DELTAMOD`

  chooses description of the Δ width and propagator. Set 0 for default relativistic width and on-shell propagator (Eqs. (6.41, 6.32)) and 1 for Manley-Saleski width and off-shell propagator (Eqs. (6.46, 6.47)).

- `FN`

  chooses the nonresonant background model. Set 0 for HNV model (Ref. [46]) and 1 for Fogli-Nardulli model (Ref. [48]).

- `PARA`

  chooses the parameterization of Δ axial form factors with all constants stored in the global table PARAMZ together with a complex phase η between Δ and background. Most common choices allow for changes of $C_5^A(0)$ and $M_{A\Delta}$:

  1. $C_5^A(Q^2) = \frac{C_5^A(0)}{(1+Q^2/\mathrm{PARAMZ}[0]^2)^2}$, $\eta = \exp(\mathrm{iPARAMZ}[1])$.
  2. $C_5^A(Q^2) = \frac{\mathrm{PARAMZ}[1]}{(1+Q^2/\mathrm{PARAMZ}[0]^2)^2}$, $\eta = \exp(\mathrm{iPARAMZ}[2])$.

I.1.1 Basic functions for scattering off free nucleon

List of functions returning cross sections used in scattering off free nucleon:

- Function

```
 double dsigma_dq0_dQ2_pars1_(const double &E,const double &q0,
const double &Q2)
```

returns the differential cross section $\frac{d^2\sigma}{dQ^2dq^0}$. It takes the neutrino energy, energy transfer q^0, Q^2. Firstly it checks, whether the $s = W^2$ is in acceptable limits (above the pion production threshold and below cut). Then it calculates the leptonic kinematics and initializes the leptonic tensor. The reduced matrix elements of weak charged current of nucleon, S_{11}, P_{11} and D_{13} resonances are as well constructed here, because they depend only on the 4-momentum transfer.
The function calculates the integral over $\cos(\Theta_\pi)$ w.r.t. momentum transfer direction) as well as all form factor sets, allowing for changes in the Δ form factor parameterizations.

- Function

```
double dsigma_dW_dQ2_(const double &E,const double &W,const double &Q2)
```

calculates the double differential cross section $\frac{d\sigma}{dQ^2dW}$. It calculates the *Delta* form factors and returns $W/M \cdot \frac{d^2\sigma}{dQ^2dq^0}$. It's a simple Jacobian multiplied previous function. One can obtain also a single differential cross section w.r.t. invariant mass W by integrating the $\frac{d\sigma}{dQ^2dW}$ over Q^2. Limits:

$$\begin{aligned}
W_{\nu N}^2 &= M^2 + 2ME \\
E_\nu^{cm} &= \frac{W_{\nu N}^2 - M^2}{2W_{\nu N}} \\
E_\mu^{cm} &= \frac{W_{\nu N}^2 - M^2 + m_\mu^2}{2W_{\nu N}} \\
Q_{min}^2 &= -m_\mu^2 + 2E_\nu^{cm}(E_\mu^{cm} - \sqrt{(E_\mu^{cm})^2 - m_\mu^2})) \\
Q_{max_0}^2 &= -m_\mu^2 + 2E_\nu^{cm}(E_\mu^{cm} + \sqrt{(E_\mu^{cm})^2 - m_\mu^2})) \qquad \text{(I.1)}
\end{aligned}$$

The *cm* index denotes here the neutrino-nucleon CMS system. In the loop one also checks, whether the maximal Q^2 is allowed a the given W^2. One uses the formula for W^2 and assumes the energy transfer to have the biggest possible value $q_{max}^0 \approx E - m_\mu$.

$$Q_{max_1}^2 = 2M(E - m_\mu) + M^2 - s; \qquad \text{(I.2)}$$

Smaller of these two maxima is taken as the integration limit.

- Function

```
double dsigma_dQ2_(const double &Energy,const double &Q2)
```

calculates the differential cross section $\frac{d\sigma(E)}{dQ^2}$.

- Function

  ```
  double dsigma_dQ2_ANL_REST( const double &Q2)
  ```

  calculates the differential cross section $\frac{d\sigma}{dQ^2}$ averaged over the ANL beam profile.

- Function

  ```
  double sigma_(const double &Energy)
  ```

  calculates the total cross section in the function of neutrino energy.

- Function

  ```
  double dsigma_dW_ANL_REST(const double &W)
  ```

  calculates the differential cross section $\frac{d\sigma}{W}$ averaged over the ANL beam profile.

I.1.2 Basic functions for scattering off deuteron

List of functions returning cross sections used in scattering off free nucleon:

- Function

  ```
  dsigma_dQ2_ANL_NEW(const double &Q2)
  ```

  calculates the ANL fluxed-averaged $\frac{d\sigma}{dQ^2}$ for neutrino scattering off deuteron with ANL kinematic cuts using GSL Vegas integration routine.

I.2 Basic code functionalities for scattering off atomic nuclei

There exist two versions of this code. First one hase been developed to calculate lepton-nucleus cros sections using the Gaussian integration technique and approximation given by Eq. (6.131). It calculates also the resonant part of cross section within the Oset model of Δ self-energy in nuclear matter given by Eq. (6.128). The second code uses the GSL Monte Carlo routines to integrate all cross sections "exactly".

I.2.1 Basic functions for approximate calculation

Here we have used object programming, generating class nucleus. Basic methods are:

- Constructor

  ```
  nucleus(unsigned int np, unsigned int  nn, double b)
  ```

  creates a nucleus with np protons and nn neutrons and mean binding energy b. It chooses LDA parameters from tables, normalizes nucleon density profiles and calculates mean Fermi momentum.

- Method

  ```
  inline void set_lepton_mass(unsigned int i)
  ```

  sets lepton mass: i=0-electron (massless), i=1-muon, i=2-taon.

- Method

  ```
  inline void set_charged_pi(bool i)
  ```

  sets pion charge from Δ decay in Eq. (6.128).

- Method

  ```
  inline void set_virt_pi_ff(bool i){virt_pi_ff=i;}
  ```

  turns on and off the virtual pion form factor given by Eq. (6.28).

- Method

  ```
  inline void set_DM(bool i){DELTAMOD=i;}
  ```

  chooses description of the Δ width and propagator. Set 0 for default relativistic width and on-shell propagator (Eqs. (6.41, 6.32)) and 1 for Manley-Saleski width and off-shell propagator (Eqs. (6.46, 6.47)).

- Method

  ```
  inline void set_dynamics(unsigned int i)
  ```

  sets the dynamical interaction channel. In case of quasielastic scattering one sets 1000 for electron, 2000 for neutrino and 3000 for antineutrino interaction. In case of Δ excitation from Eq. (6.128) one chooses channel codes from Tab. 9. In case of SPP

Table 9: Available dynamical channels for Δ resonance production with Eq. (6.128):

dynamics	channel
1096/2096/3096	$e/\nu/\overline{\nu}N \to \Delta \to N\pi$
1097/2097/3097	$e/\nu/\overline{\nu}N \to \Delta \to 2p2h$
1098/2098/3098	$e/\nu/\overline{\nu}N \to \Delta \to 3p3h$
1099/2099/3099	$e/\nu/\overline{\nu}N \to \Delta \to anything$

calculated with Eq. (6.131) one can use channel codes given in Tab. 10).

- Method

  ```
  double nucleus::d3sigma_dOmega_deprime(const double &E,
  const double &Eprime,const double &coslep)
  ```

Table 10: Available dynamical channels for SPP with Eq. (6.131):

dynamics	channel	Δ medium effects
1010	$e^-N \to N\pi^0$ resonant	off
1011	$e^-p \to n\pi^+$ resonant	off
1012	$e^-n \to p\pi^-$ resonant	off
1015	$e^-N \to N\pi^0$ resonant	on
1016	$e^-p \to n\pi^+$ resonant	on
1017	$e^-n \to p\pi^-$ resonant	on
1080	$e^-N \to N\pi^0$ full HNV	off
1081	$e^-p \to n\pi^+$ full HNV	off
1082	$e^-n \to p\pi^-$ full HNV	off
1090	$e^-N \to N\pi^0$ full HNV	on
1091	$e^-p \to n\pi^+$ full HNV	on
1092	$e^-n \to p\pi^-$ full HNV	on
2010	$\nu_l p \to l^- p\pi^+$ resonant	off
2011	$\nu_l n \to l^- p\pi^0$ resonant	off
2012	$\nu_l n \to l^- n\pi^+$ resonant	off
2016	$\nu_l p \to l^- p\pi^+$ resonant	on
2017	$\nu_l n \to l^- p\pi^0$ resonant	on
2018	$\nu_l n \to l^- n\pi^+$ resonant	on
2080	$\nu_l p \to l^- p\pi^+$ full HNV	off
2081	$\nu_l n \to l^- p\pi^0$ full HNV	off
2082	$\nu_l n \to l^- n\pi^+$ full HNV	off
2090	$\nu_l p \to l^- p\pi^+$ full HNV	on
2091	$\nu_l n \to l^- p\pi^0$ full HNV	on
2092	$\nu_l n \to l^- n\pi^+$ full HNV	on
3010	$\overline{\nu}_l n \to l^+ n\pi^-$ resonant	off
3011	$\overline{\nu}_l p \to l^+ n\pi^0$ resonant	off
3012	$\overline{\nu}_l p \to l^+ p\pi^-$ resonant	off
3016	$\overline{\nu}_l n \to l^+ n\pi^-$ resonant	on
3017	$\overline{\nu}_l p \to l^+ n\pi^0$ resonant	on
3018	$\overline{\nu}_l p \to l^+ p\pi^-$ resonant	on
3080	$\overline{\nu}_l n \to l^+ n\pi^-$ full HNV	off
3081	$\overline{\nu}_l p \to l^+ n\pi^0$ full HNV	off
3082	$\overline{\nu}_l p \to l^+ p\pi^-$ full HNV	off
3090	$\overline{\nu}_l n \to l^+ n\pi^-$ full HNV	on
3091	$\overline{\nu}_l p \to l^+ n\pi^0$ full HNV	on
3092	$\overline{\nu}_l p \to l^+ p\pi^-$ full HNV	on

returns the double differential cross section for scattering of lepton with energy E off nucleus with outgoing lepton energy Eprime and cosine of scattering angle coslep.

- Method

  `double nucleus::dsigma_deprime(const double &E,const double &Eprime)`

  returns the differential cross section for scattering of lepton with energy E off nucleus with outgoing lepton energy Eprime. Use only with neutrinos.

- Method

  `double nucleus::sigma(const double &E)`

  returns the total cross section for scattering of lepton with energy E off nucleus. Use only with neutrinos.

I.2.2 Basic functions for MC integration

This code calculates SPP cross sections using GSL Vegas routines. Basic functions are:

- `void set_nucleus(unsigned int np, unsigned int  nn)`

  calculates all density normalizations and bindings (Q-values) for chosen nucleus with np protons and nn neutrons.

- `void set_steps(unsigned int i)`

  sets the number of Vegas steps to i.

- `set_dynamics(bool lept, int typ, bool ant, unsigned int dyn, bool prot, bool charged, bool piff,bool _2nd, bool dm)`

  sets the dynamical channel:

  - lept: set 0 for electron, 1 for neutrino
  - typ: set 0 for electron, 1 for muon, 2 for taon
  - ant: set 0 for particle, 1 for antiparticle (antineutrinos).
  - dyn: choose dynamics. Set 10 for resonant pion production with no Δ in-medium effects, 11 for resonant pion production with Δ medium effects, 12, 13 for $\delta \to 2p2h$ and $\Delta \to 3p3h$ decays, 14 for any pionless Δ decay, 16 for full HNV model SPP without Δ self-energy and 17 for full HNV model SPP with Δ self-energy.
  - prot: 1 for scattering off proton and 0 for neutron.
  - charged: 1 for charged pion production and 0 for neutral pion production.
  - piff: turns on and off the virtual pion form factor given by Eq. (6.28).
  - 2nd: turn on and off the second resonance region
  - dm: chooses description of the Δ width and propagator. Set 0 for default relativistic width and on-shell propagator (Eqs. (6.41, 6.32)) and 1 for Manley-Saleski width and off-shell propagator (Eqs. (6.46, 6.47)).

- `void d3sigma_dq0_domega_a(double En, double Etr, double Theta)`

  calculates the double differential cross section for lepton with energy En, energy transfer Etr and angle Theta (in degree). Result and error estimate are written in global variables RESULT and ERROR.

- `void sigma_a(double En)`

  calculates the total cross section for lepton with energy En. Result and error estimate are written in global variables RESULT and ERROR.

J Total SPP cross section tables for ^{12}C

In this section we show our results for different neutrino flavors scattering off ^{12}C calculated in section 6.4 (Tab. 11-14). Cross sections are divided according to the final pion isospin channels and nuclear target modeling starting from free nucleons ($6p + 6n$), through Fermi motion and Pauli blocking effects ($FM + PB$) up to full medium effects considered in this thesis ($\Delta\, in - medium$). We give the results both for the full model and resonant SPP contribution only. All of the results are given in the units of [10^{-38}cm^2].

Table 11: Total cross sections in the $^{12}C(\nu_e, e^-)$ scattering in $10^{-38} cm^2$.

E_ν GeV	6p+6n Free				Fermi Motion + PB				Full Δ In-Medium				
	Resonant		+Background		Resonant		+Background		Resonant		+Background		
	π^+	π^0	π^+	π^0	π^+	π^0	π^+	π^0	π^+	π^0	π^+	π^0	$\Delta_{pionless}$
0.40	0.2274	0.0455	0.3440	0.0888	0.3153	0.0631	0.4183	0.0902	0.1675	0.0335	0.2522	0.0559	0.1412
0.45	0.4797	0.0959	0.6666	0.1646	0.6063	0.1213	0.7647	0.1646	0.3313	0.0663	0.4664	0.1038	0.2126
0.50	0.8124	0.1625	1.0674	0.2569	0.9605	0.1921	1.1667	0.2516	0.5430	0.1086	0.7304	0.1619	0.2902
0.55	1.1980	0.2396	1.5122	0.3581	1.3463	0.2693	1.5886	0.3429	0.7868	0.1574	1.0167	0.2263	0.3682
0.60	1.6110	0.3222	1.9725	0.4625	1.7449	0.3490	2.0095	0.4353	1.0477	0.2095	1.3132	0.2924	0.4429
0.65	2.0309	0.4062	2.4282	0.5658	2.1329	0.4266	2.4188	0.5223	1.3137	0.2627	1.6094	0.3560	0.5120
0.70	2.4433	0.4886	2.8661	0.6657	2.5106	0.5021	2.7844	0.6051	1.5759	0.3152	1.8882	0.4209	0.5745
0.75	2.8379	0.5676	3.2785	0.7605	2.8616	0.5723	3.1523	0.6821	1.8282	0.3656	2.1566	0.4794	0.6297
0.80	3.2100	0.6420	3.6634	0.8499	3.1820	0.6364	3.4548	0.7500	2.0667	0.4133	2.4046	0.5338	0.6781
0.85	3.5570	0.7114	4.0200	0.9338	3.4779	0.6956	3.7404	0.8164	2.2895	0.4579	2.6318	0.5875	0.7199
0.90	3.8767	0.7753	4.3482	1.0121	3.7432	0.7486	3.9988	0.8747	2.4956	0.4991	2.8464	0.6358	0.7559
0.95	4.1701	0.8340	4.6508	1.0854	3.9876	0.7975	4.2507	0.9261	2.6859	0.5372	3.0413	0.6764	0.7868
1.00	4.4394	0.8879	4.9315	1.1544	4.2180	0.8436	4.4820	0.9822	2.8609	0.5722	3.2119	0.7188	0.8131

Table 12: Total cross sections in the $^{12}C(\overline{\nu}_e, e^+)$ scattering in $10^{-38} cm^2$.

E_ν GeV	6p+6n Free				Fermi Motion + PB				Full Δ In-Medium				
	Resonant		+Background		Resonant		+Background		Resonant		+Background		
	π^-	π^0	π^-	π^0	π^-	π^0	π^-	π^0	π^-	π^0	π^-	π^0	$\Delta_{pionless}$
0.40	0.0475	0.0095	0.0836	0.0305	0.0555	0.0111	0.0848	0.0226	0.0290	0.0058	0.0545	0.0167	0.0216
0.45	0.0914	0.0183	0.1476	0.0516	0.1023	0.0205	0.1474	0.0396	0.0551	0.0110	0.0960	0.0292	0.0322
0.50	0.1460	0.0292	0.2245	0.0772	0.1597	0.0319	0.2227	0.0605	0.0891	0.0178	0.1475	0.0452	0.0442
0.55	0.2088	0.0418	0.3118	0.1065	0.2252	0.0450	0.3067	0.0844	0.1301	0.0260	0.2077	0.0638	0.0573
0.60	0.2786	0.0557	0.4079	0.1391	0.2992	0.0598	0.3995	0.1110	0.1776	0.0355	0.2763	0.0849	0.0713
0.65	0.3542	0.0708	0.5119	0.1745	0.3759	0.0752	0.4997	0.1398	0.2309	0.0462	0.3528	0.1078	0.0859
0.70	0.4351	0.0870	0.6231	0.2124	0.4630	0.0926	0.6075	0.1702	0.2893	0.0579	0.4350	0.1329	0.1010
0.75	0.5205	0.1041	0.7409	0.2525	0.5515	0.1103	0.7199	0.2011	0.3522	0.0704	0.5246	0.1598	0.1163
0.80	0.6098	0.1220	0.8648	0.2945	0.6416	0.1283	0.8391	0.2354	0.4191	0.0838	0.6192	0.1879	0.1316
0.85	0.7025	0.1405	0.9945	0.3382	0.7392	0.1478	0.9624	0.2689	0.4890	0.0978	0.7205	0.2164	0.1470
0.90	0.7980	0.1596	1.1295	0.3835	0.8359	0.1672	1.0959	0.3064	0.5613	0.1123	0.8286	0.2475	0.1623
0.95	0.8957	0.1791	1.2697	0.4301	0.9342	0.1868	1.2316	0.3407	0.6358	0.1272	0.9393	0.2788	0.1775
1.00	0.9953	0.1991	1.4147	0.4780	1.0378	0.2076	1.3656	0.3795	0.7121	0.1424	1.0583	0.3108	0.1924

Table 13: Total cross sections in the $^{12}C(\nu_\mu, \mu^-)$ scattering in $10^{-38} cm^2$.

E_ν GeV	6p+6n Free				Fermi Motion + PB				Full Δ In-Medium				
	Resonant		+Background		Resonant		+Background		Resonant		+Background		
	π^+	π^0	π^+	π^0	π^+	π^0	π^+	π^0	π^+	π^0	π^+	π^0	$\Delta_{pionless}$
0.40	0.0276	0.0055	0.0635	0.0202	0.0677	0.0135	0.1102	0.0228	0.0388	0.0078	0.0717	0.0153	0.0721
0.45	0.1378	0.0276	0.2406	0.0658	0.2528	0.0506	0.3538	0.0749	0.1316	0.0263	0.2107	0.0458	0.1317
0.50	0.4078	0.0816	0.6007	0.1507	0.5576	0.1115	0.7228	0.1545	0.2981	0.0596	0.4348	0.0956	0.2063
0.55	0.7792	0.1558	1.0495	0.2531	0.9331	0.1866	1.1481	0.2480	0.5197	0.1039	0.7122	0.1573	0.2869
0.60	1.1890	0.2378	1.5195	0.3594	1.3370	0.2674	1.5934	0.3425	0.7725	0.1545	1.0116	0.2244	0.3667
0.65	1.6128	0.3226	1.9897	0.4655	1.7418	0.3484	2.0115	0.4358	1.0382	0.2076	1.3167	0.2904	0.4417
0.70	2.0407	0.4081	2.4533	0.5704	2.1309	0.4262	2.4195	0.5230	1.3044	0.2609	1.6114	0.3554	0.5099
0.75	2.4628	0.4926	2.8998	0.6718	2.4985	0.4997	2.7860	0.6017	1.5630	0.3126	1.8779	0.4188	0.5705
0.80	2.8594	0.5719	3.3103	0.7660	2.8390	0.5678	3.1156	0.6740	1.8092	0.3618	2.1372	0.4754	0.6238
0.85	3.2263	0.6453	3.6856	0.8534	3.1519	0.6304	3.4359	0.7380	2.0404	0.4081	2.3644	0.5294	0.6700
0.90	3.5642	0.7128	4.0292	0.9346	3.4382	0.6876	3.6895	0.8048	2.2549	0.4510	2.5930	0.5776	0.7098
0.95	3.8729	0.7746	4.3429	1.0099	3.6954	0.7391	3.9564	0.8624	2.4532	0.4906	2.7903	0.6250	0.7439
1.00	4.1546	0.8309	4.6309	1.0804	3.9245	0.7849	4.1873	0.9113	2.6352	0.5270	2.9678	0.6661	0.7730

Table 14: Total cross sections in the $^{12}C(\overline{\nu}_\mu, \mu^+)$ scattering in $10^{-38} cm^2$.

E_ν GeV	6p+6n Free				Fermi Motion + PB				Full Δ In-Medium				
	Resonant		+Background		Resonant		+Background		Resonant		+Background		
	π^-	π^0	π^-	π^0	π^-	π^0	π^-	π^0	π^-	π^0	π^-	π^0	$\Delta_{pionless}$
0.40	0.0049	0.0010	0.0173	0.0097	0.0076	0.0015	0.0186	0.0059	0.0045	0.0009	0.0141	0.0052	0.0079
0.45	0.0212	0.0042	0.0495	0.0223	0.0291	0.0058	0.0533	0.0159	0.0150	0.0030	0.0361	0.0126	0.0146
0.50	0.0587	0.0117	0.1082	0.0423	0.0673	0.0135	0.1084	0.0315	0.0351	0.0070	0.0715	0.0240	0.0240
0.55	0.1089	0.0218	0.1812	0.0671	0.1193	0.0239	0.1794	0.0514	0.0645	0.0129	0.1189	0.0390	0.0354
0.60	0.1649	0.0330	0.2622	0.0952	0.1817	0.0363	0.2614	0.0748	0.1020	0.0204	0.1765	0.0568	0.0483
0.65	0.2286	0.0457	0.3545	0.1271	0.2530	0.0506	0.3546	0.1009	0.1469	0.0294	0.2432	0.0774	0.0624
0.70	0.3058	0.0612	0.4643	0.1638	0.3310	0.0662	0.4531	0.1286	0.1981	0.0396	0.3167	0.1000	0.0773
0.75	0.3968	0.0794	0.5887	0.2042	0.4151	0.0830	0.5619	0.1597	0.2550	0.0510	0.3996	0.1244	0.0927
0.80	0.4902	0.0980	0.7148	0.2458	0.5036	0.1007	0.6748	0.1913	0.3166	0.0633	0.4871	0.1509	0.1083
0.85	0.5841	0.1168	0.8425	0.2883	0.5962	0.1192	0.7937	0.2237	0.3823	0.0765	0.5811	0.1783	0.1241
0.90	0.6793	0.1359	0.9734	0.3321	0.6922	0.1384	0.9189	0.2578	0.4512	0.0902	0.6796	0.2079	0.1398
0.95	0.7762	0.1552	1.1083	0.3771	0.7901	0.1580	1.0436	0.2936	0.5229	0.1046	0.7845	0.2372	0.1555
1.00	0.8746	0.1749	1.2471	0.4232	0.8896	0.1779	1.1769	0.3287	0.5965	0.1193	0.8926	0.2685	0.1709

Table 15: Total cross sections in the $C(\nu_e, e^-) + 2p(\nu_e, e^-)$ scattering in $10^{-38} cm^2$.

E_ν GeV	8p+6n Free				Fermi Motion + PB				Full Δ In-Medium				
	Resonant		+Background		Resonant		+Background		Resonant		+Background		
	π^+	π^0	π^+	π^0	π^+	π^0	π^+	π^0	π^+	π^0	π^+	π^0	$\Delta_{pionless}$
0.40	0.2957	0.0455	0.4476	0.0888	0.3835	0.0631	0.5219	0.0902	0.2357	0.0335	0.3557	0.0559	0.1412
0.45	0.6236	0.0959	0.8669	0.1646	0.7502	0.1213	0.9649	0.1646	0.4752	0.0663	0.6667	0.1038	0.2126
0.50	1.0561	0.1625	1.3875	0.2569	1.2042	0.1921	1.4866	0.2516	0.7867	0.1086	1.0504	0.1619	0.2902
0.55	1.5574	0.2396	1.9645	0.3581	1.7057	0.2693	2.0409	0.3429	1.1462	0.1574	1.4691	0.2263	0.3682
0.60	2.0942	0.3222	2.5614	0.4625	2.2282	0.3490	2.5984	0.4353	1.5310	0.2095	1.9021	0.2924	0.4429
0.65	2.6402	0.4062	3.1515	0.5658	2.7422	0.4266	3.1422	0.5223	1.9230	0.2627	2.3327	0.3560	0.5120
0.70	3.1763	0.4886	3.7182	0.6657	3.2436	0.5021	3.6365	0.6051	2.3089	0.3152	2.7403	0.4209	0.5745
0.75	3.6893	0.5676	4.2513	0.7605	3.7130	0.5723	4.1251	0.6821	2.6795	0.3656	3.1293	0.4794	0.6297
0.80	4.1730	0.6420	4.7482	0.8499	4.1450	0.6364	4.5396	0.7500	3.0297	0.4133	3.4894	0.5338	0.6781
0.85	4.6242	0.7114	5.2080	0.9338	4.5450	0.6956	4.9283	0.8164	3.3566	0.4579	3.8198	0.5875	0.7199
0.90	5.0397	0.7753	5.6304	1.0121	4.9062	0.7486	5.2810	0.8747	3.6586	0.4991	4.1285	0.6358	0.7559
0.95	5.4211	0.8340	6.0192	1.0854	5.2386	0.7975	5.6191	0.9261	3.9369	0.5372	4.4096	0.6764	0.7868
1.00	5.7712	0.8879	6.3791	1.1544	5.5498	0.8436	5.9295	0.9822	4.1927	0.5722	4.6595	0.7188	0.8131

Table 16: Total cross sections in the $^{12}C(\overline{\nu}_e, e^+) + 2p(\overline{\nu}_e, e^+)$ scattering in $10^{-38} cm^2$.

E_ν GeV	8p+6n Free				Fermi Motion + PB				Full Δ In-Medium				
	Resonant		+Background		Resonant		+Background		Resonant		+Background		
	π^-	π^0	π^-	π^0	π^-	π^0	π^-	π^0	π^-	π^0	π^-	π^0	$\Delta_{pionless}$
0.40	0.0491	0.0095	0.0886	0.0305	0.0571	0.0111	0.0897	0.0226	0.0306	0.0058	0.0595	0.0167	0.0216
0.45	0.0945	0.0183	0.1562	0.0516	0.1053	0.0205	0.1559	0.0396	0.0581	0.0110	0.1045	0.0292	0.0322
0.50	0.1508	0.0292	0.2377	0.0772	0.1646	0.0319	0.2360	0.0605	0.0939	0.0178	0.1605	0.0452	0.0442
0.55	0.2158	0.0418	0.3304	0.1065	0.2321	0.0450	0.3252	0.0844	0.1371	0.0260	0.2264	0.0638	0.0573
0.60	0.2878	0.0557	0.4329	0.1391	0.3084	0.0598	0.4243	0.1110	0.1869	0.0355	0.3013	0.0849	0.0713
0.65	0.3660	0.0708	0.5441	0.1745	0.3877	0.0752	0.5319	0.1398	0.2427	0.0462	0.3849	0.1078	0.0859
0.70	0.4496	0.0870	0.6634	0.2124	0.4775	0.0926	0.6478	0.1702	0.3038	0.0579	0.4753	0.1329	0.1010
0.75	0.5379	0.1041	0.7903	0.2525	0.5689	0.1103	0.7694	0.2011	0.3696	0.0704	0.5739	0.1598	0.1163
0.80	0.6302	0.1220	0.9243	0.2945	0.6619	0.1283	0.8986	0.2354	0.4394	0.0838	0.6787	0.1879	0.1316
0.85	0.7259	0.1405	1.0651	0.3382	0.7627	0.1478	1.0332	0.2689	0.5124	0.0978	0.7911	0.2164	0.1470
0.90	0.8246	0.1596	1.2124	0.3835	0.8625	0.1672	1.1788	0.3064	0.5879	0.1123	0.9115	0.2475	0.1623
0.95	0.9256	0.1791	1.3659	0.4301	0.9640	0.1868	1.3277	0.3407	0.6656	0.1272	1.0355	0.2788	0.1775
1.00	1.0285	0.1991	1.5255	0.4780	1.0709	0.2076	1.4763	0.3795	0.7453	0.1424	1.1690	0.3108	0.1924

Table 17: Total cross sections in the $^{12}C(\nu_\mu, \mu^-) + 2p(\nu_\mu, \mu^-)$ scattering in $10^{-38} cm^2$.

E_ν GeV	8p+6n Free				Fermi Motion + PB				Full Δ In-Medium				
	Resonant		+Background		Resonant		+Background		Resonant		+Background		
	π^+	π^0	π^+	π^0	π^+	π^0	π^+	π^0	π^+	π^0	π^+	π^0	$\Delta_{pionless}$
0.40	0.0359	0.0055	0.0823	0.0202	0.0760	0.0135	0.1290	0.0228	0.0471	0.0078	0.0905	0.0153	0.0721
0.45	0.1791	0.0276	0.3129	0.0658	0.2941	0.0506	0.4261	0.0749	0.1729	0.0263	0.2829	0.0458	0.1317
0.50	0.5302	0.0816	0.7813	0.1507	0.6799	0.1115	0.9035	0.1545	0.4204	0.0596	0.6153	0.0956	0.2063
0.55	1.0129	0.1558	1.3644	0.2531	1.1669	0.1866	1.4631	0.2480	0.7534	0.1039	1.0271	0.1573	0.2869
0.60	1.5456	0.2378	1.9743	0.3594	1.6936	0.2674	2.0480	0.3425	1.1292	0.1545	1.4663	0.2244	0.3667
0.65	2.0967	0.3226	2.5838	0.4655	2.2257	0.3484	2.6056	0.4358	1.5220	0.2076	1.9108	0.2904	0.4417
0.70	2.6529	0.4081	3.1843	0.5704	2.7431	0.4262	3.1504	0.5230	1.9166	0.2609	2.3424	0.3554	0.5099
0.75	3.2017	0.4926	3.7621	0.6718	3.2373	0.4997	3.6482	0.6017	2.3019	0.3126	2.7402	0.4188	0.5705
0.80	3.7172	0.5719	4.2926	0.7660	3.6968	0.5678	4.0979	0.6740	2.6670	0.3618	3.1195	0.4754	0.6238
0.85	4.1942	0.6453	4.7772	0.8534	4.1198	0.6304	4.5275	0.7380	3.0083	0.4081	3.4559	0.5294	0.6700
0.90	4.6335	0.7128	5.2201	0.9346	4.5074	0.6876	4.8803	0.8048	3.3242	0.4510	3.7840	0.5776	0.7098
0.95	5.0347	0.7746	5.6238	1.0099	4.8573	0.7391	5.2375	0.8624	3.6151	0.4906	4.0714	0.6250	0.7439
1.00	5.4010	0.8309	5.9938	1.0804	5.1708	0.7849	5.5501	0.9113	3.8816	0.5270	4.3308	0.6661	0.7730

Table 18: Total cross sections in the $^{12}C(\overline{\nu}_\mu, \mu^+) + 2p(\overline{\nu}_\mu, \mu^+)$ scattering in $10^{-38} cm^2$.

E_ν GeV	8p+6n Free				Fermi Motion + PB				Full Δ In-Medium				
	Resonant		+Background		Resonant		+Background		Resonant		+Background		
	π^-	π^0	π^-	π^0	π^-	π^0	π^-	π^0	π^-	π^0	π^-	π^0	$\Delta_{pionless}$
0.40	0.0051	0.0010	0.0188	0.0097	0.0077	0.0015	0.0199	0.0059	0.0046	0.0009	0.0156	0.0052	0.0079
0.45	0.0219	0.0042	0.0531	0.0223	0.0298	0.0058	0.0569	0.0159	0.0157	0.0030	0.0397	0.0126	0.0146
0.50	0.0607	0.0117	0.1153	0.0423	0.0692	0.0135	0.1154	0.0315	0.0371	0.0070	0.0786	0.0240	0.0240
0.55	0.1125	0.0218	0.1926	0.0671	0.1229	0.0239	0.1907	0.0514	0.0681	0.0129	0.1304	0.0390	0.0354
0.60	0.1704	0.0330	0.2789	0.0952	0.1872	0.0363	0.2781	0.0748	0.1075	0.0204	0.1932	0.0568	0.0483
0.65	0.2362	0.0457	0.3773	0.1271	0.2606	0.0506	0.3774	0.1009	0.1545	0.0294	0.2659	0.0774	0.0624
0.70	0.3160	0.0612	0.4943	0.1638	0.3412	0.0662	0.4832	0.1286	0.2083	0.0396	0.3467	0.1000	0.0773
0.75	0.4100	0.0794	0.6271	0.2042	0.4283	0.0830	0.6002	0.1597	0.2682	0.0510	0.4379	0.1244	0.0927
0.80	0.5065	0.0980	0.7624	0.2458	0.5200	0.1007	0.7226	0.1913	0.3329	0.0633	0.5347	0.1509	0.1083
0.85	0.6035	0.1168	0.9001	0.2883	0.6157	0.1192	0.8514	0.2237	0.4018	0.0765	0.6388	0.1783	0.1241
0.90	0.7020	0.1359	1.0418	0.3321	0.7149	0.1384	0.9874	0.2578	0.4739	0.0902	0.7481	0.2079	0.1398
0.95	0.8021	0.1552	1.1885	0.3771	0.8160	0.1580	1.1239	0.2936	0.5488	0.1046	0.8647	0.2372	0.1555
1.00	0.9038	0.1749	1.3401	0.4232	0.9188	0.1779	1.2699	0.3287	0.6257	0.1193	0.9856	0.2685	0.1709

Table 19: Total cross sections in the $^{12}C(\nu_e, e^-)$ scattering in $10^{-38} cm^2$. M-S width.

E_ν GeV	6p+6n Free				Fermi Motion + PB				Full Δ In-Medium				
	Resonant		+Background		Resonant		+Background		Resonant		+Background		
	π^+	π^0	π^+	π^0	π^+	π^0	π^+	π^0	π^+	π^0	π^+	π^0	$\Delta_{pionless}$
0.40	0.2504	0.0501	0.3703	0.0936	0.3455	0.0691	0.4521	0.0965	0.1876	0.0375	0.2767	0.0607	0.1369
0.45	0.5150	0.1030	0.7040	0.1712	0.6526	0.1305	0.8094	0.1742	0.3638	0.0728	0.5049	0.1112	0.2080
0.50	0.8630	0.1726	1.1161	0.2649	1.0249	0.2050	1.2233	0.2630	0.5913	0.1183	0.7814	0.1726	0.2875
0.55	1.2661	0.2532	1.5701	0.3670	1.4309	0.2862	1.6577	0.3560	0.8538	0.1708	1.0865	0.2395	0.3698
0.60	1.6968	0.3394	2.0358	0.4711	1.8479	0.3696	2.0892	0.4504	1.1348	0.2270	1.3971	0.3089	0.4506
0.65	2.1334	0.4267	2.4915	0.5729	2.2555	0.4511	2.4954	0.5368	1.4209	0.2842	1.6987	0.3751	0.5271
0.70	2.5600	0.5120	2.9237	0.6699	2.6471	0.5294	2.8534	0.6187	1.7019	0.3404	1.9880	0.4387	0.5974
0.75	2.9660	0.5932	3.3247	0.7605	3.0099	0.6020	3.2237	0.6956	1.9706	0.3941	2.2550	0.4990	0.6607
0.80	3.3458	0.6692	3.6923	0.8445	3.3410	0.6682	3.5233	0.7606	2.2227	0.4445	2.4919	0.5544	0.7168
0.85	3.6967	0.7393	4.0263	0.9219	3.6432	0.7286	3.7749	0.8238	2.4560	0.4912	2.7155	0.6038	0.7661
0.90	4.0172	0.8034	4.3279	0.9930	3.9128	0.7826	4.0272	0.8764	2.6695	0.5339	2.9101	0.6493	0.8089
0.95	4.3081	0.8616	4.6000	1.0583	4.1542	0.8308	4.2522	0.9313	2.8638	0.5728	3.0791	0.6917	0.8460
1.00	4.5712	0.9142	4.8463	1.1186	4.3726	0.8745	4.4506	0.9758	3.0392	0.6078	3.2406	0.7318	0.8778

Table 20: Total cross sections in the $^{12}C(\overline{\nu}_e, e^+)$ scattering in $10^{-38} cm^2$. M-S width

E_ν GeV	6p+6n Free				Fermi Motion + PB				Full Δ In-Medium				
	Resonant		+Background		Resonant		+Background		Resonant		+Background		
	π^-	π^0	π^-	π^0	π^-	π^0	π^-	π^0	π^-	π^0	π^-	π^0	$\Delta_{pionless}$
0.40	0.0509	0.0102	0.0849	0.0294	0.0643	0.0129	0.0915	0.0234	0.0348	0.0070	0.0594	0.0171	0.0262
0.45	0.0960	0.0192	0.1487	0.0498	0.1153	0.0231	0.1574	0.0408	0.0636	0.0127	0.1027	0.0299	0.0383
0.50	0.1522	0.0304	0.2253	0.0747	0.1764	0.0353	0.2346	0.0617	0.1001	0.0200	0.1555	0.0457	0.0522
0.55	0.2168	0.0434	0.3118	0.1030	0.2447	0.0489	0.3185	0.0852	0.1429	0.0286	0.2170	0.0640	0.0674
0.60	0.2881	0.0576	0.4062	0.1343	0.3195	0.0639	0.4105	0.1110	0.1911	0.0382	0.2832	0.0847	0.0835
0.65	0.3650	0.0730	0.5076	0.1681	0.3975	0.0795	0.5058	0.1371	0.2437	0.0487	0.3574	0.1070	0.1002
0.70	0.4465	0.0893	0.6148	0.2039	0.4818	0.0964	0.6098	0.1674	0.3002	0.0600	0.4348	0.1307	0.1173
0.75	0.5316	0.1063	0.7273	0.2414	0.5670	0.1134	0.7160	0.1965	0.3596	0.0719	0.5191	0.1554	0.1347
0.80	0.6198	0.1240	0.8446	0.2805	0.6537	0.1307	0.8302	0.2268	0.4216	0.0843	0.6070	0.1813	0.1522
0.85	0.7103	0.1421	0.9662	0.3207	0.7442	0.1488	0.9414	0.2581	0.4853	0.0971	0.6970	0.2075	0.1696
0.90	0.8023	0.1605	1.0916	0.3621	0.8343	0.1669	1.0536	0.2905	0.5504	0.1101	0.7910	0.2353	0.1869
0.95	0.8954	0.1791	1.2207	0.4043	0.9244	0.1849	1.1765	0.3222	0.6165	0.1233	0.8922	0.2631	0.2040
1.00	0.9891	0.1978	1.3532	0.4474	1.0159	0.2032	1.3014	0.3566	0.6831	0.1366	0.9921	0.2918	0.2208

Table 21: Total cross sections in the $^{12}C(\nu_\mu, \mu^-)$ scattering in $10^{-38} cm^2$. M-S width

E_ν GeV	6p+6n Free				Fermi Motion + PB				Full Δ In-Medium				
	Resonant		+Background		Resonant		+Background		Resonant		+Background		
	π^+	π^0	π^+	π^0	π^+	π^0	π^+	π^0	π^+	π^0	π^+	π^0	$\Delta_{pionless}$
0.40	0.0391	0.0078	0.0786	0.0233	0.0845	0.0169	0.1304	0.0267	0.0491	0.0098	0.0850	0.0179	0.0694
0.45	0.1642	0.0328	0.2721	0.0719	0.2827	0.0565	0.3873	0.0816	0.1517	0.0303	0.2359	0.0509	0.1261
0.50	0.4423	0.0885	0.6395	0.1577	0.6027	0.1205	0.7688	0.1640	0.3295	0.0659	0.4721	0.1030	0.1991
0.55	0.8276	0.1655	1.1000	0.2619	0.9973	0.1995	1.2120	0.2599	0.5666	0.1133	0.7647	0.1675	0.2811
0.60	1.2570	0.2514	1.5826	0.3696	1.4224	0.2845	1.6652	0.3587	0.8389	0.1678	1.0845	0.2375	0.3652
0.65	1.7014	0.3403	2.0613	0.4761	1.8488	0.3698	2.1042	0.4507	1.1262	0.2252	1.4003	0.3082	0.4467
0.70	2.1473	0.4295	2.5265	0.5797	2.2586	0.4517	2.5173	0.5398	1.4143	0.2829	1.7065	0.3742	0.5228
0.75	2.5836	0.5167	2.9674	0.6781	2.6432	0.5286	2.8716	0.6222	1.6933	0.3387	1.9866	0.4392	0.5919
0.80	2.9929	0.5986	3.3684	0.7685	2.9974	0.5995	3.2129	0.6919	1.9573	0.3915	2.2444	0.4961	0.6535
0.85	3.3688	0.6738	3.7279	0.8507	3.3194	0.6639	3.5089	0.7556	2.2031	0.4406	2.4742	0.5492	0.7077
0.90	3.7114	0.7423	4.0500	0.9255	3.6093	0.7219	3.7720	0.8191	2.4286	0.4857	2.6868	0.5991	0.7549
0.95	4.0218	0.8044	4.3383	0.9938	3.8688	0.7738	3.9892	0.8677	2.6344	0.5269	2.8730	0.6431	0.7958
1.00	4.3020	0.8604	4.5972	1.0564	4.0996	0.8199	4.2028	0.9198	2.8208	0.5642	3.0448	0.6822	0.8309

Table 22: Total cross sections in the $^{12}C(\overline{\nu}_\mu, \mu^+)$ scattering in $10^{-38} cm^2$. M-S width

E_ν GeV	6p+6n Free				Fermi Motion + PB				Full Δ In-Medium				
	Resonant		+Background		Resonant		+Background		Resonant		+Background		
	π^-	π^0	π^-	π^0	π^-	π^0	π^-	π^0	π^-	π^0	π^-	π^0	$\Delta_{pionless}$
0.40	0.0064	0.0013	0.0182	0.0092	0.0111	0.0022	0.0214	0.0062	0.0068	0.0014	0.0161	0.0054	0.0105
0.45	0.0244	0.0049	0.0511	0.0214	0.0366	0.0073	0.0594	0.0165	0.0200	0.0040	0.0402	0.0129	0.0186
0.50	0.0623	0.0125	0.1088	0.0405	0.0794	0.0159	0.1176	0.0323	0.0431	0.0086	0.0781	0.0246	0.0294
0.55	0.1136	0.0227	0.1815	0.0646	0.1358	0.0272	0.1906	0.0525	0.0753	0.0151	0.1275	0.0397	0.0425
0.60	0.1718	0.0344	0.2627	0.0920	0.2019	0.0404	0.2749	0.0758	0.1151	0.0230	0.1862	0.0577	0.0572
0.65	0.2381	0.0476	0.3550	0.1230	0.2754	0.0551	0.3676	0.1014	0.1613	0.0323	0.2530	0.0777	0.0731
0.70	0.3170	0.0634	0.4630	0.1581	0.3544	0.0709	0.4670	0.1287	0.2127	0.0425	0.3259	0.0998	0.0900
0.75	0.4083	0.0817	0.5839	0.1967	0.4378	0.0876	0.5685	0.1576	0.2683	0.0537	0.4043	0.1231	0.1073
0.80	0.5029	0.1006	0.7069	0.2361	0.5244	0.1049	0.6748	0.1872	0.3275	0.0655	0.4871	0.1474	0.1250
0.85	0.5973	0.1195	0.8299	0.2761	0.6134	0.1227	0.7871	0.2186	0.3894	0.0779	0.5746	0.1732	0.1428
0.90	0.6918	0.1384	0.9543	0.3167	0.7038	0.1408	0.9070	0.2491	0.4532	0.0906	0.6632	0.2000	0.1605
0.95	0.7867	0.1573	1.0811	0.3580	0.7955	0.1591	1.0165	0.2810	0.5185	0.1037	0.7599	0.2259	0.1781
1.00	0.8820	0.1764	1.2103	0.3999	0.8878	0.1775	1.1411	0.3134	0.5848	0.1170	0.8581	0.2543	0.1955

Table 23: Total cross sections in the $C(\nu_e, e^-) + 2p(\nu_e, e^-)$ scattering in $10^{-38} cm^2$. M-S width

E_ν GeV	8p+6n Free				Fermi Motion + PB				Full Δ In-Medium				
	Resonant		+Background		Resonant		+Background		Resonant		+Background		
	π^+	π^0	π^+	π^0	π^+	π^0	π^+	π^0	π^+	π^0	π^+	π^0	$\Delta_{pionless}$
0.40	0.3255	0.0501	0.4816	0.0936	0.4206	0.0691	0.5634	0.0965	0.2627	0.0375	0.3880	0.0607	0.1369
0.45	0.6695	0.1030	0.9153	0.1712	0.8071	0.1305	1.0206	0.1742	0.5183	0.0728	0.7162	0.1112	0.2080
0.50	1.1220	0.1726	1.4503	0.2649	1.2838	0.2050	1.5575	0.2630	0.8502	0.1183	1.1156	0.1726	0.2875
0.55	1.6459	0.2532	2.0392	0.3670	1.8107	0.2862	2.1266	0.3560	1.2336	0.1708	1.5556	0.2395	0.3698
0.60	2.2059	0.3394	2.6425	0.4711	2.3570	0.3696	2.6961	0.4504	1.6439	0.2270	2.0040	0.3089	0.4506
0.65	2.7734	0.4267	3.2325	0.5729	2.8955	0.4511	3.2364	0.5368	2.0609	0.2842	2.4397	0.3751	0.5271
0.70	3.3280	0.5120	3.7912	0.6699	3.4151	0.5294	3.7209	0.6187	2.4699	0.3404	2.8556	0.4387	0.5974
0.75	3.8558	0.5932	4.3091	0.7605	3.8997	0.6020	4.2080	0.6956	2.8604	0.3941	3.2393	0.4990	0.6607
0.80	4.3496	0.6692	4.7829	0.8445	4.3447	0.6682	4.6140	0.7606	3.2265	0.4445	3.5826	0.5544	0.7168
0.85	4.8057	0.7393	5.2129	0.9219	4.7522	0.7286	4.9615	0.8238	3.5651	0.4912	3.9022	0.6038	0.7661
0.90	5.2224	0.8034	5.6003	0.9930	5.1180	0.7826	5.2995	0.8764	3.8747	0.5339	4.1825	0.6493	0.8089
0.95	5.6005	0.8616	5.9489	1.0583	5.4467	0.8308	5.6011	0.9313	4.1562	0.5728	4.4279	0.6917	0.8460
1.00	5.9426	0.9142	6.2635	1.1186	5.7439	0.8745	5.8678	0.9758	4.4106	0.6078	4.6580	0.7318	0.8778

Table 24: Total cross sections in the $^{12}C(\overline{\nu}_e, e^+) + 2p(\overline{\nu}_e, e^+)$ scattering in $10^{-38} cm^2$. M-S width

E_ν GeV	8p+6n Free				Fermi Motion + PB				Full Δ In-Medium				
	Resonant		+Background		Resonant		+Background		Resonant		+Background		
	π^-	π^0	π^-	π^0	π^-	π^0	π^-	π^0	π^-	π^0	π^-	π^0	$\Delta_{pionless}$
0.40	0.0526	0.0102	0.0902	0.0294	0.0660	0.0129	0.0969	0.0234	0.0365	0.0070	0.0647	0.0171	0.0262
0.45	0.0992	0.0192	0.1578	0.0498	0.1185	0.0231	0.1666	0.0408	0.0668	0.0127	0.1118	0.0299	0.0383
0.50	0.1573	0.0304	0.2392	0.0747	0.1814	0.0353	0.2483	0.0617	0.1052	0.0200	0.1695	0.0457	0.0522
0.55	0.2240	0.0434	0.3312	0.1030	0.2520	0.0489	0.3380	0.0852	0.1501	0.0286	0.2364	0.0640	0.0674
0.60	0.2978	0.0576	0.4322	0.1343	0.3291	0.0639	0.4364	0.1110	0.2007	0.0382	0.3092	0.0847	0.0835
0.65	0.3772	0.0730	0.5409	0.1681	0.4097	0.0795	0.5391	0.1371	0.2559	0.0487	0.3908	0.1070	0.1002
0.70	0.4613	0.0893	0.6565	0.2039	0.4966	0.0964	0.6514	0.1674	0.3150	0.0600	0.4764	0.1307	0.1173
0.75	0.5493	0.1063	0.7783	0.2414	0.5847	0.1134	0.7670	0.1965	0.3774	0.0719	0.5702	0.1554	0.1347
0.80	0.6404	0.1240	0.9059	0.2805	0.6743	0.1307	0.8915	0.2268	0.4422	0.0843	0.6683	0.1813	0.1522
0.85	0.7339	0.1421	1.0388	0.3207	0.7679	0.1488	1.0141	0.2581	0.5090	0.0971	0.7697	0.2075	0.1696
0.90	0.8291	0.1605	1.1767	0.3621	0.8610	0.1669	1.1385	0.2905	0.5771	0.1101	0.8761	0.2353	0.1869
0.95	0.9253	0.1791	1.3193	0.4043	0.9542	0.1849	1.2750	0.3222	0.6463	0.1233	0.9908	0.2631	0.2040
1.00	1.0221	0.1978	1.4665	0.4474	1.0489	0.2032	1.4147	0.3566	0.7160	0.1366	1.1053	0.2918	0.2208

Table 25: Total cross sections in the $^{12}C(\nu_\mu, \mu^-) + 2p(\nu_\mu, \mu^-)$ scattering in $10^{-38} cm^2$. M-S width

E_ν GeV	8p+6n Free				Fermi Motion + PB				Full Δ In-Medium				
	Resonant		+Background		Resonant		+Background		Resonant		+Background		
	π^+	π^0	π^+	π^0	π^+	π^0	π^+	π^0	π^+	π^0	π^+	π^0	$\Delta_{pionless}$
0.40	0.0509	0.0078	0.1020	0.0233	0.0962	0.0169	0.1537	0.0267	0.0608	0.0098	0.1083	0.0179	0.0694
0.45	0.2135	0.0328	0.3538	0.0719	0.3320	0.0565	0.4690	0.0816	0.2009	0.0303	0.3175	0.0509	0.1261
0.50	0.5750	0.0885	0.8316	0.1577	0.7354	0.1205	0.9609	0.1640	0.4622	0.0659	0.6643	0.1030	0.1991
0.55	1.0759	0.1655	1.4297	0.2619	1.2456	0.1995	1.5417	0.2599	0.8149	0.1133	1.0944	0.1675	0.2811
0.60	1.6341	0.2514	2.0557	0.3696	1.7995	0.2845	2.1382	0.3587	1.2160	0.1678	1.5575	0.2375	0.3652
0.65	2.2118	0.3403	2.6759	0.4761	2.3592	0.3698	2.7189	0.4507	1.6367	0.2252	2.0150	0.3082	0.4467
0.70	2.7915	0.4295	3.2780	0.5797	2.9029	0.4517	3.2689	0.5398	2.0586	0.2829	2.4582	0.3742	0.5228
0.75	3.3587	0.5167	3.8481	0.6781	3.4183	0.5286	3.7523	0.6222	2.4684	0.3387	2.8673	0.4392	0.5919
0.80	3.8908	0.5986	4.3659	0.7685	3.8952	0.5995	4.2102	0.6919	2.8552	0.3915	3.2418	0.4961	0.6535
0.85	4.3795	0.6738	4.8294	0.8507	4.3300	0.6639	4.6103	0.7556	3.2137	0.4406	3.5755	0.5492	0.7077
0.90	4.8248	0.7423	5.2438	0.9255	4.7227	0.7219	4.9658	0.8191	3.5420	0.4857	3.8807	0.5991	0.7549
0.95	5.2283	0.8044	5.6141	0.9938	5.0754	0.7738	5.2649	0.8677	3.8410	0.5269	4.1488	0.6431	0.7958
1.00	5.5926	0.8604	5.9457	1.0564	5.3902	0.8199	5.5513	0.9198	4.1114	0.5642	4.3933	0.6822	0.8309

Table 26: Total cross sections in the $^{12}C(\overline{\nu}_\mu, \mu^+) + (\overline{\nu}_\mu, \mu^+)2p$ scattering in $10^{-38} cm^2$. M-S width

E_ν GeV	8p+6n Free				Fermi Motion + PB				Full Δ In-Medium				
	Resonant		+Background		Resonant		+Background		Resonant		+Background		
	π^-	π^0	π^-	π^0	π^-	π^0	π^-	π^0	π^-	π^0	π^-	π^0	$\Delta_{pionless}$
0.40	0.0066	0.0013	0.0198	0.0092	0.0113	0.0022	0.0231	0.0062	0.0070	0.0014	0.0178	0.0054	0.0105
0.45	0.0252	0.0049	0.0551	0.0214	0.0374	0.0073	0.0634	0.0165	0.0208	0.0040	0.0442	0.0129	0.0186
0.50	0.0644	0.0125	0.1164	0.0405	0.0815	0.0159	0.1253	0.0323	0.0452	0.0086	0.0857	0.0246	0.0294
0.55	0.1174	0.0227	0.1936	0.0646	0.1395	0.0272	0.2027	0.0525	0.0791	0.0151	0.1396	0.0397	0.0425
0.60	0.1775	0.0344	0.2802	0.0920	0.2076	0.0404	0.2924	0.0758	0.1208	0.0230	0.2037	0.0577	0.0572
0.65	0.2460	0.0476	0.3789	0.1230	0.2833	0.0551	0.3914	0.1014	0.1692	0.0323	0.2767	0.0777	0.0731
0.70	0.3276	0.0634	0.4943	0.1581	0.3650	0.0709	0.4984	0.1287	0.2232	0.0425	0.3571	0.0998	0.0900
0.75	0.4219	0.0817	0.6239	0.1967	0.4514	0.0876	0.6084	0.1576	0.2820	0.0537	0.4443	0.1231	0.1073
0.80	0.5197	0.1006	0.7562	0.2361	0.5412	0.1049	0.7242	0.1872	0.3443	0.0655	0.5366	0.1474	0.1250
0.85	0.6172	0.1195	0.8895	0.2761	0.6333	0.1227	0.8467	0.2186	0.4093	0.0779	0.6342	0.1732	0.1428
0.90	0.7148	0.1384	1.0250	0.3167	0.7268	0.1408	0.9777	0.2491	0.4762	0.0906	0.7338	0.2000	0.1605
0.95	0.8130	0.1573	1.1638	0.3580	0.8217	0.1591	1.0993	0.2810	0.5448	0.1037	0.8427	0.2259	0.1781
1.00	0.9114	0.1764	1.3061	0.3999	0.9172	0.1775	1.2369	0.3134	0.6142	0.1170	0.9538	0.2543	0.1955

References

[1] B. T. Cleveland, T. Daily, R. Davis Jr., J. R. Distel, K. Lande, C. K. Lee, P. S. Wildenhain, and J. Ullman, Astrophys. J. **496**, 505 (1998).

[2] Y. Fukuda *et al.* [Super-Kamiokande Collaboration], Phys. Rev. Lett. **81**, 1562 (1998).

[3] Y. Ashie *et al.* [Super-Kamiokande Collaboration], Phys. Rev. D **71**, 112005 (2005).

[4] K. Abe *et al.* [T2K Collaboration], Phys. Rev. Lett. **107**, 041801 (2011).

[5] F. P. An *et al.* [DAYA-BAY Collaboration], Phys. Rev. Lett. **108**, 171803 (2012).

[6] J. K. Ahn *et al.* [RENO Collaboration], Phys. Rev. Lett. **108**, 191802 (2012).

[7] Y. Abe *et al.* [Double Chooz Collaboration], Phys. Rev. D **86**, 052008 (2012).

[8] K. Abe et al., Evidence of Electron Neutrino Appearance in a Muon Neutrino Beam, arXiv:1304.0841(hep-ex), 2013.

[9] H. Gallagher, G. Garvey, and G. P. Zeller, Ann. Rev. Nucl. Part. Sci. **61**, 355 (2011).

[10] J. G. Morfin, J. Nieves, and J. T. Sobczyk, Adv. High Energy Phys. **2012**, 934597 (2012).

[11] A. A. Aguilar-Arevalo *et al.* [MiniBooNE Collaboration], Phys. Rev. D **81**, 092005 (2010).

[12] K. Abe *et al.* [T2K Collaboration], Measurement of the inclusive numu charged current cross section on carbon in the near detector of the t2k experiment, arXiv:1302.4908 [hep-ex], 2013.

[13] M. H. Ahn *et al.* [K2K Collaboration], Phys. Rev. D **74**, 072003 (2006).

[14] C. Juszczak, J. T. Sobczyk, and J. Zmuda, Phys. Rev. C **82**, 045502 (2010).

[15] J. T. Sobczyk. and J. Zmuda, On Impact of Nuclear Effects on Weak Pion Production in Sub 1 GeV Energy Region, arXiv:1210.6149 [nucl-th], accepted for publication in Physical Review C, 2012.

[16] S. Glashow, Nucl.Phys. **22**, 579 (1961).

[17] J. Goldstone, A. Salam, and S. Weinberg, Phys.Rev. **127**, 965 (1962).

[18] A. Salam and J. C. Ward, Phys.Lett. **13**, 168 (1964).

[19] S. Weinberg, Phys. Rev. Lett. **19**, 1264 (1967).

[20] A. Salam, Conf.Proc. **C680519**, 367 (1968).

[21] S. Bilenky, Lect. Notes Phys. **817**, 1 (2010).

[22] T. P. Cheng and L. F. Li, *Gauge Theory Of Elementary Particle Physics*, Oxford, UK: Clarendon (Oxford Science Publications), 1984.

[23] J. Beringer *et al.* [Particle Data Group Collaboration], Phys. Rev. D **86**, 010001 (2012).

[24] P. F. Loverre [K2K and T2K Collaborations], J. Phys. Conf. Ser. **39**, 323 (2006).

[25] Y. Obayashi [T2K Collaboration], Reach of Future Accelerator and Reactor Neutrino Efforts, talk given at Flavor Physics and CP Violation (FPCP) conference, Taipei, Taiwan, 2008.

[26] R. P. Feynman and M. Gell-Mann, Phys. Rev. **109**, 193 (1958).

[27] J. D. Walecka, *Theoretical Nuclear and Subnuclear Physics*, Oxford University Press, Inc., 1995.

[28] M. L. Goldberger and S. B. Treiman, Phys. Rev. **110**, 1178 (1958).

[29] A. M. Ankowski, Acta Phys. Polon. B **37**, 377 (2006).

[30] R. Gran *et al.* [K2K Collaboration], Phys. Rev. D **74**, 052002 (2006).

[31] X. Espinal and F. Sanchez, AIP Conf. Proc. **967**, 117 (2007).

[32] M. Dorman *et al.* [MINOS Collaboration], AIP Conf. Proc. **1189**, 133 (2009).

[33] V. Lyubushkin *et al.* [NOMAD Collaboration], AIP Conf. Proc. **1189**, 157 (2009).

[34] A. M. Ankowski, PoS NUFACT **08**, 118 (2008).

[35] A. Ankowski, *Efekty jadrowe w oddzialywaniach neutrin*, PhD thesis, Institute of Theoretical Physics, University of Wroclaw, 2008.

[36] O. Benhar, A. Fabrocini, S. Fantoni, and I. Sick, Nucl. Phys. A **579**, 493 (1994).

[37] O. Benhar, A. Fabrocini, and S. Fantoni, Nucl. Phys. A **505**, 267 (1989).

[38] O. Benhar, A. Fabrocini, S. Fantoni, G. A. Miller, V. R. Pandharipande, and I. Sick, Phys. Rev. C **44**, 2328 (1991).

[39] O. Benhar, N. Farina, H. Nakamura, M. Sakuda, and R. Seki, Phys. Rev. D **72**, 053005 (2005).

[40] O. Benhar, P. Coletti, and D. Meloni, Phys. Rev. Lett. **105**, 132301 (2010).

[41] C. Juszczak, J. A. Nowak, and J. T. Sobczyk, Nucl. Phys. Proc. Suppl. **159**, 211 (2006).

[42] J. A. Nowak, Phys. Scripta T **127**, 70 (2006).

[43] C. Juszczak, Acta Phys. Polon. B **40**, 2507 (2009).

[44] A. M. Ankowski and J. T. Sobczyk, Phys.Rev. **C74**, 054316 (2006).

[45] L. Alvarez-Ruso, Nucl. Phys. B (Proc. Suppl.) **229-232**, 167 (2012).

[46] E. Hernandez, J. Nieves, and M. Valverde, Phys. Rev. D **76**, 033005 (2007).

[47] K. M. Graczyk, D. Kielczewska, P. Przewlocki, and J. T. Sobczyk, Phys. Rev. D **80**, 093001 (2009).

[48] G. L. Fogli and G. Nardulli, Nucl. Phys. B **160**, 116 (1979).

[49] D. Rein, Z. Phys. C **35**, 43 (1987).

[50] D. Drechsel, S. S. Kamalov, and L. Tiator, Eur. Phys. J. A **34**, 69 (2007).

[51] C. Barbero, G. Lopez Castro, and A. Mariano, Phys. Lett. B **664**, 70 (2008).

[52] S. K. Singh, M. J. Vicente-Vacas, and E. Oset, Phys. Lett. B **416**, 23 (1998), [Erratum-ibid. B **423** (1998) 428].

[53] S. Ahmad, M. Sajjad Athar, and S. K. Singh, Phys. Rev. D **74**, 073008 (2006).

[54] M. Sajjad Athar, S. Ahmad, and S. K. Singh, Nucl. Phys. A **782**, 179 (2007).

[55] S. K. Singh, M. Sajjad Athar, and S. Ahmed, AIP Conf. Proc. **967**, 182 (2007).

[56] M. Sajjad Athar, S. Chauhan, and S. K. Singh, J. Phys. G **37**, 015005 (2010).

[57] M. Sajjad Athar, S. Chauhan, and S. K. Singh, Eur. Phys. J. A **43**, 209 (2010).

[58] E. Oset and L. L. Salcedo, Nucl. Phys. A **468**, 631 (1987).

[59] L. Tiator, D. Drechsel, S. S. Kamalov, and M. Vanderhaeghen, Eur. Phys. J. ST **198**, 141 (2011).

[60] S. J. Barish, M. Derrick, T. Dombeck, L. G. Hyman, K. Jaeger, B. Musgrave, P. Schreiner, and R. Singer *et al.*, Phys. Rev. D **19**, 2521 (1979).

[61] G. M. Radecky, V. E. Barnes, D. D. Carmony, A. F. Garfinkel, M. Derrick, E. Fernandez, L. Hyman, and G. Levman *et al.*, Phys. Rev. D **26**, 3297 (1982), [Erratum-ibid. D **26** (1982) 3297].

[62] T. Kitagaki, H. Yuta, S. Tanaka, A. Yamaguchi, K. Abe, K. Hasegawa, K. Tamai, and H. Sagawa *et al.*, Phys. Rev. D **42**, 1331 (1990).

[63] A. Rodriguez and L. Whitehead *et al*, Phys. Rev. D **78**, 032003 (2008).

[64] C. Mariani *et al.* [K2K Collaboration], Phys. Rev. D **83**, 054023 (2011).

[65] A. A. Aguilar-Arevalo *et al.* [MiniBooNE Collaboration], Phys. Rev. D **83**, 052007 (2011).

[66] A. A. Aguilar-Arevalo *et al.* [MiniBooNE Collaboration], Phys. Rev. D **83**, 052009 (2011).

[67] D. Rein and L. M. Sehgal, Annals Phys. **133**, 79 (1981).

[68] R. P. Feynman, M. Kislinger, and F. Ravndal, Phys. Rev. D **3**, 2706 (1971).

[69] K. Graczyk and J. Sobczyk, Phys. Rev. D **77**, 053001 (2008), erratum-ibid. D**79** (2009) 079903.

[70] J. Nieves, I. Ruiz Simo, and M. J. Vicente Vacas, Phys. Rev. C **83**, 045501 (2011).

[71] G. Fiorentini et al., Measurement of Muon Neutrino Quasi-Elastic Scattering on a Hydrocarbon Target at $E_\nu \sim 3.5$ GeV, arXiv:1305.2243 [hep-ex], 2013.

[72] L. Fields et al., Measurement of Muon Antineutrino Quasi-Elastic Scattering on a Hydrocarbon Target at $E_\nu \sim 3.5$ GeV, arXiv:1305.2234 [hep-ex], 2013.

[73] M. Chemtob and A. Lumbroso, Nucl. Phys. B **17**, 401 (1970).

[74] M. Chemtob and M. Rho, Nucl. Phys. A **163**, 1 (1971).

[75] J. W. Van Orden, T. W. Donnelly, T. De Forest Jr., and W. C. Hermans, Phys. Lett. B **76**, 393 (1978).

[76] J. W. Van Orden and T. W. Donnelly, Annals Phys. **131**, 451 (1981).

[77] M. Kohno and N. Ohtsuka, Phys. Lett. B **98**, 335 (1981).

[78] W. M. Alberico, M. Ericson, and A. Molinari, Annals Phys. **154**, 356 (1984).

[79] W. M. Alberico, R. Cenni, A. Molinari, and P. Saracco, Phys. Rev. Lett. **65**, 1845 (1990).

[80] W. M. Alberico, T. W. Donnelly, and A. Molinari, Nucl. Phys. A **512**, 541 (1990).

[81] M. J. Dekker, P. J. Brussaard, and J. A. Tjon, Phys. Lett. B **266**, 249 (1990).

[82] M. J. Dekker, P. J. Brussaard, and J. A. Tjon, Phys. Rev. C **49**, 2650 (1994).

[83] M. J. Dekker, P. J. Brussaard, and J. A. Tjon, Phys. Rev. C **51**, 1393 (1995).

[84] W. Leidemann and G. Orlandini, Nucl. Phys. A **506**, 447 (1990).

[85] J. Carlson and R. Schiavilla, Phys. Rev. C **49**, R2880 (1994).

[86] A. Gil, J. Nieves, and E. Oset, Nucl. Phys. A **627**, 543 (1997).

[87] A. De Pace, M. Nardi, W. M. Alberico, T. W. Donnelly, and A. Molinari, Nucl. Phys. A **726**, 303 (2003).

[88] A. De Pace, M. Nardi, W. M. Alberico, T. W. Donnelly, and A. Molinari, Nucl. Phys. A **741**, 249 (2004).

[89] J. Carlson, J. Jourdan, R. Schiavilla, and I. Sick, Phys. Rev. C **65**, 024002 (2002).

[90] J. Marteau, Eur. Phys. J. A **5**, 183 (1999).

[91] M. Martini, M. Ericson, G. Chanfray, and J. Marteau, Phys. Rev. C **80**, 065501 (2009).

[92] J. Nieves, I. Ruiz Simo, and M. J. Vicente Vacas, Phys. Lett. B **707**, 72 (2012).

[93] J. E. Amaro, M. B. Barbaro, J. A. Caballero, and T. W. Donnelly, Phys. Rev. Lett. **108**, 152501 (2012).

[94] H. S. Bodek, A. Budd and M. E. Christy, Eur. Phys. J. C **71**, 1726 (2011).

[95] T. Katori, Meson Exchange Current (MEC) Models in Neutrino Interaction Generators, arXiv:1304.6014[nucl-th], 2013.

[96] M. Martini, M. Ericson, G. Chanfray, and J. Marteau, Phys. Rev. C **81**, 045502 (2010).

[97] J. Nieves, F. Sanchez, I. Ruiz Simo, and M. J. Vicente Vacas, Phys. Rev. D **85**, 113008 (2012).

[98] J. E. Amaro, M. B. Barbaro, J. A. Caballero, T. W. Donnelly, and J. M. Udias, Phys. Rev. D **84**, 033004 (2011).

[99] J. Nieves, I. R. Simo, and M. J. Vicente-Vacas, Two Particle-Hole Excitations in Charged Current Quasielastic Antineutrino-Nucleus Scattering, arXiv:1302.0703 [hep-ph], 2012.

[100] T. Golan, C. Juszczak, and J. T. Sobczyk, Phys. Rev. C **86**, 015505 (2012).

[101] C. H. Llewellyn Smith, Phys. Rept. **3**, 261 (1972).

[102] K. M. Graczyk and J. T. Sobczyk, Eur. Phys. J. C **31**, 177 (2003).

[103] K. M. Graczyk, Nucl. Phys. A **748**, 313 (2005).

[104] H. F. Jones and M. D. Scadron, Annals Phys. **81**, 1 (1973).

[105] D. Rein and L. M. Sehgal, Nucl. Phys. B **223**, 29 (1983).

[106] J. T. Sobczyk, Phys. Rev. C **86**, 015504 (2012).

[107] J. Marteau, J. Delorme, and M. Ericson, Nucl. Instrum. Meth. A **451**, 76 (2000).

[108] A. Bodek and U. K. Yang, Nucl. Phys. Proc. Suppl. **112**, 70 (2002).

[109] F. Sartogo, *Interazioni di neutrini atmosferici: un modello fenomenologico e la sua applicazione nell'interpretazione dei dati ottenibili in rivelatori sotterranei*, PhD thesis, Universita di Roma "La Sapienza", Dipartimento Di Fisica, 2002.

[110] J. Sobczyk, PoS NUFACT **08**, 141 (2008).

[111] L. L. Salcedo, E. Oset, M. J. Vicente-Vacas, and C. Garcia-Recio, Nucl. Phys. A **484**, 557 (1988).

[112] M. N. Rosenbluth, Phys. Rev. **79**, 615 (1950).

[113] T. De Forest, Nucl. Phys. A **392**, 232 (1983).

[114] H. De Vries, C. W. De Jager, and C. De Vries, Atom. Data Nucl. Data Tabl. **36**, 495 (1987).

[115] C. Garcia-Recio, J. Nieves, and E. Oset, Nucl. Phys. A **547**, 473 (1992).

[116] R. Cutkosky, J. Math. Phys. **1**, 429 (1960).

[117] P. Barreau et al., Nucl.Phys. A **402**, 515 (1983).

[118] J. O'Connell et al., Phys. Rev. C **35**, 1063 (1987).

[119] R. Sealock et al., Phys. Rev. Lett. **62**, 1350 (1989).

[120] P. K. A. de Witt Huberts, J. Phys. G **16**, 507 (1990).

[121] D. Rohe *et al.* [E97-006 Collaboration], Phys. Rev. C **72**, 054602 (2005).

[122] A. L. Fetter and J. D. Walecka, *Quantum Theory of Many-Particle Systems*, Dover Publications, 1971.

[123] S. Frullani and J. Mougey, Adv. Nucl. Phys. **14**, 1 (1984).

[124] L. Alvarez-Ruso, O. Buss, T. Leitner, and U. Mosel, AIP Conf. Proc. **1189**, 151 (2009).

[125] S. Boyd, S. Dytman, E. Hernandez, J. Sobczyk, and R. Tacik, AIP Conf. Proc. **1189**, 60 (2009).

[126] L. Alvarez-Ruso, AIP Conf. Proc. **1222**, 42 (2010).

[127] T. Leitner, *Neutrino-Nucleus Interactions in a Coupled-Channel Hadronic Transport Model*, PhD thesis, Justus-Liebig-Universitaet Giessen, Fachbereich 07 (Mathematik und Informatik, Physik, Geographie), Institut fuer Theoretische Physik, 2007.

[128] D. Rohe, C. S. Armstrong, R. Asaturyan, O. K. Baker, S. Bueltmann, C. Carasco, D. Day, and R. Ent *et al.*, Phys. Rev. Lett. **93**, 182501 (2004).

[129] D. Rohe *et al.*, Nucl. Phys. Proc. Suppl. **159**, 152 (2006).

[130] A. M. Ankowski and J. T. Sobczyk, Phys. Rev. C **77**, 044311 (2008).

[131] A. V. Butkevich, Phys. Rev. C **82**, 055501 (2010).

[132] S. Kopp, Neutrino beams, talk at NuInt09, Sitges, May 18-22 2009.

[133] J. Nowak, AIP Conf. Proc. **1189**, 351 (2009).

[134] A. A. Aguilar-Arevalo *et al.* [MiniBooNE Collaboration], Phys. Rev. Lett. **103**, 081801 (2009).

[135] G. D'Agostini, Nucl. Instrum. Meth. A **346**, 306 (1994).

[136] M. Martini, M. Ericson, and G. Chanfray, Phys. Rev. C **84**, 055502 (2011).

[137] E. Hernandez, J. Nieves, M. Singh, S. K. and Valverde, and M. J. Vicente Vacas, Phys. Rev. D **77**, 053009 (2008).

[138] M. Valverde, J. Nieves, E. Hernandez, S. K. Singh, and M. J. Vicente Vacas, Mod. Phys. Lett. A **23**, 2309 (2008).

[139] E. D. Bloom and F. J. Gilman, Phys. Rev. Lett. **25**, 1140 (1970).

[140] O. Lalakulich, E. A. Paschos, and G. Piranishvili, Phys. Rev. D **74**, 014009 (2006).

[141] J. S. O'Connell, W. R. Dodge, J. W. Lightbody, X. K. Maruyama, J. O. Adler, K. Hansen, B. Schroder, and A. M. Bernstein *et al.*, Phys. Rev. Lett. **53**, 1627 (1984).

[142] M. Christy and P. E. Bosted, Phys. Rev. C **81**, 055213 (2010).

[143] S. L. Adler, Annals Phys. **50**, 189 (1968).

[144] D. M. Manley and E. M. Saleski, Phys. Rev. D **45**, 4002 (1992).

[145] M. Post, S. Leupold, and U. Mosel, Nucl. Phys. A **741**, 81 (2004).

[146] K. M. Watson, Phys. Rev. **95**, 228 (1954).

[147] T. Leitner, O. Buss, L. Alvarez-Ruso, and U. Mosel, Phys. Rev. C **79**, 034601 (2009).

[148] T. Kitagaki et al., Phys. Rev. D **34**, 2554 (1986).

[149] L. Hulthen and M. Sugawara, *Handbuch der Physik*, volume 39, Springer Verlag, 1957.

[150] M. Lacombe, B. Loiseau, R. Vinh Mau, J. Cote, P. Pires, and R. de Tourreil, Phys. Lett. B , 139 (1981).

[151] R. Machleidt, K. Holinde, and C. Elster, Phys. Rept. , 1 (1987).

[152] E. Hernandez, J. Nieves, M. Valverde, and M. Vicente Vacas, Phys. Rev. D **81**, 085046 (2010).

[153] M. Galassi, J. Davies, J. Theiler, B. Gough, G. Jungman, P. Alken, M. Booth, and F. Rossi, *GNU Scientific Library Reference Manual (3rd Ed.)*, Network Theory LTD, 2009, GSL home page: http://www.gnu.org/software/gsl/.

[154] R. C. Carrasco and E. Oset, Nucl. Phys. A **536**, 445 (1992).

[155] C. Praet, O. Lalakulich, N. Jachowicz, and J. Ryckebusch, Phys. Rev. C **79**, 044603 (2009).

[156] M. Antonello, V. Caracciolo, G. Christodoulou, J. Dobson, E. Frank, T. Golan, V. Lee, and S. Mania, Acta Phys. Polon. B **40**, 2519 (2009).

[157] O. Lalakulich, K. Gallmeister, T. Leitner, and U. Mosel, AIP Conf.Proc. **1405**, 127 (2011).

[158] O. Lalakulich and U. Mosel, Phys. Rev. C **87**, 014602 (2013).

[159] M. El Amiri, J. Pestieau, and G. Lopez Castro, Nucl. Phys. A **543**, 673 (1992).

[160] V. Pascalutsa and M. Vanderhaeghen, Phys. Rev. D **73**, 034003 (2006).

[161] V. Pascalutsa and R. Timmermans, Phys. Rev. C **60**, 042201 (1999).

[162] A. Mariano and C. Barbero, 2p2h effects on the weak pion production cross section, arXiv:1304.6249[nucl-th], 2013.

[163] J. Nieves, J. E. Amaro, and M. Valverde, Phys. Rev. C **70**, 055503 (2004), [Erratum-ibid. C **72** (2005) 019902].

[164] J. E. Amaro, C. Maieron, M. B. Barbaro, J. A. Caballero, and T. W. Donnelly, Phys. Rev. C **82**, 044601 (2010).

[165] P. A. Schreiner and F. Von Hippel, Nucl. Phys. B **58**, 333 (1978).

[166] S. Galster, H. Klein, J. Moritz, K. H. Schmidt, D. Wegener, and J. Bleckwenn, Nucl. Phys. B **32**, 221 (1971).

[167] W. M. Alberico, S. M. Bilenky, C. Giunti, and K. M. Graczyk, Phys. Rev. C **79**, 065204 (2009).

[168] M. Warns, H. Schroder, W. Pfeil, and H. Rollnik, Z. Phys. C **45**, 627 (1990).

[169] P. Stoler, Phys. Rept. **226**, 103 (1993).

[170] O. Lalakulich, T. Leitner, O. Buss, and U. Mosel, Phys. Rev. D **82**, 093001 (2010).

[171] E. A. Paschos, J. Y. Yu, and M. Sakuda, Phys. Rev. D **69**, 014013 (2004).